

8-1-2013

Malaria kinase inhibition: a tool for antimalarial drug discovery and elucidation of cell cycle protein expression patterns

Kristen M. Bullard

Follow this and additional works at: <http://digscholarship.unco.edu/dissertations>

Recommended Citation

Bullard, Kristen M., "Malaria kinase inhibition: a tool for antimalarial drug discovery and elucidation of cell cycle protein expression patterns" (2013). *Dissertations*. Paper 86.

This Text is brought to you for free and open access by the Student Research at Scholarship & Creative Works @ Digital UNC. It has been accepted for inclusion in Dissertations by an authorized administrator of Scholarship & Creative Works @ Digital UNC. For more information, please contact Jane.Monson@unco.edu.

© 2013

KRISTEN M. BULLARD

ALL RIGHTS RESERVED

UNIVERSITY OF NORTHERN COLORADO

Greeley, Colorado

The Graduate School

MALARIA KINASE INHIBITION: A TOOL FOR
ANTIMALARIAL DRUG DISCOVERY AND
ELUCIDATION OF CELL CYCLE
PROTEIN EXPRESSION
PATTERNS

A Dissertation Submitted in Partial Fulfillment
of the Requirements for the Degree of
Doctor of Philosophy

Kristen M. Bullard

College of Natural & Health Sciences
School of Biological Sciences
Biological Education

August 2013

This Dissertation by: Kristen M. Bullard

Entitled: *Malaria Kinase Inhibition: a Tool for Antimalarial Drug Discovery and Elucidation of Cell Cycle Protein Expression Patterns*

has been approved as meeting the requirement for the Degree of Doctor of Philosophy in the College of Natural & Health Sciences in the School of Biological Sciences, Program of Biological Education

Accepted by the Doctoral Committee

Susan M. Keenan Ph. D., Chair

Tony Schountz Ph.D., Committee Member

Stephen Mackessy Ph.D., Committee Member

Aichun Dong, Ph.D., Committee Member

Date of Dissertation Defense _____

Accepted by the Graduate School

Linda L. Black, Ed.D.
Dean of the Graduate School and International Admissions

ABSTRACT

Bullard, Kristen M. *Malaria Kinase Inhibition: a Tool for Antimalarial Drug Discovery and Elucidation of Cell Cycle Protein Expression Patterns*.
Published Doctor of Philosophy in Biological Education dissertation,
University of Northern Colorado, 2013.

The protozoan parasite, *Plasmodium (P.) falciparum*, causes the most virulent form of malaria and is a significant source of mortality in the developing world. Increasing resistance of this parasite to traditional antimalarials has necessitated the identification of new targets for antimalarial drug design. Protein kinases, which mediate critical cellular processes such as proliferation, growth, and apoptosis, make attractive drug targets as the deregulation of cellular phosphorylation events has been linked to human diseases. In recent years, kinase inhibitors have successfully treated such diseases as chronic myelogenous leukemia and renal cell carcinoma. The unique structural and mechanistic aspects of many *P. falciparum* kinases make these proteins potentially useful drug targets and the inhibition of these macromolecules provides a means to examine heretofore undescribed cellular mechanisms within these dynamic parasitic organisms. First, three libraries of known kinase inhibitors were screened against the malaria kinase, PfPK7, using a ATP luminescence assay to determine which of these molecules had affinity for the ATP binding site of this kinase. Computational methods were employed to determine how small molecule inhibitors were binding to the PfPK7 ATP-binding site and properties that are important for determining the druglikeness of each

compound were predicted using commercially available software. In addition, small molecules were screened against *P. falciparum* strain W2 to determine their ability to inhibit intraerythrocytic stage growth using a SYBR Green I growth assay. Finally, the well characterized kinase inhibitor Purvalanol B was applied to blood stage cultures of *P. falciparum* strain W2 and differences in protein expression between inhibitor-treated and wildtype parasites were determined using a shotgun proteomics approach. Out of the 244 small molecules tested, eight were found to have affinity for the ATP-binding site of PfPK7 and the probable interactions that contribute to small molecule binding as well as the predicted properties that contribute to druglikeness were described. While several small molecules were able to inhibit intraerythrocytic parasite growth, most inhibitors of PfPK7 identified in the luminescence screen did not significantly inhibit *P. falciparum* growth. Disruption of parasite development with the kinase inhibitor Purvalanol B yielded differences in protein expression between wildtype and inhibitor-treated parasites. These data further characterize the orphan kinase PfPK7 and may suggest this target may not be ideal for antimalarial drug design as its inhibition does not correspond with attenuated *P. falciparum* growth in blood stage cultures. Finally, protein differences resulting from kinase inhibitor treatment during parasite cell cycle aid in the elucidation of the heretofore poorly understood *P. falciparum* cell cycle mechanisms.

ACKNOWLEDGMENTS

I would like to thank my advisor Susan M. Keenan for allowing me to perform research in her laboratory over the last five years and for her continuous support and encouragement. Dr. Keenan has facilitated my growth as a scientist and helped me to develop a skillset that will serve me well in all my future endeavors. For their time, effort, and advice I would also like to thank the other members of my committee; Dr. Tony Schountz, Dr. Stephen P. Mackessy, and Dr. Aichun Dong. In addition, I would like to acknowledge my parents, Thomas R. and Judy J. Bullard, for instilling in me the desire to learn and for supporting my dream of obtaining an advanced degree. The completion of this project would not have been possible without their steadfast encouragement. Finally, I would like to thank my future husband, Paul G. Feibelman, whose love and support made me realize what I can achieve.

TABLE OF CONTENTS

AIMS.....	1
CHAPTER	
I. REVIEW OF LITERATURE.....	3
Introduction.....	3
The History of Malaria.....	5
The <i>P. falciparum</i> Life Cycle.....	8
Morphological Characteristics.....	11
Pathogenesis of <i>P. falciparum</i> Malaria.....	15
History of Antimalarial Chemotherapy.....	16
Resistance Mechanisms.....	20
Protein Kinases.....	23
The Malaria Kinome.....	25
<i>P. falciparum</i> Protein Kinase 7 (PfPK7).....	29
Malaria Cell Cycle Regulation.....	32
II. MATERIALS AND METHODS.....	45
Compound Libraries.....	45
Small Molecule Preparation.....	45
Protein Preparation.....	46
ATP Luminescence Assay.....	46
Computational Docking of Small Molecules.....	48
Maestro and Macromodel.....	48
Docking and Scoring of Small Molecules.....	49
Computational Investigation of Druglikeness.....	49
QikProp.....	49
TOPKAT.....	50
Maintaining <i>P. falciparum</i> Cultures.....	51
SYBR Green I Growth Assay.....	52
Culturing Parasites with Purvalanol B.....	53
Protein Extraction.....	54
Mass Spectrometry Analysis.....	54
Protein Data Analysis.....	55
<i>P. falciparum</i> Quantitative Analysis.....	56

III.	SCREEN OF KNOWN KINASE INHIBITORS AGAINST PFPK7.	57
	Introduction.....	57
	Results.....	63
	ATP Luminescence Assay.....	63
	Docking of Small Molecules.....	64
	Biologically Relevant Property Prediction.....	68
	Discussion.....	81
IV.	SCREEN OF KINASE INHIBITORS AGAINST P. FALCIPARUM.	92
	Introduction.....	92
	Results.....	95
	Discussion.....	99
V.	TREATMENT OF P. FALCIPARUM WITH PURVALANOL B.....	103
	Introduction.....	103
	Results.....	105
	Discussion.....	124
VI.	CONCLUSION AND FUTURE DIRECTIONS.....	128
	REFERENCES.....	132
	APPENDIX A - PROTEINS IDENTIFIED IN PLASMODIUM FALCIPARUM MASCOT SEARCH.....	155
	APPENDIX B - PROTEINS IDENTIFIED IN HUMAN MASCOT SEARCH.....	177

LIST OF TABLES

TABLES

1	The Malaria Kinome.....	27
2	IC ₅₀ Luminescence Values for PfPK7 Small Molecule Inhibitors.....	65
3	Top Interactions Between PfPK7 Binding Site and Small Molecules.....	77
4	Structural and Physicochemical Properties of PfPK7 Inhibitors.....	78
5	Toxicity Predictions.....	82
6	Structure of Hits from Kinase Library Screen Against <i>P. falciparum</i>	96
7	IC ₅₀ concentrations for PfPK7 Inhibitors in SYBR Green I Assay.....	100
8	Proteins Only in <i>P. falciparum</i> Control Sample.....	108
9	Proteins Only in <i>P. falciparum</i> Treatment Samples.....	111
10	Differentially Regulated Proteins Between Purvalanol B-treated and Control Samples.....	123

LIST OF FIGURES

FIGURES

1	Global Distribution of Malaria.....	4
2	Life Cycle Stages of <i>P. falciparum</i>	10
3	Intraerythrocytic Life Cycle Stages of <i>P. falciparum</i>	13
4	AMP Docked to the PfPK7 ATP-Binding Site.....	67
5		
	a. 324840 in the ATP-Binding Site of PfPK7	69
	b. 428205 in the ATP-Binding Site of PfPK7.....	70
	c. 420298 in the ATP-Binding Site of PfPK7.....	71
	d. 569397 in the ATP-Binding Site of PfPK7.....	72
	e. 217714 in the ATP-Binding Site of PfPK7.....	73
	f. 218710 in the ATP-Binding Site of PfPK7.....	74
	g. 528116 in the ATP-Binding Site of PfPK7.....	75
	h. 551590 in the ATP-Binding Site of PfPK7.....	76
6	Control and Purvalanol B-treated Parasites Before and After Inhibitor Application.....	106
7	Number of Proteins in Control and Purvalanol B-treated Samples.....	107
8		
	a. Gene Ontology Cellular Compartment Subdomain Terms for <i>P. falciparum</i> Protein Search.....	116
	b. Gene Ontology Molecular Function Subdomain Terms for <i>P. falciparum</i> Protein Search.....	117
	c. Gene Ontology Biological Process Subdomain Term for <i>P. falciparum</i> Protein Search.....	118

a. Cellular Component GO Terms for <i>P. falciparum</i> Search Proteins.....	119
b. Molecular Function GO Terms for <i>P. falciparum</i> Search Proteins.....	120
c. Biological Process GO Terms for <i>P. falciparum</i> Search Protein.....	121

AIMS

Malaria is a devastating disease that is caused by protozoan parasites from the genus *Plasmodium*. One species of *Plasmodium*, *P. falciparum*, is increasingly resistant to traditional antimalarial treatments. The increase in resistance is causing a drastic surge in morbidity and mortality as well as amplifying an economic hardship for those global populations that can least afford the additional burden. Development of resistant *P. falciparum* strains calls for identification of new drug candidates for antimalarial drug design and identification of drug targets within the parasite that are unique and indispensable for normal parasite growth. Kinases from *P. falciparum* make excellent targets for drug discovery because of vast phylogenetic and mechanistic differences between parasite and human kinases. As such, inhibition of *Plasmodium* kinases may be a useful tool for pursuing compounds with potential antimalarial activity and for providing a means to investigate biological roles of these unique proteins within this parasitic organism. Firstly, this body of work describes the inhibition of a unique kinase from *P. falciparum*, PfPK7, which has been shown to be involved in the intraerythrocytic stages of parasite development within the human host. Secondly, the extent to which small molecules from three kinase-inhibitor focused libraries were able to inhibit intraerythrocytic growth of *P. falciparum* strain W2 blood stage cultures was assessed. In addition, application of the well-characterized cyclin-dependent kinase inhibitor Purvalanol B to blood stage

cultures of *P. falciparum* strain W2 allowed for the determination of protein content differences between inhibitor-treated and wildtype cultures.

Aim 1: To screen 244 known kinase inhibitors against PfPK7.

Hypothesis: Screening a kinase inhibitor-focused library against PfPK7 will identify several small molecules capable of inhibiting kinase activity at low molar concentrations.

Subaim 1: To screen 244 known kinase inhibitors using an ATP luminescence assay. An ATP luminescence assay was used to screen small molecule kinase inhibitors against PfPK7 by quantifying the protein's ability to utilize ATP as it autophosphorylates in the presence of each small molecule.

Subaim 2: To computationally determine likely associations between small molecules identified in aim 1 and the ATP-binding site of PfPK7. All 244 kinase inhibitors were docked to the ATP-binding site of the PfPK7 crystal structure using GOLD and hits from aim 1 were analyzed to determine which residues within the binding site were interacting with each small molecule.

Subaim 3: To computationally investigate the probable biologically relevant properties of PfPK7 inhibitors. Computer programs TOPKAT and QikProp were used to estimate biological properties such as toxicity, bioavailability, and absorption.

Aim 2: To screen 244 kinase inhibitors against blood stage cultures of *P. falciparum* strain W2.

Hypothesis: Small molecules from kinase inhibitor-focused libraries will inhibit parasitic growth of *P. falciparum* strain W2 in blood stage cultures. A SYBR Green I parasitic growth assay was used to evaluate the ability of small molecules in the kinase libraries to inhibit growth of intraerythrocytic stages of *P. falciparum* strain W2 in blood stage cultures.

Aim 3: To determine whether differences in protein expression occur between wildtype and Purvalanol B-treated blood stage cultures of *P. falciparum* strain W2.

Hypothesis: Administration of Purvalanol B to blood stage cultures of *P. falciparum* will result in protein expression differences between wildtype and inhibitor-treated cultures. The cyclin-dependent kinase selective inhibitor Purvalanol B was applied to tightly synchronized blood stage cultures of *P. falciparum* strain W2 at approximately 20 hours post invasion. Parasites were extracted from cultures at 32 hours post invasion. Protein was extracted from Purvalanol-B treated and control cultures. Soluble fractions from wildtype and Purvalanol B-treated cultures were analyzed with shotgun proteomics.

CHAPTER I

REVIEW OF LITERATURE

Introduction

Malaria is one of the most tragic causes of morbidity and mortality in the developing world. According to the Malaria World Report 2012, a report of malaria-related statistics compiled from data drawn from 104 countries where malaria is endemic, there were an estimated 154-289 million cases of malaria and approximately 700,000 malaria-related deaths in 2012 [1]. Malaria is the primary cause of child death in tropical areas and it predominantly impacts children under 5 years of age in Sub-Saharan Africa [2]. Young children, pregnant women, migrant workers, and travelers are generally the most vulnerable to transmission as these groups have little protective immunity [3]. Tropical and subtropical areas with temperate climates and sufficient precipitation allow for the development of the mosquito vector and thus have the greatest rates of malaria infection [4](Figure 1). Many of these areas are found in the developing world where people are plagued by socio-economic instability and other endemic diseases such as tuberculosis and HIV/AIDS [5]. One of the causes of this societal burden, the malaria parasite *Plasmodium (P.)*

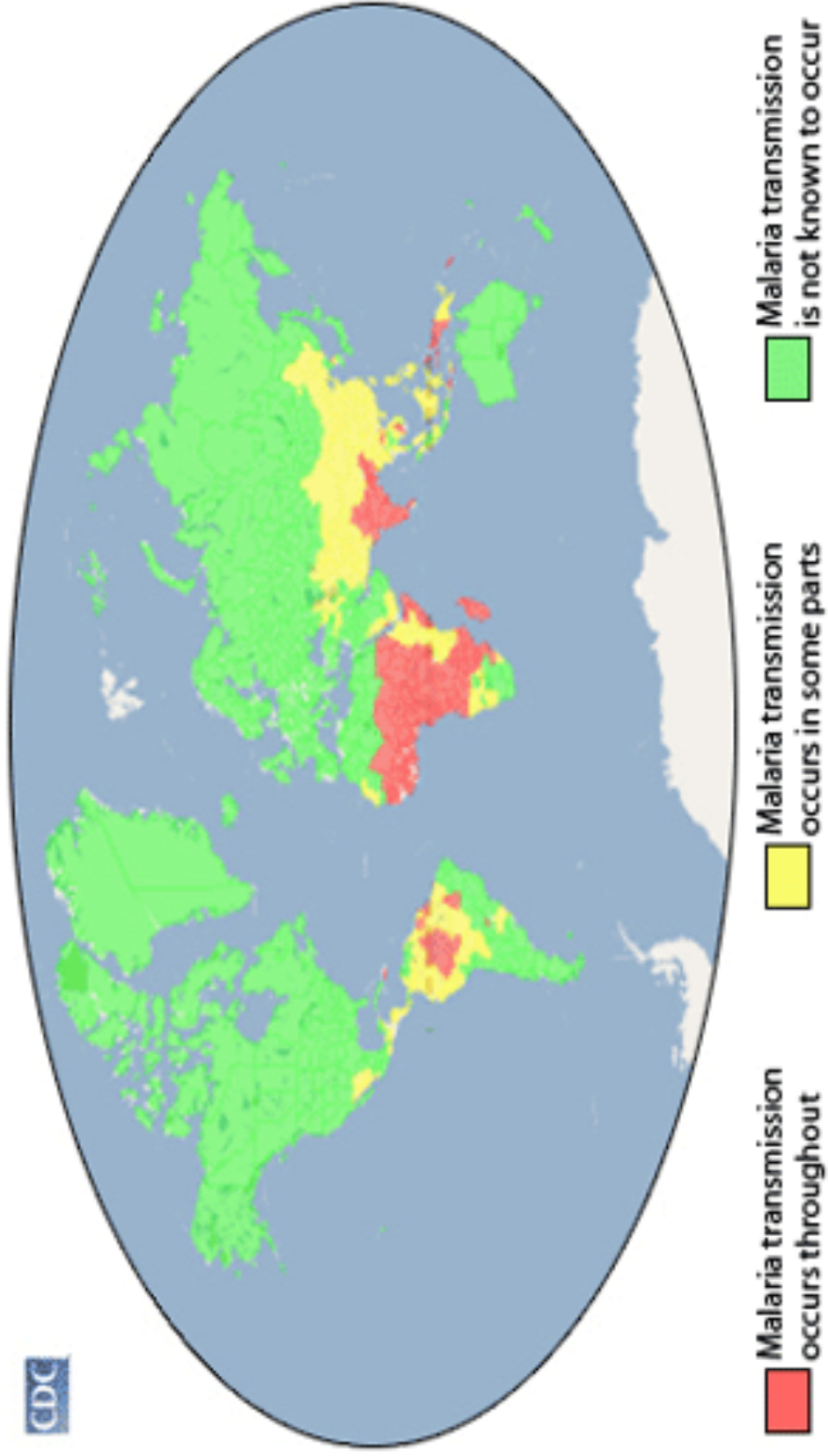


Figure 1: Global Distribution of Malaria Transmission. This map depicts areas in which malaria transmission occurs throughout the region (red), areas in which malaria transmission occurs in some parts (yellow), and those areas in which malaria transmission is not known to occur (CDC, 2010).

falciparum, is becoming increasingly resistant to known antimalarial treatments and as such there is an immediate need to identify novel antimalarial agents as well as potential drug targets that would make clear the poorly understood molecular mechanisms that govern parasite proliferation [6].

The History of Malaria

Malaria has been present and shaping human history for centuries. As long ago as 2700 BCE, the Chinese Canon of Medicine Nei Ching, described a disease that progressed with symptoms that lead to cycles of reoccurring fevers and ultimately an enlarged spleen [7]. In Egypt, Hippocrates was the first to note the relationship between transmission of the fever disease and the proximity of affected populations to bodies of stagnant water [8]. This observation was further solidified by the Romans, who came to the same conclusion and began attempting to drain swampy areas in order to prevent disease occurrence [9].

As malaria was associated with swampy areas and microorganisms were as yet undiscovered, the name for the disease came from what was assumed to be its cause: in 18th century Italian, mala was the word for “bad” and aria was the word for “air”. At the time, people believed that the symptoms of malaria infection were caused by the putrid air emanating from the stagnant waters in these swampy areas [9] and although the parasitic origin of malaria was discovered in 1880, the disease name has remained the same.

It was the French physician and student of Louis Pasteur, Charles Louis Alphonse Laveran, who first identified the cause of malaria in Algeria in 1880 [10]. Laveran observed trophozoites and gametocytes in slides made from blood

specimens of patients with malaria. He called the parasite *Oscillaria malariae*. Although his findings were largely discounted by members of the scientific community because of pressure from well-known bacteriologists who thought the cause of malaria must be bacterial, he was vindicated in 1886 with the independent observations of Louis Pasteur, William Osler, and Camillo Golgi who also observed parasites in blood smears of infected individuals [11]. In addition, Camillo Golgi was further able to distinguish between malaria parasites that cause tertian and quartan malaria, noting that parasite load contributed to the severity of malaria symptoms and that the rupture of red blood cells coincided with fever onset [12].

It was clear that the cause of malaria was an infection with a parasitic organism; however, how this organism was transmitted was still ambiguous. Patrick Manson, a British Medical Officer with an expertise in tropical medicine was the first to note microfilariae in the blood and filarial worms in the lymphatic vessels of patients suffering from elephantiasis. He was also the first to note that the microfilariae could be picked up from infected humans by mosquitos that could then transmit the disease to other humans [13]. After extensive correspondence and guidance from Dr. Patrick Manson, British army surgeon Ronald Ross felt compelled to test Manson's theory that malaria was carried and transmitted by mosquitoes much in the same way as filariae [14, 15]. Although discouraged from several unsuccessful attempts to pinpoint the malaria vector species, on August 20th 1897, he toiled at his microscope [16]. It was on this day that his labors were rewarded and when dissecting three mosquitoes from an

Indian Anopheline species he found within the midguts of these specimens a key element to malaria transmission, *Plasmodium* oocysts. Ross, a dedicated if not widely successful poet, wrote the following about his discovery:

This day relenting God
Hath placed within my hand
A wondrous thing; and God
Be praised. At his command,
Seeking His secret deeds
With tears and toiling breath,
I find thy cunning seeds,
O million-murdering Death.
I know this little thing
A myriad men will save.
O Death, where is thy sting?
Thy victory, O Grave?

Ronald Ross [17]

Anopheline mosquitos were further solidified as the malaria vector in 1898 when Giovanni Battista Grassi recruited a human volunteer and successfully transmitted malaria to a human host using mosquitos infected with *P. vivax* [18]. The next year the entire life cycle of *P. falciparum* within blood cells was observed by three researchers including Grassi [18]. Soon after the complete intraerythrocytic life cycle was observed, a heated feud ensued between Grassi and Ross when Grassi failed to recognize Ross's contributions to the malaria transmission puzzle and instead published his findings without crediting Ross for his earlier discovery [19]. However, the disagreement between the two scientists was resolved when Ross was awarded the Nobel Prize in Physiology or Medicine in 1902 [20].

Researchers then began investigating the reason why some patients with malaria infection could not be cured when treated with quinine administered less

than six days into infection. There seemed to be a brief time during the prepatent period when parasites were resistant to antimalarial drugs. The mystery of this period was solved in 1948 when Shortt and Garnham used rhesus monkeys infected with *P. cynomolgi* and later human volunteers infected with *P. vivax* to elucidate the exoerythrocytic cycle of parasite development in liver cells [21]. It was now clear that the malaria life cycle was much more complex than originally thought and this understanding allowed researchers a better grasp of parasite growth requirements.

Much had been learned about malaria using animal models and human volunteers; however, it wasn't until 1976 when William Trager and James Jensen developed a technique for culturing the intraerythrocytic life cycle stages of the parasite in blood stage cultures that malaria research became accessible to many labs across the globe [22].

The *P. falciparum* Life Cycle

There are five species in the genus *Plasmodium* that cause human pathology: *P. ovale*, *P. malariae*, *P. vivax*, *P. knowlesi*, and *P. falciparum*. Malaria caused by *P. falciparum* parasites is the most lethal [23] and as the intraerythrocytic life cycle stages of *P. falciparum* are responsible for the pathology observed in human illness, many studies are aimed at elucidating the mechanisms involved in the development of *falciparum* malaria during these stages.

The *P. falciparum* life cycle requires two vectors for completion. The sexual stages of the life cycle take place in mosquitoes from the genus

Anopheles, while the asexual exoerythrocytic (EE) and intraerythrocytic (IE) life cycle stages take place within the human host. The life cycle begins when a female *Anopheles* mosquito takes a blood meal and injects infectious sporozoites from its saliva into a vertebrate host (Figure 2). After inoculation, sporozoites travel to the liver where they infect certain hepatocytes. Inside these hepatocytes, parasites undergo exoerythrocytic schizogony, a type of multi-nuclear division that releases several thousand merozoites capable of infecting erythrocytes into the bloodstream. Upon contact with a susceptible red blood cell (RBC), the merozoite will secrete digestive enzymes from its apical surface in order to invade and take over the RBC. Once inside the cell, the parasite undergoes intraerythrocytic schizogony, the product of which is 8-24 new merozoites that are capable of infecting additional RBCs. The EE life cycle requires five and a half to six days for completion, while the IE life cycle is completed in 36 to 48 hours.

A small fraction of infected RBCs mature into micro and macro gametocytes, which travel to the peripheral blood to be taken up by a mosquito during a blood meal [24]. Sexual stage replication takes place within the mosquito midgut and the cycle is completed when sporozoites travel to the mosquito salivary glands where they mature and prepare to be inoculated into a new vertebrate host.

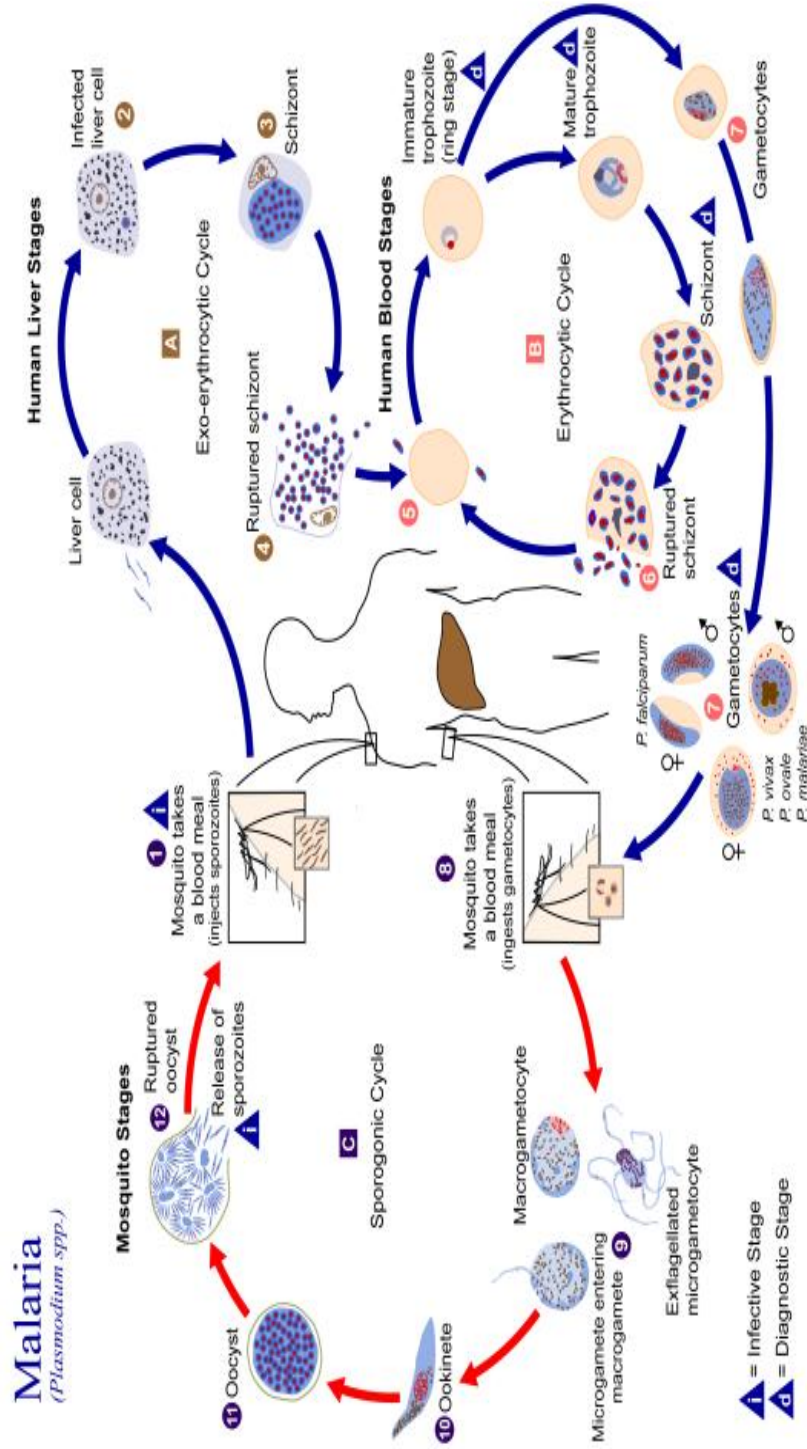


Figure 2: Life Cycle Stages of *P. falciparum*. The exo-erythrocytic life cycle stages (A) as well as the erythrocytic life cycle stages (B) take place within the human host, while the sexual stages of development (C) and sporogony take place within the mosquito vector. The cycle begins when a female mosquito takes a blood meal (1). Sporozoites travel to liver cells where they undergo exo-erythrocytic schizogony (2-4). Infectious merozoites infect RBCs where they undergo intraerythrocytic schizogony (5 & 6). Some parasites will become gametocytes (7) that are taken up by the mosquito vector (8). Gametocytes fuse to form a zygote, which eventually develops into new sporozoites during the process of sporogony (9-12)(CDC, 2010).

Morphological Characteristics of *P. falciparum*

Sporozoites, the parasite form that is transmitted to human hosts from the mosquito's saliva, are approximately 10 μm to 15 μm in length with a diameter of approximately 1 μm . The outermost structure of the sporozoite is referred to as a pellicle and is composed of one outer membrane and two inner membranes [25-27]. Just beneath the double membrane of the pellicle an organization of subpellicular microtubules resides, which functions to maintain the shape of the sporozoites and support the movement of the organisms from circulating blood to the liver parenchyma [28]. Also present in the apical portion are three polar rings and a nonfunctional cytostome. The nucleus is housed in the mid-portion of the parasite, while a mitochondrion and a spherical body occupy the posterior portion. The parasite also possess two long structures called rhoptries that extend from the apical end to the mid-portion, while the bulk of remaining anterior cytoplasm contains several electron dense micronemes [29].

Approximately 24 hours after sporozoite injection, the parasites penetrate liver parenchyma when a domain of circumsporozoite protein, a protein that covers the outside of sporozoites, attaches to a complementary surface on a receptor of the liver cell basolateral membrane [30]. Rhoptries then facilitate invasion by excreting substances that solidify parasite attachment to the RBC and make the cellular membrane of the host cell easier to disrupt [31]. Exoerythrocytic forms in liver cells become early trophozoites and apical organelles such as rhoptries and micronemes disappear as the parasite begins to take in host cell cytoplasm for digestion. Once the cell has grown in size, the

parasite undergoes schizogony and merozoites that are released from liver cells regain many of their earlier apical organelles.

The apical complex including rhoptries, micronemes, and polar bodies redevelop in order to help the invading parasite to latch onto the RBC [32]. The apical complex allows invasion by orienting the apical end of the parasite towards the RBC and secreting a series of proteins that form a “moving junction.” The moving junction effectively invaginates the host cell membrane and ushers the parasite inside the host cell while forming the protective parasitophorous vacuolar membrane between the parasite and host cell cytoplasm [33-38].

Once ensconced within the RBC, the malaria parasite again begins development as a trophozoite. The early trophozoite occupies approximately $\frac{1}{4}$ the diameter of the RBC and has the appearance of a signet ring (Figure 3, stages 1-15) with either one or two chromatin dots [39]. The ring shape is a result of the ingestion of host cell cytoplasm through the parasite’s primary cytostome. The cytoplasm is kept in a large central food vacuole that pushes the nucleus of the parasite to the periphery. As the parasite feeds on hemoglobin from the food vacuole, the food vacuole shrinks and the waste product hemozoin can be seen [40]. Hemozoin is a polymer of heme molecules and is the result of hemoglobin digestion by the parasite [41, 42]. The early trophozoite stage, sometimes referred to as the “ring stage”, is the only stage of development that is commonly observed in circulating blood with the exception of the gametocyte forms [43]. Mid and late trophozoite forms (Figure 3, stages 16-20) are darkly pigmented when stained with Giemsa as much of the RBC is taken up by newly

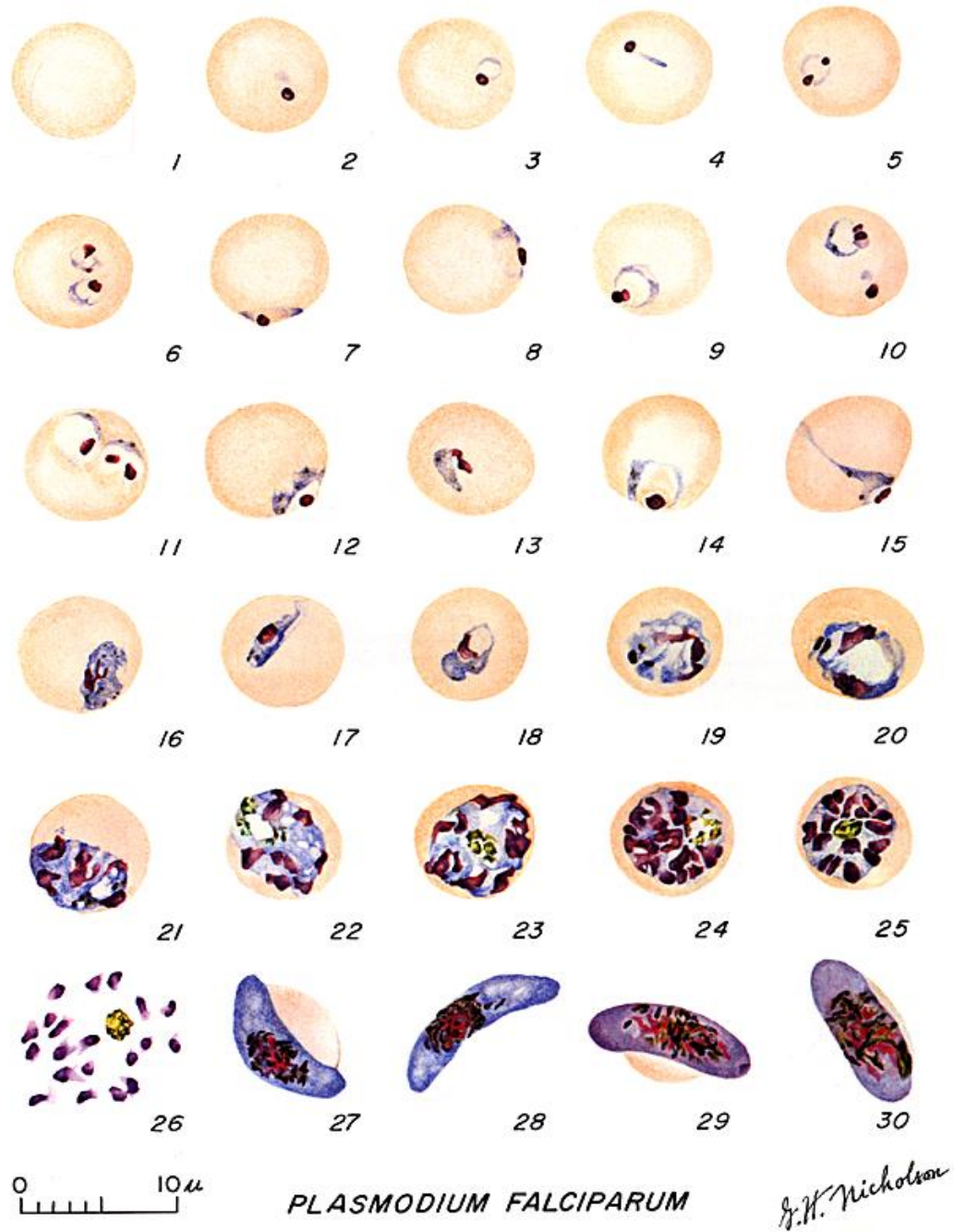


Figure 3: Intraerythrocytic life cycle stages of *P. falciparum*. Early trophozoite (1-15), mid to late trophozoite (16-20), schizont (21-25), merozoite (26), and gametocyte (27-30) stages of *P. falciparum* as would be seen in a Giemsa-stained blood smear (The National Library of Medicine, 1971).

replicated nuclear material, which the parasite has produced in preparation for intraerythrocytic schizogony [39]. Late trophozoites then transition into the schizont stage (Figure 3, stages 21-25). The 8-24 newly synthesized nuclei are surrounded packets of cytoplasm during the segmenter phase of schizogony. When the schizont bursts, metabolic wastes and residual material are released into the bloodstream along with new merozoites [44]

The exact mechanism involved in determining whether a parasite will engage in the intraerythrocytic cycle or whether it will instead develop into a gametocyte (Figure 3, stages 27-30) remains unclear [45-47]. However, it has been shown that some schizonts produce merozoites that invade RBCs and commit to the 10-12 day development period during which a single microgametocyte or macrogametocyte is formed [48-51]. Fewer microgametocytes are formed than macrogametocytes and these life cycle stages tend to be crescent shaped with a total length one and one half times greater than that of the RBC [52]. In addition, microgametocytes are darkly pigmented upon staining, have a large concentrations of hemozoin in their center, and contain evenly diffused chromatin. In contrast, the chromatin of macrogametocytes is more concentrated giving the macrogametocyte a darker color when compared to microgametocytes.

The developmental stages of *P. falciparum* that take place within the mosquito also have distinct morphological characteristics; however, they are not described here (see [53] for a review) as this body of work elucidates aspects of parasite biology during *P. falciparum* development within the human host .

Pathogenesis of *P. falciparum* Malaria

Pathology associated with malaria infections is caused by the inflammatory response of the host and by the depletion of red blood cells, which causes anemia [54, 55]. Severity of infection is largely determined by the species of *Plasmodium* with which the host is infected. *P. vivax* and *P. ovale* cause less complicated forms of malaria, but are able to lie dormant during exoerythrocytic stages of parasite development and are thus able to avoid the host immune response [56]. *P. falciparum* infections cause the most severe pathology [57]. Common symptoms during the initial stages of malaria are flu-like and involve all or some of the following: loss of appetite, muscle pain, fatigue, headache, and slight fever [58]. The first paroxysm, which is a cycle of chills and fever, occurs anywhere from 6 to 14 days post inoculation and lasts anywhere from 20-36 hours in *P. falciparum* infections as these parasites tend to be less synchronous than other malaria parasites in vivo [59-61]. Inhibition of cellular pathways involved in parasite development within human RBCs has the potential to reduce the clinical consequences of malaria infections as replication during this time results in human pathology. However, little is known about the regulation of molecular pathways that contribute to parasite proliferation during intraerythrocytic growth. By targeting and inhibiting proteins that are active during these stages it may be possible to elucidate parasite replication mechanisms and to identify potential antimalarial drug targets, which would later make the identification lead compounds for antimalarial drug design.

History of Antimalarial Chemotherapy

One of the first chemical compounds used to treat malaria was the drug quinine, which is a component of cinchona tree bark [62]. The origin of quinine in Europe as a treatment for malaria is still a mystery. One explanation suggests that in 1629 the Spanish Countess of Chincona, who was traveling with her husband, arrived in Lima, Peru and shortly thereafter became ill with fever [63, 64]. In an account from Sebastiao Bado, the Countess drank a concoction made from the bark of a local tree and was cured of her fever ailment [65]. The Countess then traveled back to Europe with her husband and introduced the bark as a treatment for malarial ailments. However, in 1930 a biography of the Count of Chinchon authored by his secretary, Don Antonio Suardo, was discovered that contradicts this series of events. Unaware of the future discovery of the diary, Carolus Linnaeus, the Swedish botanist, named the tree from which quinine is derived for the Spanish Countess [66]. Unfortunately, he misspelled the title name, Chinchon, and now the tree is referred to as the cinchona tree. Regardless of how the compound was identified, the widespread adoption of quinine as an antimalarial occurred and it can be said for certain that it was and remains a crucial compound for the treatment of malaria [67]. Indeed, until the 1940s, it was the only widespread compound used as an antimalarial [68].

The drug chloroquine, discovered by Hans Andersag in 1934, was largely ignored as a potential antimalarial because it was thought to be too toxic to administer to humans [69]. However, after US government-sponsored clinical trials, chloroquine was found to be useful as an antimalarial and in 1947 it was

introduced for prophylactic use [69]. The antimalarial effects of chloroquine are due to the ability of the drug to prevent the crystallization of heme molecules, which are a product of host cell hemoglobin digestion [70]. Loose heme molecules are toxic to the parasite, therefore, these molecules are biocrystallized into a substance called hemozoin that is much more readily tolerated by the organism [71]. Upon entering the parasite cell, chloroquine molecules quickly become protonated and are unable to leave the parasite cell by diffusion [72]. The protonated chloroquine molecules cap heme molecules, making them unable to biocrystallize heme. Modified heme molecules accumulate within the parasite, become toxic because they prevent normal function of the parasite membrane, and eventually cause lysis of the parasite cell.

While chloroquine has been shown to interfere in the metabolism of hemoglobin by the parasite, other successful antimalarials target different essential pathways in parasite development. Success treating bacterial infections with antifolates had shown researchers that these drugs were able to inhibit necessary routes of DNA synthesis within several species of bacteria [73, 74]. Researchers then began to determine whether antifolate compounds would result in similar pathway disruptions in malaria parasites. These efforts were successful and sulpha drugs and folic acid antagonists such as sulphadoxine, pyrimethamine, and proguanil were shown to inhibit parasite replication by preventing synthesis of folic and folinic acid [75, 76]. The prevention of folic and folinic acid synthesis prohibits the formation of nucleotides for DNA synthesis, which is necessary for the parasite to complete schizogony. Adoption of an

antibacterial treatment strategies for the treatment of parasitic disorders such as malaria represented a paradigm shift for researchers of tropical medicine: it may not be necessary to search through the proverbial haystack to discover antiparasitic compounds when one can harness the information gathered from previously successful drug discovery efforts.

While new strategies for antimalarial drug discovery were slowly emerging, so was parasite resistance to widely used and effective antimalarial drugs. Resistance of parasites to chloroquine was first observed in Colombia in 1956 [77]. Soon after, reports of resistance began to emerge in multiple regions from the Colombian-Venezuelan border to Kenya and Tanzania. The Vietnam war was being waged and as many as 1% of U.S. troops were succumbing to malaria infection per day [78]. In the wake of this devastation, the U.S. launched what was, at the time, the largest drug discovery effort ever undertaken. From this effort, which involved a screen of over 250,000 compounds, the drugs mefloquine and halofantrine emerged and were marketed by F. Hoffmann-La Roche and Smith Kline Beecham as Lariam and Halfan respectively [78]. While the exact mechanism of action for the aforementioned antimalarial drugs has not fully been uncovered, they are similar in structure to chloroquine and thought to act in much the same way. Since the introduction of mefloquine, adverse side effects and unfavorable drug interactions have emerged that render this drug less effective or dangerous for many individuals [79].

While the US was desperately trying to bolster its Vietnam War efforts with a massive drug discovery initiative, China was undergoing a movement that

in the west was known as the Chinese Cultural Revolution. During this time, Tu Youyou, a Chinese pharmacologist and her team of investigators were also working to identify a cure for malaria [80]. The Vietnam War and the resulting malaria infections that ensued were also wreaking havoc on the soldiers of China's ally, North Korea. In order to alleviate North Korea's malaria problem, the Chinese government set up a large drug discovery project called 523 with the express goal of pinpointing an effective cure for malaria that would allow North Korean soldiers to have the upper hand in a jungle war [81]. After screening thousands of synthetic compounds against the parasite without success, Chinese scientists resorted to reading ancient medical texts with the hope of harnessing traditional Chinese herbal remedies for a cure. It was at this time that Tu Youyou uncovered the writings of Ge Hong in a text, *Emergency Prescriptions Kept Up One's Sleeve*, written 1600 years before [80]. In this book, Ge Hong described the preparation of a tea from *Artemisia annua*, the sweet wormwood plant that was used as a treatment for intermittent fevers. Although artemisinin was tested previously with little efficacy against the parasite, the preparation method suggested in the ancient text led researchers to believe that it was necessary to prepare an artemisinin formula that would assure the compound retained activity. When Chinese researchers tested the formula, it was 100% effective at treating mice and monkeys infected with drug-resistant *Plasmodium* [81]. In 2011, Tu Youyou was awarded the Lasker~DeBakey Clinical Medical Research Award for the discovery of artemisinin. The discovery of artemisinin represents the last historically significant finding of a truly effective antimalarial compound. While

this compound has remained efficacious in treating the most deadly cases of malaria, the emergence of artemisinin-resistant parasite strains has now been observed in four nations [1].

Resistance Mechanisms

Perhaps the most alarming problem concerning malaria is the growing resistance of malaria parasites to almost all known traditional antimalarial treatments. Parasite resistance to first line drug treatments, such as chloroquine, is encountered almost everywhere malaria is endemic (www.cdc.gov/Malaria/drug_resistance). The replication rate of *Plasmodium* species allows the parasite to readily adapt to changes in its environment including the toxic drug effects of many antimalarials. Resistance quite often occurs as a result of changes in drug targets where a single point mutation in a gene in the parasitic DNA leads to an amino acid change in the protein encoded by that gene [82]. This amino acid difference decreases the affinity of the inhibitor for its target and renders the inhibitor ineffective or at least less effective. Point mutations in dihydrofolate reductase (DHFR) and dihydropteroate synthase (DHPS) are responsible for the resistance of parasites to the anti-folate drugs pyrimethamine and sulphadoxine respectively. Survival strategies are based in part on developing large numbers of daughter progeny, drug treatment eventually selects for those parasites that carry mutations for parasite survival. Malaria strains eventually evolve drug resistance, especially when drugs are administered as monotherapies or lower than therapeutic doses, and as a result are much less susceptible to treatment with commonly used antimalarials [83].

The quick and efficient replication strategy of the parasite the allows for the reestablishment of infection with the now more virulent form of *Plasmodium*.

Other parasitic resistance strategies result from the upregulation of proteins involved with shuttling substances such as antimalarial drugs out of cellular compartments or upregulation of proteins that metabolize toxic substances into less bioactive forms [84]. The upregulation of these proteins decreases the amount of drug that is available to bind the drug target and renders previously effective doses of drug ineffective. Chloroquine resistance has been an observed phenomenon since the 1960s, which was only 10 years after its introduction [85, 86]. This type of resistance mechanism has been attributed to the reduction of chloroquine concentration in the food vacuole, which is the parasitic structure affected by this drug [87]. The reduction in chloroquine concentration resulted from a mutation in the gene coding for a molecular transporter, *pfcr1* [88]. However, the exact mechanism leading to this resistance is still unknown [89]. The significant resistance of *Plasmodium* parasites to the drug mefloquine, which is in the same drug family as chloroquine and works by much the same mechanism, occurred in only six years and has been attributed to the upregulation of multidrug resistance proteins *pfmdr1* and *pfcr1*, which transport toxic substances out of the parasitophorous vacuolar membrane [90].

Artemisinin and artemisinin derivatives, which are effective against resistant strains of malaria parasites and are able to clear parasites from the body quickly, are the latest drugs for which parasites are developing resistance [1]. Researchers along the Thai-Cambodian border have warned that artemisinin

resistance is not only evolving in parasites, but also that the emergence of resistance must be contained in the very near future in order to prevent the spread of resistant parasites strains to neighboring regions; a migration which could have devastating effects [91-94]. Administering a single drug with a single molecular target as a treatment for malaria increases the risk of resistance development because it is likely to exert a selective pressure that would result in mutation of that target. As such, the World Health Organization has suggested that artemisinin combination therapy (ACT) be administered as first line drug treatment for all cases of uncomplicated *falciparum* malaria in order to reduce the likelihood of resistance development (WHO guidelines for the treatment of malaria, 2006). A recent study suggested that parasite resistance to dihydroartemisinin (DHA) was associated with an increase in both *pfmdr1*, a multidrug resistance transporter, copy number and antioxidant activity within DHA-challenged *P. falciparum* parasite clones [95]. If strains of malaria parasites develop that are increasingly resistant to ACT, a massive global public health problem will arise and for the first time in 50 years, there will be no effective treatment for the most virulent forms of malaria.

Clearly there is a need to develop novel and efficacious drug treatments for the treatment of multidrug-resistant malaria strains. When researchers began to understand that they could utilize drug development strategies that had been previously successful in the treatment of bacterial diseases and apply those strategies to treating parasitic diseases, for the first time drug discovery efforts could be directed at inhibiting specific necessary pathways within the parasite. In

recent years it has become possible to make the drug discovery process even more efficient as we are now able to target individual proteins within a disease organism or cell in order to inhibit necessary functions of that organism.

Protein Kinases

Protein kinases are biological macromolecules that regulate cellular processes by transferring a terminal phosphate group from ATP to an amino acid residue with a free hydroxyl (-OH) on a target protein. Most kinases transfer phosphate groups to either serine or threonine residues; however, there are subsets of kinases that act specifically on tyrosine or on all three types of residues. Bacterial cells, plants, and some less complex eukaryotes also contain histidine kinases, which autophosphorylate on a histidine residue and transfer a phosphate group to an aspartate residue on the target protein. The phosphorylation events that are carried out by kinases are reversible so proteins that are activated, inactivated, or otherwise modified by the addition of a phosphate group can return to their original state of activity with the removal of the phosphate group by another type of protein, a phosphatase.

Protein kinases are responsible for the regulation of cellular processes such as homeostasis, growth, and cell division [96, 97]. The deregulation of these critical proteins has been associated with disease processes such as diabetes, cancer, and several neurodegenerative disorders [98, 99]. Drug discovery aimed at the inhibition of protein kinases has afforded the development of several successful drug therapies such as imatinib, which was marketed by Novartis under the name Gleevec for the treatment of chronic myelogenous

leukemia in 2002 [100]. At the current time, more than 11 kinase inhibitors have successfully progressed through the drug discovery pipeline and been approved for clinical use by the United States Food and Drug Administration (FDA). In addition, 150 clinical trials for future kinase-targeted therapies are ongoing [101]. Of the inhibitors approved for clinical use, Sunitinib (Pfizer), Pazapanib (GlaxoSmithKline), and Sirafenib (Onyx and Bayer Pharmaceuticals) target VEGFR isoforms and Erlotinib (Roche), Gefitinib (AstraZeneca), and Lapatinib (GlaxoSmithKline) selectively target EGFR. KIT, PDGFR, and ABL1-2 are the molecular targets of Dasatinib (Bristol Myers), Nilotinib (Novartis), and Imatinib. Dasatinib targets SRC as well. Interestingly, all the aforementioned drugs act at least in part by competing for the ATP-binding site of their respective kinase targets (reviewed in [102]). These drug discovery successes lend credence to the fact that despite the general evolutionary conservation of the kinase ATP-binding site, the selective targeting kinases with ATP competitive inhibitors is not only feasible but is also an effective drug design strategy. The large quantity of research in the area of kinase inhibition, especially in oncology research, has yielded kinase inhibitors, such as cyclin-dependent kinase inhibitors, that are selective for particular kinases and can be utilized as scaffolds for future drug screening efforts. Recent achievement in the area of kinase inhibition for disease treatment along with the need to identify new and effective antimalarial drugs point to kinase inhibition as a potential tool for antimalarial drug discovery.

The Malaria Kinome

There are between 86-99 protein kinases in the *P. falciparum* genome depending on the algorithm used for classification [103, 104]. In order to preserve the ability to complete phosphate transfer, the catalytic domain of kinases has remained relatively well conserved across genomes in comparison to other non-catalytic domains within these proteins, which have been at liberty to diverge evolutionarily [105]. That kinase domains have such a great degree of conservation has raised questions as to whether it is possible to identify inhibitors that are selective for *Plasmodium* kinases. Indeed, it is imperative during the drug discovery process to evaluate the likelihood that molecules will affect host kinases and thus likely have deleterious side effects. Differences in structure and function between parasite and host kinases would increase the likelihood that inhibitors targeting *P. falciparum* kinases will not interfere with host kinase function and indeed, there are several characteristics of *P. falciparum* kinases that increase the probability of identifying parasite kinase-selective inhibitors.

Many canonical motifs are highly conserved throughout all typical protein kinases [106-110] and with few variations, these motifs are present in *P. falciparum* kinases as well. Conserved motifs are generally located within the catalytic domain of the protein, while other regulatory pockets that surround the catalytic domain and insertions of low complexity tend to be much more divergent in sequence [111, 112]. By identifying small molecules that take advantage of small differences between human and malaria kinases, it is possible to selectively target parasite proteins. The publication of the *P. falciparum* genome

sequence in 2002 and the accumulation of this sequence data in the *Plasmodium* database PlasmoDB have enabled the ongoing characterization of proteins from this genus [104, 113]. Interestingly results from analysis of the *P. falciparum* kinome revealed that many kinases from this genus are chimeras of mammalian kinases and have characteristics and sequences from more than one kinase family [104, 114]. Functional analysis of selected kinases from this dataset has revealed that sequence similarity in these proteins does not necessarily indicate protein function, which underscores the unique nature and need for further functional characterization of *Plasmodium* proteins [115, 116].

Included in the kinome are kinases that cluster within traditional eukaryotic protein kinase (ePK) families and kinases that are more divergent in sequence from traditional ePKs and cannot be clustered into a family (Table 1). The latter group of kinases is termed the orphan kinase group as its members have no ePK ortholog. One such group, the FIKK family, is limited to organisms from the phylum Apicomplexa. Generally, any given Apicomplexan organism will have no more than one representative from this kinase family within its kinome [117]. Unlike other Apicomplexan organisms, *P. falciparum* contains twenty such proteins which localize to the RBC membrane and participate in conveying extracellular signals between the parasite and host [117, 118]. The unique nature of orphan kinases make these proteins promising targets for drug design and inhibitors of orphan kinases may leave host cell kinases unaffected and cause fewer deleterious side-effects when compared to other less selectively targeted drugs.

Table 1: *The Malaria Kinome*. Distribution of *P. falciparum* kinases into eukaryotic and unclassified kinase groups as well as kinase family designation, representation of each kinase family within the *P. falciparum* kinome, and a list of characterized proteins from each group [119].

<i>Classification</i>	<i>Major Kinase Group</i>	<i>Number of Proteins within Kinome</i>	<i>Characterized Proteins</i>
Eukaryotic protein kinase (ePK)	Cyclic-nucleotide and calcium/phospholipid kinase (AGC) group	5	PfPKA (Syin et al., 2001) PfPKG (Deng & Baker, 2002) PfPKB (Kumar, Vaid, Syin, & Sharma, 2004)
	Cyclin-dependent (CDK), mitogen-activated (MAPK), glycogen-synthase (GSK), and CDK-like kinase (CMGC) group	26	Pfcrk-1 (C. Doerig et al., 1995) Pfcrk-3 (Ward, et al., 2004) Pfcrk-4 (Ward, et al., 2004) Pfcrk-5 (Ward, et al., 2004) Pfmap-1 (C. M. Doerig et al., 1996; Graeser, Kury, Franklin, & Kappes, 1997; Lin, Goldman, & Syin, 1996) Pfmap-2 (Dorin et al., 1999) PfPK5 (Ross-Macdonald, Graeser, Kappes, Franklin, & Williamson, 1994) PfPK6 (Ross-Macdonald, et al., 1994) Pfmrk (Li, Robson, Chen, Targett, & Baker, 1996)
	Calmodulin-dependent kinase (CaMK) group	13	PfCDPK1 (Zhao et al., 1994) PfCDPK3 (Li, Baker, & Cox, 2000) PfCDPK4 (Billker et al., 2004) PfCDPK5 (Dvorin et al., 2010)

Table 1 Continued

<i>Classification</i>	<i>Major Kinase Group</i>	<i>Number of Proteins within Kinome</i>	<i>Characterized Proteins</i>
	Tyrosine kinase (TyrK) group	0	NA
	Casein kinase 1 (CK1) group	1	PfCK1 (Barik, Taylor, & Chakrabarti, 1997)
	Yeast sterile mutant (STE) group	0	NA
	Tyrosine kinase-like (TKL) group	4	PfTKL3 (A. Abdi, Eschenlauer, Reininger, & Doerig, 2010)
	Aurora kinase family	3	PfArk-1 (Reininger, Wilkes, Bourgade, Miranda-Saavedra, & Doerig, 2011)
	Never in mitosis/Aspergills (NIMA) group	4	Pfnek-1 (Dorin et al., 2001; Dorin-Semlat et al., 2011) Pfnek-2 (Reininger et al., 2009) Pfnek-3 (Ward, et al., 2004) Pfnek-4 (Reininger, Garcia, Tomlins, Muller, & Doerig, 2012)
Other	FIKK family	20	
	Orphan kinases	NA	PfPK7 (Dorin, et al., 2005; Dorin-Semlat, Sicard, Doerig, & Ranford-Cartwright, 2008; Koyama et al., 2012; Merckx et al., 2008) PfPK9 (Philip & Haystead, 2007)

The cyclin-dependent (CDK), mitogen-activated, glycogen synthase, and CDK-like group (CMGC) accounts for more than 25% of all malaria kinases. In other eukaryotic organisms, this group is important for cell proliferation and development and the large representation of CMGC kinases underscores the importance of cellular replication within the parasite [120].

The CamK group is also highly represented in the parasite, which may belie the importance of calcium in parasitic signaling pathways. Also of note is the marked absence of kinases that cluster within the TyrK or STE groups and the traditional three-component MAPK pathway appears to be absent as there are no MAPKKs or MAPKKKs within *P. falciparum* [104]. The absence of these kinases may indicate modes of cellular regulation within the parasite that are distinct from those of other eukaryotic organisms. Disruption of kinase function during cell replication and analysis of downstream effects after this disruption may provide clues to the abstruse mechanisms of regulation in intraerythrocytic *P. falciparum* parasites.

***P. falciparum* Protein Kinase 7 (PfPK7)**

The phylogenetic and mechanistic differences between host and *Plasmodium* kinases are particularly pronounced in orphan kinases from this species. In an effort to uncover a MAPKK homolog in the *Plasmodium* genome, researchers identified PfPK7, a kinase that displays regions of sequence similarity to more than one protein kinase family [115]. The C-terminal region displays maximal homology with MEK3/6 while the N-terminal region is more closely related in sequence to fungal protein kinase A. This protein is expressed

in both sexual stages in the mosquito vector and asexual stages in the human host. While PfPK7 was able to autophosphorylate and to phosphorylate several substrates, it was not able to phosphorylate MAPK homologs in vitro; thus making it an improbable candidate for a *Plasmodium* MAPKK [115].

Co-crystallization of PfPK7 both with an ATP analog and with a PfPK7 inhibitor revealed several interesting structural and functional aspects of this protein. PfPK7 is 343 residues in length [121]. The N-terminal lobe contains two alpha helices, while the C-terminal lobe is comprised of twisted antiparallel β -sheets. Four low complexity inserts are found in this protein and the highly conserved serine, threonine or negatively charged residue that would normally reside in the activation loop of active kinases has been replaced in this kinase by a positively charged residue. As a consequence, PfPK7 ligands have negatively charged atoms, which bind to this site. In addition, the *P. falciparum* myelin basic protein, PFRAB11B, has been pinpointed as an endogenous substrate [121]. In the same study by Merckx et al. (2008) the researchers found that the small molecule, K510, was able to compete with ATP for the ATP-binding site and inhibit this protein during thermal shift assays.

A high-throughput screen of small molecules revealed several imidazopyridazine compounds that showed an inhibitory effect on the function of PfPK7 in vitro and chemical synthesis yielded several more molecules with the same imidazopyridazine core that had varying inhibitory effects against the enzyme [122]. One research group utilized the imidazopyridazine molecules from the previous study to build 2D and 3D QSAR models in order to predict the

binding affinity of small molecules for the PfPK7 binding site. A computational docking study of the imidazopyridazine molecules was also conducted to define probable interactions between these molecules and the PfPK7 binding site [123]. Several studies have contributed information regarding the structure of PfPK7 and its ATP-binding site; however, in order to evaluate its potential as an antimalarial drug target, it is essential to determine the effect of these inhibitory compounds in blood stage cultures of the parasite.

In another study, PfPK7(-) clones were shown to have a decreased asexual growth rate during intraerythrocytic life cycle stages as fewer merozoites were produced per schizont and a decreased capability of forming oocysts in the mosquito vector during sexual stage development was also observed [124]. A decrease in schizont population with PfPK7 inactivity can be explained in part by data that suggest PfPK7 is involved in melatonin signaling in the parasite [125]. It has previously been shown that melatonin signaling regulates the malaria cell cycle by increasing intraerythrocytic schizont stage populations by a mechanism involving an increase in cytoplasmic calcium concentrations [126, 127]. Furthermore, PfPK7(-) clones were unable to enrich schizont populations in the presence of melatonin and an expected increase in cytoplasmic calcium concentration was not detected [125]. Data from these studies suggest this kinase is involved in a molecular pathway that aids in the regulation of the malaria cell cycle. The putative role of PfPK7 in parasite proliferation during the erythrocytic stages of parasite development, which are directly responsible for disease progression combined with data that suggest disruption of PfPK7 activity

contributes to decrease intraerythrocytic growth rates make this protein an attractive target for drug intervention. Small molecule inhibitors of this protein could potentially be formulated into an antimalarial therapy that would reduce parasite burden and alleviate the devastating and often fatal symptoms associated with *P. falciparum* malaria. In addition, defining optimal characteristics of a PfPK7 inhibitor, further elucidating interactions between small molecule inhibitors and the PfPK7 ATP-binding site, and determining whether PfPK7 inhibitors affect intraerythrocyte parasite growth will aid future research aimed at pinpointing a small molecule that would selectively inhibit this kinase and allow for investigation of its biological role in the parasite.

Malaria Cell Cycle Regulation

As kinase function plays such a pivotal role in the eukaryotic cell cycle and disruption of cell cycle kinases has been shown to impede cellular replication, inhibition of kinases that function during parasite replication may provide a way to halt intraerythrocytic growth of *P. falciparum* parasites [128, 129]. The value of parasite cell cycle disruption is twofold: first, it may point to new promising drug targets that are imperative for parasite survival and second, it may serve as a valuable tool for investigating poorly understood malaria cell cycle protein expression patterns.

The overall goal of the cell cycle in eukaryotic cells is not only to achieve cell division but also to ensure that genetic information is accurately passed on from one generation to the next. *P. falciparum* also seeks with its cell cycle to create sufficient daughter progeny to ensure its own survival in the harsh

environment of the vertebrate host. The parasite accomplishes this goal by producing 8-32 daughter cells during schizogony. As discussed above, the malaria parasite must also complete replicative cycles in many different environments [130]: sexual stage development takes place inside the arthropod vector while both the exoerythrocytic and intraerythrocytic life cycle stages develop within humans. In order to complete replication, the parasite must temporally express and regulate proteins that will ensure the correct sequence of cell cycle events during each of these stages [131-133]. Here we focus on modes of cell cycle regulation that occur during the intraerythrocytic stages of parasite development as these stages are the direct cause of human pathology.

Little is known about the regulation of the parasite life cycle in comparison to the vast amount of information that is available about regulation of the mammalian cell cycle. In order to set a framework for the malaria cell cycle, the following section includes information that relates what we know about malaria cell cycle regulation to what is known about the cell cycle in more complex eukaryotic organisms. Typical higher eukaryotic cell cycle characteristics and regulators as well as known characteristics and regulators of the malaria cell cycle are discussed.

In contrast to the asexual intraerythrocytic malaria cell cycle, which produces many progeny, the end products of asexual division in higher eukaryotic cells are two daughter cells that can be considered genetically identically to the parent cell. In higher eukaryotes, regulation of this cell cycle is accomplished by kinases from Aurora, Polo, and NIMA families and particularly

by CDKs which, while not catalytically active on their own, drive and regulate the cell cycle when in conjunction with a type of regulatory protein called a cyclin [134]. The action and control of different CDK/cyclin complexes within context of the cell cycle as well as other cell cycle regulators are well characterized in higher eukaryotes [135-137]. In contrast, researchers are only now beginning to understand the biological role of these critical cell cycle molecules in the malaria parasite [138] as reviewed in [139].

While the progression of the cell cycle in malaria is not clearly understood at this time, in mammalian cells the cell cycle consists of four distinct phases. These are growth phase 1 (G_1), in which the cell grows and acquires the necessary means to duplicate the genome; synthesis (S), in which the cell semiconservatively duplicates its genome one time; growth phase 2 (G_2), in which the cell continues to grow and prepare for cell division; and mitosis (M), in which the duplicated nuclear material is divided into separate packets [140]. Mitosis generally leads to cytokinesis, which is the division of the cytoplasm. Cell cycle is highly regulated in mammalian cells and the deregulation of this process can cause cell cycle arrest and finally apoptosis or cancer, which is characterized by uncontrolled cell division [141-143]. CDKs, as previously described, contribute to these control mechanisms and exert their influence by associating with cyclins and other proteins that regulate CDK function such as CDK inhibitors (CKIs) [134, 140, 144]. Additional regulatory proteins such as p53 provide checkpoints at which time the cell can decide if all the necessary requirements to continue with cell cycle progression are met [145-147].

Most eukaryotic cells exist in a non-dividing state called (G_0) and in order to divide, a cell must enter a G_1 state and begin to synthesize necessary factors for division. The progression passed G_1 is determined by the size of the cell and the presence or absence of mitogenic factors [148, 149]. The restriction point that resides between the G_1 and S phases is controlled by retinoblastoma protein (pRb) and a family of transcription factors [150, 151]. Phosphorylation of pRb by the Cdk4, 6 – cyclin D and later Cdk2-cyclin E, which governs centrosome duplication events prior to S phase permits passage through the checkpoint [152-156]. CKIs also provide regulation at this time. The cyclin dependent kinase inhibitor p21 inhibits CDK1/2 complexes and the expression of this protein is controlled by the tumor suppressor protein p53 [157]. In addition, the cell must check for the presence of damaged DNA, which would be detrimental to newly formed daughter cells. DNA damage increases the activity of kinases that activate p53, which induces cell cycle arrest with the idea that the cell will have more time to correct DNA damage [158]. Progression through this checkpoint is also largely controlled by the presence of critical growth factors, without which the cell cycle cannot continue [149].

S phase is the DNA synthesis phase of the cell cycle. During this phase, the genomic content of the cell must be duplicated accurately. During late anaphase or early G_1 , the origins of replication complexes (ORCs) are formed along the DNA [159] and DNA synthesis begins at these complexes, which must commence only one per cell cycle [160]. In order for the transition from G_1 to S to proceed in an ordered fashion, cyclins must be expressed and then degraded

in a temporally accurate manner [161]. Cdk2-cyclin E first phosphorylates pRb. Phosphorylation of pRb permits the degradation of cyclin D and allows for the accumulation of cyclin A, which then complexes with Cdk-2 and allows for the progression into S phase [162-164]. Cyclin E is quickly degraded as cyclin A is upregulated and the Cdk2-cyclin-A complex forms [165]. This complex phosphorylates substrates and activates proteins necessary for synthesis to continue. Cdc7 kinase also positively regulates synthesis of new DNA by phosphorylating Mcm proteins that are associated with DNA [166]. An intra-S checkpoint exists to check for the presence of any abnormalities in DNA synthesis including any DNA breaks and blocked replication forks [167-169].

During G₂ phase, the cell is preparing to enter mitosis. Progression from G₂ to M phase also depends on the presence of cyclins, in particular cyclin B, which is upregulated prior to mitosis [170, 171]. Cyclin B associates with Cdk1 and the Cdk1-cyclinB complex is then shuttled to the nucleus where it permits transition into mitosis. Cdk1 is highly regulated by Cdc25, Wee1, and Myt1 and the shuttling of these inhibitory and activating molecules from the nucleus to the cytoplasm. Cdk7 is a cyclin-dependent kinase activating kinase (CAK) that positively regulates the activities of other kinases including Cdk1, Cdk2, Cdk4, and Cdk6 (as reviewed in [172]) along with the accessory proteins cyclin H and MAT1 [173-176]. Soon thereafter, cyclin B is degraded as the cell proceeds with mitosis [171]. During the G₂ checkpoint, the cell assesses whether it is safe to separate sister chromatids. During this checkpoint, the presence or absence of damaged DNA is sensed [177-182]. If DNA damage exists, protein kinases

transduce a signal indicating to the cells that damage exists and effector molecules will arrest the cell cycle.

Mitosis is cell cycle stage where the nucleus divides and two daughter cells are formed. Before entry into mitosis, the genome is duplicated as are centrosomes and histone proteins are synthesized. Asters form at microtubule organizing centers in prophase. During prometaphase, chromosomes attach to microtubules via their kinetochores from both poles of the cell. Microtubule rearrangements pull chromosomes until they line up along the metaphase plate during metaphase. During the metaphase checkpoint, chromosome alignment and spindle assembly are checked by proteins such as the Mad1/Mad2 complex and Bub1 that make up the spindle assembly checkpoint (SAC) [183-185]. The SAC ensures that anaphase does not commence until all sister chromatid pairs are attached on either end of their kinetochore. Anaphase is triggered by activation of the anaphase-promoting complex/cyclosome (APC/C) along with the associated protein Cdc20. This activation triggers a series of events that leads to release of the phosphatase Cdc14 from the nucleolus and the subsequent decrease in Cdk1 activity as well as degradation of anaphase inhibitor proteins [186, 187]. Chromosomes then migrate to opposite poles and the cell makes preparations for the final stages of mitosis. During telophase, the cleavage plane forms and cytokinesis follows shortly thereafter. The end product of this division in mammalian cells is the formation of two daughter cells.

While it is anticipated that cell cycle regulators and mechanisms are conserved to a degree, it is evident modes of *P. falciparum* cell cycle regulation

differ from those of previously well-characterized organisms. The intraerythrocytic life cycle stages, described in detail above, consist of the ring or early trophozoite stage, the feeding trophozoite stage, and the schizont stage, in which 8-32 merozoites are formed and are ultimately released to infect new erythrocytes. Therefore, in contrast to the mammalian cycle, which produces only two daughter cells per cell cycle, the parasite must produce many new daughter cells per round of replication. The preinvasion merozoite and ring stages are thought to be analogous to the G₁ phase of the mammalian cell cycle and S phase can be thought of as beginning around 18 hours post invasion (hpi) [188-192]. At this time, the haploid DNA content has been observed to be multiplied as much as 16-20 fold in 4 to 6 hours [193]. In contrast to the highly organized division of nuclear material in mammalian cells, the genetic duplications in *P. falciparum* are asynchronous both within one schizont and also between schizonts [194]. This is highly unusual considering that schizonts in a particular area of the body are subjected to the same environmental factors. Another important distinction between mammalian cell replication and that of *P. falciparum* is a difference in nuclear envelope dynamics. The nuclear envelope disintegrates in mitosis and is reformed in mammalian cells, but this structure remains intact during schizogony [195].

The phase of the parasite life cycle that is analogous to G₁ phase in mammalian cells takes place during growth of preinvasion merozoites and ring stages of *P. falciparum*. During this time, Pfcyc-1, Pfmrk, and Pfcrc-3, which are related to CDKs or their associated proteins, are expressed as are PfPK1 and

Pfmap-2. Pfmrk is a protein kinase that is related in sequence to mammalian CDK7 and is present both during G₁ phase and S phase [196]. In mammalian cells, CDK7 pairs with cyclin H and is involved in cell cycle control and indeed, Pfmrk has been shown to stably complex with human cyclin H, which increases kinase activity [197]. However, in humans CDK7 acts to regulate the activity of other human kinases such as CDK1 and it was shown that the putative *Plasmodium* homolog of CDK1, PfPK5, is not affected by interaction with Pfmrk *in vitro* [116]. This lack of activation may indicate that while Pfmrk is similar in sequence to PfPK7, it does not function as a true CAK and further studies are needed to clarify the role of this kinase during cell proliferation. Pfcyc-1 is a cyclin that is expressed prior to S phase [116]. It is most closely related in sequence to mammalian cyclin H and it has been shown that Pfcyc-1 is able to stimulate the phosphorylation of histone H1 and CTD by Pfmrk [116]. However, Pfcyc-1 has also been shown to activate PfPK5 much more strongly than Pfmrk.

Pfcrk-3 is a large *Plasmodium* kinase that is active during G₁ and S phases and has been shown to colocalize with histone proteins [198]. It displays maximal homology to eukaryotic CDKs that participate in transcription control. Data suggest that this protein acts in complex other proteins and coimmunoprecipitation of Pfcrk-3 with its associated proteins revealed a complex that possessed both kinase and histone deacetylase activities, which is consistent with the known activity of CDKs that have been shown to exert transcriptional control by associating with proteins that modify chromatin structure.

During S phase, nuclear replication takes place. In contrast to mammalian cell S phase, *P. falciparum* S phase continues even after the parasite has entered into mitosis and the parasite seems to lack a definite G₂/M period [193]. The lack of distinction between phases potentially makes distinguishing between proteins that are involved in synthesis and those that are involved in mitosis difficult. However, microarray analysis has been able to tease out proteins that are expressed during early synthesis from those that are expressed primarily in mitosis [199]. The proteins whose expression patterns overlap may prove more difficult to classify. Proteins that are expressed during parasite S phase and may be involved in cell cycle control include PfPK5, PfPK6, and two cyclins, Pfcyc-2 and Pfcyc-4.

PfPK5 is most closely related to yeast p34cdc2 (which is also known as CDK1) [200]. PfPK5 is able to phosphorylate histone H1 and casein. The activity of PfPK5 can be stimulated by the presence of cyclins and, in fact, it has been shown that PfPK5 is quite promiscuous with respect to its activation these proteins [116]. The expression of this protein peaks in late trophozoites and early schizonts and given that an accumulation of PfPK5 activity was observed in cell cycle inhibitor-treated *P. falciparum* parasites, it has been suggested that the protein may play a role in S phase regulation [189].

PfPK6 is also expressed during S phase and is similar in sequence to both CDKs and MAPKs [201]. This protein is active in the absence of cyclins and is able to phosphorylate a subunit of a protein required for synthesis of DNA components, malaria ribonucleotide reductase (R2). The same study showed

that while PfPK6 does not contain a PSTAIRE domain that would indicate the presence of a cyclin-binding site on this protein, it is inhibited by the CDK inhibitors olomoucine and roscovitine.

Both putative cyclins that are expressed during S phase Pfcyc-2 and Pfcyc-4 are strongly associated with histone H1 kinase activity; however it is unclear whether the former functions as a true cyclin [202]. The latter protein, Pfcyc-4, shows greatest expression during segmenters (phase where cytoplasm accumulates around individual nuclei). The same study characterized an additional protein, Pfcyc-3, which while not strongly expressed during S phase or schizogony, is also associated with histone H1 kinase activity and able to activate PfPK5.

Several proteins have been identified in *P. falciparum* with sequence similarity to proteins involved in DNA synthesis pathways and are maximally expressed during 35-40 hpi. These proteins include PfORC1 and PfORC5, the homologs of which function to combine into a 6 subunit origin recognition complex, which then serves as the basis for the larger pre-replication complex in other eukaryotes [203, 204]. Additional *Plasmodium* proteins have been identified and are thought to contribute to the pre-replication complex. Six *P. falciparum* minichromosome maintenance complex proteins [205], *P. falciparum* proliferating cell nuclear antigen [206], and *P. falciparum* replication protein A [207] have all been characterized. The presence of pre-replication complex components within the parasite indicate that the process of DNA synthesis may occur in much the same manner as that observed in yeast or mammalian cells.

However, as one of the purposes of pre-replication complex assembly it to assure that only one round of DNA replication takes place in other cells, clearly there are mechanisms in the parasite that allow for both pre-replication complex assembly and multiple rounds of nuclear division.

Members of the NIMA-related protein kinase family are also regulators of the parasite cell cycle. Five members of this family have been identified including Pfnek-1, Pfnek-3, and Pfnek-2. Members of this family may function as MAPKKs in a unique *Plasmodium* MAPK signaling pathway [104]. The canonical MAPK signaling pathway generally plays a role in cell cycle progression and involves a MAPKKK phosphorylating a MAPKK, which in turn phosphorylates a MAPK. However, this pathway remains a mystery in *P. falciparum* because a MAPKK has yet to be identified. Pfmap-1 and Pfmap-2 are expressed in asexual stage parasites and are closely related to ePK MAPKs and it has been shown that Pfnek-3 is able to phosphorylate Pfmap-2 [208]. In addition, it has been shown that activity of Pfnek-1 is necessary for completion of the asexual intraerythrocytic life cycle [209]

Additional noteworthy differences between *P. falciparum* and cell cycle control in other higher eukaryotes include the fact that CDKs seem to outnumber cyclins in *P. falciparum*. One must keep in mind however that 60% of the *P. falciparum* proteome is made up of proteins of unknown function, which may point to the presence of atypical cell cycle modulators [210]. Another point is that although several of these proteins display sequence similarity to ePKs, there are no definite orthologs in the *P. falciparum* kinome for specific mammalian kinases

with the exception of PfPK5 and Pfcrk-1. A final noteworthy difference is that CKIs (p21, p16), which act as negative modulators of CDK function seem to be absent in *P. falciparum* [104]. Myt1 and Wee1 orthologs are also absent as is Cdc25. In conclusion, there are many differences between the machinery and regulatory mechanisms of *P. falciparum* and mammalian cell cycle regulation. Several questions emerge when considering governing mechanisms driving *P. falciparum* and higher eukaryote cell cycle patterns. Many years of concentrated effort will be required to reconcile these differences; however, discovering the keys to malaria cell cycle dynamics may help alleviate the world's malaria burden by providing tools to stop parasite replication and thus disease progression.

Given the dearth of knowledge that currently exists regarding the biological roles of malarial kinases and the absolute necessity of finding novel antimalarial drugs, this study contributes information about the structure and function of the orphan kinase PfPK7 and provides possible leads for antimalarial drug design. In addition this study utilized the previously characterized cyclin-dependent protein kinase inhibitor Purvalanol B to explore changes in protein expression that result following inhibitor application during parasite S phase. The main research questions from this study are as follows.

- Q1 Will a screen of three well-characterized kinase inhibitor-focused libraries yield molecules that are capable of inhibiting PfPK7 in low molar concentrations.
- Q2 What interactions between the ATP-binding site of PfPK7 and small molecules determine the affinity of these small molecules for the binding site?

- Q3 Are small molecules from three kinase-inhibitor-focused libraries able to inhibit intraerythrocytic growth of *P. falciparum* strain W2 parasites in blood stage cultures?
- Q4 Are small molecule inhibitors of PfPK7 able to inhibit intraerythrocytic growth of *P. falciparum* strain W2 parasites in blood stages cultures?
- Q5 Does application of cyclin-dependent protein kinase inhibitor Purvalanol B to synchronized *P. falciparum* strain W2 blood stage cultures during S phase result in morphological differences between wildtype and inhibitor-treated parasites?
- Q6 What are the differences in protein expression profiles between *P. falciparum* blood stage cultures that have been treated with cyclin-dependent protein kinase inhibitor Purvalanol B during S phase and wild types parasites in the same stage of parasite growth?

This study contributes much needed structural information that will guide the harvesting of potential inhibitory compounds from chemical space in the future and also potentially provides a means for researchers in the future to study the effects of chemically knocking down PfPK7 function in the parasite; a process that would help elucidate the pathways in which PfPK7 functions. Further, by treating synchronized parasites with cyclin-dependent kinase inhibitor Purvalanol B during S phase and comparing protein expression profiles from these parasites to protein expression patterns of wildtype parasites during the same phase of parasite growth, this study contributes information about potential protein interactions during this phase of the cell cycle and may provide insights into the result of inhibiting S phase machinery in *P. falciparum* parasites.

CHAPTER II

MATERIALS AND METHODS

Compound Libraries

The small molecules screened were purchased from EMD Millipore Chemicals in the form of three kinase inhibitor libraries. Inhibitor Select™ 96-Well Protein Kinase Library I (539744) consisted of 80 small molecules that were primarily tyrosine kinase inhibitors. Inhibitor Select™ 96-Well Protein Kinase Inhibitor Library II (539745) consisted of 80 small molecules that were primarily selective inhibitors of kinases from the CMGC kinase group. Inhibitor Select™ 96-Well Protein Kinase Inhibitor Library III consisted of 84 small molecules, which were primarily selective targets of serine/threonine kinases. The majority of these small molecules were cell permeable and well-characterized. In addition, most were ATP-competitive and suspended in dimethyl sulfoxide (DMSO) at a 10mM concentration with the exception of three small molecules from library III, which were at a concentration of 5mM.

Small Molecule Preparation

Small molecules 324840, 428205, 676489, 203290, 420298, 569397, 217714, 218710, 506106, 528116, 551590, 506163 were ordered from EMD Millipore Chemicals and dissolved in DMSO. Purvalanol B was purchased from Tocris Bioscience. Compounds were prepared in 10 mM stock solutions, filter sterilized, and stored in single use aliquots at -80°C.

Protein Preparation

PfPK7 gene codon optimization, synthesis of the coding region of PfPK7, subcloning into a bacterial expression vector, optimization of protein expression, and verification of protein expression were carried out by GenScript Corp. New Jersey, USA. Protein was shipped on dry ice, aliquotted into single use aliquots, and stored at -80°C .

ATP Luminescence Assay

An ATP luminescence assay, which determines levels of kinase activity by measuring residual ATP after a kinase reaction, was used to quantify PfPK7 activity levels after incubation with each small molecule. Kinase-Glo® Luminescent Kinase Assay (Promega) was used and the suggested protocol was optimized for protein and ATP concentration. Kinase reactions took place at a final volume of 50 μl and each small molecule was initially screened against PfPK7 at 0.1 μM , 1 μM , and 10 μM in triplicate. Small molecules were incubated in master mix (40 mM HEPES, 15 mM MnCl_2 , 15 mM MgCl_2 , 50 mM NaCl , 2 mM DTT, 0.5 μM PfPK7) for 10 minutes at room temperature in the dark. ATP was added at 1 μM and reactions were then incubated for 30 minutes at room temperature in the dark. Following incubation with ATP, Kinase-Glo® buffer was added in equal volumes to the reaction mixtures and plates were again incubated for 10 minutes at room temperature in the dark. Plates were then read with a Wallac Victor 2 Multi-label Counter (Perkin Elmer) for luminescence. Positive control wells contained kinase buffer (40 mM HEPES, 15 mM MnCl_2 , 15 mM MgCl_2 , 50 mM NaCl , 2 mM DTT), 1 μM ATP and 2 % DMSO. Negative controls

contained master mix, 1 μM ATP, and 2 % DMSO. Percent inhibition (Equation 1) was determined for each small molecule at each concentration in order to determine hits from the screen. Molecules that had inhibited more than 70 % of kinase activity at 10 μM were considered hits and were chosen for IC_{50} determination. Z factor scores (Equation 2), a means of determining statistical effects size for high-throughput screening assays, were determined for each assay and scores were consistently above 0.7. In order to determine IC_{50} concentrations of hits from the initial screen, small molecules were diluted in 12 point 1:2 dilution series and added to wells starting at a final concentration of 200 μM . Reactions were carried out in triplicate for each concentration and each molecule was tested independently 3 times. Results were analyzed with nonlinear regression using GraphPad Prism® version 5 software with the sigmoidal dose-response (variable slope) equation. Z-factor scores for all assays in the IC_{50} determination process were above 0.7.

$$\% \text{ Inhibition} = \left[\frac{(\text{normal activity} - \text{inhibited activity})}{(\text{normal activity})} \right] \times 100$$

Equation 1: Equation for Percent Inhibition. The average of negative control wells subtracted from the average of positive control wells yields normal activity and inhibited activity is calculated by subtracting the average of inhibitor-treated wells from positive control wells. Inhibited activity was then subtracted from normal activity before dividing the answer by normal activity. The answer is then multiplied by 100 to yield percent inhibition.

$$Z\text{-factor} = 1 - \left[\frac{3(\sigma_p + \sigma_n)}{|\mu_p + \mu_n|} \right]$$

Equation 2: Definition of Z-factor. The sum of the standard deviation of positive controls (σ_p) plus the standard deviation of negative controls (σ_n) all multiplied by three all over the positive control mean (μ_p) plus the negative control mean (μ_n) subtracted from 1 yields the Z factor score. The Z-factor is a measure of statistical effects size and is used in highthroughput screens to determine if observed differences in an assay are significant.

Computational Docking of Small Molecules

Maestro and Macromodel

Structure-data files (SDF) for all small molecules were downloaded from EMD Millipore Chemicals website. The crystal structure file 2PML was used for the docking studies and was downloaded from the Protein Data Bank [121]. The crystal structure file 2PML was assembled from a protein that had been cocrystallized with an analog of ATP, at a resolution of 2.6 Å. DS ViewerPro (Accelrys) was used to visualize the protein and the ATP analog, phosphoaminophosphonic acid-adenylate ester (ANP), was removed from the ATP-binding site. Maestro and Macromodel (Schrodinger software suite) were used to add hydrogens and minimize each structure respectively. In Macromodel, structures were minimized with the dielectric constant set to 4.0 to account for an aqueous environment and maximum iteration number was set to 1000. OPLS_2005 forcefield was used to define algorithm parameters and local energy minimums were determined with Polak-Ribiere Conjugate Gradient (PRCG) methodology [211]. Solutions were considered converged at 0.05 kJ/Å-mol. After minimization, structures were exported as .mol2 files for later docking and analysis. Modified 2PML was saved as a PDB file.

Docking and Scoring of Small Molecules

The ligand-docking program GOLD was used to determine the most likely orientations of small molecules within the ATP-binding site of PfPK7. The center of the docking sphere was set by determining the coordinates of the N9 nitrogen of ANP in the 2PML text file. The centroid was set at $x=-12.021$, $y=6.897$, and $z=-19.854$ and the active site radius was set at 10 Å. The 2PML crystal structure was first validated by recapitulating the docking of ANP and adenosine monophosphate (AMP) within the crystal structure ATP-binding site. Following this validation, each small molecule was docked to the ATP-binding site and the most likely 50 orientations were determined. Each orientation was scored with the fitness function Chemscore using default search settings and annealing parameters. Docking data were analyzed in Maestro and DS ViewerPro 5.0.

Computational Investigation of Druglikeness

QikProp

Small molecule hits were evaluated for druglikeness by determining their adherence to Lipinski's rule of five. Most effective orally available medications are formulated from relatively small and lipophilic molecules. Christopher Lipinski defined the following set of criteria for determining whether a given molecule will have desirable pharmacokinetics in the body: not more than 5 hydrogen bond donors, not more than 10 hydrogen bond acceptors, a molecular mass less than 500 Daltons, and an octanol-water partition coefficient (logP) not greater than 5 [212, 213]. If a compound violates more than one of the aforementioned criteria its usefulness as a lead drug compound is limited. LogP

was calculated by the previously described model [214-216]. The Schrodinger-applied percent human oral absorption model was also employed. In addition, human colon adenocarcinoma (Caco-2) cell permeability was calculated using the model developed from Boehringer-Ingelheim and AstraZeneca in order to predict absorption across intestinal epithelium [217, 218]. Prediction of hERG inhibition was performed using the model previously described [219, 220]. The hERG predictor determines whether or not small molecules are likely to block K⁺ channels and thus alter membrane potential especially in cardiac muscle where these channels are prevalent.

TOPKAT

Prediction of Ames mutagenicity was used to determine if small molecules were likely to be mutagens. The model used to predict Ames mutagenicity was developed using compounds that were tested with the US EPA GeneTox protocol [221]. Evaluation of 894 compounds tested by the Japanese Ministry of International Trade and Industry 1 text protocol was used to develop the model used by TOPKAT to predict aerobic biodegradability. The prediction of Developmental Toxicity Potential was determined using the model developed for TOPKAT that was trained by 374 open-literature references out of the approximately 3000 studies that were reviewed by developers. A quantitative structure-toxicity relationship (QSTR) model was constructed using weight of evidence rodent carcinogenicity. According to the United States Food and Drug Administration (FDA) weight of evidence protocol, a given molecule is considered a carcinogen if it is a single site carcinogen in two or more sexes/species of test

animals or a multiple site carcinogen in one or greater sexes/species of test animal. The QSTR gives predicted carcinogenic values based on this protocol and on experimental carcinogenicity rodent model studies conducted by the National Toxicology Program (NTP) and the National Cancer Institute (NCI).

Maintaining *P. falciparum* Cultures

P. falciparum strain W2 was obtained from Malaria Research and Reference Reagent Resource Center (MR4) as part of the BEI Resources Repository, NIAID, NIH: *Plasmodium falciparum* W2, MRA-157, deposited by DE Kyle. All experiments with this strain were conducted at Biosafety Level 2. Parasites were thawed from liquid nitrogen and maintained as previously described with slight modifications [22]. Briefly, parasites were kept in malaria culture medium (MCM) (RPMI 1640 (Gibco), 25 mM HEPES, 23 mM NaHCO₃, and 25 µg/ml gentamicin sulfate (Sigma-Aldrich), pH 7.4) that was supplemented with 10 % human serum (type AB-) at 5 % hematocrit (Blood type O⁺) in an atmosphere of 5 % CO₂, 5 % O₂, and a balance of N. A temperature of 37°C was maintained. Cultures were split 1:50 when parasitemia reached 3-5 %. Parasite growth synchronization protocol was adapted from Lambros and Vanderberg, 1979 [222]. Cultures that were primarily rings at approximately 5 % parasitemia were centrifuged to pellet RBCs. CMCM was removed and 20X volume of packed cells of 5 % D-sorbitol in PBS was added. Cultures were allowed to rest at room temperature for 15 minutes and were then centrifuged to pellet RBCs. RBCs were washed once in MCM without serum and were then resuspended in MCM with serum. Synchronized cultures were split 1:10 and

allowed to grow for 48 hours after which blood smears were taken and Giemsa (HARLECO)-stained to count parasitemia levels and estimate life cycle stage. The procedure was repeated until >90 % of parasites were in the same life cycle stage as verified by Giemsa staining.

SYBR Green I Growth Assay

In the SYBR Green I assay, parasites are incubated with inhibitor for 72 hours and growth of parasites is detected by applying buffer containing the fluorescent intercalating agent SYBR Green I. Extent of SYBR Green I DNA binding can be determined by reading for fluorescence and as human RBCs are anuclear, fluorescence is the direct result of parasite DNA presence. In order to determine the extent to which small molecules can inhibit intraerythrocytic parasite growth, the SYBR Green I parasite growth assay was performed with minor alterations as previously described [223]. Briefly, a 96 well plate format was used. One hundred μl total volume was used in each well and 99 μl contained CMCM with 0.5 % parasitemia. One μl of small molecule was added in each well and each small molecule was screened in triplicate at 1 μM . Negative control wells contained CMCM, 2% hematocrit, and no parasites. Positive control wells contained CMCM and 2 % hematocrit with 0.5 % parasitemia. 1 μl of DMSO was added to all control wells. Plates were kept at 37°C in a modular incubator that was gassed at 20 L/min for 5 minutes with 5 % O₂, 5 % CO₂, and a balance of nitrogen daily. After an incubation period of 72 hours, equal volumes of lysis buffer (20mM Tris base, 5 mM EDTA, 0.008 % Saponin, 0.08 % Triton X-100, pH 7.5 with 0.2 μl SYBR Green I/ml of lysis buffer)

was added to each well. Plates were then incubated in the dark for 1 hour and then read on a Wallac Victor 2 Multi-label Counter (Perkin Elmer) for fluorescence (excitation 485 nm and emission 535 nm). IC₅₀ determinations were made by diluting 10 mM stock compounds in 12 point 1:2 dilution series from a starting final concentration of 200 μ M. The assay was performed as indicated above and final fluorescence readings were analyzed with nonlinear regression analysis using GraphPad Prism® version 5 software with the sigmoidal dose-response (variable slope) equation. Z factor scores were tabulated for all assays and were found to exceed 0.7.

Culturing Parasites with Purvalanol B

Parasites were maintained and synchronized as described above and at 5 % parasitemia, parasites were resynchronized and placed at 37°C for 24 hours. At 24 hpi, parasitemia and life cycle stage were confirmed with Giemsa-stained blood smears and 3X the IC₅₀ concentration (determined by SYBR Green I growth assay to be 29.8 μ M) of Purvalanol B (Sigma-Aldrich) in DMSO was applied to cultures, which were again gassed and incubated for 12 hours at 37°C. Three treatment cultures and three control cultures were prepared. Control cultures were incubated with DMSO only for 12 hours. At 36 hpi, parasitemia and life cycle staged were confirmed with Giemsa-stained blood smears. At 36 hpi RBCs were pelleted and washed 3X in PBS to remove serum proteins. All centrifugation steps took place at 4°C. RBCs were then lysed in 20X volume of packed cells in 0.05 % saponin (Fluka BioChemika) in PBS on ice for 10 minutes. Lysates were then washed 3X in PBS to remove RBC ghosts and once in 10 mM

Tris HCl (Sigma-Aldrich) to remove heme-binding proteins before final sedimentation. Parasites were centrifuged at 8000 rpm for 10 minutes and the resulting parasite pellets were stored at -80°C.

Protein Extraction

Parasite lysates were resuspended in 1 ml of 10 mM Tris HCl supplemented with protease inhibitor cocktail (PI) (Sigma-Aldrich) and were flash frozen 2X to begin to release proteins. Suspensions were then sonicated on ice 5X 20 seconds (1 second on and 1 second off) at 10 % amplitude to complete protein release. Samples were centrifuged at 14,000 rpm for 30 minutes at 4°C to sediment hemozoin and the resulting supernatant was removed for later analysis. Protein concentration was determined for all samples using a DC assay (Biorad). For each sample, 60 µg were sent to Colorado State University's Proteomics and Metabolomics Facility for evaluation with shotgun proteomics. Proteins underwent mass spectrometry analysis following trypsin digestion.

Mass Spectrometry Analysis

First peptides were purified and concentrated using on-line enrichment columns (Thermo Scientific 5 µm, 100 µm ID x 2 cm C18 column). Then chromatographic peptide separation was performed on a reverse phase nanospray column (Thermo Scientific EASYnano-LC, 3 µm, 75 µm ID x 100mm C18 column) using a 90 minute linear gradient from 10%-30% buffer B (100% ACN, 0.1% formic acid) at a flow rate of 400 nanoliters/min. Peptides were eluted directly into the mass spectrometer (Thermo Scientific Orbitrap Velos) and spectra were collected over a m/z range of 250-2000 Daltons using a dynamic

exclusion limit of 2 MS/MS spectra of a given peptide mass for 30 seconds (exclusion duration of 90 seconds). Samples (0.5 μ g) were analyzed in randomized duplicate injections. Compound lists of the resulting spectra were generated using Xcalibur 2.2 software (Thermo Scientific) with a S/N threshold of 1.5 and 1 scan/group.

Protein Data Analysis

MS/MS spectra were searched against the Uniprot *Plasmodium falciparum* concatenated reverse database (version 03/06/2013) using the Mascot database search engine (version 2.3) and the SorcererTMSEQUEST[®] version 3.5 LFDR (local false discovery rate) was calculated using a Bayesian algorithm to confirm peptide probabilities based on likelihoods calculated using parent mass accuracy. Search parameters were as follows: monoisotopic mass, parent ion mass tolerance of 20 ppm, fragment ion mass tolerance of 0.8 Da, fully tryptic peptides with 1 missed cleavage, variable modification of oxidation of M and fixed modification of carbamidomethylation of C. Search results for each independently analyzed sample were imported into the Scaffold software (Version 4, Proteome Software, Portland, OR). Peptide and protein probability thresholds of 95 % and 99 % respectively were applied and a minimum of two unique peptides were required. Manual validation of MS/MS spectra was performed for all protein identifications above the probability thresholds that were based on only two unique peptides. Criteria for manual validation included the following: 1) minimum of 80 % coverage of theoretical y or b ions (at least 5 in order); 2) absence of prominent unassigned peaks greater than 5 % of the

maximum intensity; and 3) indicative residue specific fragmentation, such as intense ions N- terminal to proline and immediately C- terminal to aspartate and glutamate (used as additional parameters of confirmation).

***P. falciparum* Quantitative Analysis**

Spectral counting (SpC) and average total ion current (TIC) relative quantitative analyses were performed and t-tests as well as fold changes were calculated for each method. While the two methods of analysis are distinct, they are both valid and yielded complementary results. The cutoff and thresholds used for this analysis were as follows: 1) 99 % protein probability; 2) 2 peptide minimum; and 3) 95 % peptide probability. There were a minimum of 10 spectral counts (sum) per biological group and a minimum presence (2 peptides) in 2/3 biological replicates. For each biological replicate, a scaling factor was determined by dividing the sum of spectral counts by the average spectral counts across all biological samples. Each protein was divided by the scaling factor of the biological replicate in which it was present. T-tests as well as fold change analysis were then performed on normalized data in Scaffold. Mean and standard deviation of spectral counts were calculated before and after normalization to assure that normalization had equaled out the mean spectral counts between the biological samples.

CHAPTER III
SCREEN OF KNOWN KINASE
INHIBITORS AGAINST
PFPK7

Introduction

The alarming development of *P. falciparum* resistant parasite strains, especially in the region of Southeast Asia has made necessary the identification of promising targets for antimalarial drug design. Unique structural aspects of *P. falciparum* kinases along with recent successes developing protein kinase-targeted drug therapies for the treatment of diseases including cancer, inflammatory disorders, and diabetes make selective targeting of the ATP-binding site from these macromolecules a promising antimalarial drug development strategy.

The majority of aforementioned successful kinase-targeted drugs compete for the ATP-binding site of their respective targets. However, compounds that bind to the ATP-binding site tend to cross-react with the ATP-binding sites of other kinases because of the high degree of evolutionary sequence conservation that occurs in this domain of the protein. The cross-reactivity of these small molecules is due to the characteristics that are shared not only among the ATP-binding site of kinases, but also to analogous characteristics of kinase inhibitors. For instance, a modified purine base is often used as a scaffold for kinase inhibitor development because this base preserves hydrogen bonding

interactions between small molecules and the hinge region of kinases, which links together the N- and C- terminal lobes of the proteins. This approach has the added benefit of providing molecules that can be used as a starting point in many different kinase-targeted drug discovery efforts (as reviewed in [224]). Analysis of 72 well-characterized kinase inhibitors against 442 kinases, which represents greater than 80 % of the human kinome, revealed that while some kinase inhibitors, such as the CDK inhibitor staurosporine, are widely promiscuous, others such as the EGFR/HER2 kinase inhibitor, Lapatinib, are notably selective for their respective targets [225]. Therefore, while cross-reactivity between kinases does occur, it is clearly possible to identify an inhibitor capable of exploiting the unique characteristics of its target molecule to the effect of selectively inhibiting the target protein and few others.

The wealth of structural information that has been gleaned over the past decade in the form of protein kinase crystal structures has revealed key characteristics of kinases that may govern the ability to selectively target a particular kinase and can be utilized during the rational drug design of small molecule inhibitors targeting the ATP-binding site. A hydrophobic pocket that lay adjacent to the ATP-binding region, access to which is controlled by a gatekeeper residue, may be exploited if the gatekeeper residue is a small amino acid such as a glycine and the small molecule in question is able to span the binding site to establish hydrophobic interactions within this pocket. Further, correspondence between key residues in the hinge region and areas in the small molecule allow for the formation of foundational hydrogen bonds and interactions

between the binding pocket floor also increase affinity [226]. The catalytic lysine residue and an acidic group that generally stabilize the phosphate groups of ATP may further add to affinity of small molecules by contributing to the formation of hydrogen bonds. In addition, the orientation of phenylalanine within the DGF motif further contributes optimal affinity.

The orphan kinase PfPK7 was chosen as a potential target for screening in this study because of its unique attributes. As an orphan kinase, PfPK7 has no eukaryotic kinase ortholog and maintains structural characteristics that are different from mammalian kinases [121]. Unique attributes of PfPK7 coupled with the data that show PfPK7(-) parasites display decreased growth rates compared to wildtype parasites make PfPK7 a potential target for antimalarial drug discovery [124]. Further, as the biological function of this kinase is undetermined, identification of a PfPK7 inhibitor would allow for the exploration of PfPK7 function the parasite.

Two hundred forty-four compounds from three kinase inhibitor-focused libraries were screened against PfPK7 with an ATP luminescence assay. Molecules that were able to compete for the ATP-binding site of PfPK7 were then tested to determine the IC₅₀ concentrations. In addition, these small molecules were computationally docked to the ATP-binding site of the PfPK7 crystal structure in order to determine the probable binding site interactions between inhibitors and the protein. In order to conduct the docking studies, the binding sphere was identified by determining the coordinates of the N9 nitrogen of ANP within the PDB file, 2PML, which is cocrystallized with the ATP analog within its

binding site. Docking studies were carried out using GOLD and results were visualized with DS ViewerPro and Maestro.

As kinases utilize ATP to carry out phosphotransfer activity, the ATP luminescence assay determines the ability of kinases to utilize ATP in the presence of potential small molecule inhibitors. If the small molecule is able to outcompete ATP for the binding site, more free ATP will exist in the reaction mixture following a kinase reaction. An enzyme that binds free ATP is then incubated with the reaction mixture and greater ATP concentrations result in luminescence increase, which allows for quantitation of ATP utilization compared to controls. This assay platform offers a non-radioactive method for quantitating the inhibitory effects of small molecules on ATP-utilizing target proteins and allows for high-throughput screening, which increases the number of compounds that can be evaluated in a single assay.

GOLD is a software program for predicting the probable docking modes of ligands in protein binding sites and is part of the GOLD suite (Hermes) of programs. GOLD utilizes a genetic algorithm for ligand-protein docking that predicts the minimum free energy of association during an iterative docking process, which yields multiple predicted binding modes. In addition, this program allows for a limited amount of backbone flexibility for up to ten select residues within the binding site, which aids user-directed parameterization of the docking process for a particular protein-ligand complex (kinase-ATP). One method to validate how precisely and accurately any algorithm will predict small molecule docking orientations is to strip a cocrystallized molecule from the protein crystal

structure file and then dock the ligand back into the binding site with the aid of the desired program. Following the docking, the researcher can then determine whether the algorithm is able to recapitulate the docking orientation indicated in the original crystal structure PDB file. GOLD was originally validated with a test set of 100 ligand-protein complexes and then more extensively validated in a Cambridge Crystallographic Data Center/Astex collaborative study using 305 ligand-protein complexes [227, 228]. Since that time two additional validation studies were carried out; an Astex test of 85 highly diverse ligand-protein complexes and an Astex non-native test that utilized 1112 crystal structures for 65 proteins that were in a non-native state [229, 230]. Data from the extensive validation of GOLD revealed that the algorithm was able to reproduce the experimental binding mode in 71-80 % of cases and that this percentage increased when the protein-ligand complex was well-characterized as is the case for kinase-ATP complexes.

DS ViewerPro is the molecular visualization software program in the Accelrys Discovery Studio. This program allows for easy manipulation of 3D structures such as adding and removing multiple docked small molecules from protein binding sites. The software program Maestro is the unifying interface for all Schrodinger software. It allows both 2D and 3D representation of protein-ligand complexes as well as visualization and measurement of electrostatics, binding pocket shape, and protein-ligand interactions. Maestro also allows for the superimposition of multiple structures or structure orientations, which enables detailed comparisons of possible small molecule binding modes as well as

assignment of a consensus orientation for multiple small molecules within one binding site.

The accumulation of information regarding the druglikeness of small molecules has allowed computational biologists to train *in silico* models which, when used to test compounds with similar qualities to drugs that are well-described in chemical space, are able to predict characteristics such as cell permeability, toxicity, likely metabolites, and solubility. These models predict structural properties such as number of hydrogen bond participants and molecular weight as well as physicochemical properties such as solubility and permeability. In addition, properties that contribute to pharmacokinetic activities and toxicity can also be predicted. Following the prediction of these properties, it is then possible to determine how well small molecules adhere to Lipinski's rule of five for predicting druglikeness. Testing small molecule drugs for all pharmacokinetically relevant properties that impact drug design *in vitro* becomes expensive and often unfeasible, which means that a lack of funds may result in limited exploration of compounds with potentially curative properties. Harnessing information gleaned from previously tested compounds and coupling this information with target activity data, provide a means to efficiently and economically identify lead compounds for drug design.

Combining *in vitro* activity data with *in silico* molecular interaction and pharmacological data enables the informed selection of molecules with the greatest potential of having druglike properties and acting as potent inhibitors of their intended biological targets. A screen of three kinase-inhibitor focused

libraries against the malaria kinase PfPK7 revealed compounds that were able to inhibit kinase activity at low molar concentrations and molecular interaction data that will inform future studies aimed at identifying selective PfPK7 inhibitors. In addition, the estimation of pharmacologically relevant properties distinguished those molecules that are most druglike from those with problematic characteristics for drug development.

Results

ATP Luminescence Assay

EMD kinase libraries I, II, and III were tested for their ability to inhibit malaria kinase PfPK7 at three concentrations, 0.1 μM , 1 μM , and 10 μM . The screen of these three inhibitor libraries containing a total of 244 compounds revealed 12 compounds capable of inhibiting PfPK7 as indicated by greater than 70% inhibition of kinase activity at a 10 μM concentration. Four molecule hits were identified from EMD Kinase Library I using the ATP luminescence assay: 324840, 428205, 676489, and 203290. Of the four compounds that hit from this library, 676489 and 203290 had IC_{50} values above $1.0\text{e-}4$ so these compounds were not explored further. The screen of EMD Kinase Library II revealed four compounds that were able to inhibit 70% of kinase activity at 10 μM . The compounds 420298, 569397, 217714, and 218710 were chosen for IC_{50} determination. EMD Kinase Library III was also screened and four molecules from this library were able to inhibit 70% of kinase activity at 10 μM ; 506106, 528116, 551590, and 506163. Of the four molecules that hit from the third library, 506163 had an IC_{50} value above $1.0\text{e-}4$ so it was excluded from further

analysis. 506106 was not explored further as upon exploration of available data on this compound it was found to be an allosteric inhibitor that targets the autoregulatory domain of group I p21-activated kinases and thus its inhibitory effects may not be due to competition for ATP within the PfPK7 ATP-binding site. The eight remaining compounds were tested three times in triplicate and displayed inhibitory activities ranging between $6.26e-7 \pm 1.5e-7$ M and $8.63e-5 \pm 1.46e-5$ M against PfPK7 (Table 2).

Docking of Small Molecules

In order to validate the crystal structure 2PML and to assure that the molecular docking program GOLD was able to recapitulate the orientation of the ATP analog, ANP, within the ATP-binding site, adenosine monophosphate was docked to the binding site of 2PML (Figure 4). GOLD was able to reproduce the binding orientation as well as the molecular interactions observed in the crystal structure 2PML. Results from computational docking of small molecules to the crystal structure file 2PML of PfPK7 revealed several interactions between small molecules and the ATP-binding site that contributed to the affinity of compounds for this binding site (Figure 5a-5h). Interaction profiles were determined for each small molecule thus enabling the characterization of the most favorable interactions for promoting compound affinity. PfPK7 was found to possess a

Table 2: IC_{50} Luminescence Values for PfPK7 Small Molecule Inhibitors. Column one indicates the EMD kinase library number from which the small molecule originated. Column two indicates the EMD molecule and column three gives the IC_{50} luminescence values for each compound plus the standard deviations in Molar concentration. The final column depicts the structure of each small molecule.

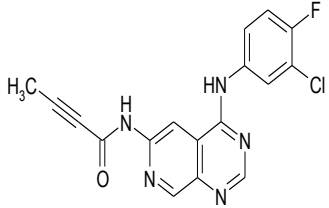
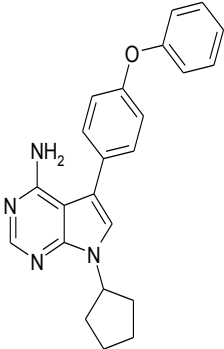
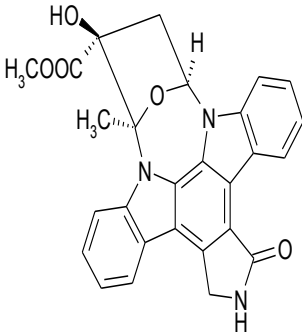
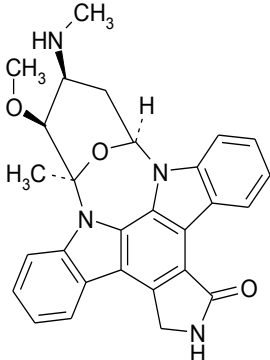
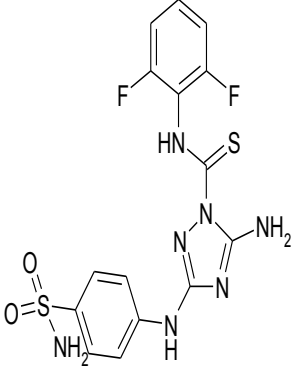
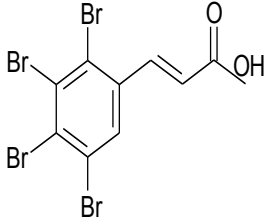
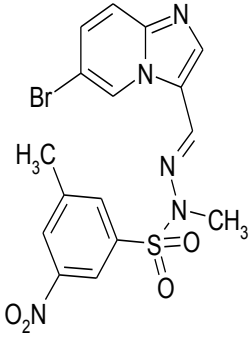
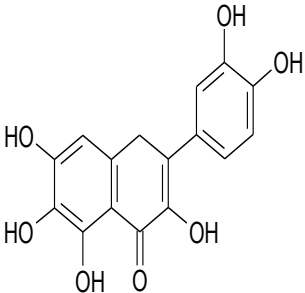
<i>Library Number</i>	<i>Compound</i>	<i>IC₅₀ Luminescence</i>	<i>Structure</i>
I	324840	$5.71e-5 \pm 1.52e-6$	
I	428205	$8.63e-5 \pm 1.46e-5$	
II	420298	$2.08e-6 \pm 1.22e-6$	
II	569397	$1.41e-6 \pm 1.35e-6$	

Table 2 Continued

<i>Library Number</i>	<i>Compound</i>	<i>IC₅₀ Luminescence</i>	<i>Structure</i>
II	217714	3.71e-5±3.75e-6	
II	218710	1.98e-5±1.26e-6	
III	528116	6.26e-7±1.5e-7	
III	551590	1.17e-5±2.24e-6	

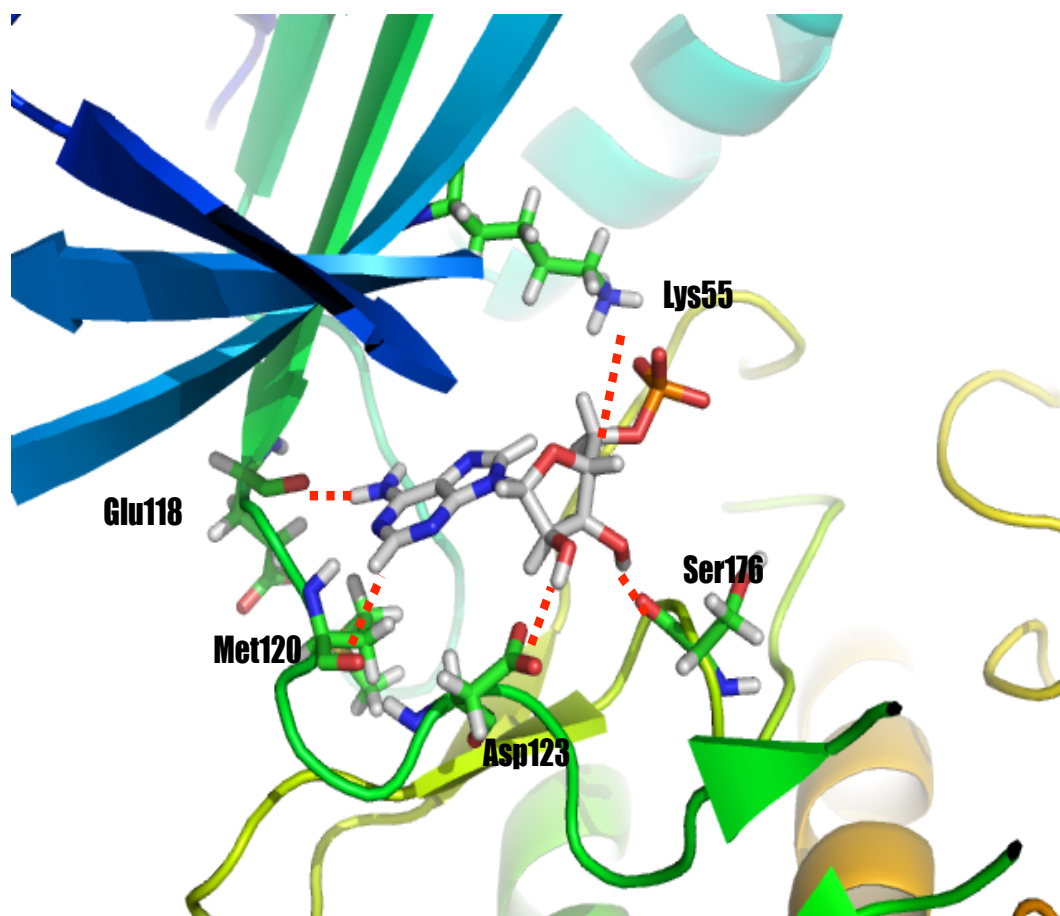


Figure 4: AMP Docked to the PfPK7 ATP-binding site. AMP docked to the ATP-binding site of the crystal structure 2PML using GOLD. Red hash marks represent hydrogen bonds between AMP and residues within the ATP binding site of 2PML. Hydrogen bonds at Glu118 and Met120 in the hinge region orient the purine backbone of AMP in the binding site and additional hydrogen bonds at Asp123 and Ser176 stabilize the molecule, while a hydrogen bond at Lys55 orients the phosphate group (Made in PyMOL).

leucine and isoleucine rich hydrophobic pocket. In general, molecules that showed high affinity for the binding site were stabilized by hydrophobic interactions at Leu34, Ile42, Ala53, Leu101, and Leu179 (Table 3). In addition, probable π/π stacking interactions in either parallel or perpendicular orientations at one or both of the tyrosine residues 117 and 119 further increased affinity of small molecules for the binding site. Hydrogen bonds, varying in number from 1 to 4, formed most often at residues Asn35, Glu118, Met120, Asp123, Ser176, and Asp190. Small molecules that displayed the highest affinity for the binding site were those that made three hydrogen bonds, maintained hydrophobic contacts with all residues in the hydrophobic pocket, and formed π/π stacking interactions with both Tyr117 and Tyr119.

Biologically Relevant Property Prediction

Software programs QikProp and TOPKAT were used to predict the biologically and pharmacologically relevant properties of the eight small molecule hits from the PfPK7 luminescence assay screen. QikProp was first used to predict the structural and physicochemical properties of the compounds (Table 4). Previous research has shown that molecules that violate no more than one of Lipinski's rules are more likely to act as good compounds for drug design than those molecules that do not adhere well to these criteria. Molecules 428205, 217714, and 551590 all violated one of Lipinski's rules, while the remaining compounds adhered to all of the criteria. Most drug-like compounds maintain a LogP octanol/water partition coefficient less than five, which assures that the

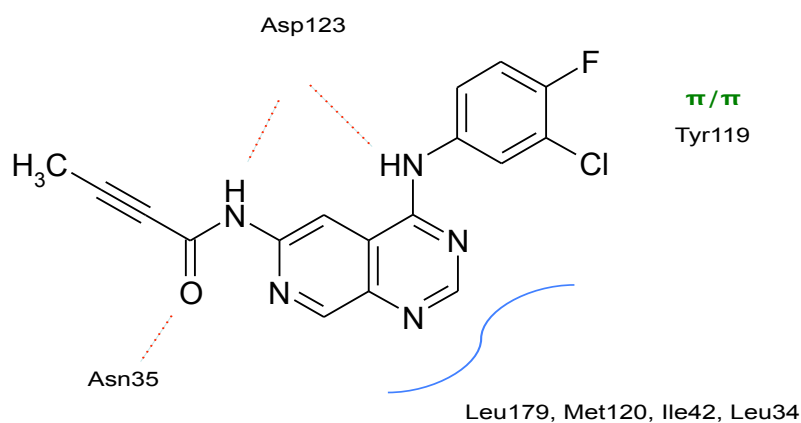
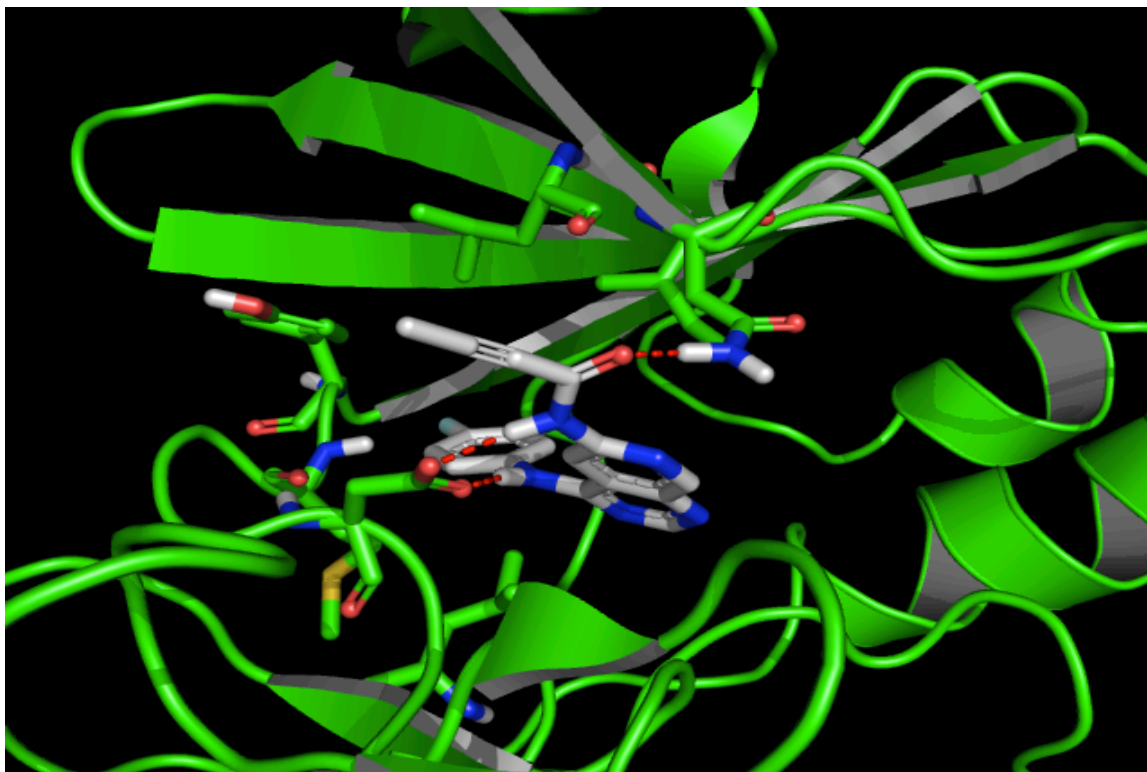


Figure 5a: 324840 in the ATP-binding site of PfPK7. Upper: representation of the small molecule 324840 in the PfPK7 ATP-binding site and dashed red lines indicate hydrogen bonds. Lower: 2D structure of small molecule 324840. Hydrogen bonds are indicated by red hash marks, blue sigmoidal curves indicate hydrophobic interactions, and the green π/π symbol indicates pi/pi stacking interactions (Made in PyMOL).

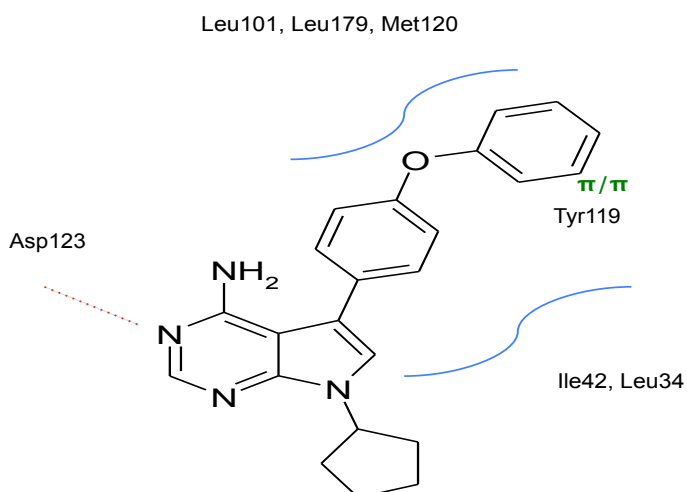
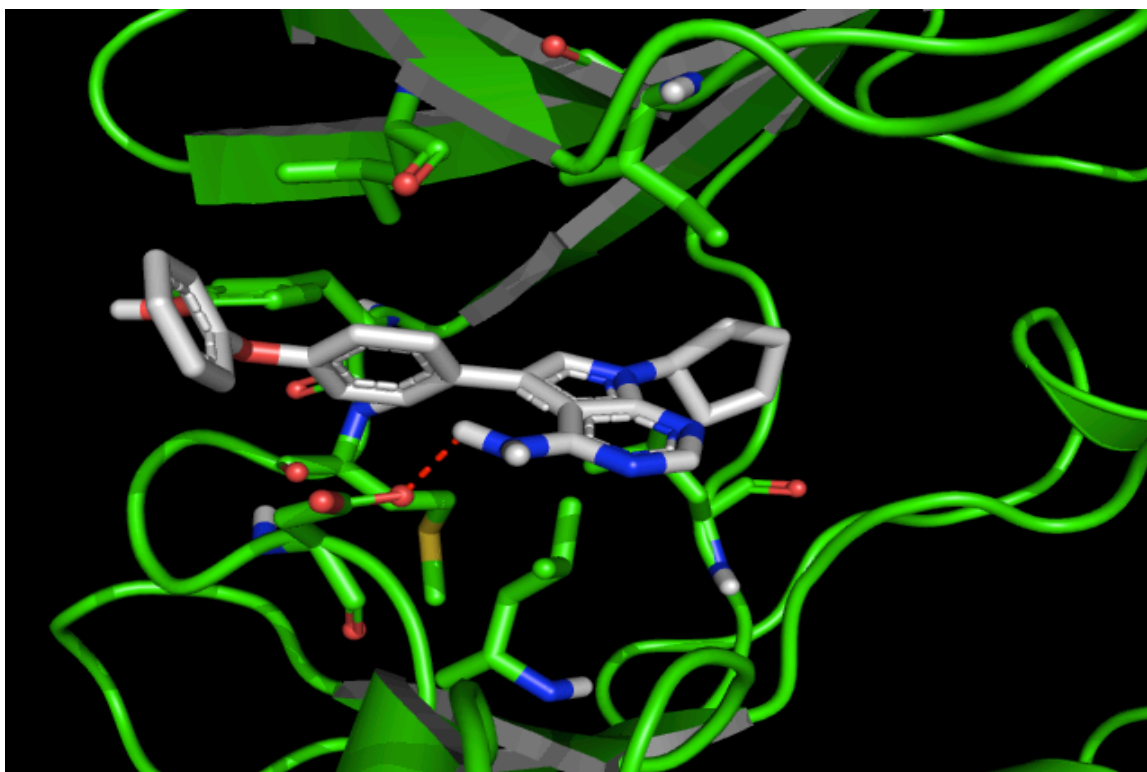


Figure 5b: 428205 in the ATP-binding site of PfPK7. Upper: a 3D representation of the small molecule 428205 in the PfPK7 ATP-binding site red dashed lines indicate hydrogen bonds. Lower: a 2D structure of small molecule 428205. Hydrogen bonds are indicated by red hash marks, blue sigmoidal curves indicate hydrophobic interactions, and the green π/π symbol indicates pi/pi stacking interactions (Made in PyMOL).

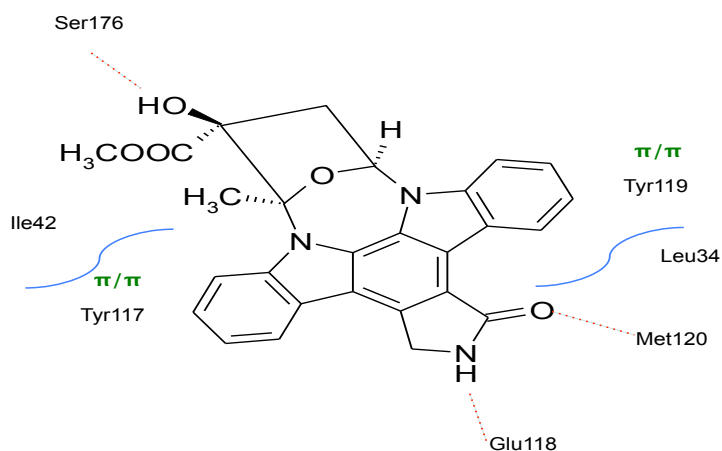
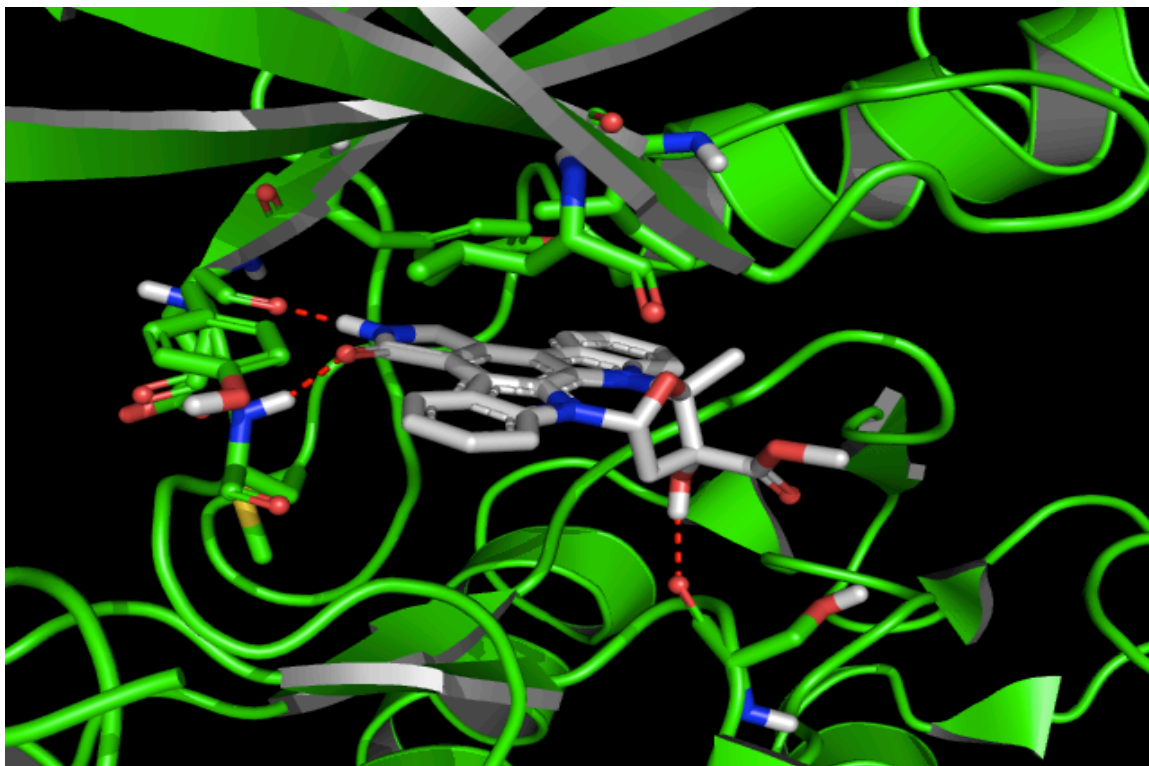


Figure 5c: 420298 in the ATP-binding site of PfPK7. Upper: a 3D representation of the small molecule 420298 in the PfPK7 ATP-binding site red dashed lines indicate hydrogen bonds. Lower: a 2D structure of small molecule 420298. Hydrogen bonds are indicated by red hash marks, blue sigmoidal curves indicate hydrophobic interactions, and the green π/π symbol indicates pi/pi stacking interactions (Made in PyMOL).

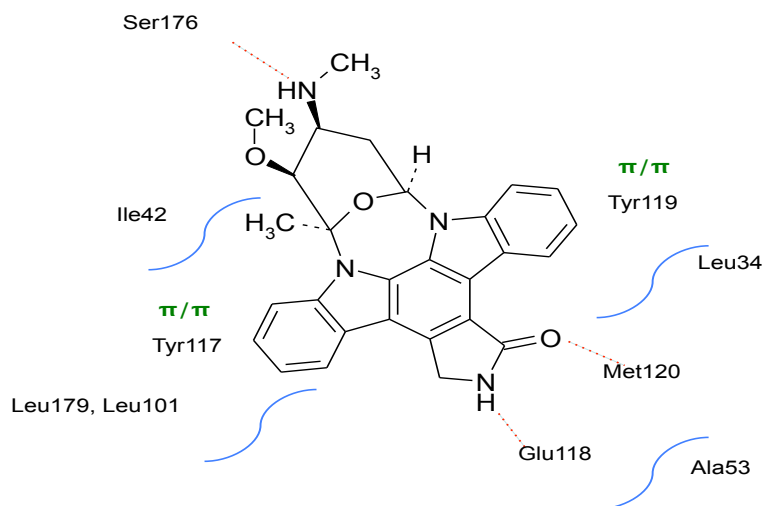
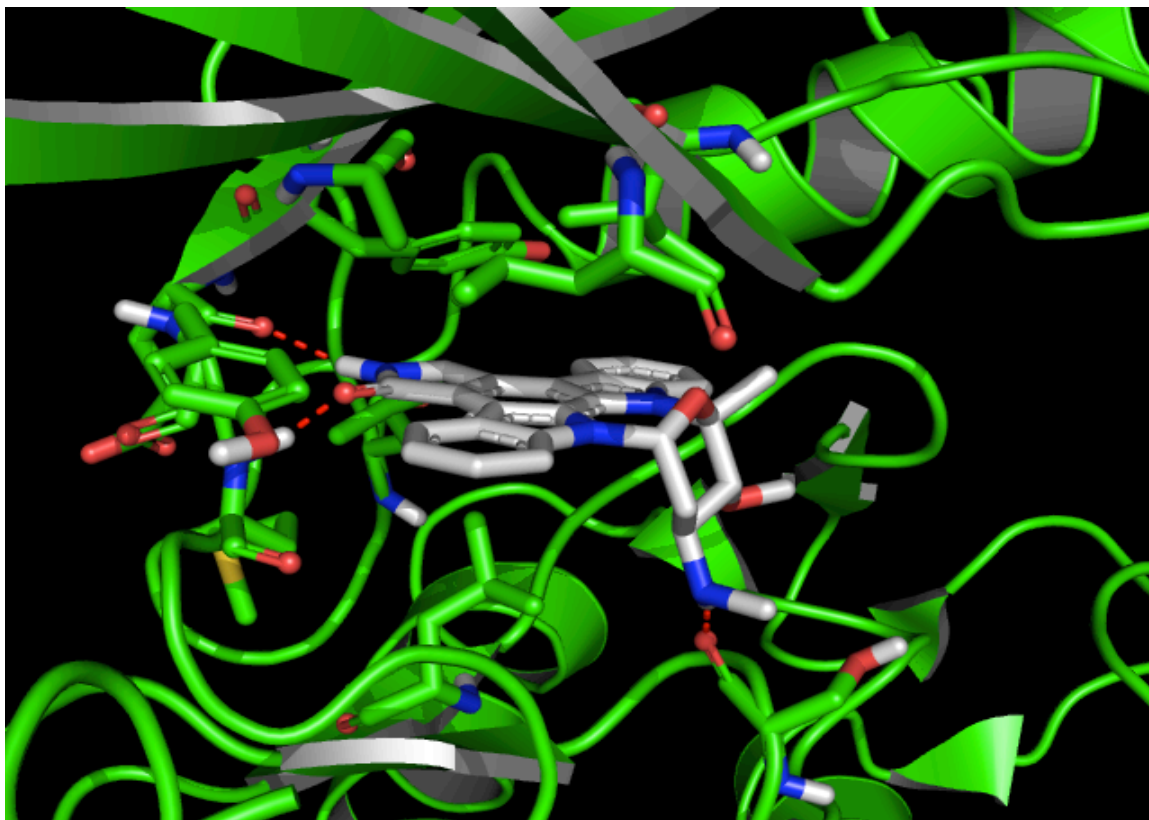


Figure 5d: 569397 in the ATP-binding site of PfPK7. Upper: a 3D representation of the small molecule 569397 in the PfPK7 ATP-binding site and red dashed lines indicate hydrogen bonds. Lower: a 2D structure of small molecule 569397. Hydrogen bonds are indicated by red hash marks, blue sigmoidal curves indicate hydrophobic interactions, and the green π/π symbol indicates pi/pi stacking interactions (Made in PyMOL).

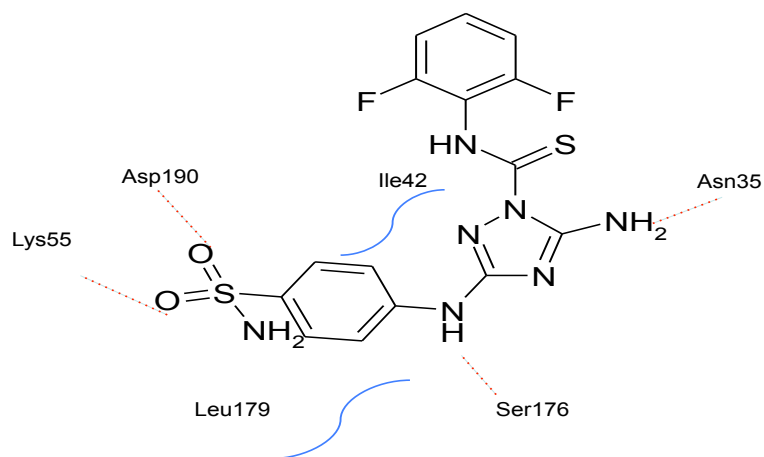
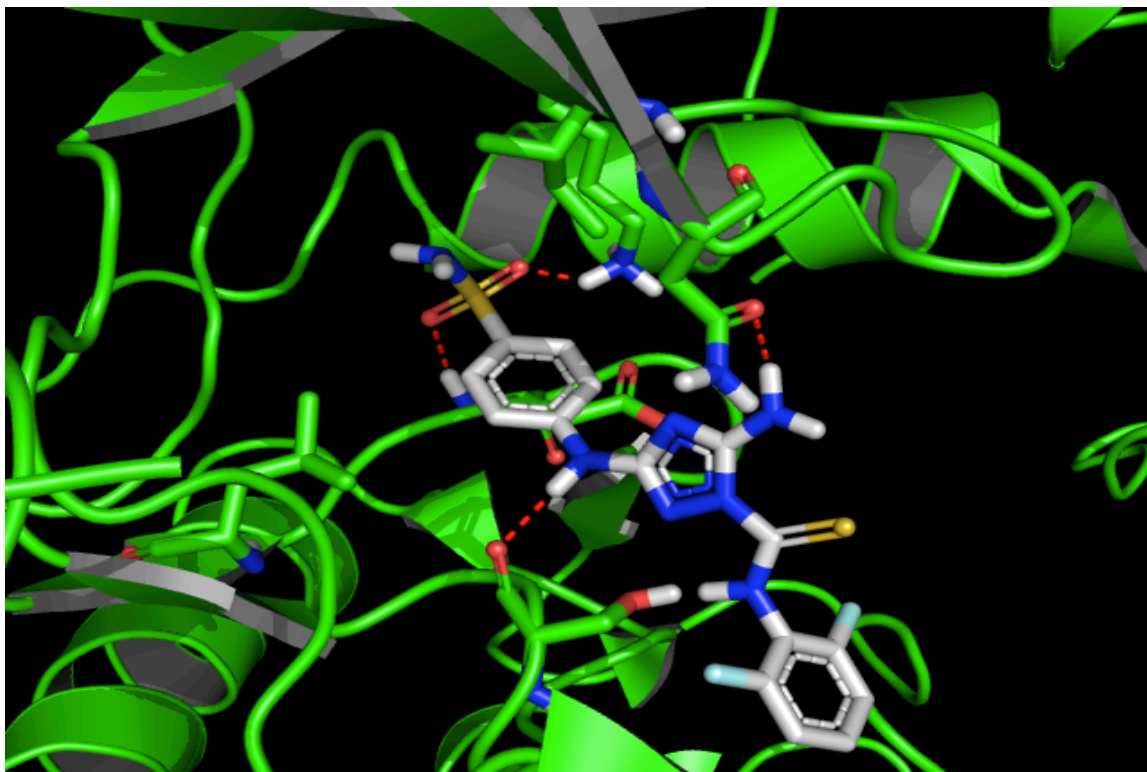


Figure 5e: 217714 in the ATP-binding site of PfPK7. Upper: a 3D representation of the small molecule 217714 in the PfPK7 ATP-binding site and red dashed lines indicate hydrogen bonds. Lower: a 2D structure of small molecule 217714. Hydrogen bonds are indicated by red hash marks, blue sigmoidal curves indicate hydrophobic interactions, and the green π/π symbol indicates pi/pi stacking interactions (Made in PyMOL).

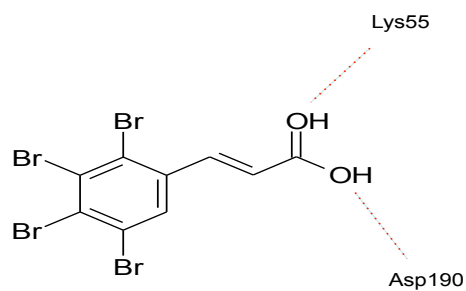
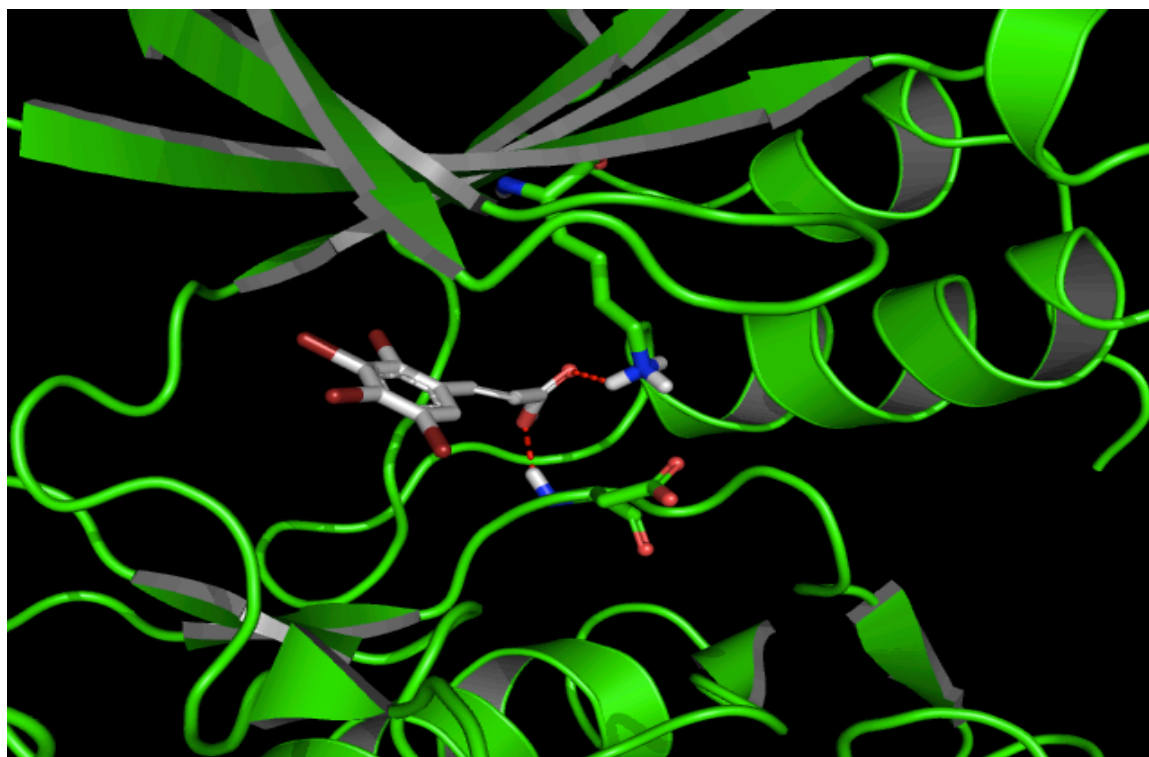


Figure 5f. 218710 in the ATP-binding site of PfPK7. Upper: a 3D representation of the small molecule 218710 in the PfPK7 ATP-binding site and red dashed lines indicate hydrogen bonds. Lower: a 2D structure of small molecule 218710. Hydrogen bonds are indicated by red hash marks, blue sigmoidal curves indicate hydrophobic interactions, and the green π/π symbol indicates pi/pi stacking interactions (Made in PyMOL).

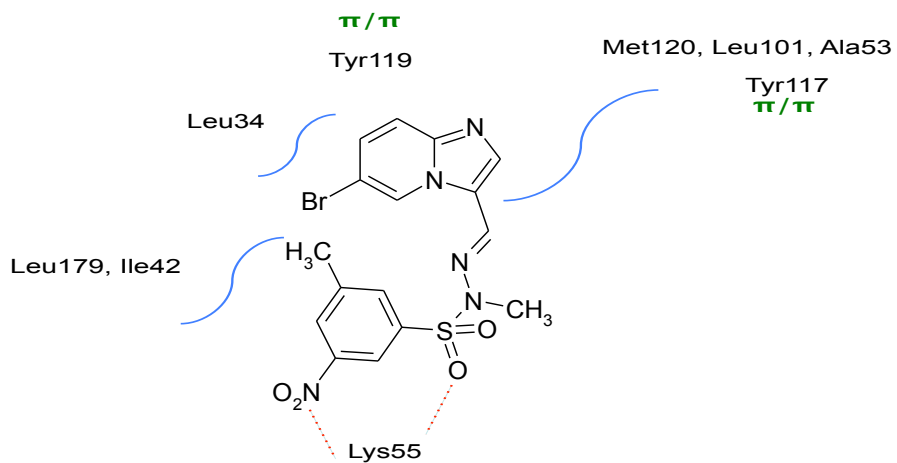
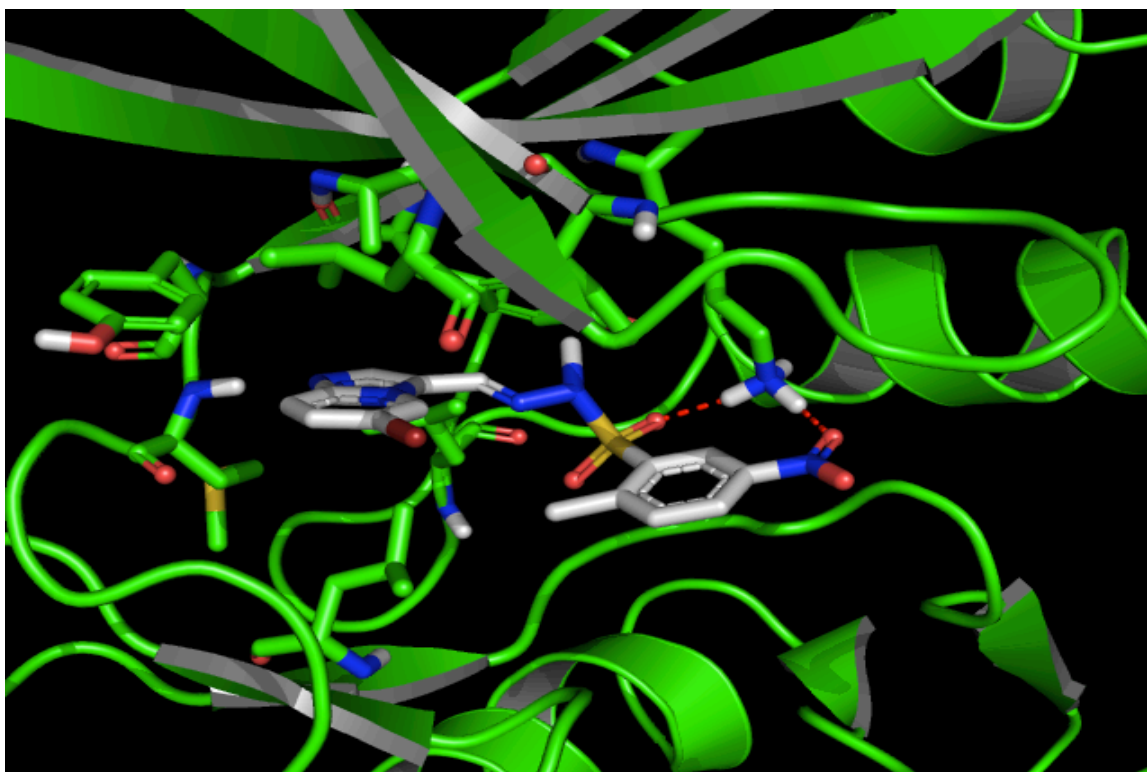


Figure 5g: 528116 in the ATP-binding site of PfPK7. Upper: a 3D representation of the small molecule 528116 in the PfPK7 ATP-binding site and red dashed lines indicate hydrogen bonds. Lower: a 2D structure of small molecule 528116. Hydrogen bonds are indicated by red hash marks, blue sigmoidal curves indicate hydrophobic interactions, and the green π/π symbol indicates pi/pi stacking interactions (Made in PyMOL).

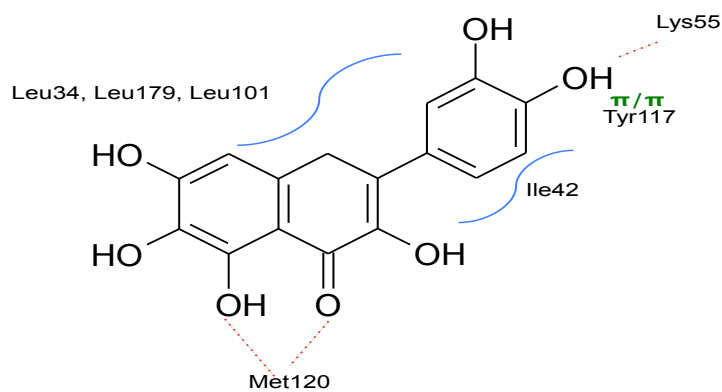
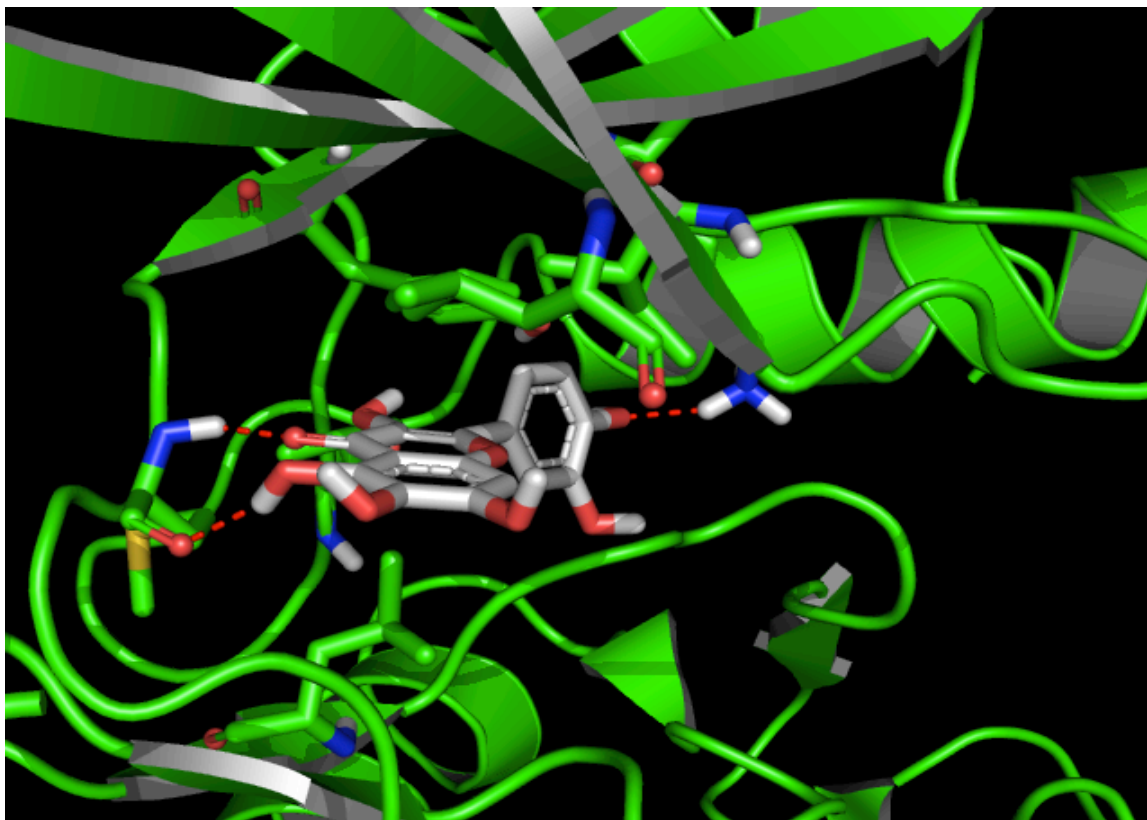


Figure 5h: 551590 in the ATP-binding site of PfPK7. Upper: a 3D representation of the small molecule 551590 in the PfPK7 ATP-binding site and red dashed lines indicate hydrogen bonds. Lower: a 2D structure of small molecule 551590. Hydrogen bonds are indicated by red hash marks, blue sigmoidal curves indicate hydrophobic interactions, and the green π/π symbol indicates pi/pi stacking interactions (Made in PyMOL).

Table 3: *Top Interactions Between PPK7 ATP-binding Site and Small Molecule Hits*. The first row lists residues and their corresponding numbers. Each following row indicates the molecular interactions that take place between the ATP-binding site of PPK7 and designated small molecules. H indicates a hydrogen bond between the corresponding residue and the small molecule, **H** indicates two hydrogen bonds between the corresponding residue and the small molecule, HI indicates presence of hydrophobic interactions between the indicated residue and the small molecule, and the π/π symbol indicates the presence of pi/pi stacking interactions between aromatic rings on the small molecule and aromatic R groups on the corresponding residue.

Compound	Leu34	Asn35	Ile42	Ala53	Lys55	Leu101	Tyr117	Glu118	Tyr119	Met120	Asp123	Ser176	Leu179	Asp190
324840	HI	H	HI	HI				π/π	HI	H			HI	
428205	HI		HI		HI			π/π	HI	H			HI	
420298	HI		HI				π/π	H		π/π	H		H	
569397	HI		HI	HI	HI		π/π	H		π/π	H		HI	
217714		H	HI		H						H		HI	H
218710					H									H
528116	HI		HI	HI	H	HI	π/π	HI	π/π	HI			HI	
551590	HI		HI		H	HI			H				HI	

Table 4: *Structural and Predicted Physicochemical Properties of PfPK7 Inhibitors*. The first column shows structures for each PfPK7 inhibitor and the second column indicates EMD compound ID numbers. The third column indicates the number of Lipinski's Rule of Five Violations (maximum is four), while the fourth column indicates LogP octanol/water partition coefficient. LogP values between -2.0 and 6.5 describe 95% of druglike molecules. The fifth column indicates LogS for aqueous solubility and 95% of druglike molecules have values between -6.5 and 0.5. Column six indicates the molecular weight. Columns seven and eight indicate predicted Caco-2 and MDCK cell permeability values reported in nm/sec. Values <25 predict poor cell permeability and values >500 predict great cell permeability. The final column indicates predicted percent human oral absorption and values >80% are high relative to 95% of druglike molecules.

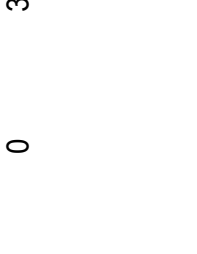
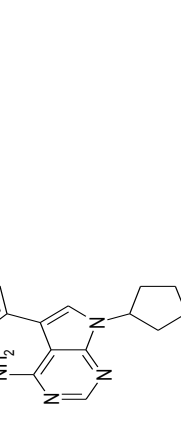
Structure	Compound	Lipinski's Rule of Five Violations	LogP for Octanol and Water	LogS for Aqueous Solubility	Molecular Weight	Caco-2 in nm/sec	MDCK in nm/sec	Percent Human Oral Absorption
	324840	0	3.48	-5.54	355.76	714	1375	100%
	428205	1	5.20	-6.67	370.45	1647	848	100%

Table 4 Continued

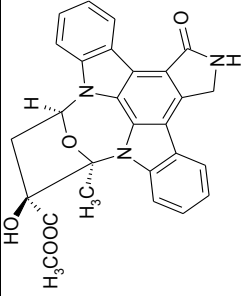
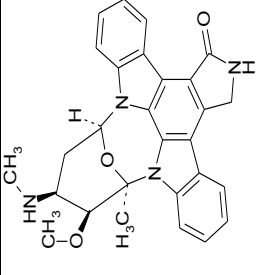
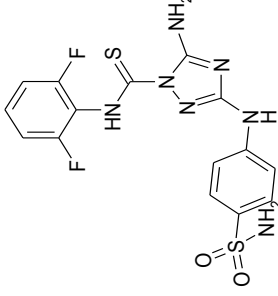
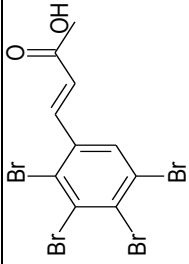
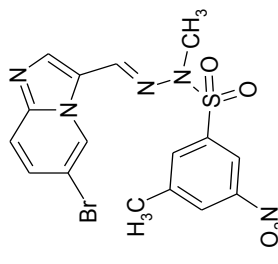
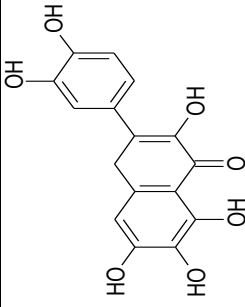
Structure	Compound	Lipinski's Rule of Five Violations	LogP for Octanol and Water	LogS for Aqueous Solubility	Molecular Weight	Caco-2 in nm/sec	MDCK in nm/sec	Percent Human Oral Absorption
	420298	0	3.94	-5.83	467.48	435	201	100%
	569397	0	3.75	-4.17	466.34	359	181	95%
	217714	1	0.703	-4.45	425.43	42	78	47%

Table 4 Continued

Structure	Compound	Lipinski's Rule of Five Violations	LogP for Octanol and Water	LogS for Aqueous Solubility	Molecular Weight	Caco-2 in nm/sec	MDCK in nm/sec	Percent Human Oral Absorption
	218710	0	3.90	-4.53	463.75	204	2681	91%
	528116	0	2.35	-3.38	452.28	145	139	80%
	551590	1	0.23	-2.49	318.24	9	3	30%

molecule is hydrophilic enough to be soluble in the aqueous environment of the body and lipophilic enough to be cell permeable. Compound 528205 was the only molecule with a LogP over five. LogS for aqueous solubility values for most drug-like molecule fall between -6.5 and 0.5. All small molecules tested were predicted to have LogS values between these numbers with the exception of 528205. The molecular weight for all compounds was below 500 Daltons and they had a wide spread of predicted cell permeability values ranging from poor to excellent. All compounds were predicted have excellent oral absorption with the exception of 217714 and 551590.

TOPKAT was used to predict small molecule toxicity values (Table 5). 218710 and 551590 were predicted to be moderate blockers of hERG K⁺ channels and only 217714 and 551590 were predicted to be mutagens. Aerobic biodegradability could not be predicted for most compounds as the structure of the compounds fell outside of the model's prediction space with the exception of 218710, which was predicted to have excellent aerobic biodegradability. Molecule 324840 was predicted to be very developmentally toxic and 428205 was predicted to be moderately developmentally toxic. Weight-of-evidence rodent carcinogenicity models predicted only small molecule 428205 would act as a carcinogen.

Discussion

Small molecule 324840 has been shown to be a potent alkynamidopyrimidine ATP competitive inhibitor of human erbB-1, erbB-2, and

Table 5: *Toxicity Predictions*. Column one depicts small molecule structures and column two indicates the EMD compound designation. Column three indicates the hERG K⁺ channel blockage value and 95% of druglike molecules have values greater than -5. Columns four, five six, and seven indicate values for Ames mutagenicity, aerobic biodegradability, developmental toxicity, and weight-of-evidence rodent carcinogenicity respectively. The last four columns are assigned a probability value between 0 and 1. Any value between 0.0 and 0.30 indicates a low probability of causing the event, values between 0.30 and 0.70 indicate an intermediate probability of causing the event, and values higher than 0.70 indicate a high probability of causing the event.

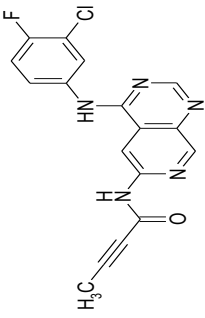
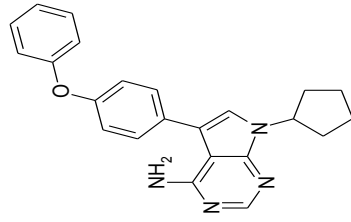
Structure	Compound	hERG K ⁺ Channel Blockage	Ames Mutagenicity	Aerobic Biodegradability	Developmental Toxicity	Weight-of- Evidence Rodent Carcinogenicity
	324840	-6.42	0.0	NA	0.90	0.0
	428205	-6.41	0.0	NA	0.35	1.0

Table 5 Continued

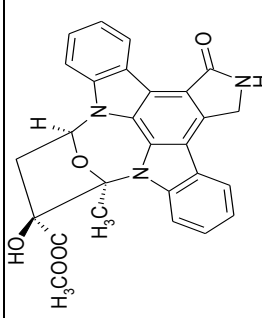
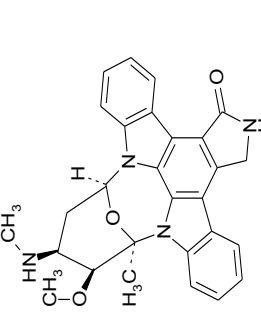
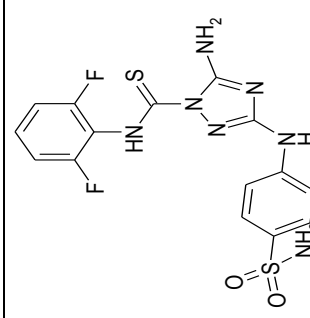
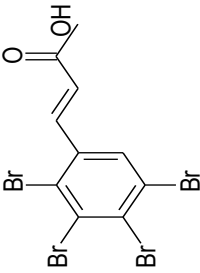
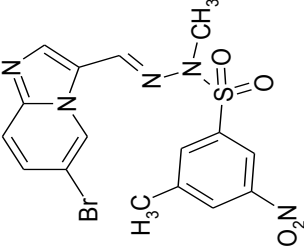
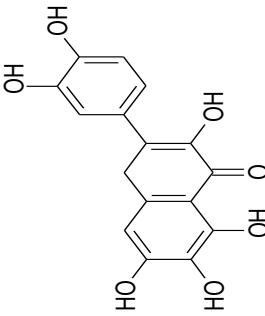
Structure	Compound	hERG K+ Channel Blockage	Ames Mutagenicity	Aerobic Biodegradability	Developmental Toxicity	Weight-of- Evidence Rodent Carcinogenicity
	420298	-5.39	0.0	NA	NA	0.0
	569397	-5.45	0.0	NA	NA	0.0
	217714	-6.34	0.0	NA	0.0	0.0

Table 5 Continued

Structure	Compound	hERG K+ Channel Blockage	Ames Mutagenicity	Aerobic Biodegradability	Developmental Toxicity	Weight-of- Evidence Rodent Carcinogenicity
	218710	-2.19	0.0	0.94	0.14	0.0
	528116	-5.01	0.0	NA	0.03	0.0
	551590	-4.81	1	NA	0.0	0.0

erbB-4 tyrosine kinase receptors with IC_{50} s in the sub nanomolar range. 324840 met all requirements for Lipinski's rule with an acceptable number of hydrogen donors and acceptors and a LogP under 5. Molecular weight was found to be 355.76 Daltons and the LogS fell within acceptable parameters indicating the small molecule would be reasonably soluble in an aqueous environment.

Additionally, 324840 was predicted to be highly cell permeable as determined by both the Caco-2 and MDCK models and percent human oral absorption was predicted to be high. Toxicity predictions revealed that the small molecule was likely to be neither mutagenic nor carcinogenic; however, the probability of developmental toxicity high and there was a slight chance the compound could act as a hERG K⁺ channel blocker and interfere with cardiac function. With an IC_{50} of almost 60 μ M, the small molecule does not possess great affinity for the PfPK7 binding site. Information from the docking study revealed that while this small molecule does form 3 hydrogen bonds with the ATP-binding site, it does not interact with the hinge region and is thus not optimally oriented to take full advantage of interactions with Tyr117 or the catalytic lysine.

Small molecule 428205 has been shown to be a pyrrolopyrimidine compound that acts as a potent and selective ATP-competitive inhibitor of human lymphocyte-specific protein tyrosine kinase, which is most highly represented in T cells. Molecule 428205 was found to violate one requirement of Lipinski's rule of five. It was found to have an acceptable number of both hydrogen bond donors and acceptors and the molecular weight was found to be 370.45 Daltons. However, LogP was predicted to be above five, which may in part explain the

predicted poor aqueous solubility as the molecule will partition more readily into a lipophilic environment. The percent human oral absorption was predicted to be high and cell permeability as predicted by both the Caco-2 and MDCK models was predicted to be high. The molecule was not predicted to be mutagenic, but was predicted to be highly carcinogenic, a HERG K⁺ channel blocker, and a developmental toxicant. Further, with an IC₅₀ of 86 μM this molecule does not have great affinity for the binding site. This lack of affinity is most likely due to the fact that its orientation within the binding site suggests only one hydrogen bond. The small molecule does form hydrophobic interactions with the leucine-rich hydrophobic pocket; however, it fails to interact with the hinge region or form pi/pi stacking interactions with Tyr117.

Small molecule 420298 has been shown to inhibit multiple human kinases including its primary target CaM kinase II. 420298 meets all requirements for Lipinski's rule of five. It has an acceptable number of both hydrogen bond donors and hydrogen bond acceptors and the molecular weight was found to be 467.48 Daltons. The aqueous solubility, LogS, was predicted to be acceptable and human percent oral absorption was predicted to be high. Additionally, the small molecule was predicted to be moderately cell permeable by the Caco-2 and MDCK models. Toxicity predictions revealed a slight probability of HERG H⁺ channel blockage, but no probability of carcinogenicity. This small molecule has affinity for the binding site with an IC₅₀ of about 2 μM. Docking studies predict the most likely orientation of this small molecule will make hydrogen bonds with residues Met120 and Glu118 in the hinge region of the kinase and form an

additional hydrogen bond with Ser176, which was an association observed in the docking of ATP as well. Further, pi/pi stacking interactions and extensive hydrophobic interaction formation all contribute to this molecule's affinity for the binding site. However, given the promiscuity of this small molecule and its size, 420298 may not make the most promising lead compound for drug design.

Small molecule 569397 is a potent ATP-competitive, promiscuous human kinase inhibitor the primary target of which is PKA. Small molecule 569397 met all requirements for Lipinski's rule of five. It has an acceptable number of hydrogen bond donors and acceptors and the molecular weight falls within the range observed for 95 % of druglike compounds at 466.34 Daltons. Aqueous solubility, LogS, and percent human oral absorption were both predicted to be high. Caco-2 and MDCK cell permeability models predicted the small molecule to be moderately cell permeable and while toxicity predictions revealed no mutagenic effects or carcinogenicity, a slight probability of HERG K⁺ channel blockage was detected. This small molecule binds to the PfPK7 ATP-binding site with a similar affinity to that of 420298 and is similar in structure. Docking studies also predict this small molecule to bind in much the same way as 420298 and similar problems with selectivity would likely occur where this small molecule to be utilized as a lead compound.

Small molecule 217714 is a triazolo-diamine and acts as a potent inhibitor of human Cdk1/cyclin B and Cdk2/Cyclin A with IC₅₀s in the picomolar range. Small molecule 217714 violated one requirement for Lipinski's rule of five with more than five hydrogen bond donors. However, the compound meets all other

requirements with hydrogen bond acceptor numbers within range and a molecular weight of 425.43 Daltons. Aqueous solubility, Log S, was within range of 95 % of all drug-like molecules and percent human oral absorption was predicted to be moderate. In addition, the small molecule was predicted to be reasonably cell permeable by both the MDCK and Caco-2 models. No probability of developmental toxicity, carcinogenicity, or mutagenicity was predicted. However, the small molecule may cause moderate hERG K⁺ channel blockage. 217714 had little affinity for the PfPK7 ATP-binding site with an IC₅₀ of 37 μM and this is most likely due to its proposed orientation within the binding site. While hydrogen bonds between the small molecule and the catalytic lysine as well as Ser176 are formed, the small molecule does not contain functional groups in close proximity to Tyr119 or Tyr117 that would allow for the formation of pi/pi stacking interactions.

Small molecule 218710 is a tetrabrominated cinnamic acid that is a potent and ATP-competitive inhibitor of human Casein Kinase II. Small molecule 218710 met all requirements for Lipinski's rule of five with hydrogen bond donor and receptor numbers within the acceptable range and a molecular weight of 463.75 Daltons. LogS predictions indicated that the molecule would be sufficiently soluble in an aqueous environment and percent human oral absorption was predicted to be excellent. Cell permeability models predicted moderate to excellent cell permeability and no probability of carcinogenicity, mutagenicity, or developmental toxicity were found using toxicity modeling equations. A slight chance of hERG K⁺ channel probability was detected. This

molecule also showed little affinity for the binding site, which is in part explained by how 218710 is oriented in the binding site. Hydrogen bonds are formed at Lys55 and Asp190; however, the small molecule fails to take advantage of the hydrophobic pocket or pi/pi stacking interactions with residues possessing aromatic R groups.

Small molecule 528116 is a imidazopyridine molecule, ATP-competitive and capable of acting as a potent inhibitor of human proteins from the phosphatidylinositol 3-kinase-related kinase family. Compound 528116 meets all requirements for Lipinski's rule of five and has acceptable numbers of hydrogen bond donors and acceptors. Molecular weight was well within the desired range at 452.28 and LogP was 2.35. The molecule was predicted to have adequate aqueous solubility as well as percent human oral absorption. Additionally, 528116 was only moderately cell permeable, however toxicity models indicated little to no probability of hERG K⁺ channel blockage, mutagenicity, carcinogenicity or developmental toxicity. 528116 was the most promising small molecule inhibitor of PfPK7 that was identified in the screen with an IC₅₀ in the nanomolar range. The compound formed a hydrogen bond with the catalytic lysine in the binding pocket and made extensive hydrophobic interactions with the leucine-rich hydrophobic pocket. While it did not form hydrogen bonds with the hinge region residues, it was oriented such that slight modification would allow for such an interaction. The NO₂ functional group is of concern as this functional group tends to form covalent bonds with interacting residues. However, future testing of 528116 analogs without this functional group would

determine whether its presence is necessary to preserve compound affinity. Unfortunately, small molecule analogs for this compound are not commercially available and would have to be synthesized before testing which would be cost prohibitive

Small molecule 551590 is a flavanol molecule that is ATP- competitive and has selective inhibitor activity against PIM1 kinase. This small molecule violates 1 of Lipinski's rule of five with more than five hydrogen bond donors. LogP and LogS value both fall within acceptable parameters and the molecule is relatively small compared with the other analyzed small molecules with a molecular weight of 318.24 Daltons. Both cell permeability and percent human oral absorption were predicted to be poor and the Ames Mutagenicity model indicated a strong probability that the compound would act as a mutagen. However, the small molecule was not predicted to be a hERG K⁺ channel blocker, a developmental toxicant or a carcinogen. This compound had moderate affinity for the PfPK7 ATP-binding site with an IC₅₀ around 12 μM. Within the binding site, the molecule made hydrogen bonds with both Met120 and Lys55 as well as established hydrophobic interactions with the hydrophobic pocket. However, the molecule did not hydrogen bond with Glu118 in the hinge region and while pi/pi stacking interactions were likely with Tyr117, the molecule was not oriented to interact with Tyr119.

Several small molecules from the kinase inhibitor-focused libraries were able to inhibit PfPK7 in low molar concentrations. In recent years, researchers have found that PfPK7 inhibitors are particularly difficult to pinpoint because the

gatekeeper residue, behind which resides a hydrophobic pocket, is a bulky tyrosine which effectively prohibits small molecules from reaching and interacting with this site in the pocket [231]. It may prove difficult to find a compound with great affinity for the binding site given this bulky impediment. Further, small molecule analogs for the eight small molecule hits from this screen were not commercially available and thus a structure-activity relationship could not be established; however the docking studies were able to indicate favorable interactions which could inform future drug discovery efforts aimed at selectively inhibiting this protein.

CHAPTER IV
SCREEN OF KINASE INHIBITORS AGAINST
PLASMODIUM FALCIPARUM STRAIN
W2 BLOOD STAGES

Introduction

Luminescence assays are able to determine the affinity of ATP-competitive small molecules for the binding site of their intended target, but they depend upon recombinant protein from the organism of interest and are carried out in controlled conditions different from the normal environment in which the organism resides. Small molecules that are able to inhibit the protein of interest may however, not make ideal lead compounds if they are not able to inhibit cell growth or development within the organism from which the target originated. Once small molecules that bind to the intended target with high affinity are identified, it is then necessary to determine the affect of those small molecules on parasite growth.

Human malaria disease symptoms are caused by a depletion of human red blood cells and the immune response elicited by infection with malaria parasites. These symptoms are a direct result of parasite propagation within human red blood cells and it is for this reason that we chose to target a kinase that is expressed during these stages of parasite growth. After identifying several compounds that were able to inhibit our intended target, PfPK7, we

next had to determine if small molecule kinase inhibitors were able to inhibit parasite growth in blood stage cultures of *P. falciparum* strain W2.

The traditional method of measuring *in vitro* growth of *Plasmodium* species blood stage cultures is the [³H] hypoxanthine incorporation assay, which was described by Chulay et al. in 1982 [232]. This assay relies upon the increased uptake of tritiated hypoxanthine by parasites. A direct relationship was found between increasing incorporation of the radioactive isotope and increasing parasite numbers. The radioisotope method was a vast improvement over previous parasite growth estimation methods, which involved the tedious counting of Giemsa-stained slides to estimate parasitemia. The [³H] hypoxanthine method was also found to be highly sensitive and reproducible. However, the use of radioactive reagents necessary for this procedure drastically limited the number of laboratories able to conduct the [³H] hypoxanthine parasite growth assay to those approved for use and able to dispose of radioactive substances. Radioisotope assays are both expensive and time consuming to carry out. In addition, the caustic components of the assay pose potential health risks to researchers performing the technique.

In 2004, Bennett et al. described a *Plasmodium* blood stage growth detection method that utilized a DNA-binding fluorophore to estimate parasite growth in place of the traditional radioisotope method [233, 234]. SYBR Green I is a dye that intercalates with DNA, prefers G and C base pairs, and preferentially binds to double stranded DNA over single stranded DNA or RNA. The broad excitation and emission spectra of this DNA-binding dye make it a

very versatile option for the development of assays to quantify DNA. As human red blood cells contain neither DNA nor RNA, the application of SYBR Green I to infected red blood cells that have been lysed with an appropriate agent allows for the quantification of only parasitic DNA. Since its introduction, the SYBR Green I parasite growth assay has been continuously validated. One study comparing known antimalarial IC₅₀ values that were determined with both the traditional radioisotope method and the SYBR Green I method found that the values resulting from the SYBR Green I growth assay were comparable to the values resulting from the [³H] hypoxanthine incorporation assay [234]. In addition, reliable IC₅₀ values were able to be determined in less time, at a lower cost, and without the hazard of handling radioactive materials. Since its validation, the SYBR Green I parasite growth assay has been used to track developing resistance to current antimalarials and to screen small molecules and naturally occurring compounds for potential antimalarial activity [235-237].

We conducted a preliminary screen of three kinase inhibitor-focused libraries against *P. falciparum* strain W2 using the SYBR Green I parasite growth assay to determine if these compounds had the ability to inhibit intraerythrocytic parasite growth. All compounds were screened in triplicate at 1 μM and percent inhibition was calculated. In addition, small molecules that were determined to be inhibitors of the parasitic kinase PfPK7 were further tested to determine IC₅₀ values for the compounds. The overall objective of the kinase inhibitor screen was to determine if the small molecules represented

in the three libraries were able to attenuate parasitic growth and to see whether or not previously identified small molecule inhibitors of PfPK7 were among the compounds able to inhibit parasite growth.

Results

The three EMD kinase libraries contained small molecules that had been previously characterized. Data regarding any human targets of the compounds as well as preliminary cytotoxicity data was known for most compounds. However, these small molecules had not yet been tested against *P. falciparum* blood stage cultures. The initial screen of three kinase inhibitor-focused libraries containing 244 small molecules yielded 22 small molecules that were able to inhibit greater than 75 percent of intraerythrocytic parasite growth at 1 μ M. Mean percent inhibition and standard deviations were calculated for all compounds at 1 μ M (Table 6).

Following the initial screen of these molecules, the PfPK7 luminescence assays were performed to determine which of the molecules were able to inhibit this protein in low molar concentrations. Out of the 244 small molecules contained in the libraries, 8 compounds displayed inhibitory activity against the protein. These eight molecules were then tested against the parasite in order to determine the IC₅₀ in blood stage cultures. The assays were performed in triplicate and each compound was tested three times. The IC₅₀ concentrations for each small molecule were calculated using GraphPad Prism (Version 5)

Table 6: *Structure of Hits from EMD Kinase Library Screen Against P. falciparum Strain W2.* The first column indicates the small molecule number and the second column contains the structures of each compound. The third column is the mean percent inhibition for each compound at 1 μ M.

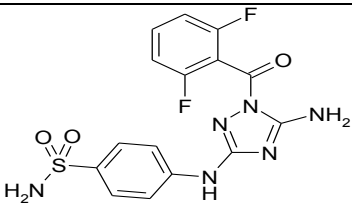
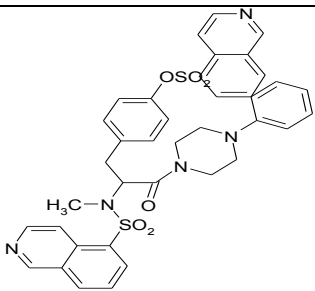
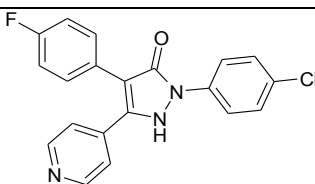
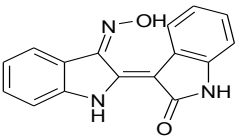
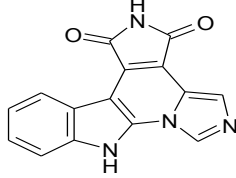
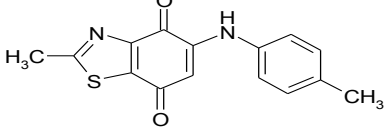
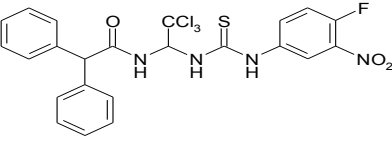
<i>Compound</i>	<i>Structure</i>	<i>Mean Percent Inhibition and Standard Deviation at 1 μM</i>
189406		79.6 \pm 2.8
422706		78.4 \pm 3.2
506126		77.3 \pm 1.9
402085		83.3 \pm 2.1
371957		76.7 \pm 1.8
219478		79.8 \pm 5.3
118501		81.8 \pm 3.1
341251	Not Available	92.4 \pm 2.5

Table 6 Continued

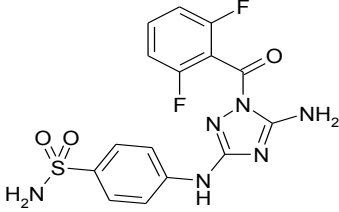
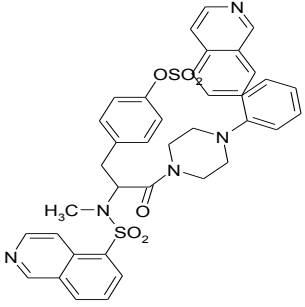
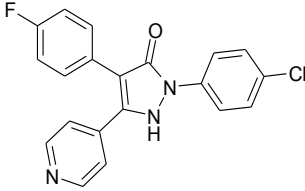
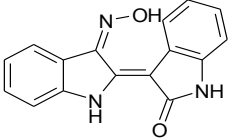
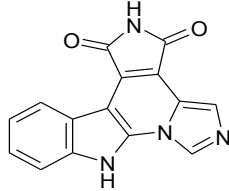
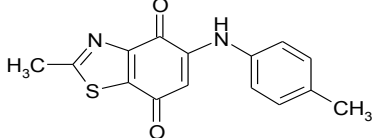
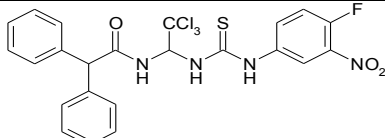
<i>Compound</i>	<i>Structure</i>	<i>Mean Percent Inhibition and Standard Deviation at 1 μM</i>
189406		79.6 \pm 2.8
422706		78.4 \pm 3.2
506126		77.3 \pm 1.9
402085		83.3 \pm 2.1
371957		76.7 \pm 1.8
219478		79.8 \pm 5.3
118501		81.8 \pm 3.1
341251	Not Available	92.4 \pm 2.5

Table 6 Continued

Compound	Structure	Mean Percent Inhibition and Standard Deviation at 1 μM
124029		75.2 \pm 1.9
365252		88.9 (500 μM) \pm 0.9
218713		78.3 \pm 5.4
203294		75.4 \pm 3.1
665203	Not Available	77.2 \pm 2.7
401486		76.1 \pm 1.1
420298		76.7 \pm 2.3

(Table 7). Small molecules 324840, 428205, 217714 and 218710 displayed weak to no inhibitory activity against *P. falciparum* blood stage parasites as indicated by SYBR Green I growth assay IC₅₀ values greater than 100 µM. 551590 was also a weak inhibitor of parasite growth and 420298, 569397, and 528116 displayed similar activities against the parasite.

Discussion

The screen of 244 inhibitors from EMD kinase libraries I, II, and III revealed 22 molecules that were able to inhibit blood stage growth of *P. falciparum* strain W2 blood stage culture at 1 µM. Interestingly, 11 of these molecules have a similar core structure and thus may bind to the same macromolecule within the parasite. Small molecules 203294, 365252, 361553, 420298, 402085, 371957, 402081, 361550, 361551, 402086, and 361556 possess an indirubin-like core structure. These molecules can be further subdivided into 402085, 402081, 361550, 361551, 402086, and 361556 which maintain the true indirubin core structure and all act as inhibitors of Cdk2/cyclin A, Cdk1/cyclin B, and GSK-3 isoforms. The remaining small molecules from this group, 203294, 365252, 361553, 420298, and 371957 are more similar in structure to the CDK inhibitor staurosporine and are inhibitors of human PKC, PKA, and GSK-3. Future studies aimed at determining the IC₅₀ values of these compounds and identifying their *in vivo* target may be fruitful as they could potentially yield a new drug target for antimalarial drug development researchers.

Table 7. IC_{50} Concentrations for PfPK7 Inhibitors in SYBR Green I Assay. Column one contains the compound name and column two indicates the structure of each compound. Column three contains the IC_{50} molar concentration for each PfPK7 inhibitor in the SYBR Green I Assay.

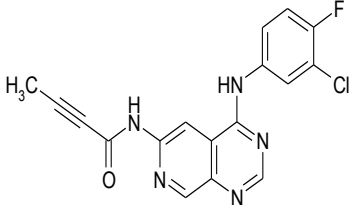
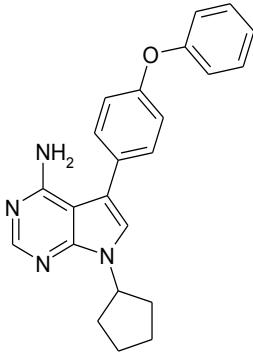
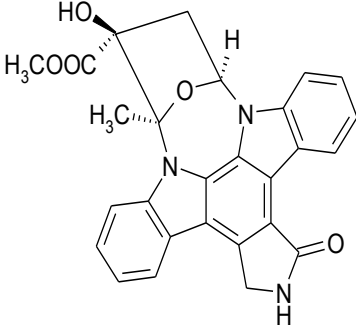
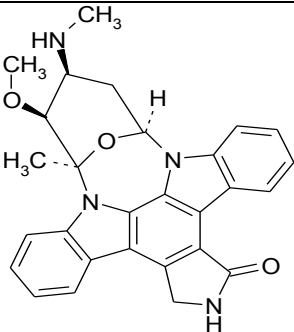
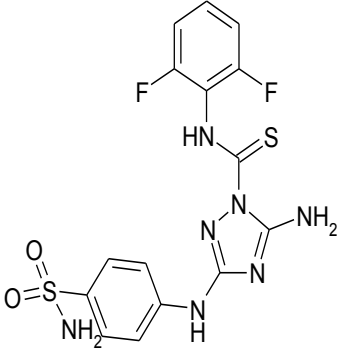
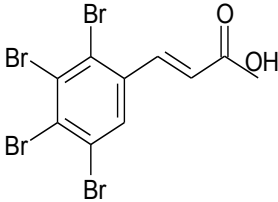
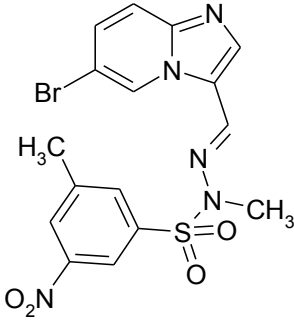
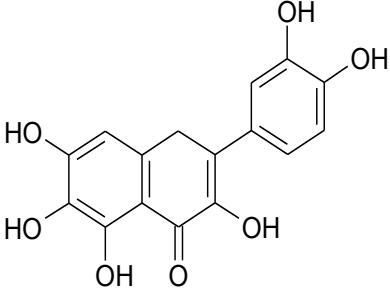
Compound	Structure	IC_{50} Concentration for PfPK7 Inhibitors in SYBR Green I Assay
324840		$>1.0e-4$
428205		$>1.0e-4$
420298		$1.08e-5 \pm 2.65e-6$
569397		$8.39e-6 \pm 6.58e-6$

Table 7 Continued

Compound	Structure	<i>IC</i> ₅₀ Concentration for PfPK7 Inhibitors in SYBR Green I Assay
217714		>1.0e-4
218710		>1.0e-4
528116		1.59e-5 ± 4.88e-6
551590		8.98e-5 ± 1.28e-5

Small molecules 324840, 428205, 217714, and 218710 were not able to efficiently inhibit intraerythrocytic development of blood stage *P. falciparum* with SYBR Green I IC50 values above 100 μ M. Molecule 324840 was predicted to be both soluble in an aqueous environment and cell permeable, but its overall affinity for the PfPK7 binding site was low and this could partially explain its failure to affect parasite growth. Conversely, 428205 had a LogP above five and was predicted to have poor aqueous solubility and these qualities could indicate this molecule is not able to function in an aqueous and hydrophilic environment such as the parasite cytoplasm. Compounds 217714 and 218710 were predicted to have adequate pharmacokinetic properties. The failure of small molecules to inhibit the protein may be due to activation of efflux pumps, which shuttle small molecules out of cellular compartments before they can reach their intended targets or perhaps to metabolism of the compounds into biologically inactive forms. 551590 was a weak inhibitor of parasite growth and this may be due to the predicted poor cell permeability of this molecule in both Caco-2 and MDCK models. Three PfPK7 inhibitor molecules were able to inhibit parasite growth; 528116, 420298, and 569397. The inhibitory activity of these small molecules on blood stage cultures of *P. falciparum* could have been due in part to the inhibition of PfPK7 as these molecules had the highest affinity for the binding site in luminescence assays; however, given the noted promiscuity of 420298 and 569397 as well as the NO₂ group of 528116, it is also likely that the inhibitory effects of these proteins on the parasite are due to off target effects.

CHAPTER V
TREATMENT OF *P. FALCIPARUM* BLOOD
STAGE CULTURES WITH
PURVALANOL B

Introduction

Since the sequencing of the *P. falciparum* genome and the initial characterization of the proteome in 2002, several studies have used molecular techniques aimed at further elucidating the similarities and differences between *Plasmodium* proteins and well-characterized proteins from other organisms. In recent years with the advent of increasingly accessible and sensitive methodology, analysis of mixed protein samples that identify hundreds of proteins at a time has become possible. Instead of characterizing the function of one protein in isolation, researchers may now begin to determine the affect that change in the cellular environment has on the entire proteomic complement of a given cell type using techniques that are able to resolve individual proteins in complex protein mixtures.

These increasingly sensitive techniques have been used to characterize the *P. falciparum* life cycle and to pinpoint several proteins that are specific for each stage of development within the parasite [210]. Similarly, potential vaccine candidates have been identified by profiling parasite isolates during crucial stages of parasite development and determining those proteins present in abundance [238].

These techniques are also able to determine relative changes in abundance between wildtype parasite and parasites that have been subjected to some environmental change such as drug challenge. MudPIT or similar complex sample analysis techniques have been used to characterize changes in *P. falciparum* protein complement that result from challenge with such antimalarials as pyrimethamine, tetracycline, chloroquine, and artemisinin [239, 240]. This large-scale approach has the benefit of characterizing the effect of drug application on many proteins in an organism at a time. Given *P. falciparum* parasite propensity to develop rapid resistance to applied drugs, it is advantageous to determine any changes in protein expression as a result of compound application. By looking at changes in protein complement, we may be able to predict resistance development before it occurs or perhaps develop strategies to stave off the effects of waning drug efficacy. Though this strategy has been applied to determine effects of many antimalarial drugs on protein expression, to date no experiment has been performed to characterize the effect of kinase inhibitors on *P. falciparum* intraerythrocytic growth.

The kinase inhibitor Purvalanol B has been shown to inhibit function of *P. falciparum* kinases including those necessary for the completion of the intraerythrocytic life cycle such as PfPK5 and PfCK1 [133, 241]. In fact an experiment using proteins isolated from *P. falciparum* culture lysates showed that when fractionated lysates were applied to a column containing immobilized Purvalanol B, the only visible band from a gel of the resulting eluent was PfCK1 [241]. However, it is important to note that given the concentration of inhibitor

applied to treatment cultures, it is likely that the small molecule affected more than one protein during the incubation period.

We incubated blood stage cultures of *P.falciparum* strain W2 with the CDK inhibitor Purvalanol B during 25-36 hpi and following inhibitor incubation, cultures were lysed and proteins were extracted. Soluble fractions were digested with trypsin and sent for analysis. Giemsa-stained slides were used to determine the ability of parasites to proceed through schizogony and a shotgun proteomics approach was used to determine relative differences in protein expression between wildtype and Purvalanol B-treated parasites.

Results

Giemsa-stained slides analyzed before inhibitor treatment indicated all parasite cultures contained approximately 6% parasitized RBCs and were composed of >90% trophozoite parasites with one nucleus (approximately 25 hpi) prior to treatment with Purvalanol B. Student t-test analysis of parasitemia counts from post-treatment slides indicated no significant change in parasitemia during the 12 hour Purvalanol B exposure period in any of the culture flasks ($p=0.7966$). However, parasite stage differences were observed between the treatment groups and those treated only with DMSO vehicle (Figure 6). While control cultures were composed of mostly multinucleated cells, the inhibitor-treated cultures contained predominantly parasites with only one nucleus. A student t-test revealed a significant difference in the number of cells that were able to form multiple nuclei between the control and inhibitor-treated cultures ($p=.00006$).

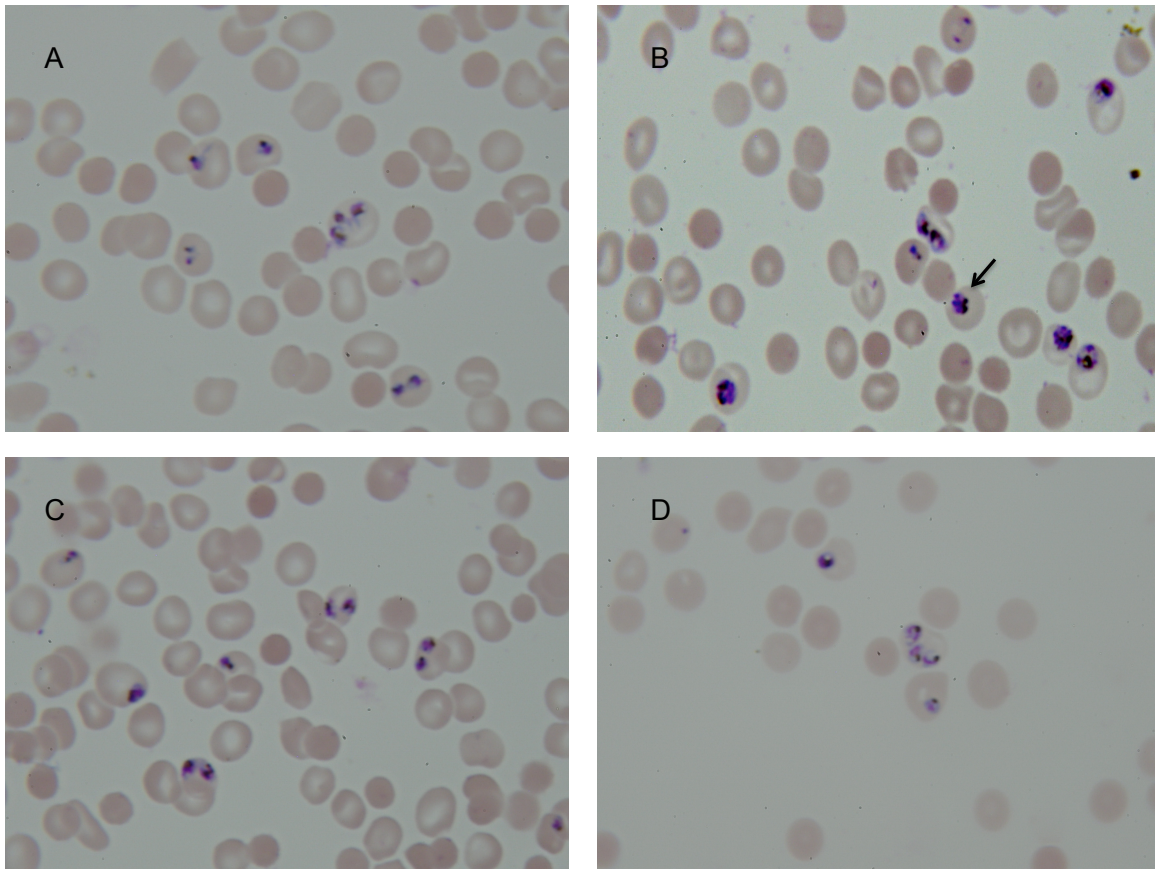


Figure 6: Control and Purvalanol B-Treated Parasites Before and After Inhibitor Application. A. representative image of cultured control parasitized RBCs prior to treatment with Purvalanol B; B. representative image of cultured control parasitized RBCs after the 12 hour treatment period. The arrow is pointing to multinucleated cells. C. parasitized RBCs from a treatment flask prior to treatment with Purvalanol B; D. is an image of parasitized RBCs 12 hours after Purvalanol B application. All slides were stained with Giemsa stain.

Of the six samples analyzed using MudPIT, three were control group biological replicates and three were Purvalanol B-treated biological replicates. A total of 52038 *P. falciparum* spectra and 25506 human spectra were identified. Peptide threshold of 95 % and decoy false discovery rate of 0.08 % and 0.01 % for *P. falciparum* and human respectively were used for the Mascot search. With a protein threshold of 99% and a minimum of two unique peptides found per

protein, the 52038 spectra identified in the *P. falciparum* Mascot search corresponded to 518 *P. falciparum* proteins among the six samples (Appendix A). The same parameters were used in the human Mascot search and the 25506 spectra were assigned to 76 human proteins (Appendix B) among the six samples. Of 518 protein identifications from the *P. falciparum* search, 414 proteins were found both in control and treatment samples (Figure 7). 57 proteins were found only in the treatment samples (Table 8), and 47 proteins were found only in the control samples (Table 9).

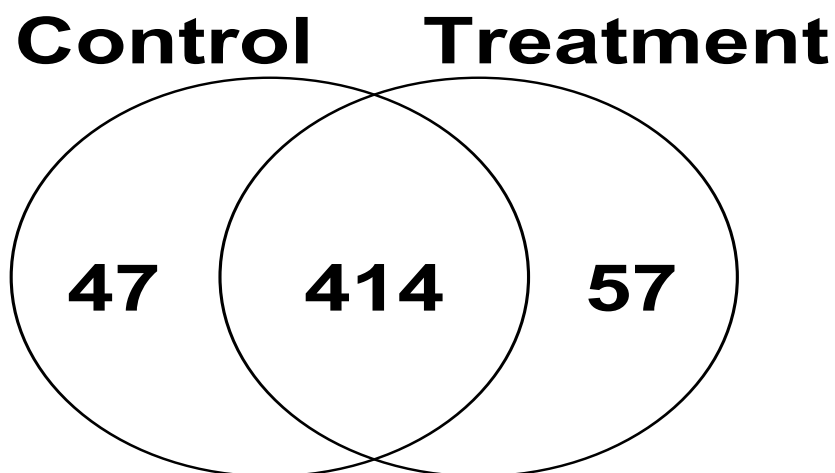


Figure 7: Number of Proteins in Control and Purvalanol B-treated Samples. Left indicates the number of proteins found only in control samples, while right indicates the number of proteins found only in treatment samples. The intersection indicates the number of proteins common to both sample types.

Table 8: *Proteins in Only P. falciparum Control Samples*. Column one provides the protein name and column two the accession number of each protein. Any identifications made from the reverse concatenated database are not represented.

<i>Protein</i>	<i>Accession Number</i>
Putative uncharacterized protein OS=Plasmodium falciparum (isolate 3D7) GN=MAL8P1.103 PE=4 SV=1	C0H4U0_PLAF7
Conserved Plasmodium protein OS=Plasmodium falciparum (isolate 3D7) GN=PFL2120w PE=4 SV=1	Q8I4Y9_PLAF7
Putative uncharacterized protein OS=Plasmodium falciparum (isolate 3D7) GN=PFE1465w PE=4 SV=1	C0H4G7_PLAF7
DNA repair protein, putative OS=Plasmodium falciparum (isolate 3D7) GN=PFE0270c PE=3 SV=1	Q8I447_PLAF7
Histidine--tRNA ligase, putative OS=Plasmodium falciparum (isolate 3D7) GN=PF14_0428 PE=4 SV=1	Q8IL22_PLAF7
40S ribosomal protein S28e, putative OS=Plasmodium falciparum (isolate 3D7) GN=PF14_0585 PE=4 SV=1	Q8IKL9_PLAF7
10b antigen, putative OS=Plasmodium falciparum (isolate 3D7) GN=PF10_0213 PE=4 SV=1	Q8IJI4_PLAF7
Ubiquitination-mediated degradation component, putative OS=Plasmodium falciparum (isolate 3D7) GN=PF08_0020 PE=4 SV=1	C0H4Y0_PLAF7
Putative uncharacterized protein OS=Plasmodium falciparum (isolate 3D7) GN=PF07_0016 PE=4 SV=1	Q8IC27_PLAF7
Vacuolar ATP synthase subunit E, putative OS=Plasmodium falciparum (isolate 3D7) GN=PF11670c PE=3 SV=2	Q8I2H3_PLAF7
V-type ATPase, subunit C, putative OS=Plasmodium falciparum (isolate 3D7) GN=PFA_0300c PE=4 SV=1	Q8I280_PLAF7
Arginyl-tRNA synthetase, putative OS=Plasmodium falciparum (isolate 3D7) GN=PFL0900c PE=3 SV=1	Q8I5M2_PLAF7
Conserved Plasmodium protein OS=Plasmodium falciparum (isolate 3D7) GN=PF11_0332 PE=4 SV=1	Q8II42_PLAF7
Putative uncharacterized protein OS=Plasmodium falciparum (isolate 3D7) GN=PFE0990w PE=4 SV=1	C0H4F1_PLAF7
Proteasome, putative OS=Plasmodium falciparum (isolate 3D7) GN=PF11545c PE=4 SV=1	Q8I0U7_PLAF7
DNA-directed RNA polymerase OS=Plasmodium falciparum (isolate 3D7) GN=PFC0805w PE=3 SV=1	O77375_PLAF7
P-type calcium transporting ATPase OS=Plasmodium falciparum GN=serca PE=3 SV=1	E1CC54_PLAFA
60S ribosomal protein L23a, putative OS=Plasmodium falciparum (isolate 3D7) GN=PF13_0132 PE=3 SV=1	Q8IE82_PLAF7
Coatomer alpha subunit, putative OS=Plasmodium falciparum (isolate 3D7) GN=PFF0330w PE=4 SV=1	C6KSR5_PLAF7
Pfmdr2 protein OS=Plasmodium falciparum GN=pfmdr2 PE=3 SV=1	Q25693_PLAFA
60S ribosomal protein L14, putative OS=Plasmodium falciparum (isolate 3D7) GN=PF14_0296 PE=4 SV=1	Q8ILE8_PLAF7

Table 8 Continued

<i>Protein</i>	<i>Accession Number</i>
Heat shock protein 90, putative OS=Plasmodium falciparum (isolate 3D7) GN=PF11_0188 PE=3 SV=1	Q8III6_PLAF7
ORF 2 protein (Fragment) OS=Plasmodium falciparum GN=ORF 2 PE=2 SV=1	Q02602_PLAFA
Ring-exported protein 1 OS=Plasmodium falciparum (isolate 3D7) GN=REX1 PE=4 SV=1	Q8I2G1_PLAF7
40S ribosomal protein S24 OS=Plasmodium falciparum (isolate 3D7) GN=PFE0975c PE=3 SV=1	Q8I3R6_PLAF7
Glutamate--cysteine ligase (Gamma-glutamylcysteine synthetase) OS=Plasmodium falciparum GN=GCS PE=2 SV=1	Q9TY17_PLAFA
Activator of Hsp90 ATPase homolog 1-like protein, putative OS=Plasmodium falciparum (isolate 3D7) GN=PFC0360w PE=4 SV=2	O97256_PLAF7
Ubiquitin conjugating enzyme E2, putative OS=Plasmodium falciparum (isolate 3D7) GN=PFL0190w PE=3 SV=1	Q8I607_PLAF7
Coatamer protein, beta subunit, putative OS=Plasmodium falciparum (isolate 3D7) GN=PF14_0277 PE=4 SV=2	Q8ILG6_PLAF7
Putative uncharacterized protein OS=Plasmodium falciparum (isolate 3D7) GN=MAL8P1.62 PE=4 SV=1	Q8IB31_PLAF7
60S ribosomal protein L36 OS=Plasmodium falciparum (isolate 3D7) GN=PF11_0106 PE=3 SV=2	Q8I713_PLAF7
Serine rich protein homologue OS=Plasmodium falciparum PE=3 SV=1	Q26015_PLAFA
6-cysteine protein, putative OS=Plasmodium falciparum (isolate 3D7) GN=Pf41 PE=4 SV=1	Q8I1Y0_PLAF7
DNA replication licensing factor mcm7 homologue, putative OS=Plasmodium falciparum (isolate 3D7) GN=PF07_0023 PE=3 SV=1	Q8IC16_PLAF7
Rab2, GTPase OS=Plasmodium falciparum (isolate 3D7) GN=Rab2 PE=3 SV=1	Q8I5A9_PLAF7
Cytidine triphosphate synthetase OS=Plasmodium falciparum (isolate 3D7) GN=PF14_0100 PE=4 SV=1	Q8ILZ3_PLAF7
Ubiquitin carboxyl-terminal hydrolase OS=Plasmodium falciparum (isolate 3D7) GN=PFE1355c PE=3 SV=1	Q8I3J3_PLAF7
Glycogen synthase kinase 3 OS=Plasmodium falciparum (isolate 3D7) GN=PfGSK-3 PE=4 SV=2	O77344_PLAF7
Acetyl-CoA synthetase OS=Plasmodium falciparum (isolate 3D7) GN=PFF1350c PE=4 SV=1	C6KTB4_PLAF7
DNAJ protein, putative OS=Plasmodium falciparum (isolate 3D7) GN=PF08_0032 PE=4 SV=1	Q8IB72_PLAF7
DNA topoisomerase 2 OS=Plasmodium falciparum (isolate 3D7) GN=PF14_0316 PE=3 SV=1	Q8ILC8_PLAF7
Conserved Plasmodium protein OS=Plasmodium falciparum (isolate 3D7) GN=PFL0895c PE=4 SV=1	Q8I5M3_PLAF7

Table 8 Continued

<i>Protein</i>	<i>Accession Number</i>
Putative uncharacterized protein OS=Plasmodium falciparum (isolate 3D7) GN=MAL8P1.103 PE=4 SV=1	C0H4U0_PLAF7
Conserved Plasmodium protein OS=Plasmodium falciparum (isolate 3D7) GN=PFL2120w PE=4 SV=1	Q8I4Y9_PLAF7
Putative uncharacterized protein OS=Plasmodium falciparum (isolate 3D7) GN=PFE1465w PE=4 SV=1	C0H4G7_PLAF7
DNA repair protein, putative OS=Plasmodium falciparum (isolate 3D7) GN=PFE0270c PE=3 SV=1	Q8I447_PLAF7
Histidine--tRNA ligase, putative OS=Plasmodium falciparum (isolate 3D7) GN=PF14_0428 PE=4 SV=1	Q8IL22_PLAF7
40S ribosomal protein S28e, putative OS=Plasmodium falciparum (isolate 3D7) GN=PF14_0585 PE=4 SV=1	Q8IKL9_PLAF7
10b antigen, putative OS=Plasmodium falciparum (isolate 3D7) GN=PF10_0213 PE=4 SV=1	Q8IJI4_PLAF7
Ubiquitination-mediated degradation component, putative OS=Plasmodium falciparum (isolate 3D7) GN=PF08_0020 PE=4 SV=1	C0H4Y0_PLAF7
Putative uncharacterized protein OS=Plasmodium falciparum (isolate 3D7) GN=PF07_0016 PE=4 SV=1	Q8IC27_PLAF7
Vacuolar ATP synthase subunit E, putative OS=Plasmodium falciparum (isolate 3D7) GN=PF11670c PE=3 SV=2	Q8I2H3_PLAF7
V-type ATPase, subunit C, putative OS=Plasmodium falciparum (isolate 3D7) GN=PFA_0300c PE=4 SV=1	Q8I280_PLAF7
Arginyl-tRNA synthetase, putative OS=Plasmodium falciparum (isolate 3D7) GN=PFL0900c PE=3 SV=1	Q8I5M2_PLAF7
Conserved Plasmodium protein OS=Plasmodium falciparum (isolate 3D7) GN=PF11_0332 PE=4 SV=1	Q8II42_PLAF7
Putative uncharacterized protein OS=Plasmodium falciparum (isolate 3D7) GN=PFE0990w PE=4 SV=1	C0H4F1_PLAF7
Proteasome, putative OS=Plasmodium falciparum (isolate 3D7) GN=PFI1545c PE=4 SV=1	Q8I0U7_PLAF7
DNA-directed RNA polymerase OS=Plasmodium falciparum (isolate 3D7) GN=PFC0805w PE=3 SV=1	O77375_PLAF7
P-type calcium transporting ATPase OS=Plasmodium falciparum GN=serca PE=3 SV=1	E1CC54_PLAFA
60S ribosomal protein L23a, putative OS=Plasmodium falciparum (isolate 3D7) GN=PF13_0132 PE=3 SV=1	Q8IE82_PLAF7
Coatmer alpha subunit, putative OS=Plasmodium falciparum (isolate 3D7) GN=PFF0330w PE=4 SV=1	C6KSR5_PLAF7
Pfmdr2 protein OS=Plasmodium falciparum GN=pfmdr2 PE=3 SV=1	Q25693_PLAFA
60S ribosomal protein L14, putative OS=Plasmodium falciparum (isolate 3D7) GN=PF14_0296 PE=4 SV=1	Q8ILE8_PLAF7

Table 9: *Proteins Only in P. falciparum Treatment Samples*. Column one provides the protein name and column two the accession number for each protein. Any identifications made from the reverse concatenated database are not represented.

<i>Protein</i>	<i>Accession Number</i>
Putative uncharacterized protein OS=Plasmodium falciparum (isolate 3D7) GN=MAL8P1.103 PE=4 SV=1	C0H4U0_PLAF7
Conserved Plasmodium protein OS=Plasmodium falciparum (isolate 3D7) GN=PFL2120w PE=4 SV=1	Q8I4Y9_PLAF7
Putative uncharacterized protein OS=Plasmodium falciparum (isolate 3D7) GN=PFE1465w PE=4 SV=1	C0H4G7_PLAF7
DNA repair protein, putative OS=Plasmodium falciparum (isolate 3D7) GN=PFE0270c PE=3 SV=1	Q8I447_PLAF7
Histidine--tRNA ligase, putative OS=Plasmodium falciparum (isolate 3D7) GN=PF14_0428 PE=4 SV=1	Q8IL22_PLAF7
40S ribosomal protein S28e, putative OS=Plasmodium falciparum (isolate 3D7) GN=PF14_0585 PE=4 SV=1	Q8IKL9_PLAF7
10b antigen, putative OS=Plasmodium falciparum (isolate 3D7) GN=PF10_0213 PE=4 SV=1	Q8IJI4_PLAF7
Ubiquitination-mediated degradation component, putative OS=Plasmodium falciparum (isolate 3D7) GN=PF08_0020 PE=4 SV=1	C0H4Y0_PLAF7
Putative uncharacterized protein OS=Plasmodium falciparum (isolate 3D7) GN=PF07_0016 PE=4 SV=1	Q8IC27_PLAF7
Vacuolar ATP synthase subunit E, putative OS=Plasmodium falciparum (isolate 3D7) GN=PFI1670c PE=3 SV=2	Q8I2H3_PLAF7
V-type ATPase, subunit C, putative OS=Plasmodium falciparum (isolate 3D7) GN=PFA_0300c PE=4 SV=1	Q8I280_PLAF7
Arginyl-tRNA synthetase, putative OS=Plasmodium falciparum (isolate 3D7) GN=PFL0900c PE=3 SV=1	Q8I5M2_PLAF7
Conserved Plasmodium protein OS=Plasmodium falciparum (isolate 3D7) GN=PF11_0332 PE=4 SV=1	Q8II42_PLAF7
Putative uncharacterized protein OS=Plasmodium falciparum (isolate 3D7) GN=PFE0990w PE=4 SV=1	C0H4F1_PLAF7
Proteasome, putative OS=Plasmodium falciparum (isolate 3D7) GN=PFI1545c PE=4 SV=1	Q8I0U7_PLAF7

Table 9 Continued

<i>Protein</i>	<i>Accession Number</i>
DNA-directed RNA polymerase OS=Plasmodium falciparum (isolate 3D7) GN=PFC0805w PE=3 SV=1	O77375_PLAF7
P-type calcium transporting ATPase OS=Plasmodium falciparum GN=serca PE=3 SV=1	E1CC54_PLAFA
60S ribosomal protein L23a, putative OS=Plasmodium falciparum (isolate 3D7) GN=PF13_0132 PE=3 SV=1	Q8IE82_PLAF7
Coatomer alpha subunit, putative OS=Plasmodium falciparum (isolate 3D7) GN=PFF0330w PE=4 SV=1	C6KSR5_PLAF7
Pfmdr2 protein OS=Plasmodium falciparum GN=pfmdr2 PE=3 SV=1	Q25693_PLAFA
60S ribosomal protein L14, putative OS=Plasmodium falciparum (isolate 3D7) GN=PF14_0296 PE=4 SV=1	Q8ILE8_PLAF7
Heat shock protein 90, putative OS=Plasmodium falciparum (isolate 3D7) GN=PF11_0188 PE=3 SV=1	Q8III6_PLAF7
ORF 2 protein (Fragment) OS=Plasmodium falciparum GN=ORF 2 PE=2 SV=1	Q02602_PLAFA
Ring-exported protein 1 OS=Plasmodium falciparum (isolate 3D7) GN=REX1 PE=4 SV=1	Q8I2G1_PLAF7
40S ribosomal protein S24 OS=Plasmodium falciparum (isolate 3D7) GN=PFE0975c PE=3 SV=1	Q8I3R6_PLAF7
Glutamate--cysteine ligase (Gamma-glutamylcysteine synthetase) OS=Plasmodium falciparum GN=GCS PE=2 SV=1	Q9TY17_PLAFA
Activator of Hsp90 ATPase homolog 1-like protein, putative OS=Plasmodium falciparum (isolate 3D7) GN=PFC0360w PE=4 SV=2	O97256_PLAF7
Ubiquitin conjugating enzyme E2, putative OS=Plasmodium falciparum (isolate 3D7) GN=PFL0190w PE=3 SV=1	Q8I607_PLAF7
Coatamer protein, beta subunit, putative OS=Plasmodium falciparum (isolate 3D7) GN=PF14_0277 PE=4 SV=2	Q8ILG6_PLAF7
Putative uncharacterized protein OS=Plasmodium falciparum (isolate 3D7) GN=MAL8P1.62 PE=4 SV=1	Q8IB31_PLAF7
60S ribosomal protein L36 OS=Plasmodium falciparum (isolate 3D7) GN=PF11_0106 PE=3 SV=2	Q8I713_PLAF7

Table 9 Continued

<i>Protein</i>	<i>Accession Number</i>
Serine rich protein homologue OS=Plasmodium falciparum PE=3 SV=1	Q26015_PLAFA
6-cysteine protein, putative OS=Plasmodium falciparum (isolate 3D7) GN=Pf41 PE=4 SV=1	Q811Y0_PLAF7
DNA replication licensing factor mcm7 homologue, putative OS=Plasmodium falciparum (isolate 3D7) GN=PF07_0023 PE=3 SV=1	Q81C16_PLAF7
Rab2, GTPase OS=Plasmodium falciparum (isolate 3D7) GN=Rab2 PE=3 SV=1	Q815A9_PLAF7
Cytidine triphosphate synthetase OS=Plasmodium falciparum (isolate 3D7) GN=PF14_0100 PE=4 SV=1	Q81LZ3_PLAF7
Ubiquitin carboxyl-terminal hydrolase OS=Plasmodium falciparum (isolate 3D7) GN=PFE1355c PE=3 SV=1	Q813J3_PLAF7
Glycogen synthase kinase 3 OS=Plasmodium falciparum (isolate 3D7) GN=PfGSK-3 PE=4 SV=2	O77344_PLAF7
Acetyl-CoA synthetase OS=Plasmodium falciparum (isolate 3D7) GN=PFF1350c PE=4 SV=1	C6KTB4_PLAF7
DNAJ protein, putative OS=Plasmodium falciparum (isolate 3D7) GN=PF08_0032 PE=4 SV=1	Q81B72_PLAF7
DNA topoisomerase 2 OS=Plasmodium falciparum (isolate 3D7) GN=PF14_0316 PE=3 SV=1	Q81LC8_PLAF7
Conserved Plasmodium protein OS=Plasmodium falciparum (isolate 3D7) GN=PFL0895c PE=4 SV=1	Q815M3_PLAF7
Spermidine synthase OS=Plasmodium falciparum (isolate 3D7) GN=PF11_0301 PE=1 SV=1	Q81I73_PLAF7
Putative uncharacterized protein OS=Plasmodium falciparum (isolate 3D7) GN=PF08_0137 PE=4 SV=1	Q81AK9_PLAF7
PfSec23 protein OS=Plasmodium falciparum (isolate 3D7) GN=Pfsec23 PE=2 SV=1	Q81B60_PLAF7
Replication factor C subunit 1 OS=Plasmodium falciparum GN=rfc1 PE=4 SV=1	Q9GQW6_PLAFA
60S ribosomal protein L8, putative OS=Plasmodium falciparum (isolate 3D7) GN=PFE0845c PE=4 SV=1	Q813T9_PLAF7

Table 9 Continued

<i>Protein</i>	<i>Accession Number</i>
Ubiquitin carboxyl-terminal hydrolase a, putative OS=Plasmodium falciparum (isolate 3D7) GN=PF0680c PE=4 SV=1	Q811U8_PLAF7
Orotate phosphoribosyltransferase OS=Plasmodium falciparum GN=opr1 PE=2 SV=1	Q8N0R1_PLAFA
Calmodulin OS=Plasmodium falciparum (isolate 3D7) GN=PF14_0323 PE=3 SV=2	CALM_PLAF7
Haloacid dehalogenase-like hydrolase, putative OS=Plasmodium falciparum (isolate 3D7) GN=PF11_0190 PE=4 SV=1	Q8III4_PLAF7
Thymidylate kinase, putative OS=Plasmodium falciparum (isolate 3D7) GN=TMK PE=1 SV=1	Q8I4S1_PLAF7
Myosin-A OS=Plasmodium falciparum (isolate FCBR / Columbia) PE=2 SV=1	MYOA_PLAFB
Probable DNA-directed RNA polymerase II subunit RPB11 OS=Plasmodium falciparum (isolate 3D7) GN=PF13_0023 PE=3 SV=1	RPB11_PLAF7
Zinc finger protein, putative OS=Plasmodium falciparum (isolate 3D7) GN=PF13_0313 PE=4 SV=1	Q8IDC0_PLAF7
60S ribosomal protein L28, putative OS=Plasmodium falciparum (isolate 3D7) GN=PF11_0437 PE=4 SV=1	Q8IHU0_PLAF7

Gene ontology (GO) terms, which used a set of defined terms to describe gene product properties, were extracted for all possible proteins. GO terms are split into three domains: 1) cellular component describes the parts of the cell or the extracellular environment in which the gene product functions; 2) molecular function describes the gene product's function at the molecular level; 3) biological process is the overall series of events in which the gene product participates (e.g. signal transduction). It is important to note that one protein may be described by several GO terms and thus fall into more than one category. The number of proteins categorized into each GO domain and subdomain were approximately the same in treated and control samples (Figure 8a-8c).

As no difference in the number of proteins that were assigned to each GO term existed between treated and control proteins, GO terms assigned to all six samples were described together (Figure 9a-9c). Within the cellular component subdomain, the predominating GO terms in descending order were unknown (278), cytoplasm (178) intracellular organelle (154), and organelle part (85). Molecular function (394), binding (242), and catalytic activity (221) were the predominating terms from the molecular function GO subdomain. Finally, the biological process subdomain GO term categorization yielded three major terms; cellular process (322), metabolic process (293), and unknown (155). All other biological process terms such as biological regulation, response to stimulus, establishment of localization, and locomotion were assigned to less than 10 % of all categorized proteins.

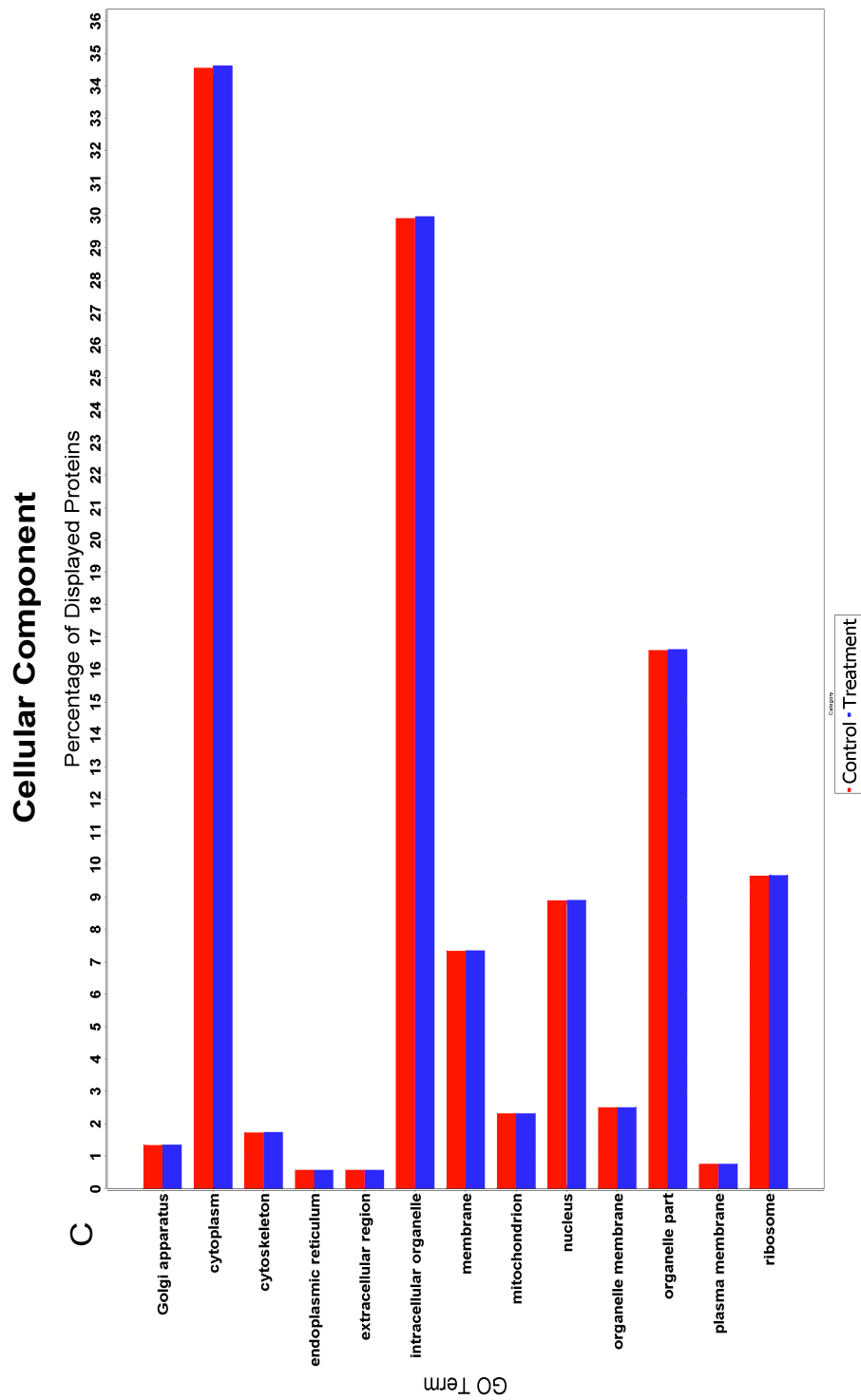


Figure 8a: Gene Ontology Cellular Component Subdomain Terms for *P. falciparum* Protein Search in Treated vs. Control Samples. The y axis indicates the GO term and the x axis indicated the percentage of proteins belonging to each GO term category. Red bars represent control proteins and blue bars represent treatment proteins.

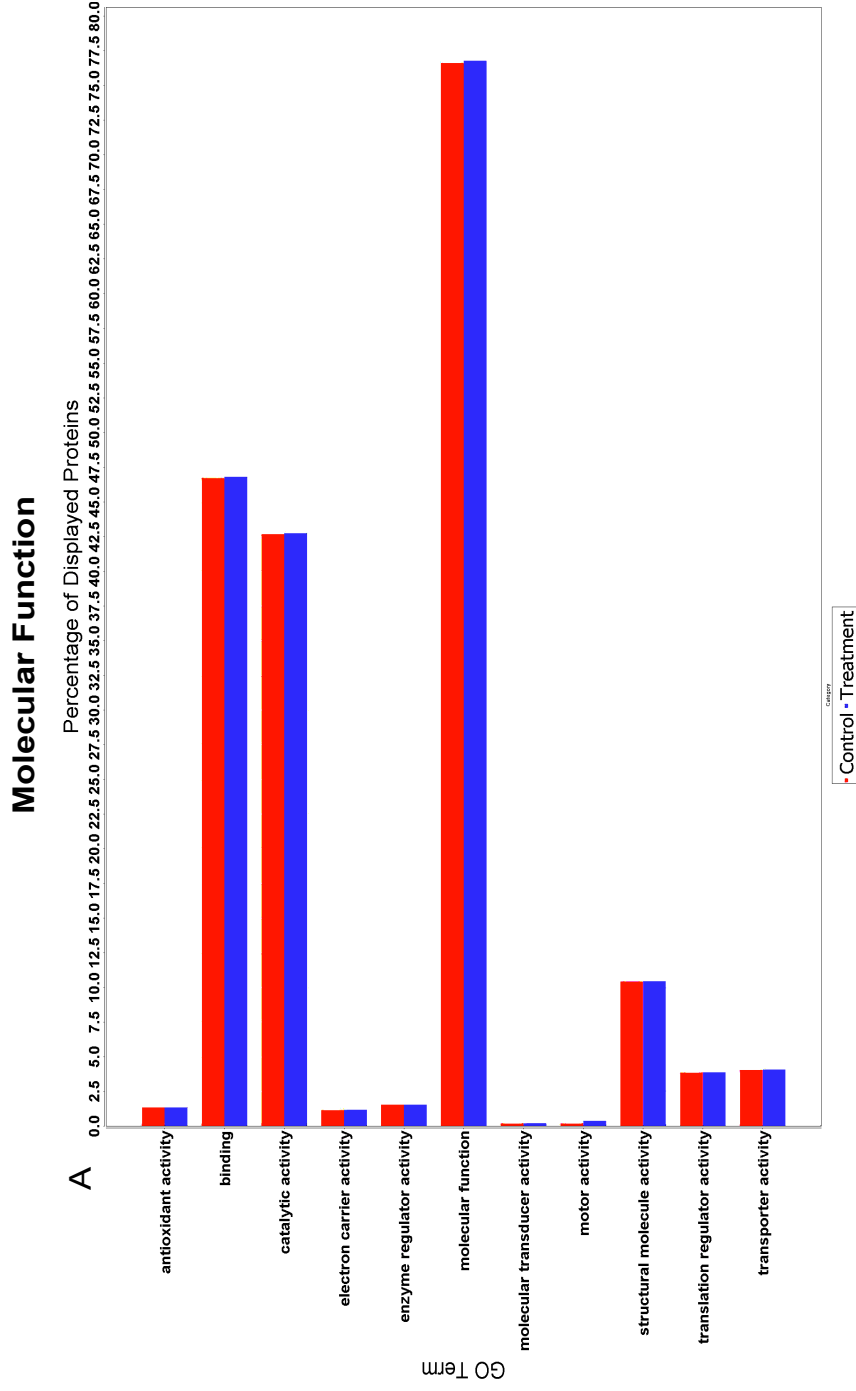


Figure 8b: Gene Ontology Molecular Function Subdomain Terms for *P. falciparum* Protein Search in Treated vs. Control Samples. The y axis indicates the GO term and the x axis indicated the percentage of proteins belonging to each GO term category. Red bars represent control proteins and blue bars represent treatment proteins.

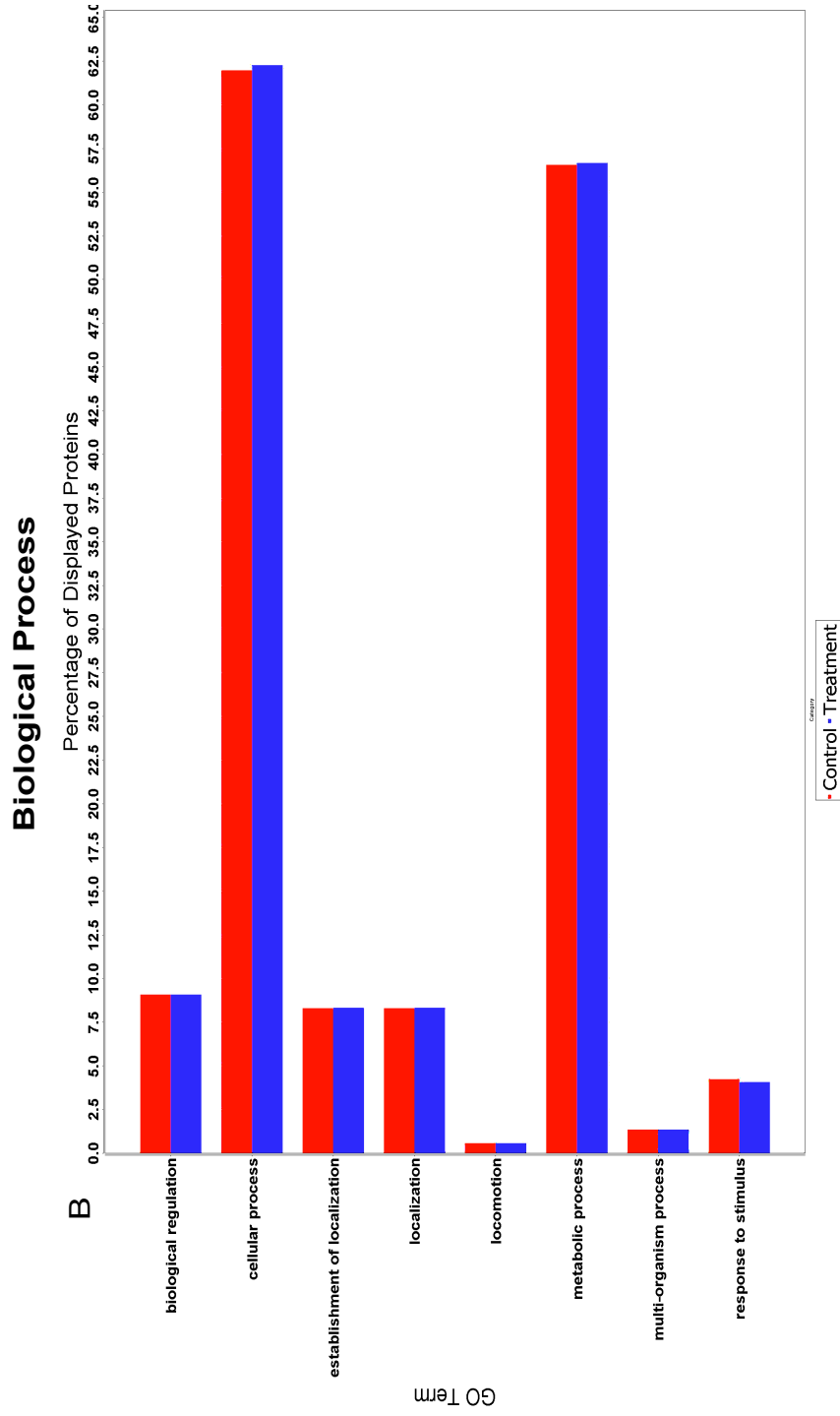


Figure 8c: Gene Ontology Biological Process Subdomain Terms for *P. falciparum* Protein Search in Treated vs. Control Samples. The y axis indicates the GO term and the x axis indicated the percentage of proteins belonging to each GO term category. Red bars represent control proteins and blue bars represent treatment proteins.

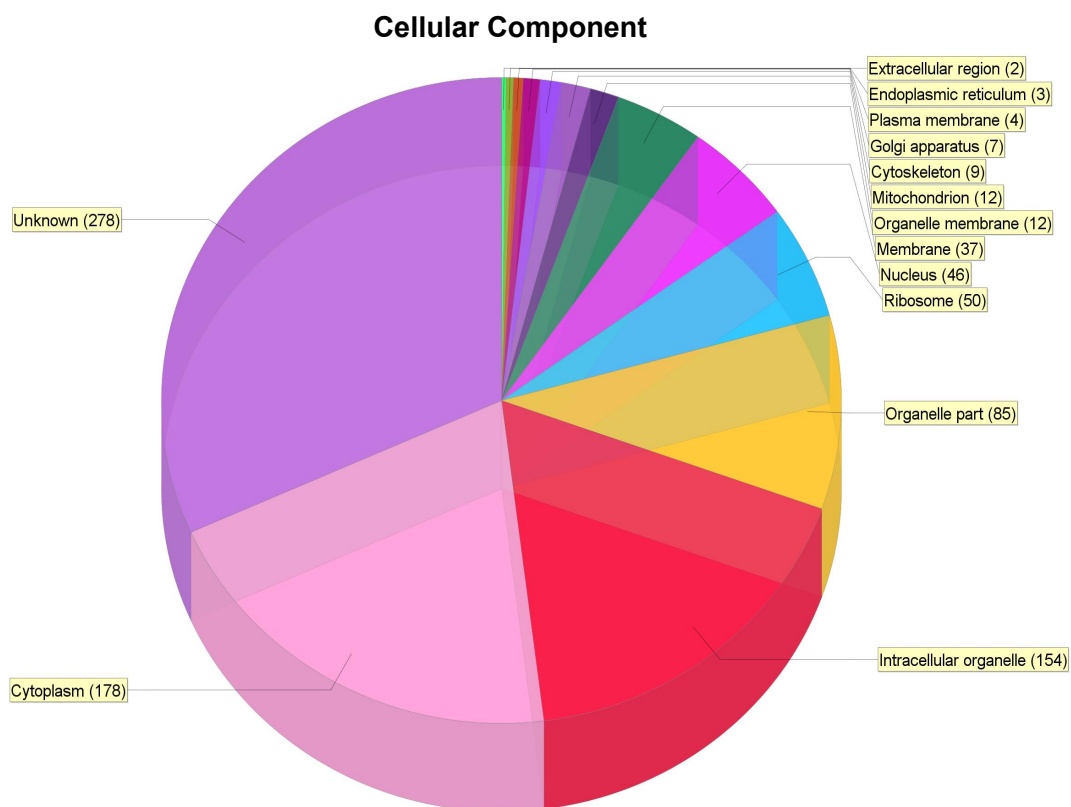


Figure 9a: Cellular Component GO Terms for *P. falciparum* Search Proteins. Each section of the pie represents a GO term and corresponding number of proteins that were assigned each term is located in brackets beside the term name.

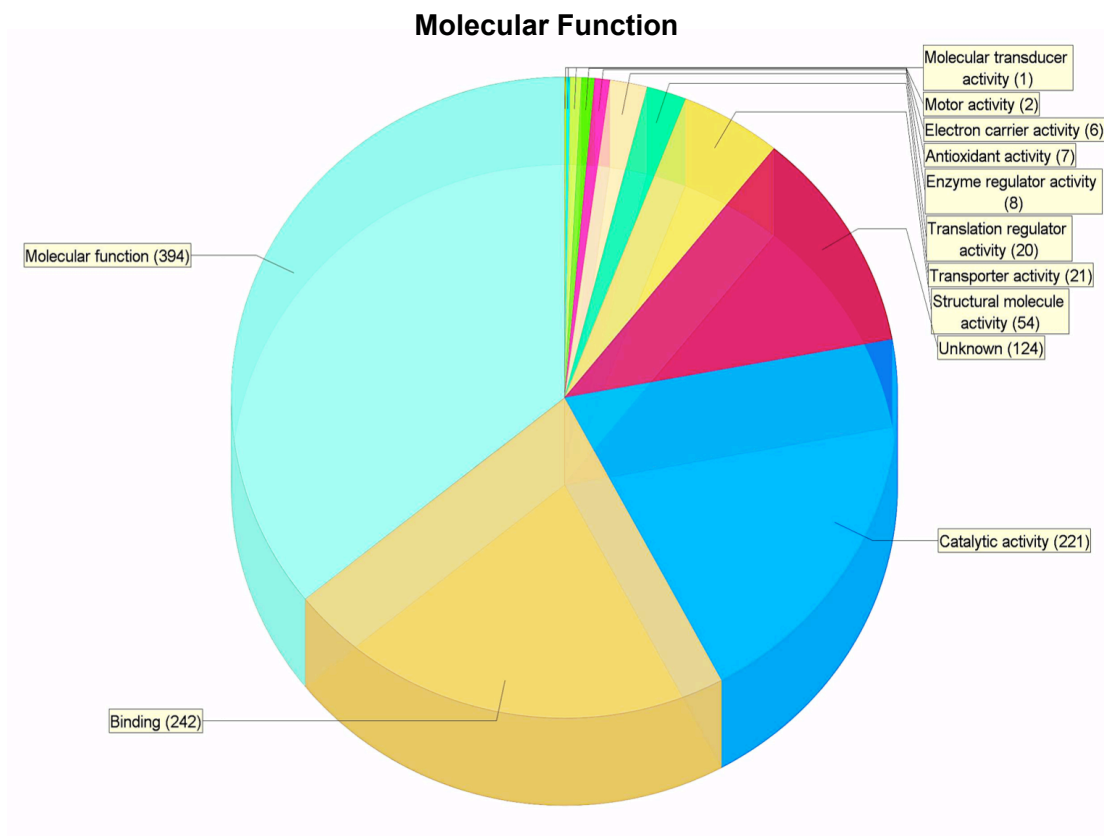


Figure 9b: Molecular Function GO Terms for *P. falciparum* Search Proteins. Each section of the pie represents a GO term and corresponding number of proteins that were assigned each term is located in brackets beside the term name.

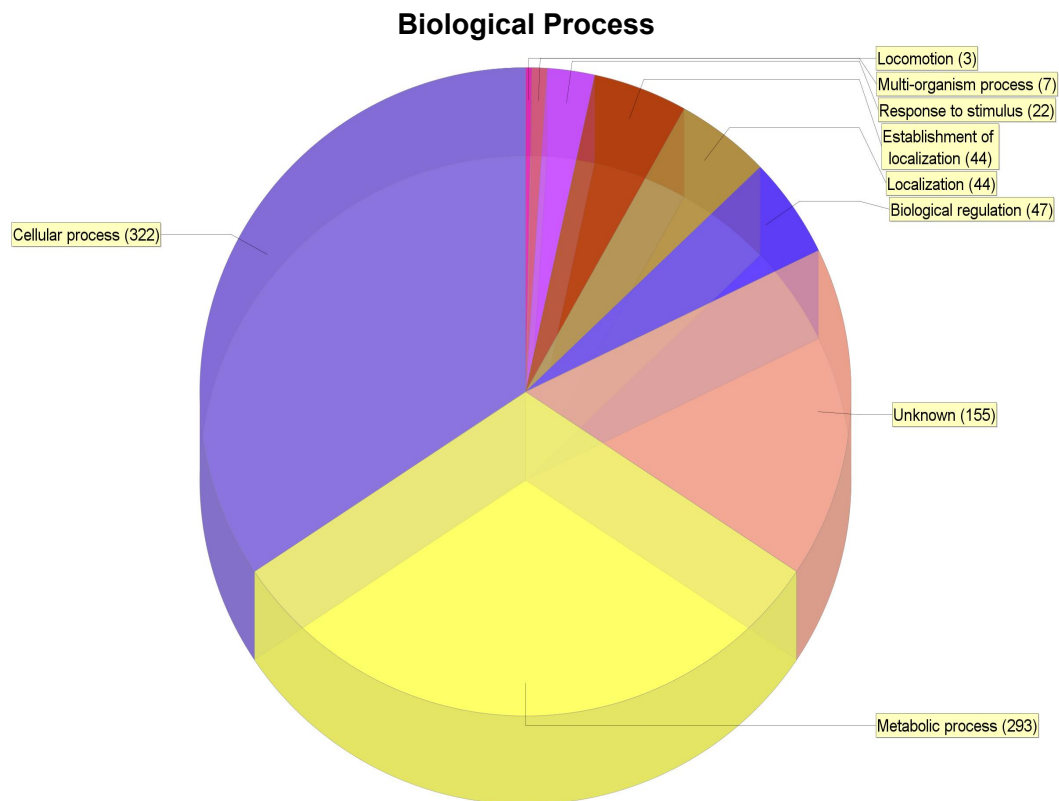


Figure 9c: Biological Process GO Terms for *P. falciparum* Search Proteins. Each section of the pie represents a GO term and corresponding number of proteins that were assigned each term is located in brackets beside the term name.

Differences in relative protein abundance between the control and Purvalanol B-treated parasites were quantified by both spectral counting (SpC) and average total ion current (TIC) analyses of normalized data in Scaffold. T-tests were performed and fold changes were calculated for each protein. Proteins with a t-test p-value below 0.05 and ≥ 1.5 fold change in either SpC or TIC analyses were considered upregulated in treatment compared to control and proteins with a p-value below 0.05 and a fold change of ≤ 0.5 in either SpC or TIC analyses were considered down regulated in treatment compared to control.

A total of 10 proteins were shown to be differentially regulated in treatment samples relative to control samples (Table 10). There were 8 proteins shown to be upregulated and 2 proteins shown to be downregulated in Purvalanol B-treated parasite samples compared to samples incubated with DMSO vehicle. Upregulated proteins included proteasome component C8 (O77396_PLAF7), subunit of proteasome activator complex (Q8I374_PLAF7), structure-specific recognition protein (Q8IL56_PLAF7), adenylosuccinate synthetase (PURA_PLAF7 (+1)), proteasome subunit alpha type (Q8IDG3_PLAF7), cysteinyl-tRNA synthetase (Q8IJP3_PLAF7), thioredoxin reductase 2 (TRXR2_PLAF7 (+1)), and 40S ribosomal protein S6 (Q8IDR9_PLAF7). Proteins that were downregulated in treatment compared to control samples included RNA binding protein (Q8I374_PLAF7) and Helicase (Q8IL13_PLAF7).

Table 10: Differentially Regulated Proteins Between Purvalanol B-treated and Control Samples. Column one indicates the protein name, while column two indicates the UniProt accession number. The t-test p-value is in the third column and fold change is indicated in the fourth column.

<i>Protein Name</i>	<i>Accession Number</i>	<i>P-value</i>	<i>Fold Change</i>
Proteasome component C8, putative OS=Plasmodium falciparum (isolate 3D7) GN=PFC0745c PE=4 SV=1	O77396_PLAF7	0.0016	2.1
Subunit of proteasome activator complex, putative OS=Plasmodium falciparum (isolate 3D7) GN=PF10370c PE=4 SV=1	Q8I374_PLAF7	0.015	2
Structure specific recognition protein OS=Plasmodium falciparum (isolate 3D7) GN=PF14_0393 PE=4 SV=1	Q8IL56_PLAF7	0.027	2.2
Adenylosuccinate synthetase OS=Plasmodium falciparum (isolate 3D7) GN=Adss PE=3 SV=1	PURA_PLAF7 (+1)	0.032	1.8
Proteasome subunit alpha type OS=Plasmodium falciparum (isolate 3D7) GN=PF13_0282 PE=3 SV=1	Q8IDG3_PLAF7	0.038	1.6
Cysteinyl-tRNA synthetase, putative OS=Plasmodium falciparum (isolate 3D7) GN=PF10_0149 PE=3 SV=2	Q8IJP3_PLAF7	0.04	2.8
Thioredoxin reductase 2 OS=Plasmodium falciparum (isolate 3D7) GN=trxr2 PE=2 SV=2	TRXR2_PLAF7 (+1)	0.049	2.9
40S ribosomal protein S6, putative OS=Plasmodium falciparum (isolate 3D7) GN=PF13_0228 PE=4 SV=1	Q8IDR9_PLAF7	0.037	1.5
Helicase, putative OS=Plasmodium falciparum (isolate 3D7) GN=b PE=3 SV=2	Q8IL13_PLAF7	0.019	0.3
RNA binding protein, putative OS=Plasmodium falciparum (isolate 3D7) GN=PF11175c PE=4 SV=1	Q8I2R8_PLAF7	0.021	0.2

Discussion

A total of 518 proteins were found among six samples using MudPIT. Treatment and control samples contained 414 proteins, while 47 and 57 proteins were found solely in the control and Purvalanol B-treated samples respectively. While differences in morphology were evident between the control and treated cultures in blood smears of intraerythrocytic *P.falciparum* parasites, GO terms extracted for proteins indicated no differences in GO subdomain assignments for cellular component, molecular function, or biological process. Calculation of fold change and t-test p-values indicated 10 proteins that were differentially regulated between control and treated groups.

Of the 10 differentially regulated proteins, 8 were found to be upregulated. 40S ribosomal protein S6 is a ribosomal protein and cycteinyI-tRNA synthetase an apicoplast- localized protein that are both involved in translation.

Adenylosuccinate synthetase is an enzyme that catalyzes the formation of adenylosuccinate from inosine monophosphate and aspartate [242]. It is important to note that *P. falciparum* lacks the necessary synthesis machinery for de novo synthesis of purine and thus all purine precursors are salvaged from the host (as reviewed in ([243]

Thioredoxin reductase is a cytoplasmic protein that is necessary for redox homeostasis. It belongs to the class-I pyridine nucleotide-disulfide oxidoreductase family and has been identified as a potential antimalarial drug target because its function is essential for parasite survival and a crystal structure is now available for this protein [244-246]. Thioredoxin in *P. falciparum* functions

as an antioxidant that helps relieve the parasite from oxidative stress [247]. Treatment with the inhibitor Purvalanol B may have increased oxidative stress on parasites and resulted in an upregulation of this protein. Additionally, in other systems, it has been shown that application of proteasome inhibitors in other cells leads to an increased vulnerability to oxidative stress and that heat shock proteins confer a degree of tolerance to oxidative damage [248]. While not expressed at the significance cutoff levels, heat shock proteins 70 (Q8I5F4_PLAF7) (p-value 0.062, fold change 0.09) and heat shock protein 86 (Q8IC05_PLAF7)(p-value 0.099 and fold change 1.2) may have been upregulated in treatment samples compared to control samples. Interestingly, as previously discussed, the potent antimalarial compound artemisinin also functions by increasing oxidative stress on the parasite.

The upregulated proteins in treatment samples included proteasome component C8 (O77396_PLAF7), which is a cytoplasmic and nuclear protein that is part of the proteasome core complex alpha-subunit and is involved in ubiquitin-dependent catabolic processes such as protein degradation. Interestingly, two additional proteasome proteins were also upregulated in the Purvalanol B-treated samples compared to controls. Subunit of proteasome activator complex (Q8I374_PLAF7) and proteasome subunit alpha (Q8IDG3_PLAF7). While some *P. falciparum* proteasome subunits have been characterized, little is known about these three protein subunits. However, it has been shown that proteasome inhibitors are able to attenuate intraerythrocytic *P. falciparum* growth [249]. Further, it has been shown that while the proteasome in other organisms plays a

role in diverse cellular processes such as response to stress and metabolic adaptation, it generally has two primary roles: 1) the ubiquitin-dependent proteolytic degradation of aberrantly folded or assembled proteins; and 2) the control of cell cycle by the temporally precise proteolysis of selected cell cycle modulators like cyclins and transcription factors (as reviewed in [250]).

It may be possible that the *P. falciparum* proteasome also plays a role in cell cycle regulation [251]. Application of Purvalanol B to synchronized *P. falciparum* cultures resulted in an inability to complete schizogony as evidenced by a significant reduction in the number of parasite cells able to form multiple nuclei when compared to control cultures and an upregulation of proteasome subunits in treatment cultures. Purvalanol B application in treatment cultures may have resulted in proteasome inhibition, which in turn lead to upregulation of proteasome subunits and the inability to degrade certain cell cycle machinery such as structure specific recognition protein (Q8IL56_PLAF7), which is a nuclear protein that is involved in single-stranded DNA binding necessary to stabilize negatively charged DNA when it is unwound.

Interestingly, while the following proteins did not meet both criteria for significance, proliferating cell nuclear antigen (PCNA_PLAF7 (+1))(p-value 0.063, fold change 1.6), cell division cycle protein 48 homolog (C6KT34_PLAF7)(p-value 0.022, fold change 1.3), and replication factor A-related protein (Q8I3A1_PLAF7)(p-value 0.08, fold change 2.8) may have been upregulated in treatment samples. Proliferating cell nuclear antigen was previously discussed and is a processivity factor for DNA polymerase. Cell division cycle protein 48 is

a homolog of yeast cdc48p and human p97 [252]. The yeast protein was first isolated in yeast mutants and the nonfunctional cdc48p was found to cause G2/M arrest. Later it was observed that cdc48p also functions during a G1 checkpoint in yeast that is equivalent to the restriction point in mammals and that progression through this checkpoint was mediated by the cdc48p-dependent degradation of cyclin-dependent kinase inhibitor Far1p [253]. The final probable upregulated cell cycle protein is replication factor A, which is a single stranded binding protein that, in yeast, is phosphorylated at the G1/S phase transition by cdc2 (CDK1) and dephosphorylated directly prior to mitosis [159, 254]. Additionally, cdc2 is the yeast homolog of PfPK5 in *P. falciparum*, which has been shown to be inhibited by the CDK inhibitor Purvalanol B at 130nM, a concentration well below the applied concentration in this experiment [255]. PfPK5 activity has also been shown to be necessary for the completion of the intraerythrocytic life cycle specifically during schizogony [133].

Taken together these data show an upregulation of proteasome components in Purvalanol B-treated parasites compared to control parasites and may indicate an increase in oxidative stress levels. Further, the inability of Purvalanol-B treated parasites to form multiple nuclei at 36 hpi and the upregulation of cell cycle proteins may indicate the Purvalanol B-mediated inhibition of a factor necessary for completion of parasite schizogony.

CHAPTER VI

CONCLUSIONS AND FUTURE DIRECTIONS

P. falciparum, a causative agent of malaria is one of the most deadly parasites known to man. Malaria devastates developing, poverty-stricken populations across the globe and given the emergence of multi-drug resistant *P. falciparum* strains, the dawn of a future with no effective treatment for this disease seems increasingly likely. However, the aid of organizations such as the Malaria Vaccine Initiative (www.malariavaccine.org) and the Roll Back Malaria Partnership (www.rollbackmalaria.org) with funding from sources such as the Bill and Melinda Gates Foundation (www.gatesfoundation.org), researchers are making strides in drug and vaccine development as well as malaria eradication strategies. However, given that malaria is still the primary killer of children under five years of age in tropical areas, it is imperative that research aimed at understanding this lethal organism continue. Drug targets as well as compounds with antimalarial activity must be identified and we must leverage what we know to better understand basic parasite biology.

The goal of this research was to investigate the *P. falciparum* kinase PfPK7 as a potential antimalarial drug target by screening a library of known kinase inhibitors against this protein and to define interactions between small molecules and the PfPK7 ATP-binding site that are potentially important for compound affinity. In addition, the screening of kinase inhibitor libraries against

P. falciparum strain W2 blood culture parasites provided information as to whether kinase inhibitors would be able to attenuate intraerythrocytic growth of the parasite and, in particular, whether application of small molecule inhibitors targeting PfPK7 would result in decreased growth rates. Finally, by treating blood stages cultures with cyclin-dependent kinase inhibitor Purvalanol B, it was possible to investigate large scale protein changes between inhibitor-treated and wildtype parasites, thus describing for the first time proteomic changes of *P. falciparum* parasites after drug challenge with a kinase inhibitor.

A screen of 244 well-characterized kinase inhibitors against recombinant PfPK7 yielded eight molecules that were able to inhibit kinase activity at concentrations below 100 μ M. *In silico* docking of these small molecules to the binding site revealed interactions between a leucine and isoleucine-rich hydrophobic pocket, pi/pi stacking interactions at Tyr119 and Tyr117, as well as hydrogen bonds at Asn35, Glu118, Met120, Asp123, and Ser176 contribute to small molecule affinity for the binding site. In addition, *in silico* methods revealed structural properties as well as predicted pharmacokinetic/pharmacodynamic properties that contribute to druglikeness. As no analogs for the eight small molecules that hit against PfPK7 in this screen were commercially available, it was not possible to establish a true structure-activity relationship. Synthesis of analogs especially for small molecule 528116 would allow for better definition properties that contribute to the affinity of these molecules for the binding site of PfPK7.

Small molecule kinase inhibitor libraries were also screened for their ability to inhibit intraerythrocytic parasite growth. Twenty-two molecules from this screen were shown to inhibit greater than 75 percent of intraerythrocytic parasite growth at 1 μ M. When PfPK7 small molecule inhibitors were tested in the SYBR Green I assay, three of the eight PfPK7 inhibitors were able to attenuate parasite growth with IC₅₀ concentrations of approximately 2 μ M; however, due to the noted promiscuity displayed by two of the three compounds, it is likely that much of the inhibitory activity of these molecules was due to off target effects. In the future it would be advantageous to determine the IC₅₀ concentrations for the 22 small molecules that were good inhibitors of intraerythrocytic parasite growth. In addition, given the structural similarity between these molecules it would be advantageous to determine the molecular target of the compounds. If many of the small molecules from this screen affect the same protein in the parasite, that protein may prove a promising target for antimalarial drug design.

Application of the CDK inhibitor Purvalanol B to blood stage cultures of *P. falciparum* strain W2 at 25 hpi resulted in morphological differences between wildtype and inhibitor-treated parasites after 12 hours of incubation. More specifically, inhibitor-treated cultures were significantly less able to form the multinucleated cells typical of *Plasmodium* schizonts when compared to control parasites. Evidence of Purvalanol B effects was further substantiated with proteomic analysis of treated and control cultures using MudPIT. The resulting data revealed a significant upregulation (p-value \geq 0.05, fold change \geq 1.5) of proteasome machinery and a protein necessary for redox homeostasis. In

addition, a trend towards upregulation of certain cell cycle modulators was also present in treatment cultures. In the future, it would be advantageous use western blot analysis to further validate the upregulation of these proteins. In addition, it has been suggested in this manuscript that the mechanism of *Plasmodium* cell cycle disruption that was observed in the Purvalanol B experiment resulted from an inhibition of the proteasome complex and the subsequent inability of the parasite to temporally regulate the destruction of cell cycle modulators such as cyclins and transcription factors. It may be possible to first determine the extent to which Purvalanol B binds to subunits of the malaria proteasome using coimmunoprecipitation and to then determine if application of Purvalanol B to parasite cultures affects the temporal presence the aforementioned Pfcyc proteins (*Plasmodium* cyclins) using western blot. If inhibition of the *Plasmodium* proteasome is able to decrease the ability of parasites to form multinucleated cells, it may be a promising and much needed drug target for antimalarial drug design.

REFERENCES

1. **World Malaria Report.** (Organization WH ed. Geneva, Switzerland: WHO Press; 2012.
2. Schellenberg AJR, Nathan R, Abdulla S, Mukasa O, Marchant TJ, Tanner M, Lengeler C: **Risk factors for child mortality in rural Tanzania.** *Trop Med Int Health* 2002, **7**:506-511.
3. Kiszewski AE, Teklehaimanot A: **A review of the clinical and epidemiologic burdens of epidemic malaria.** *Am J Trop Med Hyg* 2004, **71**:128-135.
4. Freeman T, Bradley M: **Temperature is predictive of severe malaria years in Zimbabwe.** *Trans R Soc Trop Med Hyg* 1996, **90**:232.
5. Russell S: **The economic burden of illness for households in developing countries: a review of studies focusing on malaria, tuberculosis, and human immunodeficiency virus/acquired immunodeficiency syndrome.** *Am J Trop Med Hyg* 2004, **71**:147-155.
6. Sachs J, Malaney P: **The economic and social burden of malaria.** *Nature* 2002, **415**:680-685.
7. Oaks SC, Mitchell VS, Pearson GW: *Malaria: obstacles and opportunities.* Washington D. C.: National Academy Press; 1991.
8. Cunha CB, Cunha BA: **Brief history of the clinical diagnosis of malaria: from Hippocrates to Osler.** *J Vector Borne Dis* 2008, **45**:194-199.
9. Packard RM: *The Making of a Tropical Disease: a Short History of Malaria.* Baltimore, Md: Johns Hopkins University Press; 2007.
10. Lawrence C: **Laveran remembered: malaria haemozoin in leucocytes.** *The Lancet* 1999, **353**:1852.
11. Cox FEG: **History of the discovery of the malaria parasites and their vectors.** *Parasit Vectors* 2010, **3**.
12. Santamaria L: **Camillo Golgi as clinical pathologist: epicritical reading of Golgi's works on malaria.** *Med Secoli* 1994, **6**:581-608.

13. Hagan P, Chauhan V: **Ronald Ross and the problem of malaria.** *Parasitology Today* 1997, **13**:290-295.
14. Venita J: **Sir Patrick Manson.** *Archives of pathology and laboratory medicine* 2000, **124**:1594-1595.
15. Bynum WF: **Ronald Ross and the malaria-mosquito cycle.** *Parasitologia* 1999, **41**:49-52.
16. Ross R: **The role of the mosquito in the evolution of the malarial parasite: the recent researches of Surgeon-Major Ronald Ross, I.M.S. 1898.** *Yale Journal of Biology and Medicine* 2002, **75**:103-105.
17. Sherman IW: *Malaria: Parasite Biology, Pathogenesis, and Protection.* Washington, DC: ASM Press; 1998.
18. Capanna E: **Battista Grassi entomologist and the Roman School of Malariology.** *Parassitologia* 2008, **50**:201-211.
19. Cook GC: **Ronald Ross' Opposition to Battista Grassi's malaria research.** *J Med Bigr* 2011, **19**:184.
20. Bynum WF: **Mosquitoes bite more than once.** *Science* 2002, **295**:47-48.
21. Shortt HE, Garnham PCC: **Demonstration of a persisting exo-erythrocytic cycle in Plasmodium cynomolgi and its bearing on the production of relapses.** *British Medical Journal* 1948:1225-1228.
22. Trager W, Jensen JB: **Human malaria parasites in continuous culture.** *Science* 1976, **193**:673-675.
23. Hanssen E, Goldie KN, Tilley L: **Ultrastructure of the asexual blood stages of Plasmodium falciparum.** *Methods Cell Biol* 2010, **96**:93-116.
24. Dixon ML, Thompson J, Gardiner DL, Trenholme KR: **Sex in Plasmodium: a sign of commitment.** *Trends Parasitol* 2008, **24**:168-175.
25. Aikawa M: **Ultrastructure of the pellicular complex of Plasmodium fallax.** *J Cell Biol* 1967, **35**:103-113.
26. Hepler PK, Huff CG, Sprinz H: **The fine structure of the exoerythrocytic stages of Plasmodium fallax.** *J Cell Biol* 1966, **30**:333-358.
27. Luse SA, Miller LH: **Plasmodium falciparum malaria. Ultrastructure of parasitized erythrocytes in cardiac vessels.** *Am J Trop Med Hyg* 1971, **20**:655-660.

28. Kalderon Ae KYBJ: **Chronic toxoplasmosis associated with severe hemolytic anemia: case report and electron microscopic studies.** *Archives of Internal Medicine* 1964, **114**:95-02.
29. Aikawa M: **Variations in structure and function during the life cycle of malarial parasites.** *Bull World Health Organ* 1977, **55**:139-156.
30. Cerami C, Frevort U, Sinnis P, Takacs B, Clavijo P, Santos MJ, Nussenzweig V: **The Basolateral domain of the hepatocyte plasma membrane bears receptors for the circumsporozoite protein of Plasmodium falciparum sporozoites.** *Cell* 1992, **70**:1021-1033.
31. Perkins ME: **Rhoptry organelles of Apicomplexan parasites.** *Parasitol Today* 1992, **8**:28-32.
32. Richard D, MacRaild CA, Riglar DT, Chan JA, Foley M, Baum J, Ralph SA, Norton RS, Cowman AF: **Interaction between Plasmodium falciparum apical membrane antigen 1 and the rhoptry neck protein complex defines a key step in the erythrocyte invasion process of malaria parasites.** *J Biol Chem* 2010, **285**:14815-14822.
33. Vulliez-Le Normand B, Tonkin ML, Lamarque MH, Longer S, Hoos S, Roques M, Saul FA, Faber BW, Bentley GA, Boulanger MJ, Lebrun M: **Structural and functional insights into the malaria parasite moving junction complex.** *PLoS Pathog* 2012, **8**:e1002755.
34. Uchime O, Herrera R, Reiter K, Kotova S, Shimp RL, Miura K, Jones D, Lebowitz J, Ambroggio X, Hurt DE, et al: **Analysis of the conformation and function of the Plasmodium falciparum merozoite proteins MTRAP and PTRAMP.** *Eukaryot Cell* 2012, **11**:615-625.
35. Cao J, Kaneko O, Thongkukiatkul A, Tachibana M, Otsuki H, Gao Q, Tsuboi T, Toril M: **Rhoptry neck protein RON2 forms a complex with microneme protein AMA1 in Plasmodium falciparum merozoites.** *Parasitol Int* 2009, **58**:29-35.
36. Baum J, Tonkin CJ, Paul AS, Rug M, Smith BJ, Gould SB, Richard D, Pollard TD, Cowman AF: **A malaria parasite formin regulates actin polymerization and localizes to the parasite-erythrocyte moving junction during invasion.** *Cell Host Microbe* 2008, **3**:188-198.
37. Klotz FW, Hadley TJ, Aikawa M, Leech J, Howard RJ, Miller LH: **A 60-kDa Plasmodium falciparum protein at the moving junction formed between merozoite and erythrocyte during invasion.** *Mol Biochem Parasitol* 1989, **36**:177-185.

38. Aikawa M, Miller LH, Johnson J, Rabbege J: **Erythrocyte entry by malarial parasites. A moving junction between erythrocyte and parasite.** *J Cell Biol* 1978, **77**:72-82.
39. Ladda R, Arnold J, Martin D: **Electron microscopy of Plasmodium falciparum. The structure of trophozoites in erythrocytes of human volunteers.** *Trans R Soc Trop Med Hyg* 1966, **60**:369-375.
40. Goldberg DE, Slater AF, Cerami A, Henderson GB: **Hemoglobin degradation in the malaria parasite Plasmodium falciparum : an ordered process in a unique organelle.** *Proc Natl Acad Sci U S A* 1990, **87**:2931-2935.
41. Sullivan AD, Meshnick SR: **Haemozoin: identification and quantification.** *Parasitol Today* 1996, **12**:161-163.
42. Ashong JO, Blench IP, Warhurst DC: **The composition of haemozoin from Plasmodium falciparum.** *Trans R Soc Trop Med Hyg* 1989, **83**:167-172.
43. Pouvelle B, Buffet PA, Lepolard C, Scherf A, Gysin J: **Cytoadhesion of Plasmodium falciparum ring-stage-infected erythrocytes.** *Nat Med* 2000, **6**:1264-1268.
44. Sherry BA, Alava G, Tracey KJ, Martiney J, Cerami A, Slater AF: **Malaria-specific metabolite hemozoin mediates the release of several potent endogenous pyrogens (TNF, MIP-1 alpha, and MIP-1 beta) in vitro, and altered thermoregulation in vivo.** *J Inflamm* 1995, **45**:85-96.
45. Lobo CA, Kumar N: **Sexual differentiation and development in the malaria parasite.** *Parasitol Today* 1998, **14**:148-150.
46. Alano P: **Plasmodium falciparum gametocytes; still many secrets of a hidden life.** *Mol Microbiol* 2007, **66**:291-302.
47. Liu Z, Miao J, Cui L: **Gametocytogenesis in malaria parasite; commitment, development and regulation.** *Future Microbiol* 2011, **6**:1351-1369.
48. Eksi S, Morahan BJ, Halle Y, Furuya T, Jiang H, Ali O, Xu H, Kiattibutr K, Suri A, Czesny B, et al: **Plasmodium falciparum gametocyte development 1 (Pfgdv1) and gametocytogenesis early gene identification and commitment to sexual development.** *PLoS Pathog* 2012, **8**:e1002964.
49. Inselburg J: **Gametocyte formation by the progeny of single Plasmodium falciparum schizonts.** *J Parasitol* 1983, **69**:584-591.

50. Silvestrini F, Alano P, Williams JL: **Commitment to the production of male and female gametocytes in the human malaria parasite *Plasmodium falciparum*.** *Parasitology* 2000, **5**:465-471.
51. Smith TG, Lourenco P, Carter R, Walliker D, Ranford-Cartwright LC: **Commitment to sexual differentiation in the human malaria parasite, *Plasmodium falciparum*.** *Parasitology* 2000, **121**:127-133.
52. Schall JJ: **The sex ratio of *Plasmodium* gametocytes.** *Parasitology* 1989, **98**:343-350.
53. Baton LA, Ranford-Cartwright LC: **Spreading the seeds of million-murdering death: metamorphoses of malaria in the mosquito.** *Trends Parasitol* 2005, **21**:573-580.
54. Hanssen E, McMillan PJ, Tilley L: **Cellular architecture of *Plasmodium falciparum*-infected erythrocytes.** *Int J Parasitol* 2010, **40**:1127-1135.
55. Tekeste Z, Petros B: **The ABO blood group and *Plasmodium falciparum* malaria in Awash, Metehara and Ziway areas, Ethiopia.** *Malar J* 2010, **9**:280.
56. Bottieau E, Clerinx J, Van Den Enden E, Van Esbroeck M, Colebunders R, Van Gompel A, Van Den Ende J: **Imported non-*Plasmodium falciparum* malaria: a five-year prospective study in a European referral center.** *Am J Trop Med Hyg* 2006, **75**:133-138.
57. Wellems TE, Hayton K, Fairhurst RM: **The impact of malaria parasitism: from corpuscles to communities.** *J Clin Invest* 2009, **119**:2496-2505.
58. Roestenberg M, O'Hara GA, Duncan CJ, Epstein JE, Edwards NJ, Scholzen A, van der Ven AJ, Hermsen CC, Hill AV, Sauerwein RW: **Comparison of clinical and parasitological data from controlled human malaria infection trials.** *PLoS One* 2012, **7**:e38434.
59. Miller LH, Good MF, Milon G: **Malaria pathogenesis.** *Science* 1994, **264**:1878-1883.
60. Perlmann P, Troye-Blomberg M: **Malaria blood-stage infection and its control by the immune system.** *Folia Biol (Praha)* 2000, **46**:210-218.
61. Mackintosh CL, Beeson JG, Marsh K: **Clinical features and pathogenesis of severe malaria.** *Trends Parasitol* 2004, **20**:597-603.
62. Russell PF: **The United States and malaria: debits and credits.** *Bull N Y Acad Med* 1968, **44**:623-653.

63. Meshnick SR, Dobson MJ: **The history of antimalarial drugs.** In *Antimalarial chemotherapy: Mechanisms of Action, Resistance, and New Directions in Drug Discovery*. Edited by Totowa PJR. New Jersey: Humana Press; 2001: 15-25
64. Achan J, Talisuna AO, Erhart A, Yeka A, Tibenderana JK, Baliraine FN, Rosenthal PJ, D'Alessandro U: **Quinine, an old anti-malarial drug in a modern world: role in the treatment of malaria.** *Malar J* 2011, **10**:44.
65. Rocco F: *Quinine: Malaria and the Quest for a Cure that Changed the World*. New York: Harper Collins Publishers; 2003.
66. Honigsbaum M: *The Fever Trail: In Search of the Cure for Malaria*. New York: Farrar, Straus, and Giroux; 2001.
67. Eholie S, Ehui E, Adou-Bryn K, Kouame KE, Tanon A, Kakou A, Bissagnene E, Kadio A: **Severe malaria in native adults in Abidjan (Cote d'Ivoire).** *Bull Soc Pathol Exot* 2004, **97**:340-344.
68. Abdi YA, Gustafsson LL, Ericsson O, Hellgren U: *Handbook of Drugs for Tropical Parasitic Infections*. Basingstoke: Burgess Science Press; 1995.
69. Krafts K, Hempelmann E, Skorska-Stania A: **From methylene blue to chloroquine: a brief review of the developemnt of an antimalarial therapy.** *Parasitology Research* 2012, **111**:1-6.
70. Ecker A, Adele ML, Clain J, Fidock DA: **PfCRT and its role in antimalarial drug resistance.** *Trends in Parasitology* 2012, **28**:504-514.
71. Stiebler R, Soares JB, Timm BL, Silva JR, Mury FB, Dansa-Petretski M, Oliveira MF: **On the mechanisms involved in biological heme crystallization.** *J Bioenerg Biomembr* 2011, **43**:93-99.
72. Krogstad DJ, Schlesinger PH, Gluzman IY: **Chloroquine and acid vesicle function.** *Prog Clin Biol Res* 1989:53-59.
73. Ben-ishai R, Volcani B, Bergman E: **The synthesis of the purine nucleus by Escherichia coli, a study on the mode of action of sulfa-drugs.** *Experientia* 1951, **7**:63-64.
74. Hitchings GH, Elion GB, Falco EA: **Antagonists of nucleic acid derivatives. II. Reversal studies with substances structurally related to thymine.** *J Biol Chem* 1950, **185**:643-649.
75. McCunn J: **Discussion on Synergy in Chemotherapy.** *Proceeding of the Royal Society of Medicine* 1956, **49**:871-882.

76. McGregor IA, Williams K, Goodwin LG: **Pyrimethamine and sulphadiazine in treatment of malaria.** *Br Med J* 1963, **2**:728-729.
77. Peters W: **Antimalarial drugs and their actions.** *Postgraduate Medical Journal* 1973, **49**:573-583.
78. Kitchen LW, Vaughn DW, Skillman DR: **Role of US military research programs in the development of US food and drug administration-approved antimalarial drugs.** *Clinical Infectious Diseases* 2006, **43**:67-71.
79. van Riemsdijk MM, Sturkenboom MC, Ditters JM, Ligthelm RJ, Overbosch D, Stricker BH: **Atovaquone plus chloroguanide versus mefloquine for malaria prophylaxis: a focus on neuropsychiatric adverse events.** *Clin Pharmacol Ther* 2002, **72**:294-301.
80. Tu Y: **The discovery of artemisinin (qinghaosu) and gifts from Chinese medicine.** *Nat Med* 2011, **17**:1217-1220.
81. Hsu E: **Reflections on the 'discovery' of the antimalarial qinghao.** *British Journal of Clinical Pharmacology* 2006, **61**:666-670.
82. Peek R, T VANG, Panchoe D, Greve S, Bus E, Resida L: **Drug resistance and genetic diversity of Plasmodium falciparum parasites from suriname.** *Am J Trop Med Hyg* 2005, **73**:833-838.
83. Kuhn S, Gill MJ, Kain KC: **Emergence of atovaquone-proguanil resistance during treatment of Plasmodium falciparum malaria acquired by a non-immune north American traveller to west Africa.** *Am J Trop Med Hyg* 2005, **72**:407-409.
84. Foote SJ, Kyle DE, Martin RK, Odulola AM, Forsyth K, Kemp DJ, Cowman AF: **Several alleles of the multidrug-resistance gene are closely linked to chloroquine resistance in Plasmodium falciparum.** *Nature* 1990, **345**:255-258.
85. Contacos RG, Lunn JS, Coatney GR: **Drug-resistant falciparum malaria from cambodia and malaya.** *Trans R Soc Trop Med Hyg* 1963, **57**:417-424.
86. Montgomery R, Eyles DE: **Chloroquine resistant falciparum malaria in malaya.** *Trans R Soc Trop Med Hyg* 1963, **57**:409-416.
87. Combrinck JM, Mabothe TE, Ncokazi KK, Ambele MA, Taylor D, Smith PJ, Hoppe HC, Egan TJ: **Insights into the role of heme in the mechanism of action of antimalarials.** *ACS Chem Biol* 2012, **8**:133-137.

88. Ecker A, Lehane AM, Clain J, Fidock DA: **PfCRT and its role in antimalarial drug resistance.** *Trends Parasitol* 2012, **28**:504-514.
89. May J, Meyer CG: **Association of Plasmodium falciparum chloroquine resistance transporter variant T76 with age-related plasma chloroquine levels.** *Am J Trop Med Hyg* 2003, **68**:143-146.
90. Price RN, Uhlemann AC, Brockman A, McGready R, Ashley E, Phaipun L, Patel R, Laing K, Looareesuwan S, White NJ, et al: **Mefloquine resistance in Plasmodium falciparum and increased pfmdr1 gene copy number.** *Lancet* 2004, **364**:438-447.
91. Alker AP, Lim P, Sem R, Shah NK, Yi P, Bouth DM, Tsuyuoka R, Maguire JD, Fandeur T, Arley F, et al: **Pfmdr1 and in vivo resistance to artesunate-mefloquine in falciparum malaria on the Cambodian-Thai border.** *Am J Trop Med Hyg* 2007, **76**:641-647.
92. Dondorp AM, Nosten F, Yi P, Das D, Phyo AP, Tarning J, Lwin KM, Arie F, Hanpithakpong W, Lee SJ, et al: **Artemisinin resistance in Plasmodium falciparum malaria.** *N Engl J Med* 2009, **361**:455-467.
93. Witkowski B, Khim M, Chim P, Kim S, Ke S, Kloeung N, Chy S, Duong S, Leang R, Ringwald P, et al: **Reduced artemisinin susceptibility of Plasmodium falciparum ring stages in Western Cambodia.** *Antimicrob Agents Chemother* 2013, **57**:914-923.
94. Talisuna AO, Karema C, Ogutu B, Juma E, Logedi J, Nyandigisi A, Mulenga M, Mbacham WF, Roper C, Guerin PJ, et al: **Mitigating the threat of artemisinin resistance in Africa: improvement of drug-resistance surveillance and response systems.** *Lancet Infect Dis* 2012, **12**:888-896.
95. Cui L, Wang Z, Miao J, Miao M, Chandra R, Jiang H, Su XZ, Cui L: **Mechanisms of in vitro resistance to dihydroartemisinin in Plasmodium falciparum.** *Mol Microbiol* 2012, **86**:111-128.
96. Jirage D, Keenan KM, Waters NC: **Targeting the malaria kinome: discovering kinase inhibitors as novel antimalarial agents.** In *Antiparasitic and antibacterial drug discovery: from molecular targets to drug candidates.* Edited by Selzer PM. Weinheim: Wiley-VCH Verlag GmbH & Co. KGaA; 2009
97. Leroy D, Doerig C: **Drugging the Plasmodium kinome: the benefits of academia-industry synergy.** *Trends Pharmacol Sci* 2008, **29**:241-249.
98. Weinblatt ME, Kavanaugh A, Genovese MC, Musser TK, Grossbard EB, Magilavy DB: **An oral spleen tyrosine kinase (Syk) inhibitor for rheumatoid arthritis.** *N Engl J Med* 2010, **363**:1303-1312.

99. Rungseesantivanon S, Thenchaisri N, Ruangvejvorachai P, Patumraj S: **Curcumin supplementation could improve diabetes-induced endothelial dysfunction associated with decreased vascular superoxide production and PKC inhibition.** *BMC Complement Altern Med* 2010, **10**:57.
100. Sanford M, Scott LJ: **Imatinib: as adjuvant therapy for gastrointestinal stromal tumour.** *Drugs* 2010, **70**:1963-1972.
101. Zhang J, Yang PL, Gray NS: **Targeting cancer with small molecule kinase inhibitors.** *Nat Rev Cancer* 2009, **9**:28-39.
102. Fabbro D, Cowan-Jacob SW, Mobitz H, Martiny-Baron G: **Targeting cancer with small-molecular weight kinase inhibitors.** *Methods Mol Biol* 2012, **795**:1-34.
103. Anamika, Srinivasan N, Krupa A: **A genomic perspective of protein kinases in Plasmodium falciparum.** *Proteins* 2005, **58**:180-189.
104. Ward P, Equinet L, Packer J, Doerig C: **Protein kinases of the human malaria parasite Plasmodium falciparum: the kinome of a divergent eukaryote.** *BMC Genomics* 2004, **5**:79.
105. Yang J, Wu J, Steichen JM, Kornev AP, Deal MS, Li S, Sankaran B, Woods VL, Taylor SS: **A conserved Glu-Arg salt bridge connects co-evolved motifs that define the eukaryote protein kinase fold.** *J Mol Biol* 2012, **315**:666-679.
106. Scheeff ED, Bourne PE: **Structural Evolution of the Protein Kinase,ÄiLike Superfamily.** *PLoS Comput Biol* 2005, **1**:e49.
107. Hanks SK: **Genomic analysis of the eukaryotic protein kinase superfamily: a perspective.** *Genome Biol* 2003, **4**:111.
108. Manning G, Plowman GD, Hunter T, S. S: **Evolution of protein kinase signaling from yeast to man.** *Trends Biochem Sci* 2002, **27**:514-520.
109. Taylor SS, Radzio-Andzelm E: **Three protein kinase structures define a common motif.** *Structure* 1994, **2**:345-355.
110. Knighton DR, Zheng JH, Ten Eych LF, Ashford VA, Xuong NH, Taylor SS, Sowadski JM: **Crystal structure of the catalytic subunit of cyclic adenosine monophosphate-dependent protein kinase.** *Science* 1991, **253**:407-414.
111. Talevich E, Mirza A, Kannan N: **Structural and evolutionary divergence of eukaryotic protein kinases in Apicomplexa.** *BMC Evol Biol* 2011, **11**:321.

112. Talevich E, Tobin AB, Kannan N, Doerig C: **An evolutionary perspective on the kinome of malaria parasites.** *Philos Trans R Soc Lond B Biol Sci* 2012, **367**:2607-2618.
113. Gardner MJ, Hall N, Fung E, White O, Berriman M, Hyman RW, Carlton JM, Pain a, Nelson KE, Bowman S, et al: **Genome sequence of the human malaria parasite *Plasmodium falciparum*.** *Nature* 2002, **419**:498-511.
114. Doerig C, Billker O, Haystead T, Sharma P, Tobin AB, Waters NC: **Protein kinases of malaria parasites: an update.** *Trends Parasitol* 2008, **24**:570-577.
115. Dorin D, Semblat JP, Pouillet P, Alano P, Goldring JP, Whittle C, Patterson S, Chakrabarti D, Doerig C: **PfPK7, an atypical MEK-related protein kinase, reflects the absence of classical three-component MAPK pathways in the human malaria parasite *Plasmodium falciparum*.** *Mol Microbiol* 2005, **55**:184-196.
116. Le Roch K, Sestier C, Dorin D, Waters N, Kappes B, Chakrabarti D, Meijer L, Doerig C: **Activation of a *Plasmodium falciparum* cdc2-related kinase by heterologous p25 and cyclin H. Functional characterization of a *P. falciparum* cyclin homologue.** *J Biol Chem* 2000, **275**:8952-8958.
117. Schneider AG, Mercereau-Pujjalon O: **A new Apicomplexa-specific protein kinase family: multiple members in *Plasmodium falciparum*, all with an export signature.** *BMC Genomics* 2005, **6**:30.
118. Nunes MC, Okada M, Scheidig-Benatar C, Cooke BM, Scherf A: ***Plasmodium falciparum* FIKK kinase members target distinct components of the erythrocyte membrane.** *PLoS One* 2010, **5**:e11747.
119. Lucet IS, Tobin A, Drewry D, Wilks AF, Doerig C: ***Plasmodium* kinases as targets for new-generation antimalarials.** *Future Medicinal Chemistry* 2012, **4**:2295-2310.
120. Miranda-Saavedra D, Barton GJ: **Classification and functional annotation of eukaryotic protein kinases.** *Proteins* 2007, **68**:893-914.
121. Merckx A, Echalié A, Langford K, Sicard A, Langsley G, Joore J, Doerig C, Noble M, Endicott J: **Structures of *P. falciparum* protein kinase 7 identify an activation motif and leads for inhibitor design.** *Structure* 2008, **16**:228-238.

122. Boulloc N, Large JM, Smiljanic E, Whalley D, Ansell KH, Edlin CD, Bryans JS: **Synthesis and in vitro evaluation of imidazopyridazines as novel inhibitors of the malarial kinase PfPK7.** *Bioorg Med Chem Lett* 2008, **18**:5294-5298.
123. Sahu NK, Kohli DV: **Structural insights for imidazopyridazines as malarial kinase PfPK7 inhibitors using QSAR techniques.** *Med Chem* 2012, **8**:636-648.
124. Dorin-Semblat D, Sicard A, Doerig C, Ranford-Cartwright L: **Disruption of the PfPK7 gene impairs schizogony and sporogony in the human malarial parasite Plasmodium falciparum.** *Eukaryot Cell* 2008, **7**:279-285.
125. Koyama FC, Ribeiro RY, Garcia JL, Azevedo MF, Chakrabarti D, Garcia CRS: **Ubiquitin proteasome system and the atypical kinase PfPK7 are involved in melatonin signaling in Plasmodium falciparum.** *J Pineal Res* 2012, **53**:147-153.
126. Beraldo FH, Garcia CR: **Products of tryptophan catabolism induce Ca²⁺ release and modulate the cell cycle of Plasmodium falciparum malaria parasites.** *J Pineal Res* 2005, **39**:224-230.
127. Hotta CT, Gazarini ML, Beraldo FH, Varotti FP, Lopes C, Markus RP, Pozzan T, Garcia CR: **Calcium-dependent modulation by melatonin of the circadian rhythm in malarial parasites.** *Nat Cell Biol* 2000, **2**:466-468.
128. Baldwin A, Grueneberg DA, Hellner K, Sawyer J, Grace M, Li W, Harlow E, Munger K: **Kinase requirements in human cells: V. Synthetic lethal interactions between p53 and the protein kinases SGK2 and PAK3.** *Proc Natl Acad Sci U S A* 2010, **107**:12463-12468.
129. Bohorquez EB, Juliano JJ, Kim HS, Meshnick SR: **Mefloquine exposure induces cell cycle delay and reveals stage-specific expression of the pfmdr1 gene.** *Antimicrob Agents Chemother* 2013, **57**:833-839.
130. Banniser L, Mitchell G: **The ins, outs and roundabouts of malaria.** *Trends Parasitol* 2003, **19**:209-213.
131. Ngwa CJ, Scheuermayer M, Mair GR, Kern S, Brugn T, Wirth CC, Aminake MN, Wiesner J, Fischer R, Vilcinskis A, Pradel G: **Changes in the transcriptome of the malaria parasite Plasmodium falciparum during the initial phase of transmission from the human to the mosquito.** *BMC Genomics* 2013, **14**:256.

132. Oehring SC, Woodcroft BJ, Moes S, Wetzel J, Dietz O, Pulfer A, Dekiwadia C, Maeser P, Flueck C, Witmer K, et al: **Organellar proteomics reveals hundreds of novel nuclear proteins in the malaria parasite *Plasmodium falciparum***. *Genome Biol* 2012, **13**:R108.
133. Solyakov L, Halbert J, Alam MM, Semblat JP, Reininger L, Bottrill AR, Mistry S, Abdi A, Fennell C, Holland Z, et al: **Global kinomic and phospho-proteomic analyses of the human malaria parasite *Plasmodium falciparum***. *Nat Commun* 2011, **2**:565.
134. Evans T, Rosenthal ET, Youngblom J, Distel D, Hunt T: **Cyclin: a protein specified by maternal mRNA in sea urchin eggs that is destroyed at each cleavage division**. *Cell* 1983, **33**:389-396.
135. Cross FR: **DAF1, a mutant gene affecting size control, pheromone arrest, and cell cycle kinetics of *Saccharomyces cerevisiae***. *Mol Cell Biol* 1988, **8**:4675-4684.
136. Nash R, Tokiwa G, Anand S, Erickson K, Fitcher AB: **The WHI1+ gene of *Saccharomyces cerevisiae* tethers cell division to cell size and is a cyclin homolog**. *EMBO* 1988, **7**:4335-3446.
137. Golias CH, Charalabopoulos A, Charalabopoulos K: **Cell proliferation and cell cycle control: a mini review**. *Int J Clin Pract* 2004, **58**:1134-1141.
138. Jirage D, Chen Y, Caridha D, O'Neil MT, Eyase FL, Witola WH, Mamoun CB, Waters NC: **The malarial CDK Pfmrk and its effector PfmAT1 phosphorylate DNA replication proteins and co-localize in the nucleus**. *Mol Biochem Parasitol* 2010, **172**:9-18.
139. Carvalho TG, Doerig C, Reininger L: **Nima- and Aurora-related kinases of malaria parasites**. *Biochim Biophys Acta* 2013, **1834**:1336-1345.
140. Gillet CE, Barnes DM: **Demystified...cell cycle**. *Mol Pathol* 1998, **51**:310-316.
141. Bonvin E, Falletta P, Shaw H, Delmas V, Goding CR: **A phosphatidylinositol 3-kinase-Pax3 axis regulates Brn-2 expression in melanoma**. *Mol Cell Biol* 2012, **32**:4674-4683.
142. Egeberg DL, Lethan M, Manguso R, Schneider L, Awan A, Jorgensen TS, Byskov AG, Pedersen LB, Christensen ST: **Primary cilia and aberrant cell signaling in epithelial ovarian cancer**. *Cilia* 2012, **1**:15.

143. Visser R, Landman EB, Goeman J, Wit JM, Karperien M: **Sotos syndrome is associated with deregulation of the MAPK/ERK-signaling pathway.** *PLoS One* 2012, **7**:e49229.
144. Chellappan SP, Giordano A, Fisher PB: **Role of cyclin-dependent kinases and their inhibitors in cellular differentiation and development.** *Curr Top Microbiol Immunol* 1998, **227**:57-103.
145. Kung AL, Sherwood SW, Schimke RT: **Cell line-specific differences in the control of cell cycle progression in the absence of mitosis.** *Proc Natl Acad Sci U S A* 1990, **87**:9553-9557.
146. Lee JM, Bernstein A: **p53 mutations increase resistance to ionizing radiation.** *Proc Natl Acad Sci U S A* 1993, **90**:5742-5746.
147. Zhan Q, Carrier F, Fornace AJ: **Induction of cellular p53 activity by DNA-damaging agents and growth arrest.** *Mol Cell Biol* 1993, **13**:4242-4250.
148. Pardee AB: **A restriction point for control of normal animal cell proliferation.** *Proc Natl Acad Sci U S A* 1974, **71**:1286-1290.
149. Pardee AB: **G1 events and regulation of cell proliferation.** *Science* 1989, **246**:603-608.
150. Sherr CJ, Roberts JM: **Inhibitors of mammalian G1 cyclin-dependent kinases.** *Genes Dev* 1995, **9**:1149-1163.
151. Yao G, Lee TJ, Mori S, Nevins JR, You L: **A bistable Rb-E2F switch underlies the restriction point.** *Nat Cell Biol* 2008, **10**:476-482.
152. Lukas J, Bartkova J, Bartek J: **Convergence of mitogenic signalling cascades from diverse classes of receptors at the cyclin D-cyclin-dependent kinase-pRb-controlled G1 checkpoint.** *Mol Cell Biol* 1996, **16**:6917-6925.
153. Matsumoto Y, Hayashi K, Nishida E: **Cyclin-dependent kinase 2 (Cdk2) is required for centrosome duplication in mammalian cells.** *Curr Biol* 1999, **9**:429-432.
154. Hinchcliffe EH, Li C, Thompson EA, Maller JL, Sluder G: **Requirement of Cdk2-cyclin E activity for repeated centrosome reproduction in Xenopus egg extracts.** *Science* 1999, **283**:851-854.
155. Tokuyama Y, Horn HF, Kawamura K, Tarapore P, Fukasawa K: **Specific phosphorylation of nucleophosmin on Thr(199) by cyclin-dependent kinase 2-cyclin E. and its role in centrosome duplication.** *J Biol Chem* 2001, **276**:21529-21537.

156. Tarapore P, Okuda M, Fukasawa K: **A mammalian in vitro centriole duplication system: evidence for involvement of CDK2/cyclin E and nucleophosmin/B23 in centrosome duplication.** *Cell Cycle* 2002, **1**:75-81.
157. Harper JW, Adami GR, Wei N, Keyomarsi K, Elledge SJ: **The p21 Cdk-interacting protein Cip1 is a potent inhibitor of G1 cyclin-dependent kinases.** *Cell* 1993, **75**:805-816.
158. Kastan MB, Onyekwere O, Sidransky D, Vogelstein B, Craig RW: **Participation of p53 protein in the cellular response to DNA damage.** *Cancer Res* 1991, **51**:6304-6311.
159. Dutta A, Bell SP: **Initiation of DNA replication in eukaryotic cells.** *Annu Rev Cell Dev Biol* 1997, **13**:293-332.
160. Matsuda K, Makise M, Sueyasu Y, Takehara M, Asano T, Mizushima T: **Yeast two-hybrid analysis of the origin recognition complex of *Saccharomyces cerevisiae*: interaction between subunits and identification of binding proteins.** *FEMS Yeast Res* 2007, **7**:1263-1269.
161. Moore GD, Ayabe T, Kopf GS, Schultz RM: **Temporal patterns of gene expression of G1-S cyclins and cdk's during the first and second mitotic cell cycles in mouse embryos.** *Mol Reprod Dev* 1996, **45**:264-275.
162. Hinds PW, Mittnacht S, Dulic V, Arnold A, I. RS, Weinberg RA: **Regulation of retinoblastoma protein functions by ectopic expression of human cyclins.** *Cell* 1992, **70**:993-1006.
163. Nawal B, Benedicte L, Blanchard JM, Arsic N: **Cyclin A2 mutagenesis analysis: a new insight into CDK Activation and Cellular Localization Requirements.** *PLoS One* 2011, **6**:e22879.
164. Henglein B, Chenivesse X, Wang J, Eick D, Brechot C: **Structure and cell cycle-regulated transcription of the human cyclin A gene.** *Proc Natl Acad Sci U S A* 1994, **91**:5490-5494.
165. Jeffrey PD, Russo AA, Polyak K, Gibbs E, Hurwitz J, Massague J, Pavletich NP: **Mechanism of CDK activation revealed by the structure of a cyclinA-CDK2 complex.** *Nature* 1995, **376**:313-320.
166. Stillman B: **Cell cycle control of DNA replication.** *Science* 1996, **274**:1659-1564.
167. Matsuoka S, Huang M, Elledge SJ: **Linkage of ATM to cell cycle regulation by the Chk2 protein kinase.** *Science* 1998, **282**:1893-1897.

168. Chaturvedi P, Eng WK, Zhu Y, Mattern MR, Mishra R, Hurlle MR, Zhang X, Annan RS, Lu Q, Faucette LF, et al: **Mammalian Chk2 is a downstream effector of the ATM-dependent DNA damage checkpoint pathway.** *Oncogene* 1999, **18**:4047-4054.
169. Zhou XY, Wang X, Hu B, Guan J, Illiakis G, Wang Y: **An ATM-independent S-phase checkpoint response involves CHK1 pathway.** *Cancer Res* 2002, **62**:1598-1603.
170. Ito M: **Factors controlling cyclin B expression.** *Plant Mol Biol* 2000, **43**:677-690.
171. Hershko A: **Mechanisms and regulation of the degradation of cyclin B.** *Philos Trans R Soc Lond B Biol Sci* 1999, **354**:1571-1576.
172. Lolli B, Johnson LN: **CAK-Cyclin-dependent Activating Kinase: a key kinase in cell cycle control and a target for drugs?** *Cell Cycle* 2005, **4**:572-577.
173. Fisher RP, Morgan DO: **A novel cyclin associates with MO15/CDK7 to form the CDK-activating kinase.** *Cell* 1994, **78**:713-724.
174. Rossingnol M, Kolb-Cheynel I, Egly JM: **Substrate specificity of the cdk-activating kinase (CAK) is altered upon association with TFIIH.** *EMBO* 1997, **16**:1628-1637.
175. Yee A, Nichols MA, Wu L, Hall FL, Kobayashi R, Xiong Y: **Molecular cloning of CDK7-associated human MAT1, a cyclin-dependent kinase-activating kinase (CAK) assembly factor.** *Cancer Res* 1995, **55**:6058-6062.
176. Makela TP, Tassan JP, Nigg EA, Frutiger S, Hughes GJ, Weinberg RA: **A cyclin associated with the CDK-activating kinase MO15.** *Nature* 1994, **371**:254-257.
177. Lundgren K, Walworth N, Booher R, Dembski M, Kirschner M, Beach D: **mik1 and wee1 cooperate in the inhibitory tyrosine phosphorylation of cdc2.** *Cell* 1991, **64**:1111-1122.
178. Raleigh JM, O'Connell MJ: **The G(2) DNA damage checkpoint targets both Wee1 and Cdc25.** *J Cell Sci* 2000, **113**:1727-1736.
179. al-Khodairy F, Carr AM: **DNA repair mutants defining G2 checkpoint pathways in Schizosaccharomyces pombe.** *EMBO* 1992, **11**:1343-1350.
180. Thelen MP, Venclovas C, Fidelis K: **A sliding clamp model for the Rad1 family of cell cycle checkpoint proteins.** *Cell* 1999, **96**:769-770.

181. Walworth N, Davey S, Beach D: **Fission yeast chk1 protein kinase links the rad checkpoint pathway to cdc2.** *Nature* 1993, **363**:368-371.
182. Verkade HM, Bugg SJ, Lindsay HD, Carr AM, O'Connell MJ: **Rad18 is required for DNA repair and checkpoint responses in fission yeast.** *Mol Biol Cell* 1999, **19**:2905-2918.
183. Roberts BT, Farr KA, Hoyt MA: **The *Saccharomyces cerevisiae* checkpoint gene BUB1 encodes a novel protein kinase.** *Mol Cell Biol* 1994, **14**:8282-8291.
184. Hardwick KG, Murray AW: **Mad1p, a phosphoprotein component of the spindle assembly checkpoint in budding yeast.** *J Cell Biol* 1995, **131**:709-720.
185. Li R, Murray AW: **Feedback control of mitosis in budding yeast.** *Cell* 1991, **66**:519-531.
186. Shirayama M, Toth A, Galova M, Nasmyth K: **APC(Cdc20) promotes exit from mitosis by destroying the anaphase inhibitor Pds1 and cyclin Clb5.** *Nature* 1999, **402**:203-207.
187. Visintin R, Craig K, Hwang ES, Prinz S, Tyers M, Amon A: **The phosphatase Cdc14 triggers mitotic exit by reversal of Cdk-dependent phosphorylation.** *Mol Cell* 1998, **2**:709-718.
188. W. JJ, Horan PK, Hare JD: **Cell cycle analysis of asexual stages of erythrocytic malaria parasites.** *Cell Prolif* 1992, **25**:431-445.
189. Graeser R, Wernli B, Franklin RM, Kappes B: **Plasmodium falciparum protein kinase 5 and the malarial nuclear division cycles.** *Mol Biochem Parasitol* 1996, **82**:37-49.
190. Arnot DE, Gull K: **The Plasmodium cell-cycle: facts and questions.** *Ann Trop Med Parasitol* 1998, **92**:361-365.
191. Kozlov S, Waters NC, Chavchich M: **Leveraging cell cycle analysis in anticancer drug discovery to identify novel plasmodial drug targets.** *Infect Disord Drug Targets* 2010, **10**:165-190.
192. Gritzmacher CA, Reese RT: **Protein and nucleic acid synthesis during synchronized growth of Plasmodium falciparum.** *J Bacteriol* 1984, **160**:1165-1167.
193. Jacobberger JW, Horan PK, Hare JD: **Cell cycle analysis of asexual stages of erythrocytic malaria parasites.** *Cell Prolif* 1992, **25**:431-445.

194. Mitchell JL, Carr TW: **Synchronous versus asynchronous oscillations for antigenically varying Plasmodium falciparum with host immune response.** *J Biol Dyn* 2012, **6**:333-357.
195. Weiner A, Dahan-Pasternak N, Shimoni E, Shinder V, von Huth P, Elbaum M, Dzikowski R: **3D nuclear architecture reveals coupled cell cycle dynamics of chromatin and nuclear pores in the malaria parasite Plasmodium falciparum.** *Cell Microbiol* 2011, **13**:967-977.
196. Li JL, Robson KJ, Chen JL, Targett GA, Baker DA: **Pfmrk, a MO15-related protein kinase from Plasmodium falciparum. Gene cloning, sequence, stage-specific expression and chromosome localization.** *Eur J Biochem* 1996, **241**:805-813.
197. Waters NC, Woodard CL, Prigge ST: **Cyclin H activation and drug susceptibility of the Pfmrk cyclin dependent protein kinase from Plasmodium falciparum.** *Mol Biochem Parasitol* 2000, **107**:45-55.
198. Halbert J, Ayong L, Equinet L, Le Roch K, Hardy M, Goldring D, Reininger L, Waters N, Chakrabarti D, Doerig C: **A Plasmodium falciparum transcriptional cyclin-dependent kinase-related kinase with a crucial role in parasite proliferation associates with histone deacetylase activity.** *Eukaryot Cell* 2010, **9**:952-959.
199. Le Roch KG, Zhou Y, Blair PL, Grainger M, Moch JK, Haynes JD, P. DLV, Holder AA, Batalov S, Carucci DJ, Winzeler EA: **Discovery of gene function by expression profiling of the malaria parasite life cycle.** *Science* 2003, **301**:1503-1508.
200. Ross-Macdonald PB, Graeser R, Kappes B, Franklin RM, Williamson DH: **Isolation and expression of a gene specifying a cdc2-like protein kinase from the human malaria parasite Plasmodium falciparum.** *Eur J Biochem* 1994, **220**:693-701.
201. Bracchi-Ricard V, Barik S, Delvecchio C, Doerig C, Chakrabarti R, Chakrabarti D: **PfPK6, a novel cyclin-dependent kinase/mitogen-activated protein kinase-related protein kinase from Plasmodium falciparum.** *Biochem J* 2000, **347 Pt 1**:255-263.
202. Merckx A, Le Roch K, Nivez MP, Dorin D, Alano P, Gutierrez GJ, Nebreda AR, Goldring D, Whittle C, Patterson S, et al: **Identification and initial characterization of three novel cyclin-related proteins of the human malaria parasite Plasmodium falciparum.** *J Biol Chem* 2003, **278**:39839-39850.

203. Gupta A, Mehra P, Kumar Dhar S: **Plasmodium falciparum origin recognition complex subunit 5: functional characterization and role in DNA replication foci formation.** *Molecular Microbiology* 2008, **69**:646-665.
204. Li JL, Cox LS: **Characterisation of a sexual stage-specific gene encoding ORC1 homologue in the human malaria parasite Plasmodium falciparum.** *Parasitol Int* 2003, **52**:41-52.
205. Patterson S, Robert C, Whittle C, Chakrabarti R, Doerig C, Chakrabarti D: **Pre-replication complex organization in the atypical DNA replication cycle of Plasmodium falciparum: characterization of the mini-chromosome maintenance (MCM) complex formation.** *Mol Biochem Parasitol* 2006, **145**:50-59.
206. Kilbey BJ, Fraser I, McAleese S, Goman M, Ridley RG: **Molecular characterizaition and stage-specific expression of proliferating cell nuclear antigen (PCNA) from the malarial parasite, Plasmodium falciparum.** *Nucleic Acids Res* 1993, **21**:239-243.
207. Voss TS, Mini T, Jenoe P, Beck HP: **Plasmodium falciparum possesses a cell cycle-regulated short type replication protein A large subunit encoded by an unusual transcript.** *J Biol Chem* 2002, **277**:17493-17501.
208. Dorin D, Le Roch K, Sallicandro P, Alano P, Parzy D, Pouillet P, Meijer L, Doerig C: **Pfnek-1, a NIMA-related kinase from the human malaria parasite Plasmodium falciparum Biochemical properties and possible involvement in MAPK regulation.** *Eur J Biochem* 2001, **268**:2600-2608.
209. Dorin-Semblat D, Schmitt S, Semblat JP, Sicard A, Reininger L, Goldring D, Patterson S, Quashie N, Chakrabarti D, Meijer L, Doerig C: **Plasmodium falciparum NIMA-related kinase Pfnek-1: sex specificity and assessment of essentiality for the erythrocytic asexual cycle.** *Microbiology* 2011, **157**:2785-2794.
210. Florens L, Washburn MP, Raine JD, Anthony RM, Grainger M, Haynes JD, Moch JK, Muster N, Sacci JB, Tabb DL, et al: **A proteomic view of the Plasmodium falciparum life cycle.** *Nature* 2002, **419**:520-526.
211. Banks JL, Beard HS, Cao Y, Cho AE, Damm W, Farid R, Felts AK, Halgren TA, Mainz DT, Maple JR, et al: **Integrated modeling program, applied chemical theory (IMPACT).** *J Comput Chem* 2005, **26**:1752-1780.

212. Lipinski CA: **Drug-like properties and the causes of poor solubility and poor permeability.** *J Pharmacol Toxicol Methods* 2000, **44**:235-249.
213. Lipinski CA, F. L, Dominy BW, Feeney PJ: **Experimental and computational approaches to estimate solubility and permeability in drug discovery and development settings.** *Adv Drug Deliv Rev* 2001, **46**:3-26.
214. Jorgensen WL: **Prediction of drug solubility from Monte Carlo simulations.** *Bioorg Med Chem Lett* Duffy, E. M., **10**:1155-1158.
215. Jorgensen WL, Duffy EM: **Prediction of drug solubility from structure.** *Adv Drug Deliv Rev* 2002, **54**:355-366.
216. Duffy EM, Jorgensen WL: **Prediction of properties from simulations: free energies of solvation in hexacecane, octanol, and water.** *J Am Chem Soc* 2000, **122**:2878-2888.
217. Stenberg P, Norinder U, Luthman K, Artursson P: **Experimental and computational screening models for the prediction of intestinal drug absorption.** *J Med Chem* 2001, **44**:1927-1937.
218. Yazdanian M, Glynn SL, Wright JL, Hawi A: **Correlating partitioning and caco-2 cell permeability of structurally diverse small molecular weight compounds.** *Pharm Res* 1998, **15**:1490-1494.
219. Cavalli A, Poluzzi E, De Ponti F, Recanatini M: **Toward a pharmacophore for drugs inducing the long QT syndrome: insights from a CoMFA study of HERG K(+) channel blockers.** *J Med Chem* 2002, **45**:3844-3853.
220. De Ponti F, Poluzzi E, Montanaro N: **Organising evidence on QT prolongation and occurrence of Torsades de Pointes with non-antiarrhythmic drugs: a call for consensus.** *Eur J Clin Pharmacol* 2001, **57**:185-209.
221. Enslein K, Gombar VK, Blake BW: **International Commission for Protection Against Environmental Mutagens and Carcinogens. Use of SAT in computer-assisted prediction of carcinogenicity and mutagenicity of chemicals by the TOPKAT program.** *Mutat Res* 1994, **305**:47-61.
222. Lambros C, Vanderberg JP: **Synchronization of Plasmodium falciparum erythrocytic stages in culture.** *J Parasitol* 1979, **65**:418-420.

223. Smilkstein M, Sriwilaijaroen N, Kelly JX, Wilairat P, Riscoe M: **Simple and inexpensive fluorescence-based technique for high-throughput antimalarial drug screening.** *Antimicrob Agents Chemother* 2004, **48**:1803-1806.
224. Banborough P, Drewry D, Harper G, Smith GK, Schneider K: **Assessment of chemical coverage of kinome space and its implications for kinase drug discovery.** *J Med Chem* 2008, **51**:7898-7914.
225. Davis MI, Hunt JP, Herrgard S, Ciceri P, Wodicka LM, Pallares G, Hocker M, Treiber DK, Zarrinkar PP: **Comprehensive analysis of kinase inhibitor selectivity.** *Nat Biotechnol* 2011, **29**:1046-1051.
226. Bullard KM, DeLisle RK, Keenan SM: **Malarial kinases: novel targets for in silico approaches to drug discovery.** In *In Silico Models for Drug Discovery* Edited by Kortagere S. New York: Humana Press Inc.; 2013:205-229.
227. Jones G, Willett P, Glen RC, Leach AR, Taylor R: **Development and validation of a genetic algorithm for flexible docking.** *J Mol Biol* 1997, **267**:727-748.
228. Nissink JW, Murray C, Hartshorn M, Verdonk ML, Cole JC, Taylor R: **A new test set for validating predictions of protein-ligand interaction.** *Proteins* 2002, **49**:457-471.
229. Hartshorn MJ, Verdonk ML, Chessari G, Brewerton SCM, W. T., Mortenson PN, Murray CW: **Diverse, high-quality test set for the validation of protein-ligand docking performance.** *J Med Chem* 2007, **50**:726-741.
230. Verdonk ML, Mortenson PN, Hall RJ, Hartshorn MJ, Murray CW: **Protein-ligand docking against non-native protein conformers.** *J Chem Inf Model* 2008, **48**:2214-2225.
231. Lucet IS, Tobin A, Drewry D, Wilks AF, Doerig C: **Plasmodium kinases as targets for new-generation antimalarials.** *Future Med Chem* 2012, **4**:2295-2310.
232. Chulay JD, Haynes JD, Diggs CL: **Plasmodium falciparum: assessment of in vitro growth by [3H] hypoxanthine incorporation.** *Exp Parasitol* 1983, **55**:138-143.
233. Bennett TN, Paguio M, Gligorijevic B, Seudieu C, Kosar AD, Davidson E, Roepe PD: **Novel, rapid, and inexpensive cell-based quantification of antimalarial drug efficacy.** *Antimicrob Agents Chemother* 2004, **48**:1807-1810.

234. Johnson JD, Denuall RA, Gerena L, Lopez-Sanchez M, Roncal NE, Waters NC: **Assessment and continued validation of the malaria SYBR green I-based fluorescence assay for use in malaria drug screening.** *Antimicrob Agents Chemother* 2007, **51**:1926-1933.
235. Eyase FL, Adala HM, Ingasia L, Cheruiyot A, Omondi A, Okudo C, Juma D, Yeda R, Andagalu B, Wanja E, et al: **The role of pfmdr1 and pfcr1 in changing chloroquine, amodiaquine, mefloquine and lumefantrine susceptibility in Western-Kenya P. falciparum samples during 2008-2011.** *PLoS One* 2013, **8**:e642999.
236. Kaushik NK, Bagavan A, Rahuman AA, Mohanakrishnan D, Kamaraj C, Elango G, Zahir AA, Sahal D: **Antiplasmodial potential of selected medicinal plants from Eastern Ghats of South India.** *Exp Parasitol* 2013, **134**:26-32.
237. Sharma N, Mohanakrishnan D, Sharda A, Sharma A, Saima, Sinha AK, Sahal D: **Stilbene-chalcone hybrids: design, synthesis, and evaluation as a new class of antimalarial scaffolds that trigger cell death through stage specific apoptosis.** *J Med Chem* 2012, **55**:297-311.
238. Lasonder E, Ishihama Y, Andersen JS, Vermunt AMW, Pain A, Sauerwein RW, Eling WMC, Hall N, Waters AP, Stunnenberg HG, Mann M: **Analysis of the Plasmodium falciparum proteome by high-accuracy mass spectrometry.** *Nature* 2002, **413**:537-542.
239. Niroshini N, Sims PFG, Hyde JE: **Quantitative proteomics of the human malaria parasite Plasmodium falciparum and its application to studies of development and inhibition.** *Molecular Microbiology* 2004, **52**:1187-1199.
240. Prieto JH, Koncarevic S, Park SK, Yates JR, Becker K: **Large-Scale Differential Proteome Analysis in Plasmodium falciparum under Drug Treatment.** *PLoS One* 2008, **3**:e4098.
241. Knockaert M, Gray N, Damiens E, Chang YT, Grellier P, Grant K, Fergusson D, Mottram JC, Soete M, Dubremetz JF, et al: **Intracellular targets of cyclin-dependent kinase inhibitors: identification by affinity chromatography using immobilised inhibitors.** *Chem Biol* 2000, **7**:411-422.
242. Benson CE, Love SH, Remy CN: **Inhibition of de novo purine biosynthesis and interconversion by 6-methylpurine in Escherichia coli.** *J Bacteriol* 1970, **101**:872-880.

243. Downie MJ, Kirk K, Mamoun CB: **Purine salvage pathways in the intraerythrocytic malaria parasite plasmodium falciparum.** *Eukaryotic Cell* 2008, **7**:1231-1237.
244. Boumis B, Giardian B, Angelucci F, Bellelli A, Brunori M, Dimastrogiovanni D, Saccoccia F, Miele AE: **Crystal structure of Plasmodium falciparum thioredoxin reductase, a validated drug target.** *Biochem Biophys Res Commun* 2012, **425**:806-811.
245. Theobald AJ, Caballero I, Coma I, Colmenarejo G, Cid C, Gamo FJ, Hibbs MJ, Bass AL, Thomas DA: **Discovery and biochemical characterization of Plasmodium thioredoxin reductase inhibitors from an antimalarial set.** *Biochemistry* 2012, **51**:4764-4771.
246. Krnajski Z, Gilberger TW, Walter RD, Cowman AF, Muller S: **Thioredoxin reductase is essential for the survival of Plasmodium falciparum erythrocytic stages.** *J Biol Chem* 2002, **277**:25970-25975.
247. Kehr S, Sturm N, Rahlfs S, Przyborski JM, Becker K: **Compartmentation of redox metabolism in malaria parasites.** *PLoS Pathog* 2012, **6**:e1001241.
248. Ding Q, Keller JN: **Proteasome inhibition in oxidative stress neurotoxicity: implications for heat shock proteins.** *Journal of Neurochemistry* 2001, **77**:1010-1017.
249. Gantt SM, Myung JM, Briones MRS, Li WD, Corey EJ, Omura S, Nussenzweig V, Sinnis P: **Proteasome Inhibitors Block Development of Plasmodium spp.** *Antimicrob Agents Chemother* 1998, **57**:2731-2738.
250. Ichihara A, Tanaka K: **Roles of proteasomes in cell growth.** *Molecular Biology Reports* 1995, **21**:49-52.
251. Paugam A, Bulteau A, Dupouy-Carnet J, Creuzet C, Friguet B: **Characterization and role of protozoan parasite proteasomes.** *Trends in Parasitology* 2003, **19**:55-59.
252. Frohlich KU, Fries HW, Rudinger M, Erdmann R, Botstein D, Mecke D: **Yeast cell cycle protein CDC48p shows full-length homology to the mammalian protein VCP and is a member of a protein family involved in secretion, peroxisome formation, and gene expression.** *J Cell Biol* 1991, **114**:443-453.
253. Fu X, Ng C, Feng D, Liang C: **Cdc48p is required for the cell cycle commitment point at Start via degradation of the G1-CDK inhibitor Far1p.** *J Cell Biol* 2003, **163**:21-26.

254. Dutta A, Din S, Brill SJ, Stillman B: **Phosphorylation of replication protein A: a role for cdc2 kinase in G1/S regulation.** *Cold Spring Harb Symp Quant Biol* 1991, **56**:315-324.
255. Holton S, Merckx A, Burgess D, Doerig C, Noble M, Endicott J: **Structures of *P. falciparum* PfPK5 test the CDK regulation paradigm and suggest mechanisms of small molecule inhibition.** *Structure* 2003, **11**:1329-1337.

APPENDIX A
PROTEINS IDENTIFIED IN PLASMODIUM
FALCIPARUM MASCOT SEARCH

Identified Proteins	UniProt Accession Number	Molecular Weight	Sample					
			W2C1	W2C2	W2C3	W2T1	W2T2	W2T3
Enolase OS=Plasmodium falciparum (isolate 3D7) GN=ENO PE=3 SV=1	ENO_PLA F7	49 kDa	X	X	X	X	X	X
Glyceraldehyde-3-phosphate dehydrogenase OS=Plasmodium falciparum (isolate 3D7) GN=GAPDH PE=3 SV=1	Q8IKK7_P LAF7 (+1)	37 kDa	X	X	X	X	X	X
Heat shock 70 kDa protein OS=Plasmodium falciparum (isolate 3D7) GN=PF08_0054 PE=3 SV=1	Q8IB24_P LAF7	74 kDa	X	X	X	X	X	X
Phosphoglycerate kinase OS=Plasmodium falciparum (isolate 3D7) GN=PGK PE=1 SV=1	PGK_PLA F7	45 kDa	X	X	X	X	X	X
L-lactate dehydrogenase OS=Plasmodium falciparum GN=LDH-P PE=1 SV=1	Q71T02_P LAFA	34 kDa	X	X	X	X	X	X
Elongation factor 1-alpha OS=Plasmodium falciparum (isolate 3D7) GN=PF13_0304 PE=3 SV=1	Q8I0P6_P LAF7	49 kDa	X	X	X	X	X	X
Heat shock protein 86 OS=Plasmodium falciparum (isolate 3D7) GN=PF07_0029 PE=1 SV=1	Q8IC05_P LAF7	86 kDa	X	X	X	X	X	X
Ornithine aminotransferase OS=Plasmodium falciparum (isolate 3D7) GN=OAT PE=1 SV=1	OAT_PLA F7 (+1)	46 kDa	X	X	X	X	X	X
Phosphoethanolamine N-methyltransferase OS=Plasmodium falciparum GN=PMT PE=1 SV=1	Q6T755_P LAFA (+1)	31 kDa	X	X	X	X	X	X
Heat shock protein 70 (HSP70) homologue OS=Plasmodium falciparum (isolate 3D7) GN=PF10875w PE=3 SV=1	Q8I2X4_P LAF7	72 kDa	X	X	X	X	X	X
Adenosine deaminase, putative OS=Plasmodium falciparum (isolate 3D7) GN=PF10_0289 PE=4 SV=1	Q8IJA9_P LAF7	42 kDa	X	X	X	X	X	X
Fructose-bisphosphate aldolase OS=Plasmodium falciparum (isolate 3D7) GN=PF14_0425 PE=3 SV=1	ALF_PLA F7 (+1)	40 kDa	X	X	X	X	X	X
Merozoite surface protein 1 OS=Plasmodium falciparum (isolate mad20 / Papua New Guinea) GN=MSP-1 PE=3 SV=3	MSP1_PL AFM	194 kDa	X	X	X	X	X	X
M1-family aminopeptidase OS=Plasmodium falciparum (isolate 3D7) GN=MAL13P1.56 PE=4 SV=1	Q8IEK1_P LAF7	126 kDa	X	X	X	X	X	X
Elongation factor 2 OS=Plasmodium falciparum (isolate 3D7) GN=PF14_0486 PE=4 SV=1	Q8IKW5_ PLAF7	94 kDa	X	X	X	X	X	X
Histone H4 (Fragment) OS=Plasmodium falciparum PE=3 SV=1	Q7JSX6_ PLAFA (+1)	11 kDa	X	X	X	X	X	X
Hypoxanthine phosphoribosyltransferase OS=Plasmodium falciparum (isolate 3D7) GN=PF10_0121 PE=4 SV=1	Q8IJS1_P LAF7	26 kDa	X	X	X	X	X	X
Protein disulfide isomerase OS=Plasmodium falciparum (isolate 3D7) GN=PfPDI-8 PE=3 SV=1	C0H4Y6_ PLAF7	56 kDa	X	X	X	X	X	X
14-3-3 protein, putative OS=Plasmodium falciparum (isolate 3D7) GN=MAL8P1.69 PE=3 SV=1	C0H4V6_ PLAF7	30 kDa	X	X	X	X	X	X
Endoplasmic homolog, putative OS=Plasmodium falciparum (isolate 3D7) GN=PFL1070c PE=1 SV=1	Q8I0V4_P LAF7	95 kDa	X	X	X	X	X	X
Pyruvate kinase OS=Plasmodium falciparum (isolate 3D7) GN=PFF1300w PE=1 SV=1	C6KTA4_ PLAF7	56 kDa	X	X	X	X	X	X
Cell division cycle protein 48 homologue, putative OS=Plasmodium falciparum (isolate 3D7) GN=PFF0940c PE=3 SV=1	C6KT34_ PLAF7	92 kDa	X	X	X	X	X	X
Antigen Pfg27/25 OS=Plasmodium falciparum GN=Pfg 27-25 PE=2 SV=1	Q27336_P LAFA (+1)	26 kDa	X	X	X	X	X	X
Triosephosphate isomerase OS=Plasmodium falciparum (isolate 3D7) GN=TP1 PE=3 SV=1	TPIS_PLA F7 (+1)	28 kDa	X	X	X	X	X	X
Histone H2B OS=Plasmodium falciparum (isolate 3D7) GN=PF11_0062 PE=3 SV=1	Q8IIV1_P LAF7	13 kDa	X	X	X	X	X	X
GTP-binding nuclear protein ran/tc4 OS=Plasmodium falciparum (isolate 3D7) GN=Ran PE=4 SV=1	Q7KQK6_ PLAF7	25 kDa	X	X	X	X	X	X

Identified Proteins	UniProt Accession Number	Molecular Weight	Sample					
			W2C1	W2C2	W2C3	W2T1	W2T2	W2T3
S-adenosylmethionine synthetase OS=Plasmodium falciparum (isolate 3D7) GN=PfSAMS PE=3 SV=1	Q7K6A4_ PLAF7	45 kDa	X	X	X	X	X	X
Purine nucleotide phosphorylase, putative OS=Plasmodium falciparum (isolate 3D7) GN=PFE0660c PE=1 SV=1	Q8I3X4_P LAF7	27 kDa	X	X	X	X	X	X
CG4 OS=Plasmodium falciparum GN=cg4 PE=3 SV=1	O15797_P LAFA	98 kDa	X	X	X	X	X	X
Actin-1 OS=Plasmodium falciparum (isolate HB3) PE=1 SV=1	ACT1_PL AFX	42 kDa	X	X	X	X	X	X
Tubulin beta chain OS=Plasmodium falciparum (isolate 3D7) GN=PF10_0084 PE=3 SV=1	TBB_PLA F7 (+1)	50 kDa	X	X	X	X	X	X
Histone H2A OS=Plasmodium falciparum (isolate 3D7) GN=PFF0860c PE=3 SV=1	C6KT18_ PLAF7 (+1)	14 kDa	X	X	X	X	X	X
Histone H2A OS=Plasmodium falciparum (isolate 3D7) GN=PFC0920w PE=3 SV=1	O97320_P LAF7	16 kDa	X	X	X	X	X	X
Peptidyl-prolyl cis-trans isomerase OS=Plasmodium falciparum PE=1 SV=1	Q25756_P LAFA (+1)	19 kDa	X	X	X	X	X	X
RhopH2 OS=Plasmodium falciparum GN=rhopH2 PE=2 SV=1	B0M0V9_ PLAFA (+1)	163 kDa	X	X	X	X	X	X
Endoplasmic reticulum-resident calcium binding protein OS=Plasmodium falciparum (isolate 3D7) GN=ERC PE=4 SV=1	Q8IIR7_P LAF7	39 kDa	X	X	X	X	X	X
Karyopherin beta OS=Plasmodium falciparum PE=4 SV=1	Q7KAU3_ PLAFA (+1)	127 kDa	X	X	X	X	X	X
Phosphoglycerate mutase, putative OS=Plasmodium falciparum (isolate 3D7) GN=PF11_0208 PE=1 SV=1	Q8II6_P LAF7	29 kDa	X	X	X	X	X	X
DNA/RNA-binding protein Alba, putative OS=Plasmodium falciparum (isolate 3D7) GN=PF08_0074 PE=4 SV=1	Q8IAX8_P LAF7	27 kDa	X	X	X	X	X	X
6-phosphofructokinase, putative OS=Plasmodium falciparum (isolate 3D7) GN=PF10755c PE=4 SV=1	Q8I2Z8_P LAF7	159 kDa	X	X	X	X	X	X
Myo-inositol 1-phosphate synthase, putative OS=Plasmodium falciparum (isolate 3D7) GN=PFE0585c PE=4 SV=1	Q8I3Y8_P LAF7	69 kDa	X	X	X	X	X	X
Exp-2 protein OS=Plasmodium falciparum GN=Exp-2 PE=4 SV=1	O61141_P LAFA (+1)	33 kDa	X	X	X	X	X	X
Histone H3 OS=Plasmodium falciparum PE=2 SV=1	Q27719_P LAFA	15 kDa	X	X	X	X	X	X
RhopH3 OS=Plasmodium falciparum (isolate 3D7) GN=PFI0265c PE=4 SV=1	Q8I395_P LAF7	105 kDa	X	X	X	X	X	X
Falcilysin OS=Plasmodium falciparum (isolate 3D7) GN=fIN PE=1 SV=1	Q76NL8_ PLAF7	139 kDa	X	X	X	X	X	X
Aspartic acid-rich protein OS=Plasmodium falciparum GN=ARP PE=2 SV=1	Q8I9F4_P LAFA	32 kDa	X	X	X	X	X	X
Heat shock protein hsp70 homologue OS=Plasmodium falciparum (isolate 3D7) GN=PF11_0351 PE=3 SV=1	Q8II24_PL AF7	73 kDa	X	X	X	X	X	X
Glucose-6-phosphate isomerase OS=Plasmodium falciparum (isolate 3D7) GN=PF14_0341 PE=1 SV=1	Q8IIA4_P LAF7	67 kDa	X	X	X	X	X	X
Histone H2B OS=Plasmodium falciparum (isolate 3D7) GN=PF07_0054 PE=3 SV=1	Q8IBV7_P LAF7	14 kDa	X	X	X	X	X	X
M17 leucyl aminopeptidase OS=Plasmodium falciparum (isolate 3D7) GN=LAP PE=1 SV=1	Q8II11_P LAF7	68 kDa	X	X	X	X	X	X
4-methyl-5(B-hydroxyethyl)-thiazol monophosphate biosynthesis enzyme OS=Plasmodium falciparum (isolate 3D7) GN=PFF1335c PE=4 SV=1	C6KTB1_ PLAF7	20 kDa	X	X	X	X	X	X
Peptidase, putative OS=Plasmodium falciparum (isolate 3D7) GN=PF14_0517 PE=3 SV=1	Q8IKT5_P LAF7	89 kDa	X	X	X	X	X	X

Identified Proteins	UniProt Accession Number	Molecular Weight	Sample					
			W2C1	W2C2	W2C3	W2T1	W2T2	W2T3
Putative uncharacterized protein OS=Plasmodium falciparum (isolate 3D7) GN=MAL8P1.95 PE=4 SV=1	C0H4U4_PLAF7	36 kDa	X	X	X	X	X	X
Elongation factor 1-gamma, putative OS=Plasmodium falciparum (isolate 3D7) GN=PF13_0214 PE=4 SV=2	Q8IDV0_PLAF7	48 kDa	X	X	X	X	X	X
Pyridoxine/pyridoxal 5-phosphate biosynthesis enzyme OS=Plasmodium falciparum (isolate 3D7) GN=PFF1025c PE=4 SV=1	C6KT50_PLAF7	33 kDa	X	X	X	X	X	X
Uncharacterized protein OS=Plasmodium falciparum (isolate 3D7) GN=MAL13P1.237 PE=4 SV=1	Q8IDM3_PLAF7	42 kDa	X	X	X	X	X	X
QF122 antigen OS=Plasmodium falciparum (isolate 3D7) GN=PF10_0115 PE=4 SV=1	Q8IJS7_PLAF7	132 kDa	X	X	X	X	X	X
Histone H3 OS=Plasmodium falciparum PE=3 SV=1	Q86QI3_PLAFA	15 kDa	X	X	X	X	X	X
Rhoptry-associated protein 1 OS=Plasmodium falciparum PE=4 SV=1	D7NSU0_PLAFA	90 kDa	X	X	X	X	X	X
Heat shock protein 60 OS=Plasmodium falciparum (isolate 3D7) GN=PF10_0153 PE=3 SV=1	Q8IJN9_PLAF7	63 kDa	X	X	X	X	X	X
RhopH1/Clag3.1 OS=Plasmodium falciparum GN=rhopH1/clag3.1 PE=2 SV=1	Q4AE85_PLAFA	169 kDa	X	X	X	X	X	X
Acidic leucine-rich nuclear phosphoprotein 32-related protein OS=Plasmodium falciparum (isolate 3D7) GN=PF14_0257 PE=3 SV=1	AN32_PLAF7	33 kDa	X	X	X	X	X	X
Helicase 45 OS=Plasmodium falciparum (isolate 3D7) GN=H45 PE=3 SV=1	Q8IKF0_PLAF7	45 kDa	X	X	X	X	X	X
Plasmeprin IV OS=Plasmodium falciparum (isolate 3D7) GN=PF14_0075 PE=1 SV=1	Q8IM16_PLAF7	51 kDa	X	X	X	X	X	X
Polyubiquitin OS=Plasmodium falciparum (isolate 3D7) GN=pUB PE=4 SV=1	Q7KQK2_PLAF7 (+1)	43 kDa	X	X	X	X	X	X
Adenosylhomocysteinase OS=Plasmodium falciparum (isolate 3D7) GN=PFE1050w PE=1 SV=2	SAHH_PLAF7	54 kDa	X	X	X	X	X	X
Eukaryotic initiation factor 5a, putative OS=Plasmodium falciparum (isolate 3D7) GN=PFL0210c PE=4 SV=1	Q8I603_PLAF7 (+1)	18 kDa	X	X	X	X	X	X
DNA/RNA-binding protein, putative OS=Plasmodium falciparum (isolate 3D7) GN=PF10_0063 PE=4 SV=1	Q8IJX8_PLAF7	12 kDa	X	X	X	X	X	X
Mature parasite-infected erythrocyte surface antigen (MESA) or PfEMP2 OS=Plasmodium falciparum (isolate 3D7) GN=MESA PE=4 SV=1	Q8I492_PLAF7	168 kDa	X	X	X	X	X	X
Hexokinase OS=Plasmodium falciparum (isolate 3D7) GN=PFF1155w PE=3 SV=1	C6KT76_PLAF7	55 kDa	X	X	X	X	X	X
DEAD box helicase, UAP56 OS=Plasmodium falciparum (isolate 3D7) GN=UAP56 PE=4 SV=1	Q9TY94_PLAF7	52 kDa	X	X	X	X	X	X
Polyadenylate-binding protein OS=Plasmodium falciparum PE=2 SV=1	A1EAA0_PLAFA (+1)	97 kDa	X	X	X	X	X	X
Proliferating cell nuclear antigen OS=Plasmodium falciparum (isolate 3D7) GN=PCNA PE=3 SV=1	PCNA_PLAF7 (+1)	31 kDa	X	X	X	X	X	X
Putative uncharacterized protein OS=Plasmodium falciparum (isolate 3D7) GN=PF11270w PE=4 SV=1	Q8I2Q0_PLAF7	25 kDa	X	X	X	X	X	X
STI1-like protein OS=Plasmodium falciparum (isolate 3D7) GN=PF14_0324 PE=4 SV=1	STI1_PLAF7	66 kDa	X	X	X	X	X	X
Merozoite capping protein 1 OS=Plasmodium falciparum (isolate 3D7) GN=PF10_0268 PE=4 SV=1	Q8IJD0_PLAF7	44 kDa	X	X	X	X	X	X
V-type proton ATPase catalytic subunit A OS=Plasmodium falciparum (isolate 3D7) GN=vapA PE=3 SV=1	VATA_PLAF7 (+1)	69 kDa	X	X	X	X	X	X

Identified Proteins	UniProt Accession Number	Molecular Weight	Sample					
			W2C1	W2C2	W2C3	W2T1	W2T2	W2T3
Alpha tubulin OS=Plasmodium falciparum (isolate 3D7) GN=PF10180w PE=3 SV=1	Q6ZLZ9_ PLAF7 (+1)	50 kDa	X	X	X	X	X	X
Malaria protein EXP-1 OS=Plasmodium falciparum GN=EXP-1 PE=2 SV=2	EXP1_PL AFA	17 kDa	X	X	X	X	X	X
Thioredoxin OS=Plasmodium falciparum GN=trx PE=3 SV=1	Q9NFK9_ PLAFA (+1)	12 kDa	X	X	X	X	X	X
Putative uncharacterized protein OS=Plasmodium falciparum (isolate 3D7) GN=PFD0090c PE=4 SV=1	Q8I206_P LAF7	50 kDa	X	X	X	X	X	X
Nucleosome assembly protein 1, putative OS=Plasmodium falciparum (isolate 3D7) GN=PFL0185c PE=1 SV=2	Q8I608_P LAF7	40 kDa	X	X	X	X	X	X
T-complex protein beta subunit, putative OS=Plasmodium falciparum (isolate 3D7) GN=PFC0285c PE=3 SV=3	O97247_P LAF7	59 kDa	X	X	X	X	X	X
Peptidyl-prolyl cis-trans isomerase OS=Plasmodium falciparum GN=CyP gene PE=2 SV=1	Q27745_P LAFA (+1)	22 kDa	X	X	X	X	X	X
Putative uncharacterized protein OS=Plasmodium falciparum (isolate 3D7) GN=PF11780w PE=4 SV=1	Q8I2F2_P LAF7	46 kDa	X	X	X	X	X	X
HAP protein OS=Plasmodium falciparum (isolate 3D7) GN=PF14_0078 PE=1 SV=1	Q8IM15_P LAF7	52 kDa	X	X	X	X	X	X
Serine hydroxymethyltransferase OS=Plasmodium falciparum (isolate 3D7) GN=PFL1720w PE=3 SV=1	Q8I566_P LAF7 (+1)	50 kDa	X	X	X	X	X	X
Thioredoxin peroxidase 1 OS=Plasmodium falciparum (isolate 3D7) GN=TPx1 PE=4 SV=1	Q8IL80_P LAF7 (+1)	22 kDa	X	X	X	X	X	X
40S ribosomal protein S3, putative OS=Plasmodium falciparum (isolate 3D7) GN=PF14_0627 PE=3 SV=1	Q8IKH8_P LAF7	25 kDa	X	X	X	X	X	X
ADP-ribosylation factor 1 OS=Plasmodium falciparum (isolate 3D7) GN=ARF1 PE=1 SV=1	ARF1_PL AF7 (+1)	21 kDa	X	X	X	X	X	X
Plasmeprin 2 (Fragment) OS=Plasmodium falciparum PE=3 SV=1	Q17SC2_ PLAFA	51 kDa	X	X	X	X	X	X
Heat shock protein 70 (Hsp70), putative OS=Plasmodium falciparum (isolate 3D7) GN=MAL13P1.540 PE=3 SV=1	C0H5H0_ PLAF7	108 kDa	X	X	X	X	X	X
Receptor for activated C kinase homolog, PfRACK OS=Plasmodium falciparum (isolate 3D7) GN=PfRACK PE=4 SV=1	Q8IBA0_P LAF7	36 kDa	X	X	X	X	X	X
60S ribosomal protein P0 OS=Plasmodium falciparum (isolate 3D7) GN=PF11_0313 PE=3 SV=1	Q8II61_PL AF7	35 kDa	X	X	X	X	X	X
Translationally-controlled tumor protein homolog OS=Plasmodium falciparum (isolate 3D7) GN=TCTP PE=1 SV=1	TCTP_PL AF7	20 kDa	X	X	X	X	X	X
Haloacid dehalogenase-like hydrolase, putative OS=Plasmodium falciparum (isolate 3D7) GN=PF10_0325 PE=4 SV=1	Q8IJ74_P LAF7	33 kDa	X	X	X	X	X	X
Rhoptry neck protein 3, putative OS=Plasmodium falciparum (isolate 3D7) GN=PFL2505c PE=4 SV=1	Q8I4R5_P LAF7	263 kDa	X	X	X	X	X	X
T-complex protein 1 subunit delta OS=Plasmodium falciparum (isolate 3D7) GN=MAL13P1.283 PE=3 SV=1	C0H5I7_P LAF7	58 kDa	X	X	X	X	X	X
Methionine-tRNA ligase, putative OS=Plasmodium falciparum (isolate 3D7) GN=PF10_0340 PE=4 SV=1	Q8IJ60_P LAF7	104 kDa	X	X	X	X	X	X
Ethanolamine kinase, putative OS=Plasmodium falciparum (isolate 3D7) GN=PF11_0257 PE=4 SV=1	Q8IIB7_P LAF7	50 kDa	X	X	X	X	X	X
RNA binding protein, putative OS=Plasmodium falciparum (isolate 3D7) GN=PF10_0068 PE=4 SV=1	Q8IJX3_P LAF7	30 kDa	X	X	X	X	X	X
Ribosomal P2 phosphoprotein OS=Plasmodium falciparum GN=P2 PE=4 SV=1	Q548Y1_ PLAFA (+1)	12 kDa	X	X	X	X	X	X

Identified Proteins	UniProt Accession Number	Molecular Weight	Sample					
			W2C1	W2C2	W2C3	W2T1	W2T2	W2T3
Lysine--tRNA ligase OS=Plasmodium falciparum (isolate 3D7) GN=PF13_0262 PE=3 SV=1	Q8IDJ8_P LAF7	68 kDa	X	X	X	X	X	X
T-complex protein 1, gamma subunit, putative OS=Plasmodium falciparum (isolate 3D7) GN=PFL1425w PE=3 SV=1	Q8I5C4_P LAF7	61 kDa	X	X	X	X	X	X
Uncharacterized protein OS=Plasmodium falciparum (isolate 3D7) GN=MAL13P1.308 PE=4 SV=1	C0H5J9_P LAF7	289 kDa	X	X	X	X	X	X
CAMP-dependent protein kinase regulatory subunit, putative OS=Plasmodium falciparum (isolate 3D7) GN=PKAr PE=4 SV=1	Q7KQK0_ PLAF7 (+1)	51 kDa	X	X	X	X	X	X
Ribonucleotide reductase small subunit OS=Plasmodium falciparum (isolate 3D7) GN=PF14_0053 PE=4 SV=1	Q8IM38_P LAF7	41 kDa	X	X	X	X	X	X
Cofilin/actin-depolymerizing factor homolog 1 OS=Plasmodium falciparum (isolate 3D7) GN=PFE0165w PE=1 SV=1	CADF1_P LAF7 (+1)	14 kDa	X	X	X	X	X	X
Vacuolar ATP synthase subunit b OS=Plasmodium falciparum (isolate 3D7) GN=PFD0305c PE=3 SV=1	Q6ZMA8_ PLAF7 (+1)	56 kDa	X	X	X	X	X	X
Nucleic acid binding protein, putative OS=Plasmodium falciparum (isolate 3D7) GN=MAL13P1.233 PE=4 SV=1	Q8IDN4_P LAF7	25 kDa	X	X	X	X	X	X
Putative uncharacterized protein OS=Plasmodium falciparum (isolate 3D7) GN=PF14_0329 PE=4 SV=1	Q8ILB6_P LAF7	29 kDa	X	X	X	X	X	X
HSP40, subfamily A, putative OS=Plasmodium falciparum (isolate 3D7) GN=PF14_0359 PE=4 SV=1	Q8IL88_P LAF7	48 kDa	X	X	X	X	X	X
Nucleoside diphosphate kinase b, putative OS=Plasmodium falciparum (isolate 3D7) GN=PF13_0349 PE=1 SV=1	Q8ID43_P LAF7	17 kDa	X	X	X	X	X	X
Early transcribed membrane protein 10.2 (Fragment) OS=Plasmodium falciparum PE=4 SV=1	C5HWR7_ PLAFA (+1)	36 kDa	X	X	X	X	X	X
Protein phosphatase 2C OS=Plasmodium falciparum (isolate 3D7) GN=PF11_0396 PE=3 SV=2	Q8IHY0_P LAF7	105 kDa	X	X	X	X	X	X
Proteasome subunit alpha type OS=Plasmodium falciparum (isolate 3D7) GN=PF07_0112 PE=3 SV=1	Q8IBI3_P LAF7	28 kDa	X	X	X	X	X	X
T-complex protein 1 subunit alpha OS=Plasmodium falciparum (isolate 3D7) GN=PF11_0331 PE=3 SV=1	Q8II43_PL AF7	60 kDa	X	X	X	X	X	X
Thioredoxin-related protein, putative OS=Plasmodium falciparum (isolate 3D7) GN=PF13_0272 PE=4 SV=1	Q8IDH5_P LAF7	24 kDa	X	X	X	X	X	X
Casein kinase II, alpha subunit OS=Plasmodium falciparum (isolate 3D7) GN=CK2alpha PE=4 SV=1	Q8IIR9_P LAF7	40 kDa	X	X	X	X	X	X
Conserved GTP-binding protein, putative OS=Plasmodium falciparum (isolate 3D7) GN=MAL7P1.122 PE=4 SV=1	Q8IBM9_ PLAF7	45 kDa	X	X	X	X	X	X
Adenylate kinase 2 OS=Plasmodium falciparum PE=1 SV=1	Q7Z0H0_ PLAFA	28 kDa	X	X	X	X	X	X
Macrophage migration inhibitory factor homologue OS=Plasmodium falciparum (isolate 3D7) GN=MIF PE=1 SV=1	Q8I5C5_P LAF7	13 kDa	X	X	X	X	X	X
Isoleucine-tRNA ligase, putative OS=Plasmodium falciparum (isolate 3D7) GN=PF13_0179 PE=3 SV=1	Q8IDZ9_P LAF7	151 kDa	X	X	X	X	X	X
40S ribosomal protein S2, putative OS=Plasmodium falciparum (isolate 3D7) GN=PF14_0448 PE=3 SV=1	Q8IL02_P LAF7	30 kDa	X	X	X	X	X	X
Conserved protein OS=Plasmodium falciparum (isolate 3D7) GN=PF11_0055 PE=4 SV=1	Q8IIV8_P LAF7	49 kDa	X	X	X	X	X	X

Identified Proteins	UniProt Accession Number	Molecular Weight	Sample					
			W2C1	W2C2	W2C3	W2T1	W2T2	W2T3
Proliferation-associated protein 2g4, putative OS=Plasmodium falciparum (isolate 3D7) GN=PF14_0261 PE=4 SV=1	Q81L12_PL AF7	43 kDa	X	X	X	X	X	X
Putative uncharacterized protein OS=Plasmodium falciparum (isolate 3D7) GN=PFD0080c PE=4 SV=1	Q81207_P LAF7	60 kDa	X	X	X	X	X	X
Ubiquitin-activating enzyme E1, putative OS=Plasmodium falciparum (isolate 3D7) GN=PFL1245w PE=4 SV=1	Q815F9_P LAF7	132 kDa	X	X	X	X	X	X
Putative uncharacterized protein OS=Plasmodium falciparum (isolate 3D7) GN=PFE1600w PE=4 SV=1	Q813F1_P LAF7	60 kDa	X	X	X	X	X	X
Acyl-CoA synthetase, PfACS10 OS=Plasmodium falciparum (isolate 3D7) GN=PfACS10 PE=4 SV=1	Q813L4_P LAF7	77 kDa	X	X	X	X	X	X
60S ribosomal protein L4, putative OS=Plasmodium falciparum (isolate 3D7) GN=PFE0350c PE=4 SV=1	Q81431_P LAF7	46 kDa	X	X	X	X	X	X
Asparagine-tRNA ligase, putative OS=Plasmodium falciparum (isolate 3D7) GN=PFB0525w PE=3 SV=1	O96198_P LAF7	71 kDa	X	X	X	X	X	X
RabGDI protein OS=Plasmodium falciparum GN=rabGDI PE=2 SV=1	Q26001_P LAFA (+1)	52 kDa	X	X	X	X	X	X
40S ribosomal protein S19, putative OS=Plasmodium falciparum (isolate 3D7) GN=PFD1055w PE=4 SV=1	Q81FP2_P LAF7	20 kDa	X	X	X	X	X	X
Proteasome subunit alpha type 2, putative OS=Plasmodium falciparum (isolate 3D7) GN=PFF0420c PE=4 SV=1	C6KST3_ PLAF7	27 kDa	X	X	X	X	X	X
Importin subunit alpha OS=Plasmodium falciparum PE=3 SV=1	Q7KAV0_ PLAFA (+1)	61 kDa	X	X	X	X	X	X
Nascent polypeptide associated complex alpha chain, putative OS=Plasmodium falciparum (isolate 3D7) GN=PFF1050w PE=4 SV=1	C6KT55_ PLAF7	21 kDa	X	X	X	X		X
Histone binding protein, putative OS=Plasmodium falciparum (isolate 3D7) GN=PFL0280c PE=4 SV=1	Q815Y9_P LAF7	39 kDa	X	X	X	X	X	X
Ubiquitin domain containing protein OS=Plasmodium falciparum (isolate 3D7) GN=PF11_0142 PE=4 SV=1	Q81IM8_P LAF7	43 kDa	X	X	X	X	X	X
40S ribosomal protein S6, putative OS=Plasmodium falciparum (isolate 3D7) GN=PF13_0228 PE=4 SV=1	Q81DR9_P LAF7	35 kDa	X	X	X	X	X	X
Profilin OS=Plasmodium falciparum (isolate 3D7) GN=Pfn PE=3 SV=1	PROF_PL AF7	19 kDa	X	X	X	X	X	X
Transketolase OS=Plasmodium falciparum (isolate 3D7) GN=PfTK PE=4 SV=1	C6KSV3_ PLAF7	76 kDa	X	X	X	X	X	X
Chaperonin CPN60, mitochondrial OS=Plasmodium falciparum (isolate FCR-3 / Gambia) PE=3 SV=1	CH60_PL AFG	79 kDa	X	X	X	X	X	X
T-complex protein 1 epsilon subunit, putative OS=Plasmodium falciparum (isolate 3D7) GN=PFC0900w PE=3 SV=1	O97282_P LAF7	59 kDa	X	X	X	X	X	X
Threonine--tRNA ligase, putative OS=Plasmodium falciparum (isolate 3D7) GN=PF11_0270 PE=3 SV=1	Q81IA4_P LAF7	120 kDa	X	X	X	X	X	X
Glutamate--tRNA ligase, putative OS=Plasmodium falciparum (isolate 3D7) GN=PF13_0257 PE=3 SV=1	Q81DK7_P LAF7	101 kDa	X	X	X	X	X	X
High mobility group protein OS=Plasmodium falciparum (isolate 3D7) GN=PfHMGB2 PE=4 SV=1	Q81B14_P LAF7	12 kDa	X	X	X		X	
Pre-mRNA splicing factor, putative OS=Plasmodium falciparum (isolate 3D7) GN=PFD0265w PE=4 SV=1	Q811X5_P LAF7	366 kDa	X	X	X	X		
Proteasome subunit alpha type 1, putative OS=Plasmodium falciparum (isolate 3D7) GN=PF14_0716 PE=4 SV=1	Q81K90_P LAF7	29 kDa	X	X	X	X	X	X
Nuclear transport factor 2, putative OS=Plasmodium falciparum (isolate 3D7) GN=PF14_0122 PE=4 SV=2	Q81LX1_P LAF7	14 kDa	X	X	X	X	X	X
26S proteasome regulatory subunit 7, putative OS=Plasmodium falciparum (isolate 3D7) GN=PF13_0063 PE=3 SV=2	Q81EK3_P LAF7	47 kDa	X	X	X	X		X

Identified Proteins	UniProt Accession Number	Molecular Weight	Sample						
			W2C1	W2C2	W2C3	W2T1	W2T2	W2T3	
Antigen 332, DBL-like protein OS=Plasmodium falciparum (isolate 3D7) GN=PF11_0506 PE=4 SV=2	Q8IHN4_P LAF7	689 kDa	X				X		X
Phosphoribosylpyrophosphate synthetase OS=Plasmodium falciparum (isolate 3D7) GN=PF13_0143 PE=3 SV=1	Q8IE67_P LAF7	49 kDa	X	X	X	X	X	X	X
Early transcribed membrane protein 5, ETRAMP5 OS=Plasmodium falciparum (isolate 3D7) GN=ETRAPM5 PE=4 SV=1	Q8I3F3_P LAF7	19 kDa	X	X	X	X	X	X	X
Eukaryotic translation initiation factor 3 37.28 kDa subunit, putative OS=Plasmodium falciparum (isolate 3D7) GN=MAL7P1.81 PE=4 SV=1	Q8IBT2_P LAF7	37 kDa	X	X	X	X	X	X	X
Ribonucleoside-diphosphate reductase OS=Plasmodium falciparum (isolate 3D7) GN=PF14_0352 PE=3 SV=1	Q8IL94_P LAF7	97 kDa	X	X	X	X	X	X	X
40S ribosomal protein S8 OS=Plasmodium falciparum (isolate 3D7) GN=PF14_0083 PE=3 SV=1	Q8IM10_P LAF7	25 kDa	X	X	X	X	X	X	X
Small ubiquitin-related modifier, putative OS=Plasmodium falciparum (isolate 3D7) GN=PfSUMO PE=4 SV=1	Q8I444_P LAF7	11 kDa	X	X	X	X	X	X	X
Putative uncharacterized protein OS=Plasmodium falciparum (isolate 3D7) GN=PF14_0546 PE=4 SV=1	Q8IKQ7_P LAF7	76 kDa	X	X	X	X	X	X	X
60S ribosomal protein L7, putative OS=Plasmodium falciparum (isolate 3D7) GN=PFC0300c PE=4 SV=2	O97250_P LAF7	31 kDa	X	X	X	X	X	X	X
Conserved Plasmodium protein OS=Plasmodium falciparum (isolate 3D7) GN=PF11_0302 PE=4 SV=1	Q8II72_PL AF7	52 kDa	X	X	X	X	X	X	X
Translation elongation factor 1 beta OS=Plasmodium falciparum GN=EF-1b PE=2 SV=1	Q9NI00_P LAFA	32 kDa	X	X	X	X	X	X	X
Insulinase, putative OS=Plasmodium falciparum (isolate 3D7) GN=PF11_0189 PE=3 SV=1	Q8III5_PL AF7	174 kDa	X	X	X	X	X	X	X
1-cys peroxiredoxin OS=Plasmodium falciparum (isolate 3D7) GN=1-cyspxn PE=4 SV=1	Q8IAM2_ PLAF7 (+1)	25 kDa	X	X	X	X	X	X	X
26S proteasome regulatory subunit, putative OS=Plasmodium falciparum (isolate 3D7) GN=PF13_0033 PE=3 SV=1	Q8IEQ1_P LAF7	45 kDa	X	X	X	X	X	X	X
Eukaryotic translation initiation factor 3 subunit 7, putative OS=Plasmodium falciparum (isolate 3D7) GN=PF10_0077 PE=4 SV=1	Q8IJW4_P LAF7	63 kDa	X	X	X	X	X	X	X
RNA binding protein, putative OS=Plasmodium falciparum (isolate 3D7) GN=PF13_0315 PE=4 SV=1	Q8IDB7_P LAF7	57 kDa	X	X	X	X	X	X	X
Adenylosuccinate synthetase OS=Plasmodium falciparum (isolate 3D7) GN=Adss PE=3 SV=1	PURA_PL AF7 (+1)	50 kDa	X	X	X	X	X	X	X
Ran binding protein 1, putative OS=Plasmodium falciparum (isolate 3D7) GN=PFD0950w PE=4 SV=1	Q76NN6_ PLAF7 (+1)	33 kDa	X	X	X	X	X	X	X
60S ribosomal protein L12, putative OS=Plasmodium falciparum (isolate 3D7) GN=PFE0850c PE=3 SV=2	Q8I3T8_P LAF7	18 kDa	X	X	X	X	X	X	X
Plasmeprin-1 OS=Plasmodium falciparum PE=1 SV=2	PLM1_PL AFA (+1)	51 kDa	X	X	X	X	X	X	X
Ribonucleotide reductase small subunit, putative OS=Plasmodium falciparum (isolate 3D7) GN=PF10_0154 PE=4 SV=2	Q8IJN8_P LAF7	40 kDa	X	X	X	X	X	X	X
Inosine-5'-monophosphate dehydrogenase OS=Plasmodium falciparum PE=2 SV=1	O96387_P LAFA (+1)	56 kDa	X	X	X	X	X	X	X
Putative uncharacterized protein OS=Plasmodium falciparum (isolate 3D7) GN=PFD1170c PE=4 SV=1	Q8IFM0_P LAF7	36 kDa	X	X	X	X	X	X	X

Identified Proteins	UniProt Accession Number	Molecular Weight	Sample					
			W2C1	W2C2	W2C3	W2T1	W2T2	W2T3
7,8-dihydro-6-hydroxymethylpterin pyrophosphokinase-dihydropteroate synthase OS=Plasmodium falciparum GN=PPPK-DHPS PE=4 SV=1	Q25704_P LAFA	83 kDa	X	X	X	X		X
60S ribosomal protein L5, putative OS=Plasmodium falciparum (isolate 3D7) GN=PF14_0230 PE=3 SV=1	Q8ILL3_P LAF7	34 kDa	X	X	X	X	X	X
Small heat shock protein, putative OS=Plasmodium falciparum (isolate 3D7) GN=PF13_0021 PE=3 SV=1	Q8IES0_P LAF7	25 kDa	X	X	X	X	X	X
Glutaredoxin OS=Plasmodium falciparum GN=fulmal4 PE=4 SV=1	Q7KXR4_ PLAFA (+1)	12 kDa	X	X		X		
Proteasome subunit alpha type OS=Plasmodium falciparum (isolate 3D7) GN=MAL13P1.270 PE=3 SV=1	Q8IDG2_ PLAF7	27 kDa	X	X	X	X	X	X
T-complex protein 1 subunit eta OS=Plasmodium falciparum (isolate 3D7) GN=MAL3P3.6 PE=3 SV=1	TCPH_PL AF7	60 kDa	X	X	X	X	X	X
60S ribosomal protein L3, putative OS=Plasmodium falciparum (isolate 3D7) GN=PF10_0272 PE=3 SV=1	Q8IJC6_P LAF7	44 kDa	X		X			X
Beta3 proteasome subunit, putative OS=Plasmodium falciparum (isolate 3D7) GN=PFA_0400c PE=4 SV=1	Q8I261_P LAF7	23 kDa	X	X	X	X	X	
Hsp70-x OS=Plasmodium falciparum (isolate 3D7) PE=2 SV=1	K7NTP5_ PLAF7	75 kDa	X	X	X	X	X	X
Chromatin assembly factor 1 protein WD40 domain, putative OS=Plasmodium falciparum (isolate 3D7) GN=PFA_0520c PE=4 SV=1	Q8I238_P LAF7	51 kDa	X	X	X	X	X	X
Putative uncharacterized protein OS=Plasmodium falciparum (isolate 3D7) GN=PPF1295w PE=4 SV=1	C6KTA3_ PLAF7	44 kDa	X	X	X	X	X	X
Calcyclin binding protein, putative OS=Plasmodium falciparum (isolate 3D7) GN=PFL1845c PE=4 SV=2	Q8I542_P LAF7	27 kDa	X	X	X	X	X	X
Cysteine-rich surface protein (Fragment) OS=Plasmodium falciparum PE=4 SV=1	C5HXB3_ PLAFA	91 kDa	X	X	X	X	X	X
p23 co-chaperone, putative OS=Plasmodium falciparum (isolate 3D7) GN=SBA1 PE=4 SV=2	Q8IKU1_P LAF7	30 kDa	X	X	X	X	X	X
Glutamate dehydrogenase, putative OS=Plasmodium falciparum (isolate 3D7) GN=PF08_0132 PE=4 SV=1	Q8IAM0_ PLAF7	160 kDa	X			X	X	X
Putative uncharacterized protein OS=Plasmodium falciparum (isolate 3D7) GN=PPF0220w PE=4 SV=1	C6KSP3_ PLAF7	334 kDa	X		X	X	X	X
DNAJ protein, putative OS=Plasmodium falciparum (isolate 3D7) GN=PF14_0700 PE=4 SV=1	Q8IKA6_P LAF7	52 kDa	X	X	X	X	X	X
40S ribosomal protein SA OS=Plasmodium falciparum (isolate 3D7) GN=PF10_0264 PE=3 SV=1	RSSA_PL AF7	30 kDa	X	X	X	X	X	X
Valine-tRNA ligase, putative OS=Plasmodium falciparum (isolate 3D7) GN=PF14_0589 PE=3 SV=1	Q8IKL5_P LAF7	128 kDa	X	X	X	X	X	X
Glutathione S-transferase OS=Plasmodium falciparum (isolate 3D7) GN=GST PE=3 SV=1	GST_PLA F7 (+1)	25 kDa	X	X	X	X	X	X
Eukaryotic translation initiation factor 3 subunit 10, putative OS=Plasmodium falciparum (isolate 3D7) GN=PFL0625c PE=4 SV=1	Q8I5S6_P LAF7	166 kDa	X			X		X
Putative uncharacterized protein OS=Plasmodium falciparum (isolate 3D7) GN=MAL7P1.171 PE=4 SV=1	Q8IBF2_P LAF7	244 kDa	X		X	X		X
Multidrug resistance protein OS=Plasmodium falciparum (isolate 3D7) GN=PfMDR1 PE=3 SV=1	Q7K6A5_ PLAF7	162 kDa	X	X	X	X	X	X
Ubiquitin conjugating enzyme E2, putative OS=Plasmodium falciparum (isolate 3D7) GN=PFC0255c PE=1 SV=1	O97241_P LAF7	16 kDa	X		X	X	X	
Probable cathepsin C OS=Plasmodium falciparum (isolate 3D7) GN=PF11_0174 PE=1 SV=1	CATC_PL AF7	80 kDa	X	X		X	X	

Identified Proteins	UniProt Accession Number	Molecular Weight	Sample					
			W2C1	W2C2	W2C3	W2T1	W2T2	W2T3
ATPase OS=Plasmodium falciparum PE=3 SV=1	Q27721_P LAFA (+2)	122 kDa	X		X	X		X
Eukaryotic translation initiation factor 2 gamma subunit, putative OS=Plasmodium falciparum (isolate 3D7) GN=PF14_0104 PE=4 SV=1	Q8ILY9_P LAF7	51 kDa	X	X	X	X	X	X
Eukaryotic translation initiation factor 3 subunit B OS=Plasmodium falciparum (isolate 3D7) GN=PFE0885w PE=3 SV=1	Q8I3T1_P LAF7	84 kDa	X	X	X	X	X	X
6-phosphogluconate dehydrogenase, decarboxylating OS=Plasmodium falciparum (isolate 3D7) GN=PF14_0520 PE=3 SV=1	Q8IKT2_P LAF7	53 kDa	X	X	X	X	X	X
26S proteasome subunit, putative OS=Plasmodium falciparum (isolate 3D7) GN=PF14_0632 PE=4 SV=1	Q8IKH3_P LAF7	133 kDa	X		X	X	X	X
Seryl-tRNA synthetase, putative OS=Plasmodium falciparum (isolate 3D7) GN=PF07_0073 PE=4 SV=1	Q8IBS3_P LAF7	62 kDa	X	X	X	X	X	X
Clathrin heavy chain, putative OS=Plasmodium falciparum (isolate 3D7) GN=PFL0930w PE=4 SV=1	Q8I5L6_P LAF7	233 kDa	X			X	X	X
Proteasome subunit alpha type OS=Plasmodium falciparum (isolate 3D7) GN=PF13_0282 PE=3 SV=1	Q8IDG3_ PLAF7	28 kDa	X	X	X	X	X	X
Prefoldin subunit 2, putative OS=Plasmodium falciparum (isolate 3D7) GN=PF14_0167 PE=4 SV=1	Q8ILS7_P LAF7	17 kDa	X	X	X		X	X
Leucyl tRNA synthase OS=Plasmodium falciparum (isolate 3D7) GN=PFF1095w PE=3 SV=1	C6KT64_ PLAF7	170 kDa	X		X	X	X	X
40S ribosomal protein S18, putative OS=Plasmodium falciparum (isolate 3D7) GN=PF11_0272 PE=3 SV=1	Q8IIA2_P LAF7	18 kDa	X	X	X	X	X	X
Glycophorin-binding protein OS=Plasmodium falciparum (isolate FCR-3 / Gambia) GN=GBP PE=2 SV=2	GBP_PLA FG	90 kDa	X	X	X	X		X
FK506-binding protein (FKBP)-type peptidyl-propyl isomerase OS=Plasmodium falciparum (isolate 3D7) GN=FKBP35 PE=1 SV=1	Q8I4V8_P LAF7	35 kDa	X		X	X	X	
26S protease subunit regulatory subunit 6a, putative OS=Plasmodium falciparum (isolate 3D7) GN=PF11_0314 PE=3 SV=1	Q8II60_PL AF7	50 kDa	X	X	X	X	X	X
tRNA binding protein, putative OS=Plasmodium falciparum (isolate 3D7) GN=PF14_0401 PE=4 SV=1	Q8IL48_P LAF7	46 kDa	X	X	X	X	X	X
10 kd chaperonin OS=Plasmodium falciparum (isolate 3D7) GN=Cpn10 PE=3 SV=2	Q8I5Q3_P LAF7	11 kDa	X	X	X	X	X	X
Alanine--tRNA ligase, putative OS=Plasmodium falciparum (isolate 3D7) GN=PF13_0354 PE=3 SV=1	Q8ID31_P LAF7	165 kDa	X	X	X	X	X	X
Tat-binding protein homolog OS=Plasmodium falciparum (isolate 3D7) GN=PFL2345c PE=3 SV=1	Q8I4U5_P LAF7	50 kDa	X			X	X	
Hsp70 interacting protein, putative OS=Plasmodium falciparum (isolate 3D7) GN=PFE1370w PE=4 SV=1	Q8I3J0_P LAF7	51 kDa	X	X	X	X	X	X
26S proteasome AAA-ATPase subunit RPT3, putative OS=Plasmodium falciparum (isolate 3D7) GN=PFD0665c PE=3 SV=1	Q8I1V1_P LAF7	45 kDa	X	X	X	X	X	X
Putative uncharacterized protein OS=Plasmodium falciparum (isolate 3D7) GN=PF14_0344 PE=4 SV=1	Q8ILA1_P LAF7	112 kDa	X	X	X	X	X	X
Proteasome 26S regulatory subunit, putative OS=Plasmodium falciparum (isolate 3D7) GN=PFB0260w PE=4 SV=3	O96153_P LAF7	108 kDa	X	X	X	X	X	X
GMP synthetase OS=Plasmodium falciparum (isolate 3D7) GN=PF10_0123 PE=1 SV=1	Q8IJR9_P LAF7	64 kDa	X	X	X	X	X	X
Proline reductase OS=Plasmodium falciparum (isolate 3D7) GN=MAL13P1.284 PE=1 SV=1	Q8IDC6_P LAF7	28 kDa	X	X	X	X	X	X
Small GTP-binding protein sar1 OS=Plasmodium falciparum (isolate 3D7) GN=sar1 PE=3 SV=1	Q8I1S0_P LAF7 (+1)	22 kDa	X	X	X	X	X	X

Identified Proteins	UniProt Accession Number	Molecular Weight	Sample					
			W2C1	W2C2	W2C3	W2T1	W2T2	W2T3
Conserved Plasmodium membrane protein OS=Plasmodium falciparum (isolate 3D7) GN=PFL1825w PE=4 SV=1	Q8I546_P LAF7	24 kDa	X	X	X		X	
Liver stage antigen 3 OS=Plasmodium falciparum GN=LSA-3 PE=4 SV=1	C7DU25_ PLAFA (+1)	171 kDa	X				X	X
Helicase, putative OS=Plasmodium falciparum (isolate 3D7) GN=PF14_0437 PE=3 SV=2	Q8IL13_P LAF7	60 kDa	X	X	X	X		X
Plastidic co-chaperonin OS=Plasmodium falciparum GN=Cpn20 PE=2 SV=1	Q50JA7_P LAFA (+1)	29 kDa	X	X	X	X	X	X
Proteasome subunit alpha, putative OS=Plasmodium falciparum (isolate 3D7) GN=MAL8P1.128 PE=4 SV=2	Q8IAR3_P LAF7	30 kDa		X	X	X	X	X
Merozoite surface protein 1 OS=Plasmodium falciparum (isolate 3D7) GN=MSP1 PE=4 SV=1	Q8IU8_P LAF7	196 kDa	X	X		X	X	X
Merozoite surface protein 9 (Fragment) OS=Plasmodium falciparum PE=4 SV=1	C5HEE5_ PLAFA	83 kDa	X	X	X	X	X	X
Proteasome subunit beta type OS=Plasmodium falciparum (isolate 3D7) GN=MAL8P1.142 PE=3 SV=1	Q7K6A9_ PLAF7 (+1)	31 kDa	X	X	X	X	X	
Dynamin-like protein OS=Plasmodium falciparum (isolate 3D7) GN=dyn1 PE=3 SV=1	Q8IHR4_P LAF7	96 kDa	X		X	X	X	X
High mobility group protein OS=Plasmodium falciparum PE=4 SV=1	Q25871_P LAFA (+2)	11 kDa	X		X	X		
Proline--tRNA ligase OS=Plasmodium falciparum (isolate 3D7) GN=proRS PE=1 SV=1	SYP_PLA F7	87 kDa	X	X	X	X	X	X
Rhoptry-associated protein 2 (Fragment) OS=Plasmodium falciparum GN=RAP2 PE=4 SV=1	B9VGG5_ PLAFA (+3)	42 kDa	X	X	X	X	X	X
Proteasome subunit beta type OS=Plasmodium falciparum (isolate 3D7) GN=PFE0915c PE=3 SV=1	C0H4E8_ PLAF7	27 kDa	X	X	X	X	X	X
PfRab7, GTPase OS=Plasmodium falciparum (isolate 3D7) GN=Rab7 PE=3 SV=1	C0H516_ PLAF7 (+1)	24 kDa	X	X	X	X	X	X
Heat shock protein 101, putative OS=Plasmodium falciparum (isolate 3D7) GN=PF11_0175 PE=3 SV=1	Q8IIJ8_PL AF7	103 kDa	X		X	X	X	X
60S ribosomal protein P1, putative OS=Plasmodium falciparum (isolate 3D7) GN=PF11_0043 PE=4 SV=1	Q8IIX0_P LAF7	13 kDa	X	X	X	X	X	
40S ribosomal protein S14, putative OS=Plasmodium falciparum (isolate 3D7) GN=PFE0810c PE=3 SV=1	Q8I3U6_P LAF7	16 kDa	X	X	X	X	X	X
DNAJ protein, putative OS=Plasmodium falciparum (isolate 3D7) GN=RESA PE=4 SV=1	Q8IU6_P LAF7	127 kDa	X	X	X	X	X	X
Acyl-coA synthetase, PfACS5 OS=Plasmodium falciparum (isolate 3D7) GN=PfACS5 PE=4 SV=1	Q8I6Z1_P LAF7	93 kDa	X	X	X	X	X	X
Protein disulfide isomerase OS=Plasmodium falciparum (isolate 3D7) GN=PDI-11 PE=4 SV=1	Q8II23_PL AF7	49 kDa	X		X	X	X	X
Proteasome component C8, putative OS=Plasmodium falciparum (isolate 3D7) GN=PFC0745c PE=4 SV=1	O77396_P LAF7	29 kDa	X	X		X	X	X
Bifunctional dihydrofolate reductase-thymidylate synthase OS=Plasmodium falciparum GN=DHFR-TS PE=1 SV=1	D9N170_ PLAFA	72 kDa	X	X	X	X		X
Eukaryotic translation initiation factor 3 subunit 8, putative OS=Plasmodium falciparum (isolate 3D7) GN=PFL0310c PE=4 SV=1	Q8I5Y3_P LAF7	116 kDa	X	X	X	X	X	X
T-complex protein 1, putative OS=Plasmodium falciparum (isolate 3D7) GN=PFB0635w PE=3 SV=3	O96220_P LAF7	61 kDa	X	X	X	X	X	X
Putative uncharacterized protein OS=Plasmodium falciparum (isolate 3D7) GN=MAL7P1.202 PE=4 SV=1	C0H4L1_ PLAF7	146 kDa	X	X	X	X	X	X

Identified Proteins	UniProt Accession Number	Molecular Weight	Sample					
			W2C1	W2C2	W2C3	W2T1	W2T2	W2T3
Merozoite surface protein 1 OS=Plasmodium falciparum GN=msp1 PE=4 SV=1	Q764L1_P LAFA	193 kDa	X	X	X	X	X	X
Structure specific recognition protein OS=Plasmodium falciparum (isolate 3D7) GN=PF14_0393 PE=4 SV=1	Q8IL56_P LAF7	59 kDa	X		X	X	X	X
Putative uncharacterized protein OS=Plasmodium falciparum (isolate 3D7) GN=MAL7P1.29 PE=4 SV=1	REVERSE_Q8IBZ1_PLAF7-R	274 kDa	X		X			X
PIESP2 erythrocyte surface protein OS=Plasmodium falciparum (isolate 3D7) GN=PFE0060w PE=4 SV=1	Q8I488_P LAF7	49 kDa	X	X		X	X	
Falstatin (Fragment) OS=Plasmodium falciparum PE=2 SV=1	Q2PZB1_PLAFA(+1)	44 kDa	X	X	X		X	
Mannose-6-phosphate isomerase, putative OS=Plasmodium falciparum (isolate 3D7) GN=MAL8P1.156 PE=4 SV=1	Q8IAL6_P LAF7	118 kDa	X		X		X	X
Putative uncharacterized protein OS=Plasmodium falciparum (isolate 3D7) GN=PF10495w PE=4 SV=1	REVERSE_Q8I350_PLAF7-R	368 kDa	X					
Exportin 1, putative OS=Plasmodium falciparum (isolate 3D7) GN=PFC0135c PE=4 SV=2	O77312_P LAF7	148 kDa	X		X	X	X	X
40S ribosomal protein S12 OS=Plasmodium falciparum (isolate 3D7) GN=RPS12 PE=3 SV=1	RS12_PL AF7	15 kDa	X	X	X	X	X	X
DNA replication licensing factor MCM2 OS=Plasmodium falciparum GN=mcm2 PE=3 SV=1	Q9GR05_PLAFA	112 kDa	X	X	X	X	X	X
40S ribosomal protein S3a OS=Plasmodium falciparum (isolate 3D7) GN=MAL3P7.35 PE=3 SV=1	RS3A_PL AF7	30 kDa	X	X	X	X	X	X
60S ribosomal protein L1, putative OS=Plasmodium falciparum (isolate 3D7) GN=PF14_0391 PE=4 SV=1	Q8IL58_P LAF7	25 kDa	X	X	X	X		X
Translation initiation factor eIF-1A, putative OS=Plasmodium falciparum (isolate 3D7) GN=PF11_0447 PE=3 SV=2	Q8IHT2_P LAF7	18 kDa	X	X		X		X
Sec31p putative OS=Plasmodium falciparum (isolate 3D7) GN=Sec31p PE=4 SV=3	O96221_P LAF7	167 kDa	X	X	X	X	X	X
Merozoite surface protein 7 OS=Plasmodium falciparum PE=4 SV=1	C5HWK9_PLAFA	41 kDa	X		X	X		X
Deoxyribose-phosphate aldolase, putative OS=Plasmodium falciparum (isolate 3D7) GN=PF10_0210 PE=4 SV=1	Q8IJ17_PL AF7	29 kDa	X	X	X		X	
40S ribosomal protein S4, putative OS=Plasmodium falciparum (isolate 3D7) GN=PF11_0065 PE=4 SV=2	Q8IIU8_P LAF7	30 kDa	X	X	X	X	X	X
Chromodomain protein OS=Plasmodium falciparum (isolate 3D7) GN=PFL1005c PE=4 SV=1	Q8I5K4_P LAF7	31 kDa	X	X	X	X	X	
Proteasome subunit beta type OS=Plasmodium falciparum (isolate 3D7) GN=PF13_0156 PE=3 SV=1	Q8I6T3_P LAF7	30 kDa	X	X	X	X	X	
26S proteasome regulatory subunit 4, putative OS=Plasmodium falciparum (isolate 3D7) GN=PF10_0081 PE=3 SV=2	Q8IJW0_P LAF7	50 kDa	X		X	X	X	X
Serine repeat antigen 5 (Fragment) OS=Plasmodium falciparum GN=sera5 PE=3 SV=1	I0I2S8_PL AFA	109 kDa	X		X	X	X	X
Putative uncharacterized protein OS=Plasmodium falciparum (isolate 3D7) GN=MAL7P1.225.1 PE=4 SV=1	C0H4J3_P LAF7 (+1)	34 kDa	X	X	X	X	X	
RNA binding protein, putative OS=Plasmodium falciparum (isolate 3D7) GN=MAL8P1.40 PE=4 SV=1	Q8IB66_P LAF7	32 kDa	X		X		X	
Surface protein, Pf113 OS=Plasmodium falciparum (isolate 3D7) GN=PF113 PE=4 SV=1	Q8ILP3_P LAF7	113 kDa	X				X	
Putative uncharacterized protein OS=Plasmodium falciparum (isolate 3D7) GN=PF14_0191 PE=4 SV=1	Q8ILQ3_P LAF7	60 kDa	X	X	X	X		X

Identified Proteins	UniProt Accession Number	Molecular Weight	Sample					
			W2C1	W2C2	W2C3	W2T1	W2T2	W2T3
Thioredoxin reductase 2 OS=Plasmodium falciparum (isolate 3D7) GN=trxr2 PE=2 SV=2	TRXR2_P LAF7 (+1)	69 kDa			X	X	X	X
MIF4G domain containing protein OS=Plasmodium falciparum (isolate 3D7) GN=PF11_0086 PE=4 SV=1	Q8IIS9_P LAF7	382 kDa	X		X			X
Eukaryotic translation initiation factor 2 alpha subunit, putative OS=Plasmodium falciparum (isolate 3D7) GN=PF07_0117 PE=4 SV=1	Q8IBH7_P LAF7	38 kDa	X				X	
Transcriptional regulator, putative OS=Plasmodium falciparum (isolate 3D7) GN=PFE0870w PE=4 SV=1	Q8I3T4_P LAF7	133 kDa	X		X	X	X	X
Putative uncharacterized protein OS=Plasmodium falciparum (isolate 3D7) GN=PFC0435w PE=4 SV=1	O77361_P LAF7	154 kDa	X	X				X
Subunit of proteasome activator complex, putative OS=Plasmodium falciparum (isolate 3D7) GN=PFI0370c PE=4 SV=1	Q8I374_P LAF7	33 kDa	X	X	X	X	X	X
GTPase (Rab6) OS=Plasmodium falciparum GN=rab6 PE=1 SV=1	Q26000_P LAFA	24 kDa	X	X	X	X	X	X
Pre-mRNA splicing factor, putative OS=Plasmodium falciparum (isolate 3D7) GN=PF10_0217 PE=4 SV=1	Q8IJU0_PL AF7	62 kDa	X		X	X		X
Proton-pumping vacuolar pyrophosphatase OS=Plasmodium falciparum GN=VP1 PE=3 SV=1	O97154_P LAFA (+1)	76 kDa	X	X	X	X	X	
Putative uncharacterized protein OS=Plasmodium falciparum (isolate 3D7) GN=PF14_0649 PE=4 SV=1	Q8IKF6_P LAF7	296 kDa	X		X	X	X	X
Conserved Plasmodium protein OS=Plasmodium falciparum (isolate 3D7) GN=PFB0115w PE=4 SV=1	O96127_P LAF7	142 kDa	X	X	X			X
Carbamoyl phosphate synthetase II OS=Plasmodium falciparum PE=4 SV=1	Q27732_P LAFA	276 kDa	X		X	X		X
Eukaryotic translation initiation factor 3 subunit E OS=Plasmodium falciparum (isolate 3D7) GN=PFE1405c PE=3 SV=1	Q8I315_PL AF7	61 kDa	X	X	X	X	X	X
Minichromosome maintenance protein 3, putative OS=Plasmodium falciparum (isolate 3D7) GN=PFE1345c PE=3 SV=1	Q8I3J5_P LAF7	110 kDa	X	X	X	X	X	X
Co-chaperone GrpE, putative OS=Plasmodium falciparum (isolate 3D7) GN=PF11_0258 PE=3 SV=2	Q8IIB6_P LAF7 (+1)	35 kDa	X		X	X	X	X
60S ribosomal protein L7-3, putative OS=Plasmodium falciparum (isolate 3D7) GN=PF14_0231 PE=4 SV=2	Q8ILL2_P LAF7	33 kDa	X	X	X	X		X
Glutathione reductase OS=Plasmodium falciparum (isolate K1 / Thailand) GN=GR2 PE=1 SV=3	GSHR_PL AFK	57 kDa	X		X	X		X
Glideosome-associated protein 50 OS=Plasmodium falciparum (isolate 3D7) GN=GAP50 PE=1 SV=1	Q8I2X3_P LAF7	45 kDa	X	X	X	X		X
Rab1b, GTPase OS=Plasmodium falciparum (isolate 3D7) GN=Rab1b PE=4 SV=1	Q7K6A8_ PLAF7	23 kDa	X	X		X		
Basic transcription factor 3b, putative OS=Plasmodium falciparum (isolate 3D7) GN=PF14_0241 PE=4 SV=1	Q8ILK2_P LAF7	19 kDa		X	X	X	X	X
26s proteasome subunit p55, putative OS=Plasmodium falciparum (isolate 3D7) GN=PF10_0174 PE=4 SV=1	Q8IJM0_P LAF7	55 kDa	X	X	X	X	X	X
40S ribosomal protein S17, putative OS=Plasmodium falciparum (isolate 3D7) GN=PFL2055w PE=3 SV=1	Q8I502_P LAF7	16 kDa	X	X	X	X	X	X
Prefoldin subunit 3, putative OS=Plasmodium falciparum (isolate 3D7) GN=MAL7P1.94 PE=4 SV=1	Q8IBR6_P LAF7	23 kDa	X	X	X	X	X	X
Adenine nucleotide translocase OS=Plasmodium falciparum PE=2 SV=1	Q25692_P LAFA (+1)	34 kDa	X	X		X		X
Uncharacterized protein OS=Plasmodium falciparum (isolate 3D7) GN=PF13_0153 PE=4 SV=1	Q8IE45_P LAF7	116 kDa	X		X	X	X	X
Elongation factor 1 (EF-1), putative OS=Plasmodium falciparum (isolate 3D7) GN=PFC0870w PE=4 SV=2	O97319_P LAF7	18 kDa	X	X	X		X	
Chaperone, putative OS=Plasmodium falciparum (isolate 3D7) GN=PFF0430w PE=3 SV=1	C6KST5_ PLAF7	62 kDa	X	X		X		X

Identified Proteins	UniProt Accession Number	Molecular Weight	Sample					
			W2C1	W2C2	W2C3	W2T1	W2T2	W2T3
Tyrosyl-tRNA synthetase, putative OS=Plasmodium falciparum (isolate 3D7) GN=MAL8P1.125 PE=1 SV=1	Q8IAR7_P LAF7	43 kDa		X	X	X	X	
Cytoadherence linked asexual protein (Fragment) OS=Plasmodium falciparum GN=clag9 PE=2 SV=1	O77090_P LAFA	161 kDa	X					X
Translation initiation factor IF-2, putative OS=Plasmodium falciparum (isolate 3D7) GN=PFF0345w PE=4 SV=1	C6KSR8_ PLAF7	112 kDa	X			X		X
RNA binding protein, putative OS=Plasmodium falciparum (isolate 3D7) GN=PF14_0096 PE=4 SV=1	Q8IILZ7_P LAF7	59 kDa	X	X	X	X	X	X
60S ribosomal protein L27, putative OS=Plasmodium falciparum (isolate 3D7) GN=PF14_0579 PE=4 SV=2	Q8IKM5_ PLAF7	17 kDa	X	X	X	X	X	X
Chromatin assembly protein (ASF1), putative OS=Plasmodium falciparum (isolate 3D7) GN=PFL1180w PE=4 SV=1	Q8I5H2_P LAF7	32 kDa	X	X	X		X	X
cAMP-dependent protein kinase catalytic subunit OS=Plasmodium falciparum (isolate 3D7) GN=PfPKAc PE=4 SV=1	Q7K6A0_ PLAF7	40 kDa	X	X	X	X	X	
Eukaryotic translation initiation factor 3 subunit G OS=Plasmodium falciparum (isolate 3D7) GN=MAL8P1.83 PE=3 SV=1	Q8IAZ3_P LAF7	31 kDa	X	X	X		X	X
Putative uncharacterized protein OS=Plasmodium falciparum (isolate 3D7) GN=PF08_0081 PE=4 SV=1	C0H4U5_ PLAF7	77 kDa	X		X		X	X
Putative uncharacterized protein OS=Plasmodium falciparum (isolate 3D7) GN=PFE1605w PE=4 SV=1	Q8I3F0_P LAF7	61 kDa	X		X	X	X	
Splicing factor, putative OS=Plasmodium falciparum (isolate 3D7) GN=PFE0865c PE=4 SV=2	Q8I3T5_P LAF7	35 kDa	X			X		
Uncharacterized protein OS=Plasmodium falciparum (isolate 3D7) GN=PF13_0165 PE=4 SV=1	Q8IE18_P LAF7	68 kDa			X	X		
Putative uncharacterized protein OS=Plasmodium falciparum (isolate 3D7) GN=MAL8P1.103 PE=4 SV=1	C0H4U0_ PLAF7	71 kDa				X		X
40S ribosomal protein S7, putative OS=Plasmodium falciparum (isolate 3D7) GN=PF13_0014 PE=4 SV=1	Q8IET7_P LAF7	22 kDa	X	X	X	X	X	
Rhoptry associated membrane antigen (Fragment) OS=Plasmodium falciparum PE=4 SV=1	C5HXN1_ PLAFA	92 kDa	X		X	X		X
40S ribosomal protein S25, putative OS=Plasmodium falciparum (isolate 3D7) GN=PF14_0205 PE=4 SV=2	Q8ILN8_P LAF7	12 kDa	X	X		X	X	X
Clustered-asparagine-rich protein OS=Plasmodium falciparum (isolate 3D7) GN=PFL1745c PE=4 SV=2	Q8I562_P LAF7	52 kDa	X	X	X	X	X	
Polyadenylate-binding protein, putative OS=Plasmodium falciparum (isolate 3D7) GN=MAL13P1.303 PE=4 SV=1	C0H5J5_P LAF7	48 kDa	X				X	X
Erythrocyte membrane-associated antigen OS=Plasmodium falciparum (isolate 3D7) GN=MAL7P1.12 PE=4 SV=1	Q8IC35_P LAF7	263 kDa	X			X		
Tudor staphylococcal nuclease OS=Plasmodium falciparum (isolate 3D7) GN=TSN PE=4 SV=1	Q8II01_PL AF7	129 kDa			X	X	X	X
Conserved Plasmodium protein OS=Plasmodium falciparum (isolate 3D7) GN=PF10_0361 PE=4 SV=1	Q8IJ39_P LAF7	193 kDa	X		X	X	X	
Putative uncharacterized protein OS=Plasmodium falciparum (isolate 3D7) GN=PF14_0046 PE=4 SV=1	Q8IM45_P LAF7	35 kDa	X	X	X	X	X	0
Conserved Plasmodium protein OS=Plasmodium falciparum (isolate 3D7) GN=PFL2120w PE=4 SV=1	Q8I4Y9_P LAF7	155 kDa				X	X	X
Actin-2 OS=Plasmodium falciparum (isolate 3D7) GN=PF14_0124 PE=3 SV=1	ACT2_PL AF7 (+2)	43 kDa	X		X	X	X	
ATP synthase subunit beta OS=Plasmodium falciparum (isolate 3D7) GN=PFL1725w PE=3 SV=1	Q8I0V2_P LAF7	58 kDa	X	X	X	X	X	

Identified Proteins	UniProt Accession Number	Molecular Weight	Sample					
			W2C1	W2C2	W2C3	W2T1	W2T2	W2T3
Glutamate-rich protein OS=Plasmodium falciparum GN=GLURP PE=4 SV=1	Q9GTX2_ PLAFA	141 kDa	X				X	X
Phenylalanyl-tRNA synthetase beta chain, putative OS=Plasmodium falciparum (isolate 3D7) GN=PF11_0051 PE=4 SV=1	Q8IIW2_P LAF7	73 kDa	X		X	X	X	X
Conserved Plasmodium protein OS=Plasmodium falciparum (isolate 3D7) GN=PF11_0413 PE=4 SV=2	Q8IHW3_ PLAF7	53 kDa	X	X	X	X	X	X
Glutathione peroxidase OS=Plasmodium falciparum PE=3 SV=1	Q27742_P LAFA (+1)	24 kDa	X			X	X	X
PF11785w OS=Plasmodium falciparum PE=2 SV=1	B2BZB8_ PLAFA	43 kDa	X	X	X	X	X	
Aspartate aminotransferase OS=Plasmodium falciparum (isolate 3D7) GN=PFB0200c PE=1 SV=1	O96142_P LAF7	47 kDa	X		X	X	X	X
40S ribosomal protein S15/S19, putative OS=Plasmodium falciparum (isolate 3D7) GN=MAL13P1.92 PE=3 SV=1	COH5C2_ PLAF7	17 kDa	X		X			X
Uncharacterized protein OS=Plasmodium falciparum (isolate 3D7) GN=PF13_0275 PE=4 SV=1	Q8IDG9_ PLAF7	33 kDa	X		X	X	X	
Putative uncharacterized protein OS=Plasmodium falciparum (isolate 3D7) GN=PFE1465w PE=4 SV=1	COH4G7_ PLAF7	188 kDa				X		
Casein kinase 1, PfCK1 OS=Plasmodium falciparum (isolate 3D7) GN=PfCK1 PE=4 SV=1	C6S3F7_ PLAF7	38 kDa	X		X	X	X	X
Ubiquitin conjugating enzyme, putative OS=Plasmodium falciparum (isolate 3D7) GN=PFE1350c PE=1 SV=1	Q8I3J4_P LAF7	17 kDa	X			X	X	X
Fibrillarlin, putative OS=Plasmodium falciparum (isolate 3D7) GN=PF14_0068 PE=3 SV=1	Q8IM23_P LAF7	34 kDa	X		X			
Aspartyl-tRNA synthetase, putative OS=Plasmodium falciparum (isolate 3D7) GN=PFA_0145c PE=3 SV=1	Q8I2B1_P LAF7	73 kDa	X		X	X		X
Vacuolar ATP synthase subunit G, putative OS=Plasmodium falciparum (isolate 3D7) GN=PF13_0130 PE=4 SV=1	Q8IE84_P LAF7	14 kDa	X	X	X			X
Rhoptry-associated protein 3 OS=Plasmodium falciparum GN=RAP3 PE=4 SV=1	Q8MUN1_ PLAFA	47 kDa	X	X		X	X	
60S ribosomal protein L21e, putative OS=Plasmodium falciparum (isolate 3D7) GN=PF14_0240 PE=4 SV=1	Q8ILK3_P LAF7	19 kDa		X	X		X	X
26S proteasome regulatory complex subunit, putative OS=Plasmodium falciparum (isolate 3D7) GN=PF11_0303 PE=4 SV=2	Q8II71_PL AF7	47 kDa	X		X	X	X	X
Glycine-tRNA ligase, putative OS=Plasmodium falciparum (isolate 3D7) GN=PF14_0198 PE=4 SV=2	Q8ILP6_P LAF7	104 kDa	X				X	X
DNA repair protein, putative OS=Plasmodium falciparum (isolate 3D7) GN=PFE0270c PE=3 SV=1	Q8I447_P LAF7	156 kDa						X
Histidine--tRNA ligase, putative OS=Plasmodium falciparum (isolate 3D7) GN=PF14_0428 PE=4 SV=1	Q8IL22_P LAF7	134 kDa	X			X		
Protein disulfide isomerase OS=Plasmodium falciparum (isolate 3D7) GN=PfPDI-9 PE=4 SV=1	Q8I2V9_P LAF7	61 kDa	X			X		
Putative uncharacterized protein OS=Plasmodium falciparum (isolate 3D7) GN=PFC0910w PE=4 SV=1	O97284_P LAF7	50 kDa	X	X	X	X	X	X
Superoxide dismutase [Fe] OS=Plasmodium falciparum (isolate 3D7) GN=SODB PE=1 SV=1	SODF_PL AF7 (+2)	23 kDa	X	X			X	X
Putative uncharacterized protein OS=Plasmodium falciparum (isolate 3D7) GN=PF08_0004 PE=4 SV=1	Q8IBD0_P LAF7	16 kDa	X			X		X
Proteasome regulatory subunit, putative OS=Plasmodium falciparum (isolate 3D7) GN=MAL13P1.343 PE=4 SV=1	Q8ID28_P LAF7	35 kDa	X					

Identified Proteins	UniProt Accession Number	Molecular Weight	Sample					
			W2C1	W2C2	W2C3	W2T1	W2T2	W2T3
Proteasome subunit alpha type 5, putative OS=Plasmodium falciparum (isolate 3D7) GN=PF08_0109 PE=4 SV=1	Q8IAR6_P LAF7	55 kDa	X					X
DNA replication licensing factor MCM4-related OS=Plasmodium falciparum (isolate 3D7) GN=PF13_0095 PE=3 SV=1	Q8IEE5_P LAF7	115 kDa	X	X	X	X		X
Glutamine synthetase, putative OS=Plasmodium falciparum (isolate 3D7) GN=PF11110w PE=3 SV=1	C0H551_ PLAF7	63 kDa	X		X	X		
Cof-like hydrolase, had-superfamily, subfamily iib OS=Plasmodium falciparum (isolate 3D7) GN=PFL1270w PE=4 SV=1	Q8I5F4_P LAF7	33 kDa	X				X	X
Sec24 subunit, putative OS=Plasmodium falciparum (isolate 3D7) GN=PF13_0324 PE=4 SV=1	C0H5J6_P LAF7	107 kDa			X	X	X	X
60S ribosomal protein L6, putative OS=Plasmodium falciparum (isolate 3D7) GN=PF13_0129 PE=4 SV=1	Q8IE85_P LAF7	22 kDa	X					X
2-Cys peroxiredoxin, putative OS=Plasmodium vivax (strain Salvador I) GN=PVX_118545 PE=1 SV=1	A5K421_P LAVS	22 kDa		X				
40S ribosomal protein S28e, putative OS=Plasmodium falciparum (isolate 3D7) GN=PF14_0585 PE=4 SV=1	Q8IKL9_P LAF7	7 kDa					X	
10b antigen, putative OS=Plasmodium falciparum (isolate 3D7) GN=PF10_0213 PE=4 SV=1	Q8IJ4_PL AF7	267 kDa						X
Ubiquitination-mediated degradation component, putative OS=Plasmodium falciparum (isolate 3D7) GN=PF08_0020 PE=4 SV=1	C0H4Y0_ PLAF7	155 kDa				X		
eIF4E OS=Plasmodium falciparum PE=2 SV=1	A0MTS9_ PLAFA (+1)	27 kDa	X	X				
Skeleton binding protein 1 OS=Plasmodium falciparum GN=sbp1 PE=4 SV=1	Q9NFF5_ PLAFA	37 kDa	X	X		X		X
Lsm6 homologue, putative OS=Plasmodium falciparum (isolate 3D7) GN=PF13_0142 PE=4 SV=1	Q8IE68_P LAF7	9 kDa			X	X	X	
60S ribosomal protein L10, putative OS=Plasmodium falciparum (isolate 3D7) GN=PF14_0141 PE=4 SV=1	Q8ILV2_P LAF7	25 kDa			X	X		
60S ribosomal protein L6-2, putative OS=Plasmodium falciparum (isolate 3D7) GN=PF13_0213 PE=4 SV=1	Q8IDV1_P LAF7	26 kDa	X		X		X	X
Replication factor A-related protein, putative OS=Plasmodium falciparum (isolate 3D7) GN=PF10235w PE=4 SV=1	Q8I3A1_P LAF7	56 kDa			X	X	X	
Putative uncharacterized protein OS=Plasmodium falciparum (isolate 3D7) GN=PFA_0410w PE=4 SV=1	Q8I259_P LAF7	255 kDa	X		X		X	X
Protein kinase c inhibitor-like protein, putative OS=Plasmodium falciparum (isolate 3D7) GN=PF08_0059 PE=4 SV=2	Q7K6B1_ PLAF7	21 kDa	X					
Putative uncharacterized protein OS=Plasmodium falciparum (isolate 3D7) GN=PF07_0016 PE=4 SV=1	Q8IC27_P LAF7	218 kDa				X		
40S ribosomal protein S9, putative OS=Plasmodium falciparum (isolate 3D7) GN=PFE1005w PE=3 SV=1	Q8I3R0_P LAF7	22 kDa	X		X	X	X	X
Phosphoglucomutase, putative OS=Plasmodium falciparum (isolate 3D7) GN=PF10_0122 PE=3 SV=1	Q8IJS0_P LAF7	68 kDa	X			X		
Cysteinyl-tRNA synthetase, putative OS=Plasmodium falciparum (isolate 3D7) GN=PF10_0149 PE=3 SV=2	Q8IJP3_P LAF7	80 kDa		X		X		X
Falcpain-3 OS=Plasmodium falciparum (isolate 3D7) GN=PF11_0162 PE=3 SV=1	Q8IIL0_PL AF7	57 kDa		X				
60S ribosomal protein L17, putative OS=Plasmodium falciparum (isolate 3D7) GN=PF13_0268 PE=3 SV=1	Q8IDI5_P LAF7	23 kDa	X			X		X

Identified Proteins	UniProt Accession Number	Molecular Weight	Sample					
			W2C1	W2C2	W2C3	W2T1	W2T2	W2T3
Vacuolar ATP synthase subunit E, putative OS=Plasmodium falciparum (isolate 3D7) GN=PF11670c PE=3 SV=2	Q812H3_P LAF7	27 kDa					X	X
Putative uncharacterized protein OS=Plasmodium falciparum (isolate 3D7) GN=PF07_0008 PE=4 SV=1	Q81C42_P LAF7	28 kDa	X		X	X		
Hexose transporter 1 OS=Plasmodium falciparum GN=ht1 PE=2 SV=1	O97467_P LAFA (+1)	56 kDa	X	X	X	X		X
V-type ATPase, subunit C, putative OS=Plasmodium falciparum (isolate 3D7) GN=PFA_0300c PE=4 SV=1	Q81280_P LAF7	45 kDa					X	
Enhancer of rudimentary homolog OS=Plasmodium falciparum (isolate 3D7) GN=ERH PE=3 SV=1	Q81J30_P LAF7	12 kDa	X				X	
Conserved Plasmodium protein OS=Plasmodium falciparum (isolate 3D7) GN=PF11_0292 PE=4 SV=1	Q81I82_PL AF7	29 kDa	X	X			X	
Uncharacterized protein MAL13P1.336 OS=Plasmodium falciparum (isolate 3D7) GN=MAL13P1.336 PE=4 SV=1	Y13P2_PL AF7	79 kDa	X				X	X
Uncharacterized protein OS=Plasmodium falciparum (isolate 3D7) GN=PF13_0099 PE=4 SV=1	Q81EE2_P LAF7	23 kDa				X		
Protein phosphatase, putative OS=Plasmodium falciparum (isolate 3D7) GN=PF11_0281 PE=4 SV=2	Q81I93_PL AF7	34 kDa	X			X		
Arginyl-tRNA synthetase, putative OS=Plasmodium falciparum (isolate 3D7) GN=PFL0900c PE=3 SV=1	Q815M2_P LAF7	68 kDa						X
40S ribosomal protein S13, putative OS=Plasmodium falciparum (isolate 3D7) GN=PF13_0316 PE=3 SV=1	Q81DB0_P LAF7	17 kDa	X				X	X
Heat shock protein DnaJ homologue Pfj4 OS=Plasmodium falciparum GN=pfj4 PE=4 SV=1	Q9GUX2_ PLAFA	28 kDa	X					
Putative uncharacterized protein OS=Plasmodium falciparum (isolate 3D7) GN=PF14_0390 PE=4 SV=1	Q81L59_P LAF7	26 kDa				X	X	X
ATP-dependent DNA helicase, putative OS=Plasmodium falciparum (isolate 3D7) GN=PF13_0330 PE=4 SV=1	Q81D85_P LAF7	55 kDa	X					
Transportin OS=Plasmodium falciparum GN=PFTRN PE=4 SV=1	Q8WSV8_ PLAFA	132 kDa	X					
Conserved Plasmodium protein OS=Plasmodium falciparum (isolate 3D7) GN=PF11_0332 PE=4 SV=1	Q81I42_PL AF7	32 kDa					X	
Probable prefoldin subunit 6 OS=Plasmodium falciparum (isolate 3D7) GN=PFE0595w PE=3 SV=2	PFD6_PL AF7	14 kDa	X					X
40S ribosomal protein S16, putative OS=Plasmodium falciparum (isolate 3D7) GN=PF08_0076 PE=3 SV=1	Q81AX5_P LAF7	16 kDa	X	X	X	X		
Putative uncharacterized protein OS=Plasmodium falciparum (isolate 3D7) GN=PFF1410c PE=4 SV=1	C6KTC6_ PLAF7	77 kDa	X			X	X	X
DEAD-box helicase 11 OS=Plasmodium falciparum PE=3 SV=1	A7U5X1_ PLAFA (+2)	109 kDa	X					
Inorganic pyrophosphatase, putative OS=Plasmodium falciparum (isolate 3D7) GN=PFC0710w.1 PE=4 SV=1	C0H477_ PLAF7	51 kDa	X				X	
Uncharacterized protein OS=Plasmodium falciparum (isolate 3D7) GN=PF13_0136 PE=4 SV=1	REVERSE _Q81E78_ PLAF7-R	45 kDa	X					
Putative uncharacterized protein OS=Plasmodium falciparum (isolate 3D7) GN=PF11590c PE=4 SV=1	Q81218_PL AF7	159 kDa	X				X	
Putative uncharacterized protein OS=Plasmodium falciparum (isolate 3D7) GN=PFE0990w PE=4 SV=1	C0H4F1_ PLAF7	23 kDa					X	X
Ribosomal protein L15 OS=Plasmodium falciparum (isolate 3D7) GN=PFD0770c PE=3 SV=1	C0H4A6_ PLAF7	24 kDa				X	X	X
Conserved Plasmodium protein OS=Plasmodium falciparum (isolate 3D7) GN=PFB0490c PE=4 SV=1	O96191_P LAF7	33 kDa	X				X	
PfSec61 OS=Plasmodium falciparum GN=PfSec61 PE=3 SV=1	O60992_P LAFA (+1)	52 kDa	X					

Identified Proteins	UniProt Accession Number	Molecular Weight	Sample						
			W2C1	W2C2	W2C3	W2T1	W2T2	W2T3	
Proteasome regulatory component, putative OS=Plasmodium falciparum (isolate 3D7) GN=MAL13P1.190 PE=4 SV=1	Q8IDV2_P LAF7	59 kDa	X				X		X
Conserved Plasmodium protein OS=Plasmodium falciparum (isolate 3D7) GN=PFB0835c PE=4 SV=1	O96259_P LAF7	61 kDa	X				X		X
PfRab18, GTPase OS=Plasmodium falciparum (isolate 3D7) GN=rab18 PE=3 SV=1	Q7K6B0_ PLAF7 (+1)	23 kDa	X				X		
RNA binding protein, putative OS=Plasmodium falciparum (isolate 3D7) GN=PFF0250w PE=4 SV=1	C6KSP9_ PLAF7	86 kDa			X				
60S ribosomal protein L23, putative OS=Plasmodium falciparum (isolate 3D7) GN=PF13_0171 PE=3 SV=1	Q8IE09_P LAF7	15 kDa		X					X
Proteasome, putative OS=Plasmodium falciparum (isolate 3D7) GN=PF11545c PE=4 SV=1	Q8I0U7_P LAF7	33 kDa					X	X	
DNA-directed RNA polymerase OS=Plasmodium falciparum (isolate 3D7) GN=PFC0805w PE=3 SV=1	O77375_P LAF7	279 kDa					X		
Centrin-2 OS=Plasmodium falciparum (isolate 3D7) GN=CEN2 PE=4 SV=1	Q8IL07_P LAF7	19 kDa	X				X		
PfSNF2L OS=Plasmodium falciparum (isolate 3D7) GN=PF11_0053 PE=4 SV=1	Q8IIW0_P LAF7	167 kDa	X						
RNAse L inhibitor protein, putative OS=Plasmodium falciparum (isolate 3D7) GN=MAL13P1.344 PE=3 SV=1	Q8I6Z4_P LAF7	70 kDa	X						
Phosphatase, putative OS=Plasmodium falciparum (isolate 3D7) GN=PF13_0222 PE=4 SV=1	Q8IDT0_P LAF7	68 kDa	X		X		X	X	
Glutamyl-tRNA synthetase, putative OS=Plasmodium falciparum (isolate 3D7) GN=PF13_0170 PE=3 SV=1	Q8IE10_P LAF7	109 kDa	X						X
Pfs38 OS=Plasmodium falciparum PE=4 SV=1	A8QVQ2_ PLAFA	41 kDa	X	X				X	
Isocitrate dehydrogenase [NADP] OS=Plasmodium falciparum (isolate 3D7) GN=PF13_0242 PE=3 SV=1	Q8I6T2_P LAF7	54 kDa	X	X	X				
Conserved Plasmodium protein OS=Plasmodium falciparum (isolate 3D7) GN=PF11_0069 PE=4 SV=2	Q8IIU5_P LAF7	31 kDa	X				X		
60S ribosomal protein L18a OS=Plasmodium falciparum (isolate 3D7) GN=PF13_0224 PE=3 SV=1	Q8IDS6_P LAF7	22 kDa	X		X		X		
Cytosolic glyoxalase II OS=Plasmodium falciparum (isolate 3D7) GN=cGloII PE=3 SV=1	C0H490_ PLAF7	31 kDa			X		X		
40S ribosomal protein S21 OS=Plasmodium falciparum (isolate 3D7) GN=PF11_0454 PE=3 SV=1	Q8IHS5_P LAF7	9 kDa	X				X		
Methionine aminopeptidase OS=Plasmodium falciparum (isolate 3D7) GN=PF14_0327 PE=3 SV=1	Q8ILB8_P LAF7	72 kDa			X		X		
P-type calcium transporting ATPase OS=Plasmodium falciparum GN=serca PE=3 SV=1	E1CC54_ PLAFA	140 kDa							X
60S ribosomal protein L23a, putative OS=Plasmodium falciparum (isolate 3D7) GN=PF13_0132 PE=3 SV=1	Q8IE82_P LAF7	22 kDa					X		
Coatamer alpha subunit, putative OS=Plasmodium falciparum (isolate 3D7) GN=PFF0330w PE=4 SV=1	C6KSR5_ PLAF7	177 kDa							X
Pfmdr2 protein OS=Plasmodium falciparum GN=pfmdr2 PE=3 SV=1	Q25693_P LAFA (+1)	119 kDa					X		
60S ribosomal protein L14, putative OS=Plasmodium falciparum (isolate 3D7) GN=PF14_0296 PE=4 SV=1	Q8ILE8_P LAF7	19 kDa					X		
Smarca-related protein OS=Plasmodium falciparum (isolate 3D7) GN=PFF1185w PE=4 SV=1	C6KT82_ PLAF7	316 kDa	X						
Small GTPase rab11 OS=Plasmodium falciparum GN=rab11 PE=2 SV=1	Q25999_P LAFA (+1)	25 kDa	X				X		
Proteasome subunit beta type OS=Plasmodium falciparum (isolate 3D7) GN=PF10_0111 PE=3 SV=1	Q8IJT1_P LAF7	31 kDa	X				X	X	

Identified Proteins	UniProt Accession Number	Molecular Weight	Sample					
			W2C1	W2C2	W2C3	W2T1	W2T2	W2T3
Heat shock protein DnaJ homologue Pfj2 OS=Plasmodium falciparum GN=pfj2 PE=4 SV=1	O77048_P LAFA (+1)	62 kDa	X		X			X
Proteasome regulatory protein, putative OS=Plasmodium falciparum (isolate 3D7) GN=PFC0785c PE=4 SV=1	O77379_P LAF7	26 kDa		X				
Heat shock protein 90, putative OS=Plasmodium falciparum (isolate 3D7) GN=PF11_0188 PE=3 SV=1	Q8116_PL AF7	108 kDa				X		X
DNA replication licensing factor MCM5, putative OS=Plasmodium falciparum (isolate 3D7) GN=PFL0580w PE=3 SV=1	Q815T4_P LAF7	86 kDa	X				X	
Ubiquitin conjugating enzyme, putative OS=Plasmodium falciparum (isolate 3D7) GN=PF13_0301 PE=3 SV=1	Q81DD9_P LAF7	23 kDa	X				X	X
Falcpain-2' OS=Plasmodium falciparum PE=3 SV=1	Q56CY9_ PLAFA (+1)	56 kDa	X	X				X
Putative uncharacterized protein OS=Plasmodium falciparum (isolate 3D7) GN=PF08_0091 PE=4 SV=1	Q81AV1_P LAF7	144 kDa	X					
ORF 2 protein (Fragment) OS=Plasmodium falciparum GN=ORF 2 PE=2 SV=1	Q02602_P LAFA	87 kDa						X
Replication factor a protein, putative OS=Plasmodium falciparum (isolate 3D7) GN=PFD0470c PE=4 SV=1	Q9U0J0_ PLAF7	134 kDa			X			
Ring-exported protein 1 OS=Plasmodium falciparum (isolate 3D7) GN=REX1 PE=4 SV=1	Q812G1_P LAF7	83 kDa					X	
40S ribosomal protein S24 OS=Plasmodium falciparum (isolate 3D7) GN=PFE0975c PE=3 SV=1	Q813R6_P LAF7	15 kDa					X	
Glutamate--cysteine ligase (Gamma-glutamylcysteine synthetase) OS=Plasmodium falciparum GN=GCS PE=2 SV=1	Q9TY17_ PLAFA (+1)	137 kDa					X	
Activator of Hsp90 ATPase homolog 1-like protein, putative OS=Plasmodium falciparum (isolate 3D7) GN=PFC0360w PE=4 SV=2	O97256_P LAF7 (+1)	16 kDa						X
Putative uncharacterized protein OS=Plasmodium falciparum (isolate 3D7) GN=PF14_0092 PE=4 SV=2	Q81M01_P LAF7	31 kDa	X					
Ubiquitin conjugating enzyme E2, putative OS=Plasmodium falciparum (isolate 3D7) GN=PFL0190w PE=3 SV=1	Q81607_P LAF7	17 kDa						X
Coatamer protein, beta subunit, putative OS=Plasmodium falciparum (isolate 3D7) GN=PF14_0277 PE=4 SV=2	Q81LG6_P LAF7	160 kDa					X	X
Putative uncharacterized protein OS=Plasmodium falciparum (isolate 3D7) GN=MAL8P1.62 PE=4 SV=1	Q81B31_P LAF7	32 kDa					X	X
Replication licensing factor, putative OS=Plasmodium falciparum (isolate 3D7) GN=PF13_0291 PE=3 SV=1	Q81DF0_P LAF7	106 kDa	X	X				
M18 aspartyl aminopeptidase OS=Plasmodium falciparum (isolate 3D7) GN=PfM18AAP PE=1 SV=1	Q812J3_P LAF7	66 kDa			X	X		
60S ribosomal protein L36 OS=Plasmodium falciparum (isolate 3D7) GN=PF11_0106 PE=3 SV=2	Q81713_P LAF7	13 kDa					X	
Putative uncharacterized protein OS=Plasmodium falciparum (isolate 3D7) GN=PFE0050w PE=4 SV=1	Q81490_P LAF7	31 kDa	X				X	
Serine rich protein homologue OS=Plasmodium falciparum PE=3 SV=1	Q26015_P LAFA	120 kDa					X	
Apicoplast 1-acyl-sn-glycerol-3-phosphate acyltransferase, putative OS=Plasmodium falciparum (isolate 3D7) GN=PF14_0421 PE=4 SV=2	Q81L28_P LAF7	34 kDa	X				X	X
Putative uncharacterized protein OS=Plasmodium falciparum (isolate 3D7) GN=PF14_0228 PE=4 SV=1	Q81LL5_P LAF7	184 kDa	X					
6-cysteine protein, putative OS=Plasmodium falciparum (isolate 3D7) GN=Pf41 PE=4 SV=1	Q811Y0_P LAF7	43 kDa					X	

Identified Proteins	UniProt Accession Number	Molecular Weight	Sample						
			W2C1	W2C2	W2C3	W2T1	W2T2	W2T3	
Putative uncharacterized protein OS=Plasmodium falciparum (isolate 3D7) GN=PFA_0420w PE=4 SV=1	Q8I257_P LAF7	20 kDa	X				X		X
DNA replication licensing factor mcm7 homologue, putative OS=Plasmodium falciparum (isolate 3D7) GN=PF07_0023 PE=3 SV=1	Q8IC16_P LAF7	94 kDa					X	X	
RNA binding protein, putative OS=Plasmodium falciparum (isolate 3D7) GN=PF11175c PE=4 SV=1	Q8I2R8_P LAF7	23 kDa	X	X	X			X	
60S ribosomal protein L19, putative OS=Plasmodium falciparum (isolate 3D7) GN=PF0700c PE=4 SV=1	C6KSY6_ PLAF7	22 kDa	X				X		
Putative uncharacterized protein OS=Plasmodium falciparum (isolate 3D7) GN=PF0880c PE=4 SV=1	C6KT22_ PLAF7	23 kDa	X						
60S ribosomal protein L30e, putative OS=Plasmodium falciparum (isolate 3D7) GN=PF10_0187 PE=4 SV=1	Q8IJK8_P LAF7	12 kDa				X	X		
Rab2, GTPase OS=Plasmodium falciparum (isolate 3D7) GN=Rab2 PE=3 SV=1	Q8I5A9_P LAF7	24 kDa							X
Cytidine triphosphate synthetase OS=Plasmodium falciparum (isolate 3D7) GN=PF14_0100 PE=4 SV=1	Q8ILZ3_P LAF7	99 kDa							X
Proteasome subunit, putative OS=Plasmodium falciparum (isolate 3D7) GN=PF14_0025 PE=4 SV=1	Q8IM66_P LAF7	78 kDa	X						
Merzoite surface protein 1 OS=Plasmodium reichenowi GN=msp1 PE=4 SV=1	Q4W2V7_ PLARE	198 kDa	X						
Ubiquitin carboxyl-terminal hydrolase OS=Plasmodium falciparum (isolate 3D7) GN=PFE1355c PE=3 SV=1	Q8I3J3_P LAF7	71 kDa					X	X	
Proteasome subunit beta type OS=Plasmodium falciparum (isolate 3D7) GN=PF14_0676 PE=3 SV=2	Q8IKC9_P LAF7	23 kDa		X				X	
Conserved protein OS=Plasmodium falciparum (isolate 3D7) GN=PF11_0287 PE=4 SV=2	Q8II87_PL AF7	35 kDa		X					
Uncharacterized protein OS=Plasmodium falciparum (isolate 3D7) GN=PF13_0190 PE=4 SV=1	Q8IDY6_P LAF7	63 kDa	X				X		
Proliferating cell nuclear antigen OS=Plasmodium falciparum (isolate 3D7) GN=PCNA2 PE=3 SV=1	Q7KQJ9_ PLAF7	30 kDa	X		X	X			
Early transcribed membrane protein 4, ETRAMP4 OS=Plasmodium falciparum (isolate 3D7) GN=ETRAPM4 PE=4 SV=1	Q8IFM9_P LAF7	15 kDa	X						X
Glycogen synthase kinase 3 OS=Plasmodium falciparum (isolate 3D7) GN=PfGSK-3 PE=4 SV=2	O77344_P LAF7	52 kDa					X		
Dynamain homologue OS=Plasmodium falciparum GN=dyn PE=3 SV=1	Q6KF55_ PLAFA	82 kDa	X						
Asparagine synthetase OS=Plasmodium falciparum (isolate 3D7) GN=PFC0395w PE=4 SV=1	O77330_P LAF7	70 kDa	X					X	
Acetyl-CoA synthetase OS=Plasmodium falciparum (isolate 3D7) GN=PF1350c PE=4 SV=1	C6KTB4_ PLAF7	114 kDa							X
Chloroquine resistance transporter OS=Plasmodium falciparum GN=CRT PE=1 SV=1	CRT_PLA FA	49 kDa	X	X		X			
DNAJ protein, putative OS=Plasmodium falciparum (isolate 3D7) GN=PF08_0032 PE=4 SV=1	Q8IB72_P LAF7	77 kDa					X		X
NAD synthase, putative OS=Plasmodium falciparum (isolate 3D7) GN=PF11310w PE=4 SV=1	Q8I2P2_P LAF7	98 kDa				X			X
Translation elongation factor EF-1, subunit alpha, putative OS=Plasmodium falciparum (isolate 3D7) GN=PF11_0245 PE=4 SV=1	Q8IIC9_P LAF7	63 kDa	X						
DNA primase small subunit OS=Plasmodium falciparum (isolate K1 / Thailand) PE=3 SV=1	PRI1_PLA FK	53 kDa	X						
Elongation factor 2 OS=Plasmodium falciparum (isolate 3D7) GN=PF14_0486 PE=4 SV=1	REVERSE_ _Q8IKW5 _PLAF7-R	94 kDa							X

Identified Proteins	UniProt Accession Number	Molecular Weight	Sample					
			W2C1	W2C2	W2C3	W2T1	W2T2	W2T3
DNA topoisomerase 2 OS=Plasmodium falciparum (isolate 3D7) GN=PF14_0316 PE=3 SV=1	Q8ILC8_P LAF7	169 kDa						X
Conserved Plasmodium protein OS=Plasmodium falciparum (isolate 3D7) GN=PFL0895c PE=4 SV=1	Q8I5M3_P LAF7	123 kDa				X		X
Spermidine synthase OS=Plasmodium falciparum (isolate 3D7) GN=PF11_0301 PE=1 SV=1	Q8II73_PL AF7 (+1)	37 kDa				X		
Putative uncharacterized protein OS=Plasmodium falciparum (isolate 3D7) GN=PF08_0137 PE=4 SV=1	Q8IAK9_P LAF7	147 kDa				X		
ATP synthase (C/AC39) subunit, putative OS=Plasmodium falciparum (isolate 3D7) GN=PF14_0615 PE=4 SV=1	Q8IKJ0_P LAF7	45 kDa			X		X	
Conserved Plasmodium protein OS=Plasmodium falciparum (isolate 3D7) GN=PFL2355w PE=4 SV=1	Q8I4U3_P LAF7	45 kDa	X		X	X		
PfSec23 protein OS=Plasmodium falciparum (isolate 3D7) GN=Pfsec23 PE=2 SV=1	Q8IB60_P LAF7	86 kDa					X	
Helicase (Fragment) OS=Plasmodium falciparum PE=2 SV=1	A6N5Z1_ PLAFA	66 kDa	X					
Replication factor C subunit 1 OS=Plasmodium falciparum GN=rfc1 PE=4 SV=1	Q9GQW6_ _PLAFA	104 kDa				X		
60S ribosomal protein L8, putative OS=Plasmodium falciparum (isolate 3D7) GN=PFE0845c PE=4 SV=1	Q8I3T9_P LAF7	28 kDa					X	
40S ribosomal protein S26e, putative OS=Plasmodium falciparum (isolate 3D7) GN=PFB0830w PE=4 SV=1	O96258_P LAF7	13 kDa	X				X	X
Vacuolar proton translocating ATPase subunit A, putative OS=Plasmodium falciparum (isolate 3D7) GN=PF08_0113 PE=4 SV=1	Q8IAQ8_P LAF7	123 kDa		X				
Ran-binding protein, putative OS=Plasmodium falciparum (isolate 3D7) GN=PF10490c PE=4 SV=1	C0H530_ PLAF7	139 kDa	X					
Ubiquitin carboxyl-terminal hydrolase a, putative OS=Plasmodium falciparum (isolate 3D7) GN=PFD0680c PE=4 SV=1	Q81U8_P LAF7	98 kDa				X		
Putative uncharacterized protein OS=Plasmodium falciparum (isolate 3D7) GN=MAL8P1.52 PE=4 SV=1	Q8IB48_P LAF7	14 kDa	X				X	
Aquaglyceroporin OS=Plasmodium falciparum (isolate 3D7) GN=AQP PE=3 SV=1	Q8II36_PL AF7 (+1)	28 kDa	X					
40S ribosomal protein S5, putative OS=Plasmodium falciparum (isolate 3D7) GN=PF07_0088 PE=3 SV=1	Q8IBN5_P LAF7	22 kDa	X					
Orotate phosphoribosyltransferase OS=Plasmodium falciparum GN=opr1 PE=2 SV=1	Q8N0R1_ PLAFA	33 kDa				X		
Uncharacterized protein OS=Plasmodium falciparum (isolate 3D7) GN=MAL13P1.257 PE=1 SV=1	Q8ID18_P LAF7	19 kDa	X			X		
Ser/Arg-rich splicing factor, putative OS=Plasmodium falciparum (isolate 3D7) GN=PFE0160c PE=4 SV=1	Q8I468_P LAF7	38 kDa	X					
Calmodulin OS=Plasmodium falciparum (isolate 3D7) GN=PF14_0323 PE=3 SV=2	CALM_PL AF7 (+1)	17 kDa						X
MYND finger protein, putative OS=Plasmodium falciparum (isolate 3D7) GN=PFF0105w PE=4 SV=1	C6KSM2_ PLAF7	29 kDa			X	X		
Merozoite-related surface protein 2 (Fragment) OS=Plasmodium falciparum PE=4 SV=1	C5HE50_ PLAFA (+5)	33 kDa	X					
Haloacid dehalogenase-like hydrolase, putative OS=Plasmodium falciparum (isolate 3D7) GN=PF11_0190 PE=4 SV=1	Q8III4_PL AF7	36 kDa				X		
Sexual stage antigen s16 OS=Plasmodium falciparum GN=s16 PE=4 SV=1	Q9U6T9_ PLAFA	17 kDa	X			X		
Nuclear movement protein, putative OS=Plasmodium falciparum (isolate 3D7) GN=PF13_0204 PE=4 SV=1	Q8IDW4_ PLAF7	46 kDa	X					

Identified Proteins	UniProt Accession Number	Molecular Weight	Sample					
			W2C1	W2C2	W2C3	W2T1	W2T2	W2T3
Bacterial histone-like protein OS=Plasmodium falciparum (isolate 3D7) GN=PfHU PE=4 SV=1	Q8I3A2_P LAF7	23 kDa	X					
Thymidylate kinase, putative OS=Plasmodium falciparum (isolate 3D7) GN=TMK PE=1 SV=1	Q8I4S1_P LAF7	25 kDa					X	
Phosphoenolpyruvate carboxylase, putative OS=Plasmodium falciparum (isolate 3D7) GN=PF14_0246 PE=4 SV=1	Q8ILJ7_P LAF7	134 kDa	X					
Myosin-A OS=Plasmodium falciparum (isolate FCBR / Columbia) PE=2 SV=1	MYOA_PL AFB	92 kDa					X	
Bet3 transport protein, putative OS=Plasmodium falciparum (isolate 3D7) GN=PF0895c PE=4 SV=1	Q8I1Q2_P LAF7	21 kDa			X			
Putative uncharacterized protein OS=Plasmodium falciparum (isolate 3D7) GN=MAL7P1.67 PE=4 SV=1	C0H4M7_ PLAF7	24 kDa	X					
Probable DNA-directed RNA polymerase II subunit RPB11 OS=Plasmodium falciparum (isolate 3D7) GN=PF13_0023 PE=3 SV=1	RPB11_P LAF7	14 kDa					X	
Zinc finger protein, putative OS=Plasmodium falciparum (isolate 3D7) GN=PF13_0313 PE=4 SV=1	Q8IDC0_P LAF7	70 kDa					X	
60S ribosomal protein L28, putative OS=Plasmodium falciparum (isolate 3D7) GN=PF11_0437 PE=4 SV=1	Q8IHU0_P LAF7	14 kDa						X
Skp1 family protein, putative OS=Plasmodium falciparum (isolate 3D7) GN=MAL13P1.337 PE=4 SV=2	Q8ID38_P LAF7	19 kDa	X				X	
60S ribosomal protein L31, putative OS=Plasmodium falciparum (isolate 3D7) GN=PFE0185c PE=4 SV=1	Q8I463_P LAF7	14 kDa			X			
Conserved Plasmodium protein OS=Plasmodium falciparum (isolate 3D7) GN=PFB0620w PE=4 SV=1	O96217_P LAF7	18 kDa	X					

APPENDIX B
PROTEINS IDENTIFIED IN HUMAN
MASCOT SEARCH

Identified Proteins	UniProt Accession Number	Molecular Weight	Sample					
			W2C1	W2C2	W2C3	W2T1	W2T2	W2T3
Spectrin alpha chain, erythrocytic 1 OS=Homo sapiens GN=SPTA1 PE=1 SV=5	sp P02549 SPTA1_HUMAN	280 kDa	X	X	X	X	X	X
Spectrin beta chain, erythrocytic OS=Homo sapiens GN=SPTB PE=1 SV=5	sp P11277 SPTB1_HUMAN	246 kDa	X	X	X	X	X	X
Band 3 anion transport protein OS=Homo sapiens GN=SLC4A1 PE=1 SV=3	B3AT_HUMAN	102 kDa	X	X	X	X	X	X
Hemoglobin subunit beta OS=Homo sapiens GN=HBB PE=1 SV=2	HBB_HUMAN	16 kDa	X	X	X	X	X	X
Isoform Er11 of Ankyrin-1 OS=Homo sapiens GN=ANK1	sp P16157-12 ANK1_HUMAN(+3)	209 kDa	X	X	X	X	X	X
Hemoglobin subunit alpha OS=Homo sapiens GN=HBA1 PE=1 SV=2	HBA_HUMAN	15 kDa	X	X	X	X	X	X
Actin, cytoplasmic 1 OS=Homo sapiens GN=ACTB PE=1 SV=1	ACTB_HUMAN	42 kDa	X	X	X	X	X	X
Isoform Long of Erythrocyte membrane protein band 4.2 OS=Homo sapiens GN=EPB42	sp P16452-2 EPB42_HUMAN	80 kDa	X	X	X	X	X	X
Isoform 2 of Protein 4.1 OS=Homo sapiens GN=EPB41	sp P11171-2 41_HUMAN(+2)	93 kDa	X	X	X	X	X	X
Glyceraldehyde-3-phosphate dehydrogenase OS=Homo sapiens GN=GAPDH PE=1 SV=3	G3P_HUMAN	36 kDa	X	X	X	X	X	X
Histone H4 OS=Homo sapiens GN=HIST1H4A PE=1 SV=2	H4_HUMAN	11 kDa	X	X	X	X	X	X
Elongation factor 1-alpha 2 OS=Homo sapiens GN=EEF1A2 PE=1 SV=1	EF1A2_HUMAN	50 kDa	X	X	X	X	X	X
Erythrocyte band 7 integral membrane protein OS=Homo sapiens GN=STOM PE=1 SV=3	sp P27105 STOM_HUMAN	32 kDa	X	X	X	X	X	X
Heat shock protein HSP 90-beta OS=Homo sapiens GN=HSP90AB1 PE=1 SV=4	HS90B_HUMAN	83 kDa	X	X	X	X	X	X
Solute carrier family 2, facilitated glucose transporter member 1 OS=Homo sapiens GN=SLC2A1 PE=1 SV=2	GTR1_HUMAN	54 kDa	X	X	X	X	X	X
Apolipoprotein A-I OS=Homo sapiens GN=APOA1 PE=1 SV=1	APOA1_HUMAN	31 kDa	X	X	X	X	X	X
Isoform 2 of Heat shock cognate 71 kDa protein OS=Homo sapiens GN=HSPA8	sp P11142-2 HSP7C_HUMAN(+1)	54 kDa	X	X	X	X	X	X

Identified Proteins	UniProt Accession Number	Molecular Weight	Sample					
			W2C1	W2C2	W2C3	W2T1	W2T2	W2T3
Isoform 2 of Tropomyosin alpha-3 chain OS=Homo sapiens GN=TPM3	sp P06753- 2 TPM3_HUMAN	29 kDa	X	X	X	X	X	X
Selenium-binding protein 1 OS=Homo sapiens GN=SELENBP1 PE=1 SV=2	sp Q13228 SBP1 _HUMAN	52 kDa	X	X	X	X	X	X
Calpain-1 catalytic subunit OS=Homo sapiens GN=CAPN1 PE=1 SV=1	CAN1_HUMAN	82 kDa	X	X	X	X	X	X
Superoxide dismutase [Cu-Zn] OS=Homo sapiens GN=SOD1 PE=1 SV=2	SODC_HUMAN	16 kDa	X	X	X	X	X	X
Alpha-adducin OS=Homo sapiens GN=ADD1 PE=2 SV=1	E7ENY0_HUMA N (+1)	73 kDa	X	X	X	X	X	X
Hemoglobin subunit delta OS=Homo sapiens GN=HBD PE=1 SV=2	HBD_HUMAN	16 kDa	X	X	X	X	X	X
Isoform Short of Dematin OS=Homo sapiens GN=EPB49	sp Q08495- 2 DEMA_HUMAN	43 kDa	X	X	X	X	X	X
Tropomodulin-1 OS=Homo sapiens GN=TMOD1 PE=1 SV=1	TMOD1_HUMAN	41 kDa	X	X	X	X	X	X
Carbonic anhydrase 1 OS=Homo sapiens GN=CA1 PE=1 SV=2	CAH1_HUMAN	29 kDa	X	X	X	X	X	X
Peroxiredoxin-2 OS=Homo sapiens GN=PRDX2 PE=1 SV=5	sp P32119 PRDX 2_HUMAN	22 kDa	X	X		X	X	X
Beta-adducin OS=Homo sapiens GN=ADD2 PE=1 SV=3	sp P35612 ADDB _HUMAN	81 kDa	X	X	X	X	X	X
Catalase OS=Homo sapiens GN=CAT PE=1 SV=3	CATA_HUMAN	60 kDa	X	X			X	
Isoform 2 of Triosephosphate isomerase OS=Homo sapiens GN=TPI1	sp P60174- 1 TPIS_HUMAN (+1)	27 kDa	X	X	X	X	X	X
Keratin, type II cytoskeletal 1 OS=Homo sapiens GN=KRT1 PE=1 SV=6	K2C1_HUMAN	66 kDa	X	X		X		X
Polyubiquitin-C (Fragment) OS=Homo sapiens GN=UBC PE=2 SV=1	F5H388_HUMAN	17 kDa	X	X	X	XX	X	X
Calpain small subunit 1 OS=Homo sapiens GN=CAPNS1 PE=1 SV=1	CPNS1_HUMAN	28 kDa	X	X	X	X	X	X
Tubulin beta-4B chain OS=Homo sapiens GN=TUBB4B PE=1 SV=1	TBB4B_HUMAN	50 kDa	X	X	X	X	X	X
Keratin, type I cytoskeletal 10 OS=Homo sapiens GN=KRT10 PE=1 SV=6	K1C10_HUMAN	59 kDa		X				
Isoform 8a of Blood group Rh(CE) polypeptide OS=Homo sapiens GN=RHCE	sp P18577- 11 RHCE_HUMA N (+1)	38 kDa	X	X	X			

Identified Proteins	UniProt Accession Number	Molecular Weight	Sample					
			W2C1	W2C2	W2C3	W2T1	W2T2	W2T3
Histone H2A type 2-A OS=Homo sapiens GN=HIST2H2AA3 PE=1 SV=3	H2A2A_HUMAN (+1)	14 kDa	X	X	X	X	X	X
Flotillin-1 OS=Homo sapiens GN=FLOT1 PE=1 SV=3	FLOT1_HUMAN	47 kDa	X	X	X	X	X	X
Histone H2B type 1-M OS=Homo sapiens GN=HIST1H2BM PE=1 SV=3	H2B1M_HUMAN	14 kDa		X				
78 kDa glucose-regulated protein OS=Homo sapiens GN=HSPA5 PE=1 SV=2	GRP78_HUMAN	72 kDa		X				
Isoform Glycophorin-D of Glycophorin-C OS=Homo sapiens GN=GYPC	sp P04921- 2 GLPC_HUMAN (+1)	11 kDa	X	X	X	X	X	X
Golgi-associated plant pathogenesis- related protein 1 OS=Homo sapiens GN=GLIPR2 PE=1 SV=3	GAPR1_HUMAN	17 kDa		X	X		X	
14-3-3 protein gamma OS=Homo sapiens GN=YWHAG PE=1 SV=2	1433G_HUMAN	28 kDa	X	X	X	X	X	X
Isoform 2 of Dynein heavy chain 9, axonemal OS=Homo sapiens GN=DNAH9	REVERSE_sp Q 9NYC9- 2 DYH9_HUMAN -DECOY (+2)	503 kDa		X				
Tropomyosin alpha-1 chain OS=Homo sapiens GN=TPM1 PE=2 SV=1	B7Z596_HUMAN (+2)	32 kDa	X	X		X		X
Apolipoprotein B-100 OS=Homo sapiens GN=APOB PE=1 SV=2	APOB_HUMAN	516 kDa	X		X	X	X	X
Flotillin-2 OS=Homo sapiens GN=FLOT2 PE=1 SV=2	FLOT2_HUMAN	47 kDa	X		X	X	X	X
Tubulin alpha-8 chain (Fragment) OS=Homo sapiens GN=TUBA8 PE=2 SV=1	C9J2C0_HUMAN (+2)	52 kDa	X			X	X	X
Flavin reductase (NADPH) OS=Homo sapiens GN=BLVRB PE=1 SV=3	BLVRB_HUMAN	22 kDa	X				X	
GTP-binding nuclear protein Ran (Fragment) OS=Homo sapiens GN=RAN PE=2 SV=1	F5H018_HUMAN	23 kDa	X		X			
Acylamino-acid-releasing enzyme OS=Homo sapiens GN=APEH PE=1 SV=4	ACPH_HUMAN (+1)	81 kDa	X				X	
Ras-related protein Rap-2b OS=Homo sapiens GN=RAP2B PE=1 SV=1	RAP2B_HUMAN	21 kDa	X					
Transitional endoplasmic reticulum ATPase OS=Homo sapiens GN=VCP PE=1 SV=4	TERA_HUMAN	89 kDa	X			X		

Identified Proteins	UniProt Accession Number	Molecular Weight	Sample					
			W2C1	W2C2	W2C3	W2T1	W2T2	W2T3
Isoform 2 of 55 kDa erythrocyte membrane protein OS=Homo sapiens GN=MPP1	sp Q00013-2 EM55_HUMAN (+1)	49 kDa	X		X	X	X	X
Uncharacterized protein (Fragment) OS=Homo sapiens PE=3 SV=1	K7N7A8_HUMAN	48 kDa	X				X	
Apolipoprotein A-II OS=Homo sapiens GN=APOA2 PE=1 SV=1	APOA2_HUMAN	11 kDa	X		X	X		X
26S protease regulatory subunit 4 OS=Homo sapiens GN=PSMC1 PE=2 SV=1	B4DR63_HUMAN	41 kDa	X					
Ras-related protein Rab-7a (Fragment) OS=Homo sapiens GN=RAB7A PE=2 SV=1	C9IZZ0_HUMAN (+6)	13 kDa	X					
Tubulin beta-3 chain OS=Homo sapiens GN=TUBB3 PE=1 SV=2	TBB3_HUMAN	50 kDa			X			X
Complement C3 OS=Homo sapiens GN=C3 PE=1 SV=2	CO3_HUMAN	187 kDa			X	X		
Isoform 2 of Apolipoprotein L1 OS=Homo sapiens GN=APOL1	sp O14791-2 APOL1_HUMAN	46 kDa					X	X
Actin, alpha skeletal muscle OS=Homo sapiens GN=ACTA1 PE=1 SV=1	ACTS_HUMAN	42 kDa						X
Glycophorin A OS=Homo sapiens GN=GYP A PE=2 SV=1	B8Q182_HUMAN (+2)	14 kDa						X
Complement C4-B OS=Homo sapiens GN=C4B PE=1 SV=2	CO4B_HUMAN	193 kDa			X	X		
Alpha-1-antitrypsin OS=Homo sapiens GN=SERPINA1 PE=1 SV=3	sp P01009 A1AT_HUMAN	47 kDa			X	X		
Keratin, type I cytoskeletal 9 OS=Homo sapiens GN=KRT9 PE=1 SV=3	K1C9_HUMAN	62 kDa					X	
Apolipoprotein E OS=Homo sapiens GN=APOE PE=1 SV=1	APOE_HUMAN	36 kDa			X			